Author:
Wilson-Kovacs, Robert S

Title:
Towards the Living Supramolecular Polymerisation of Tetra(aniline)-Functionalised Perylene Diimides

Towards the Living Supramolecular Polymerisation of Tetra(aniline)-Functionalised Perylene Diimides

Robert Stefan Wilson-Kovacs

A dissertation submitted to the University of Bristol in accordance with the requirements of the degree of Master of Science by Research in the Faculty of Science, School of Chemistry.

September 2020

Word count: 25,197 words.

Abstract

Perylene diimides (PDIs) provide a promising platform to create functionalised supramolecular polymers with controlled morphology and optoelectronic properties. The imide substitution of PDIs can finely tune the morphology and mode of growth of PDI supramolecular polymers, whilst the addition of functional moieties at the imide position yields supramolecular materials with new functionalities. Meanwhile, two major challenges in the field of poly(aniline)-based nanomaterials - improving their conductivity and stimuli response - can be addressed by finely controlling their nanostructure. This project envisions that incorporation of poly(anilines) into the imide substituents of PDIs will create controlled, functional supramolecular polymers to solve these challenges and open up new horizons in the field of multifunctional supramolecular polymers and devices.

In this thesis, the rational design, synthesis and supramolecular polymerisation of a tetra(aniline) functionalised PDI, **PDI-2-TANI**, is reported. Comprehensive synthetic pathways were trialled and optimised to create **PDI-2-TANI** through a series of heterocoupling reactions. The modularity of these coupling reactions allowed **PDI-2-TANI** to be synthesised through several different routes and provides a flexible framework to create other tetra(aniline)-substituted PDIs for future research.

The supramolecular polymerisation of **PDI-2-TANI** was studied via transmission electron microscopy and ultraviolet-visible spectroscopy. Thermally self-seeded aggregates of **PDI-2-TANI**, prepared via heating and cooling, consisted of ordered fibre bundles, with each fibre corresponding to an H-aggregated supramolecular polymer. The low dispersity of these fibres indicated that **PDI-2-TANI** underwent a living supramolecular polymerisation. Seeded growth experiments partially confirmed this, but a cooperative growth mechanism was not established via ultraviolet-visible spectroscopy. The **PDI-2-TANI** polymers were found to be out-of-equilibrium self-assemblies, requiring high temperatures to activate the unimer, whereupon it polymerised upon cooling. The discovery of this out-of-equilibrium behaviour yields a promising route to refine spectroscopic and seeded growth experiments and establish thermal self-seeding as a new method to perform living supramolecular polymerisations.

Acknowledgements

I would like to express my deepest appreciation and gratitude to my supervisor, Professor Charl Faul, for his patience, support and guidance. I am fortunate to have worked with him, both over the course of this project and during my Integrated Masters. Through his dedication to creating an encouraging, inspiring and collaborative research environment, and the opportunities he has provided to push my skills further, he has given me the best start to a research career.

I would also like to express my gratitude to Henry Symons for his support and insight throughout the project, and the many hours he spent helping me with theory and practical techniques. I would also like to thank Esther Townsend and Maha Alotaibi for their valuable advice on synthetic procedures. Additionally, I would like to thank all members of the Faul Group, whose support, optimism and camaraderie over the years have made my first steps into research thoroughly rewarding and enjoyable.

Author's Declaration

I declare that the work in this dissertation was carried out in accordance with the requirements of the University's *Regulations and Code of Practice for Research Degree Programmes* and that it has not been submitted for any other academic award. Except where indicated by specific reference in the text, the work is the candidate's own work. Work done in collaboration with, or with the assistance of, others, is indicated as such. Any views expressed in the dissertation are those of the author.

SIGNED: Robert Stefan Wilson-Kovacs DATE: 14th September 2020

Table of Contents

List of Abbreviations

Abbreviations are listed by the order in which they appear in the text.

PDI - Perylene diimide

HOMO - Highest occupied molecular orbital

LUMO - Lowest unoccupied molecular orbital

OPV - Organic photovoltaic

DMPAA - 2-*N*,*N*-dimethylamino-3-phenylpropanamine

PANI - Poly(aniline)

TANI - Tetra(aniline)

TANI - The TANI species used in this project - Boc-protected Ph/NH_2 TANI.

LEB - Leucoemeraldine base

EB - Emeraldine base

PB - Pernigraniline base

ES - Emeraldine salt

PDI-TANI - The conceptual class of unimers containing PDI and TANI moieties.

PDI-2-TANI - The specific PDI-TANI unimer trialled in this project.

NMR - Nuclear magnetic resonance

UV/Vis - Ultraviolet-visible (referring to this region of the electromagnetic spectrum)

TLC - Thin-layer chromatography

Boc - *Tert*-butyl carbamate

THF - Tetrahydrofuran

DCM - Dichloromethane

TBATB - Tetrabutylammonium tribromide

DMAP - 4-dimethylaminopyridine

$Pd(dba)_2$ - Palladium(0) bis(dibenzylideneacetone)

PTCDA - Perylenetetracarboxylic dianhydride

DMSO - Dimethyl sulfoxide

EDC - 1-ethyl-3-(3-dimethylaminopropyl)carbodiimide

DCC - Dicyclohexylcarbodiimide

HBTU - Hexafluorophosphate benzotriazole tetramethyl uronium

HOBt - Hydroxybenzotriazole

TEM - Transmission electron microscopy

List of Figures

List of Schemes

List of Tables

1. Introduction

1.1 Supramolecular Polymers

Supramolecular chemistry and polymer chemistry are closely interlinked; intermolecular interactions between polymer chains give rise to emergent physical properties, and even enable new functions. For example nylons, one of the first widely-used commercial covalent polymer classes, are prized for their thermoplasticity, an emergent property which arises due inter-chain hydrogen bonding, which promotes the formation of semicrystalline regions below its melt temperature (**Figure 1**).[1] In the natural world, the functions of many long-chain proteins, such as enzymes, are dictated by their secondary, tertiary and quaternary structures, which all stem from intra- and inter-chain noncovalent interactions. However, a relatively new class of materials, supramolecular polymers, aim to bring the fields of supramolecular chemistry and polymer chemistry even further together: with their polymerisations driven by intermolecular interactions instead of covalent bonds, these polymers can exhibit superior processability and recyclability,[2] self-healing[3] and dynamic morphologies which allow them to be used as sensors,[4] biomaterials,[5] artificial enzymes[6] and components for artificial photosynthetic devices.[7]

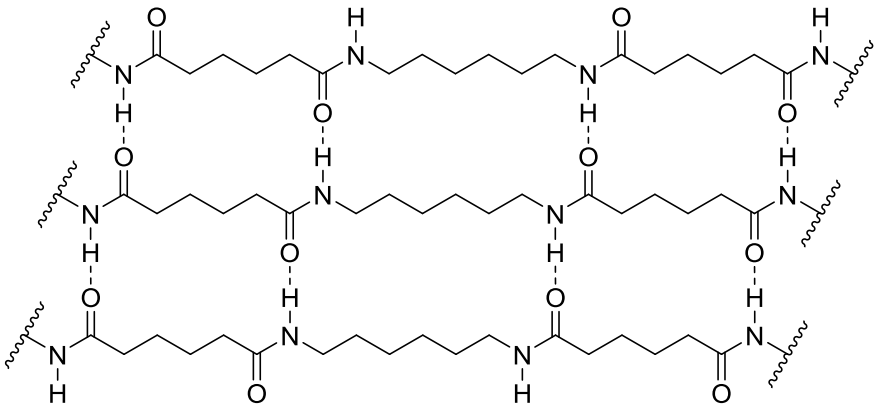

Figure 1 *An example of noncovalent interactions in polymer chemistry: hydrogen bonding in nylon 66.*

Supramolecular polymerisation is driven by the directional, noncovalent binding of covalent molecules or discrete-size supramolecular assemblies (e.g. metal-porphyrin complexes,[8] or hydrogen-bonded ensembles[9]), termed unimers. As such, supramolecular polymerisation is a subtype of molecular self-assembly; more precisely, it is the one-dimensional self-assembly of unimers. This self-assembly can be driven by a range of interactions, such as hydrogen bonding, π-stacking, metal–ligand interactions and hydrophobic interactions (**Figure 2**). It may be mediated by a range of complementary interactions, such as in the case of host–guest driven supramolecular polymerisations.[10] These interactions are often highly dependent on ambient conditions, such as temperature, concentration and solvent quality, and due to the reversible nature of noncovalent interactions, depolymerisation can readily occur. Through employing strong, or highly specific, complementary interactions, these challenges can be overcome.[11]

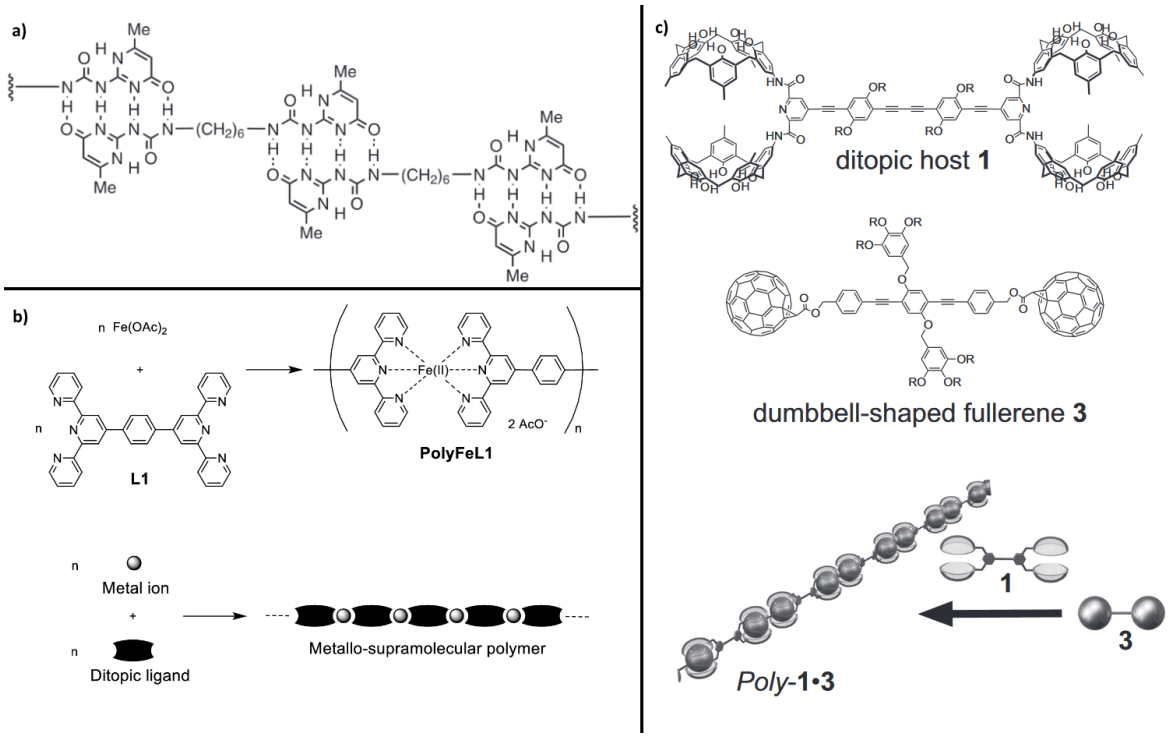

Figure 2 *Different examples of supramolecular polymers, driven by* ***a)*** *quadruple hydrogen bonding,* ***b)*** *metal-ligand interactions and* ***c)*** *aromatic interactions (π-stacking between fullerene and calixarene).*[12,13]

Like covalent polymerisation, supramolecular polymerisation can proceed via several growth mechanisms. In covalent polymerisation, the mode of growth is dependent on the presence of chemically active sites; for example, chain-growth polymerisation occurs when a growing chain has one active site which is regenerated upon the addition of further monomer, and step-growth polymerisation occurs when all monomers are chemically active. However, as supramolecular polymerisation is not driven by bond formation or scission, but instead by noncovalent interactions, the mode of growth of a supramolecular polymer is determined by aggregation and disaggregation kinetics (binding strength) between unimers, and how this binding strength changes as a function of polymer length. This behaviour is commonly simplified into two stages: the nucleation stage, where small oligomers and solvated unimers rapidly interconvert in a pre-equilibrium state, eventually forming stable seeds, and the elongation stage, where these seeds polymerise further as solvated unimers or seeds bind to them. Thus, the mechanism of a supramolecular polymerisation can be defined by the K_2-K model (**Figure 3**), which describes whether nucleation (commonly dimerization) kinetics, K_2, or growth (aggregation) kinetics, K, dominate.[14]

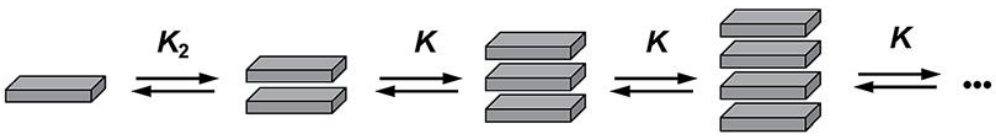

Figure 3 *An illustration of the K_2-K model for an abstracted supramolecular polymer.*[15]

The K_2-K model thus succinctly describes the modes of growth supramolecular polymers can undertake. When K_2 and K are equal, nucleation and aggregation kinetics are equally favoured, resulting in isodesmic growth, a mechanism analogous to step-growth covalent polymerisation. However, when K is larger than K_2, aggregation kinetics dominate, leading to a small population of seeds which readily polymerise, resulting in cooperative growth - this resembles chain-growth covalent polymerisation (**Figure 4**), and also exhibits a critical concentration or temperature where

the degree of aggregation α_A rapidly increases.[11] When K is smaller than K_2, the inverse occurs; nucleation kinetics dominate, leading to a large population of seeds whose growth is kinetically unfavourable, thus leading to aggregates with a supressed size. This process is referred to as anticooperative growth, a mechanism unique to supramolecular polymerisation. Unlike the step or chain growth of covalent polymerisation, these supramolecular growth mechanisms exist as a spectrum; for example, a polymerisation where K_2 is only slightly larger than K may be weakly anticooperative, and still readily form large aggregates, whilst a polymerisation where K_2 is orders of magnitude larger than K would be dominated by dimers and short oligomers, even when α_A is close to unity.

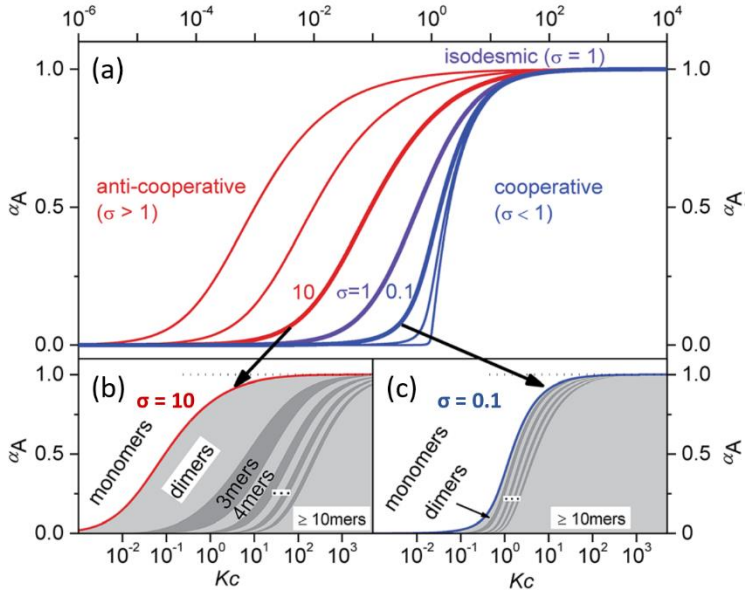

Figure 4 a) *Plots of* α_A *vs. equilibrium constant* K_c *for model isodesmic (σ=1), cooperative (σ<1) and anticooperative (σ>1) modes of growth.* ***b)*** *Plot of aggregate populations as a function of* K_c *and* α_A *for anticooperative growth.* ***c)*** *Plot of aggregate populations as a function of* K_c *and* α_A *for cooperative growth. σ is defined as the ratio* K_2/K.

1.2 Properties and Applications of Perylene Diimides

Discovered in 1913, perylene diimides (PDIs) were initially commercially used as high-performance pigments, where their stability and low solubility made them excellent candidates for coatings, paints and textile colourants.[16] Academic and commercial interest in PDIs was renewed with the onset of organic electronics and organic photovoltaics during the 1970s, due to the molecule's high thermal and redox stability, fluorescence and visible light absorption, and the high charge carrier mobility and exciton diffusion length within PDI aggregates.[17] Changes in optoelectronic properties from the molecular to aggregate state also make PDIs promising candidates for optical sensors and chemiresistors, and their biological inertness makes them suitable for in-vitro and in-vivo use.[18,19]

The key feature of PDIs is the π-conjugated perylene core, a rigid chromophore which bears a HOMO-LUMO gap corresponding to wavelengths of 500-700 nm, making these compounds strongly absorbent in the visible region of the electromagnetic spectrum, thus giving rise to intense colours. The perylene core also exhibits intense fluorescence (>95% quantum yield) due to its low-energy triplet excited state whose vibrational levels do not overlap with its excited singlet state, thus minimising intersystem crossing.[20] In PDIs, the perylene core is electron-poor due to its conjugation with two imide groups; the four carbonyls from the imides create a significant inductive effect. Thus, the core is resistant to oxidative degradation, and this resistance to oxidation is also extended to its reduced species, the PDI dianion.[21] This stability, as well as the preservation of core rigidity in the anionic form, makes PDIs an excellent candidate for n-type semiconductors.[22] N-type semiconductivity is relatively rare in the current field of organic electronics,[23] and thus PDIs have a distinct advantage over other molecules; literature examples exist of both p- and n-type doped PDIs.[24]

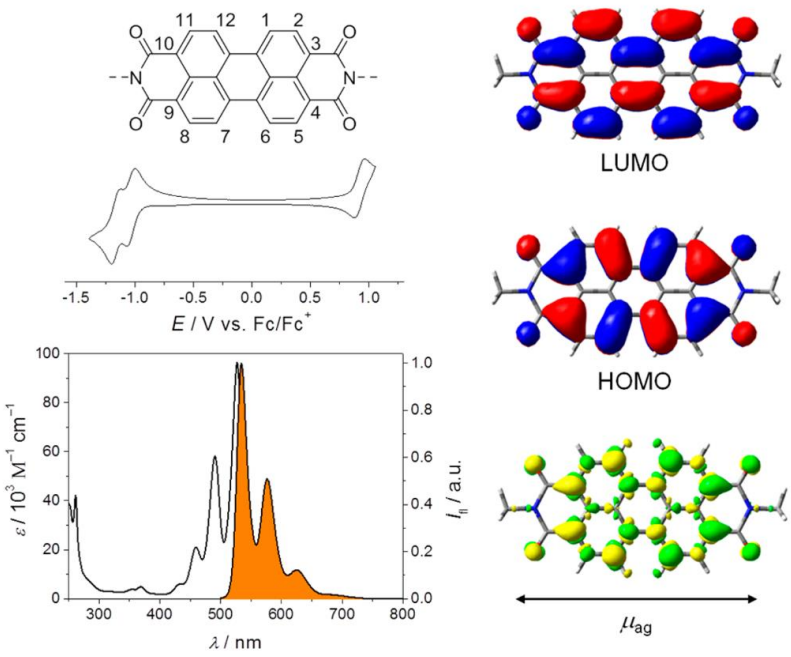

Figure 5 *The molecular structure of the PDI chromophore, a typical cyclic voltammogram illustrating its redox stability, UV/Vis spectrum and fluorescence (orange) spectrum, B3LYP/6-31++G** calculated HOMO and LUMO, and the S_0 to S_1 (ground and excited state singlet) transition density.*[25]

The π-conjugated perylene core of PDIs also drives the self-assembly of these molecules; like other conjugated aromatic systems, PDIs are commonly driven to self-assemble via π-stacking. Aromatic systems have strong quadrupole moments; in benzene, the C-H ring sigma bonds contain a lower electron density than the electron-rich conjugated π system, creating a 'sandwich' of partial positive charge (the ring) flanked by partial negative charge (the π orbitals). The polarity of this quadrupole is reversed in electron-poor aromatics such as the PDI core - the core's π-orbitals contain a lower electron density than its sigma bonds.[26] As aromatic molecules self-assemble, they seek orientations to relieve electron deficiency (**Figure 6**): for example, benzene will often undergo face-to-edge stacking, where the electron-poor 'edge' sigma orbits are electrostatically attracted to the electron-rich 'face' π-orbitals of a neighbouring molecule, creating a T-shaped aggregate.[27] In PDIs, the driving force towards π-stacking is the electrostatic attraction between the electron-poor core and the electron-rich carbonyls of the imide group, creating an offset stack.

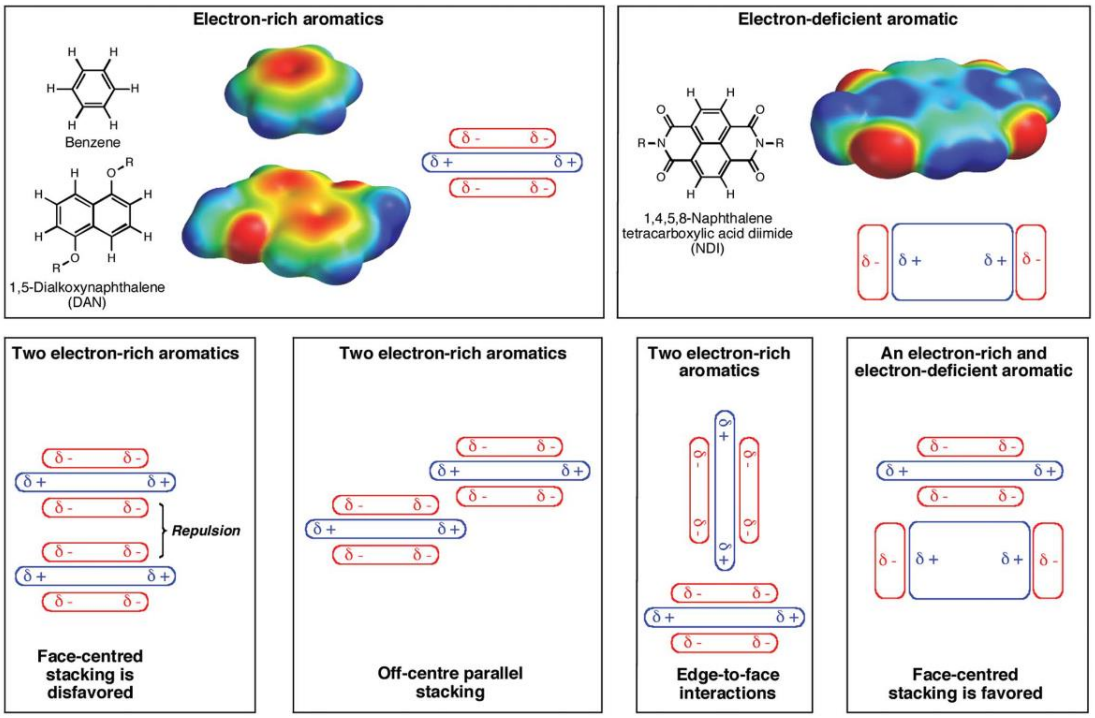

Figure 6 *Examples of electron-rich and electron-poor aromatic compounds, their B3LYP/6-31G* calculated electrostatic potential surfaces (red areas indicate high electron density, blue areas indicate low electron density), and simplified models of π-stacking based on electrostatic interactions.*[27]

Even though direct face-to-face stacking of the perylene cores is disfavoured due to electrostatic repulsion, the strong core-carbonyl attraction leads to an aggregate where the π-orbitals of neighbouring perylene cores are close enough to overlap. This π-overlap leads to orbital splitting and modulation of the HOMO-LUMO gap; thus, the optical and electronic properties of aromatic aggregates differ from their disaggregated molecules.[28] In the case of PDIs, their HOMO-LUMO transitions lie within the visible region of the spectrum, and thus their aggregation is often accompanied by a pronounced colour change. By controlling the amount of π-overlap between neighbouring PDI molecules, for example, by derivatising PDIs with sterically demanding substituents, this HOMO-LUMO gap can be tuned to obtain different colours: shades of red, brown, violet and black.[29]

As the self-assembly of PDIs involves a degree of π-orbital overlap, electronic coupling occurs between neighbouring PDI molecules in an aggregate, facilitating the intermolecular transfer of electrons or holes via electron hopping.[30] Electron transfer within solids is described by polaron theory, whereby atoms surrounding an electron distort to shield the electron's charge, forming a polaron.[31] Thus, molecular or lattice distortion energy affects the mobility of polarons in a solid. In organic supramolecular aggregates, intramolecular distortion and relaxation is minimised due to the relative inflexibility of covalent bonds (compared to lattices).[32] However, intermolecular transfer of these polarons incurs an energy barrier due to intermolecular distortion and reorganisation, negatively impacting charge carrier mobility.[33] The strong π-stacking of PDI aggregates, their high structural order, and one-dimensional intermolecular charge transfer minimises this effect, and as such PDI aggregates have high charge carrier mobilities, comparable to that of amorphous silicon.[34] Slight variations in the energy barrier for intermolecular polaron transfer between PDIs (e.g. due to variations in their distance and conformation) lead to broadening of molecular HOMO and LUMO orbitals into a band structure for PDI aggregates (**Figure 7**).[35] The small HOMO-LUMO gap of PDIs results in a small band-gap in their aggregate state; thus PDI aggregates are semiconductive. As the HOMO and LUMO of PDI molecules can be readily modulated by molecular substitutions, and the bands of aggregates modulated by the mode of aggregation, PDIs can be designed to be either p- or n-type semiconductors, their conductivity relying on either electron or electron hole transport.

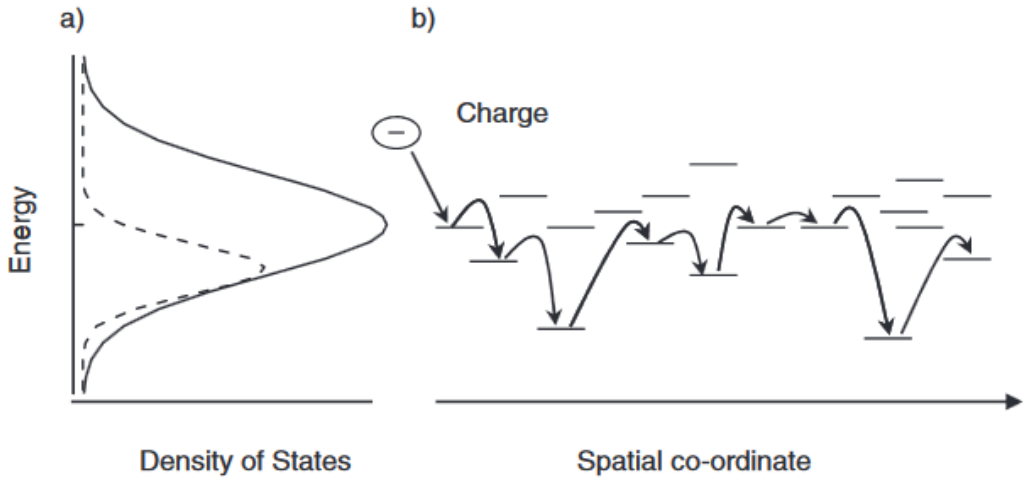

Figure 7 a) *The density of LUMO states (solid line) and occupied LUMO states for an aggregated semiconductor.* ***b)*** *Energy levels of a LUMO polaron on different molecules in a disordered ensemble of molecules. The pathway an electron takes as it moves between molecules can results in a range of different energies, resulting in a band.*[35]

As PDIs can form both p- and n-type semiconductors, they have attracted much interest in the field of organic photovoltaics (OPVs). Photovoltaic devices rely on electron transport and exciton diffusion within a p-n junction; the interface of a p-type (hole-doped) and n-type (electron-doped) semiconductor. As electrons diffuse randomly throughout the material, a charge bias is built up at the p-n junction; holes from the p-type semiconductor migrate to the n-type semiconductor, building up a positive charge, and electrons migrate from the n-type semiconductor to the p-type semiconductor, building up a negative charge. At the p-n interface, electrons and holes readily recombine, creating a depletion region with filled conduction bands (no holes) and empty valence bands (no electrons). Electromagnetic radiation absorbed by the material promotes electrons from the conduction to valence bands, creating a type of polaron termed an exciton (an electron-hole pair); this regenerates the electron and hole populations in the depletion region. Due to the p-n junction's charge bias, these electrons and holes become separated in a process termed charge separation, and thus they create a current (**Figure 8**).[36]

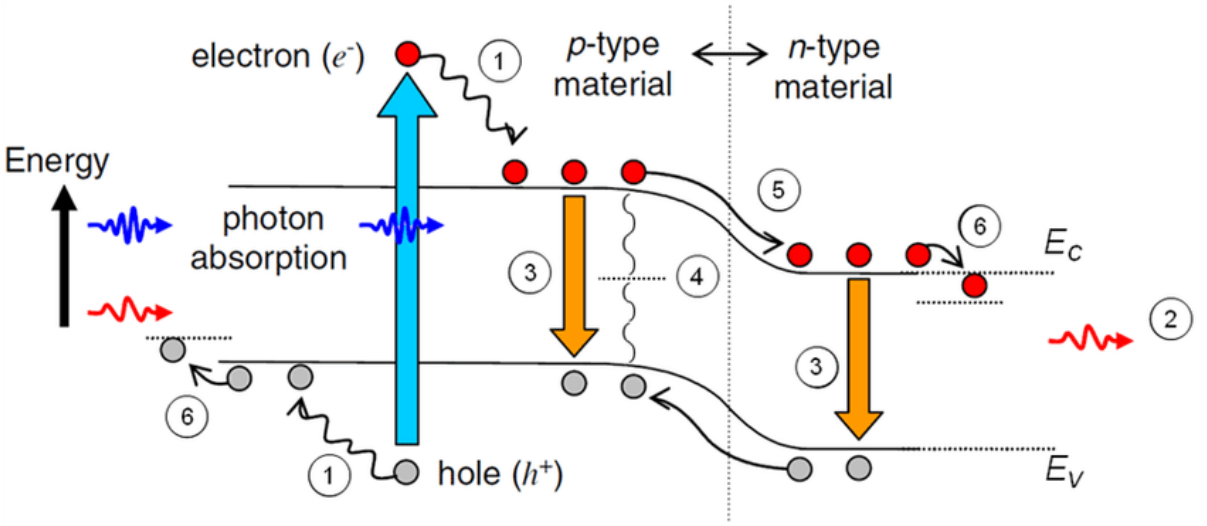

Figure 8 *The processes which occur in a p-n junction upon illumination. 1) Irradiation with light above the band-gap energy creates an exciton, which via thermalisation relaxes to the band-gap energy. 2) Irradiation with light below the band-gap energy results in transmission and no exciton formation. 3) Radiative recombination and 4) nonradiative recombination result in the quenching of excitons and lower exciton diffusion lengths. 5) Excitons diffuse across the junction - electrons migrate to the positively charged n-type terminus and holes migrate to the negatively charged p-type terminus. 6) If excitons are not quenched, they reach the termini, resulting in a potential difference and current.*[37]

A key challenge in photovoltaics is minimising the recombination of electron-hole pairs before they are separated by the p-n junction's charge bias. As such, maximising exciton diffusion length (how far electron-hole pairs migrate before they recombine) in a material is key to improving solar cell efficiency. PDIs have been reported with exciton diffusion lengths of up to 2.5 µm,[38] orders of magnitude higher than other organic semiconductors (which typically range from 5-50 nm).[39] This is aided by singlet fission, a process which occurs in PDIs whereby a singlet can split into two opposite-spin triplet states.[40] Since singlet fission is spin-allowed, the process rapidly occurs, outcompeting radiative recombination and preserving excitons. Furthermore, minimising radiative recombination allows for the preservation of high-energy excitons (e.g. those formed from blue or UV light) by minimising thermalisation, potentially allowing for PDI solar cells to be designed with efficiencies over 34% - the Shockley-Queisser limit for solar cell efficiency.[41] This minimisation, combined with the intense fluorescence of PDIs (which can be preserved in its J-aggregate – see below) and its strong absorption in the visible spectrum, makes these molecules ideal candidates for high-efficiency OPVs.

Two modes of π-stacking exist in supramolecular aggregates - H-aggregation, where interaction energy is minimised by the formation of near-parallel stacks, and J-aggregation, where the energy minima is achieved by extremely offset, 'head-to-tail' stacking. In H-aggregates, this parallel stacking results in aligned dipole moments, creating an in-phase (symmetry allowed) LUMO with a higher energy compared to the disaggregated molecule (**Figure 9**).[42] Thus, H-aggregates have a larger HOMO-LUMO gap with a hypsochromic (blue-shifted) aggregate peak. In J-aggregates, the converse is true; the head-to-tail alignment of dipole moments creates an in-phase LUMO with a lower energy, thus narrowing the HOMO-LUMO gap relative to the disaggregated molecule and leading to a bathochromic (red-shifted) aggregate peak.[42] PDI H- and J-aggregates have several differing properties: J-aggregates do not exhibit aggregation-induced fluorescence quenching[43] and can have higher exciton diffusion lengths, improving the performance of organic photovoltaics,[44] whilst H-aggregates have higher n-type carrier mobilities, advantageous in n-type semiconductors and spintronics.[45]

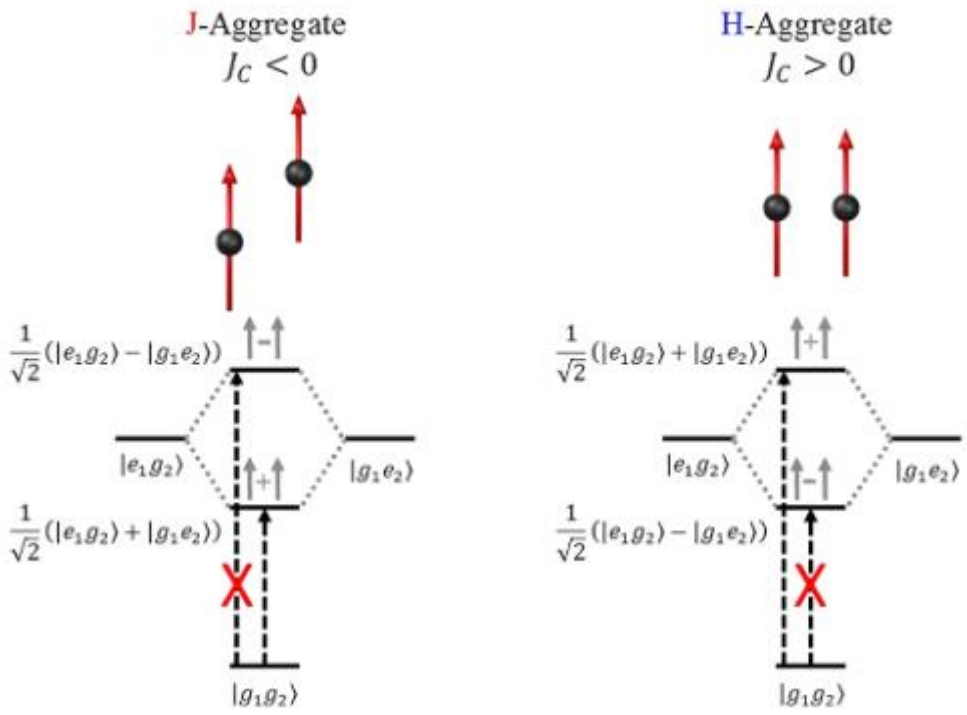

Figure 9 *Energy level diagrams for H- and J-aggregate dimers, showing the splitting of two localised excited states, $|e_1g_2\rangle$ and $|g_1e_2\rangle$, into two delocalised excited states via coulombic coupling (J_c). Transitions between the $|g_1g_2\rangle$ ground state are only symmetry-allowed to the delocalised excited state with an in-phase transition dipole moment; in J-aggregates this transition is lower-energy than in H-aggregates ($J_c<0$ and $J_c>0$ respectively).*[42]

PDIs are commonly substituted at two sites: the bay position, and the imide position (PDIs can also be substituted at the *ortho* position, but due to their limited relevancy to this project, *ortho* substitutions are not discussed here). Substitution at the bay position directly affects the energy of HOMO and LUMO orbitals within the perylene chromophore, thus affecting the redox potentials and absorption properties of PDI molecules. Electron donating groups at the bay positions lower redox potentials, whilst electron withdrawing groups raise reduction potentials and can suppress electrochemical oxidation.[46] Electron-withdrawing or electron-donating substituents at the bay position can also self-dope a PDI, imparting p- or n-type semiconductivity to the perylene core through modulation of the HOMO and LUMO which form the valence and conduction bands.[47] Sterically demanding bay substituents can lead to a twisting of the perylene core, disrupting π-stacking and preventing aggregation-induced fluorescence quenching.[48] Meanwhile, substitution at the imide position preserves the perylene core's HOMO-LUMO gap, and thus does not impact on the PDI's electronic and

optical properties in the molecular state. However, imide substitution can have a marked effect on the aggregation of PDI molecules, modulating their solvophilicity, mode of aggregation and the extent of π-orbital overlap in PDI aggregates. Thus, bay and imide substitutions can be employed orthogonally to modulate the HOMO-LUMO gap and aggregation properties of PDIs, giving these molecules an advantage over other π-conjugated chromophores for electronic and optical applications.

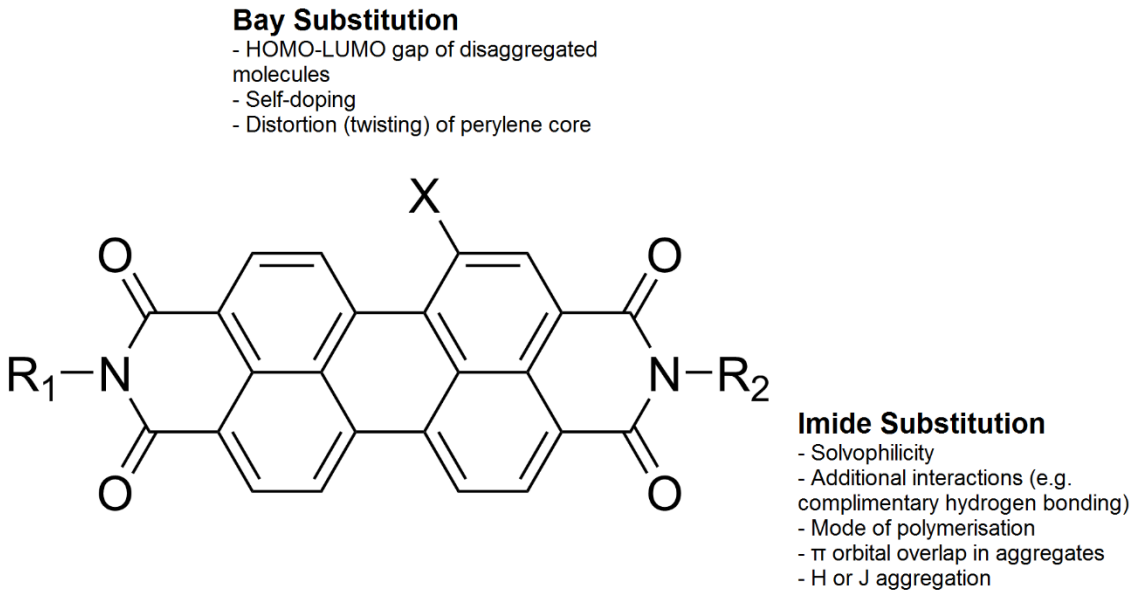

Figure 10 *The effects of bay and imide substitution on PDI properties. Note that whilst bay substitution will have effects on intermolecular interactions, solvophilicity and thus aggregate properties, these effects are commonly encoded for via imide substituents.*

1.3 Controlling Polymerisations of Perylene Diimides

As discussed in **Section 1.1**, the growth of PDIs, as with all supramolecular polymers, is mediated by the interplay of a range of kinetic processes; nucleation, elongation, off-pathway aggregation and kinetic trapping. These processes are determined by the balance of inter- and intramolecular forces between unimers, solvent and other compounds present in the growth medium, and as such can be encoded for on a molecular level. In the case of PDIs, the presence of the conjugated perylene core gives rise to strong π-stacking and supramolecular polymerisation (**Section 1.2**), but the mode of this growth can be encoded for by the PDI's bay and imide substituents. Examples of controlled isodesmic, cooperative and anticooperative growth of PDIs have been reported, and from these findings PDIs can be rationally designed to follow a specific mechanism.

Fine control over isodesmic growth is difficult to achieve - by definition, the kinetics of nucleation and elongation cannot be discriminated between for isodesmic polymerisation. Likewise, designing a PDI for isodesmic growth presents its own challenges, as PDI unimer and aggregate binding kinetics must be equally favoured. Thus, isodesmic aggregates are more commonly used as a means of control for a cooperative or anticooperative supramolecular polymerisation (e.g. by being an off-pathway aggregate) rather than being length-controlled themselves.[49,50] In nature, where the growth mechanism of protein aggregates must be finely controlled, few proven examples of isodesmic growth exist,[51–53] and these are mainly confined to amyloid growth following protein misfolding.[54] Nevertheless, examples of growth control for isodesmic PDI polymerisations exist. For example, the Faul group has utilised PDIs that were imide-substituted with a phenylalanine analogue (DMAPAA). These DMAPAA groups readily oxidised to ammonium salts (**Figure 11**), driving PDI-DMAPAA polymerisation via ionic self-assembly and π-stacking.[55] However, the steric bulkiness of DMAPAA suppressed nucleation and growth kinetics, leading to a population of unimers, dimers and trimers, whose average length could be linearly controlled via adjusting PDI-DMAPAA concentration.

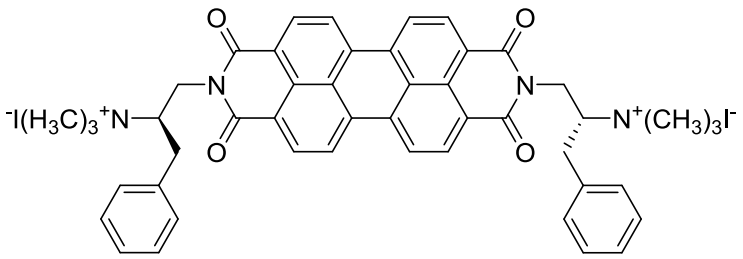

Figure 11 *The chiral DMPAA substituted PDI utilised by the Faul group, whose* N*-methylated ammonium iodide salt moieties induce ionic self-assembly, but also provide significant steric hinderance upon aggregation.*

Another method to control the isodesmic growth of supramolecular polymers is to utilise an end-cap - a molecule which inhibits further growth at a site. An example would be a monofunctional unimer (which only has one site to bind at); this unimer can bind to a growing chain end but does not have a second binding site to continue growth, thus capping the chain. Some progress towards this has been made in the field of PDIs - for example, the Nakashima group's research into PDI dimers, covalently bonded via the imide positions to a chiral binaphthalene moiety (**Figure 12**).[56] Enantiopure solutions of these chiral molecules self-assembled into nanowires via an isodesmic process, but this growth could be disrupted if the minor enantiomer was introduced to a growing polymer. After several additions of the 'capping' minor enantiomer, polymer growth halted entirely. Whilst this is not an example of true end-capping as several 'caps' were required to terminate growth; appreciable length control was achieved by varying enantiomeric excess.

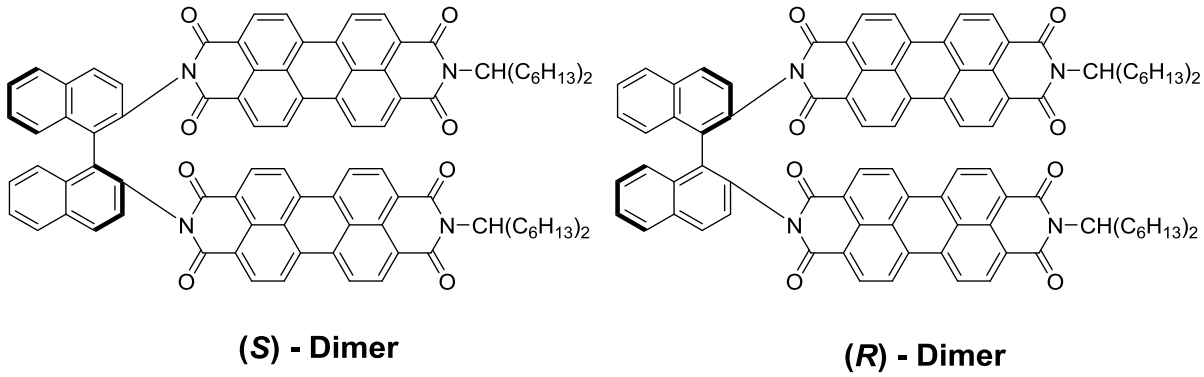

Figure 12 *The binaphthalene-linked PDI dimer utilised by the Nakashima group, in its (S) and (R) isomers.*

Unlike isodesmic growth, cooperative growth presents a viable way to finely control the length of supramolecular polymers on several length scales. As discussed in **Section 1.1**, the unfavourable nucleation kinetics of cooperative growth makes seeded growth of polymers to be viable. Under ideal 'living' conditions, a seeded-growth polymerisation contains a fixed number of seeds, and the addition of unimer does not cause further nucleation and seed formation, but instead controls the length of polymers formed from existing seeds. Living seeded growth has been used in corannulenes,[57] block copolymers[58] and platinum complexes[59] to yield polymers with low dispersities (1.1 to 1.3) and lengths that could be controlled linearly over several hundred nanometres by adjusting the seed:unimer ratio. Furthermore, seeded growth has been used to prepare block supramolecular copolymers, with the length of each block finely controlled. A striking example uses polyferrocenylsilane-based block copolymers, some of which are fluorescent. These undergo which undergo a seeded growth supramolecular polymerisation to create fluorescent 'barcodes' (**Figure 13**). The pattern of these 'barcodes' could be determined by the sequential addition of fluorescent or non-fluorescent unimers to the growing polymers.[60]

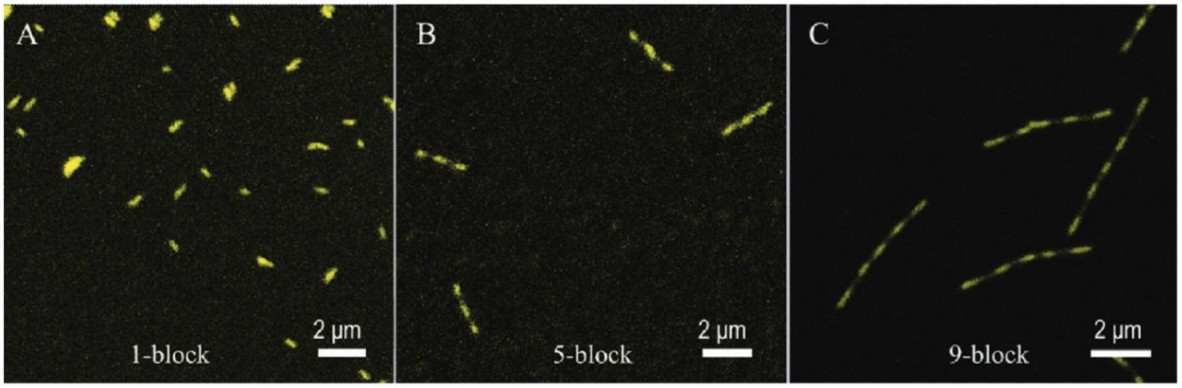

Figure 13 a) *Laser confocal microscopy images of the fluorescent one-block (A) aggregates* ***b)*** *5-block supramolecular copolymer of fluorescent (A) and nonfluorescent (B) aggregates (ABABA) and* ***c)*** *9-block supramolecular copolymers (ABABABABA).*[60]

Several examples of cooperative, seeded and living growth of PDIs exist in literature, and clear design principles have been formulated to encode PDIs for cooperative growth. For example, by incorporating dipole-bearing amide or carbamate moieties into PDIs, macrodipoles are induced in PDI supramolecular polymers (**Figure 14**). These macrodipoles strengthen as the supramolecular polymer grows, improving the binding energy of larger aggregates and thus promoting growth kinetics over nucleation kinetics.[57] This cooperativity can be further reinforced by rigidifying these dipole-bearing moieties, limiting conformational changes which could disrupt the formation of macrodipoles in aggregates. For example, PDIs substituted at the imide position with a motif which combined an ethyl spacer, a carbamate linker and a sterol group showed strong cooperative growth with the formation of a macrodipole confirmed by dielectric measurements. The ethyl spacer afforded the PDI enough flexibility for its carbamate linkers to align into macrodipoles, whilst the rigid sterol preserved the alignment of the carbamate linkers as the PDIs aggregated.[61]

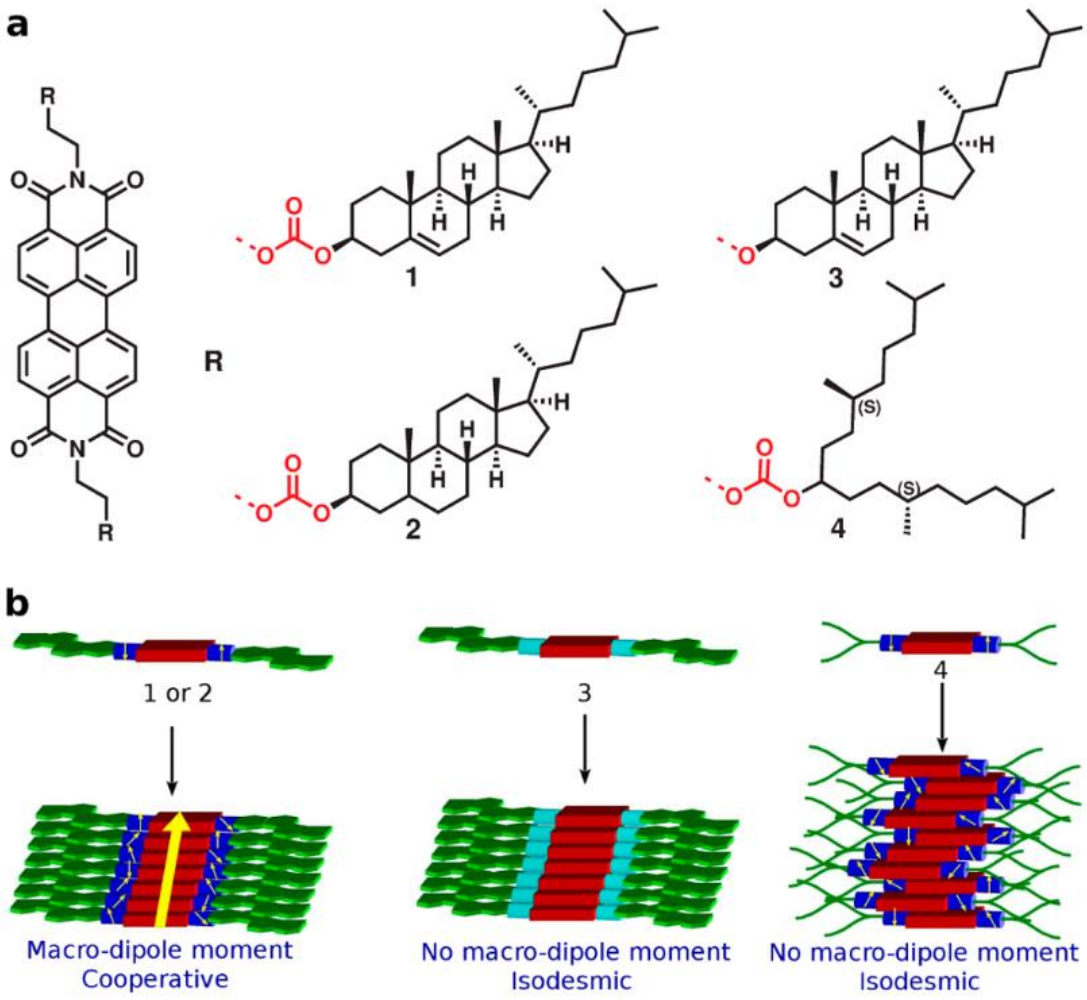

Figure 14 a) *Structures of the substituted PDIs studied by the George group - 1, 2) Carbamate-linked sterols, 3) Ether-linked sterol and 4) Carbamate-linked alkyl swallowtail.* ***b)*** *The dipole moments (arrows in dark blue boxes), macrodipole moments and growth mechanisms for 1, 2, 3 and 4.*[61]

Amongst the cooperative-growth PDI supramolecular polymers, amide-bearing PDIs are one of the most extensively studied, mostly notably by the Würthner group. The incorporation of amides within a PDI allows for intermolecular hydrogen bonding, promoting the aggregation of PDIs in aromatic solvents which would normally disrupt π-stacking of the perylene cores.[62] This also allows for the formation of strong macrodipoles to promote cooperative growth. Furthermore, these PDI-amides can be readily functionalised, for example via *N*-methylation, to create monofunctional unimers which can serve as end-caps. The use of alkyl spacer and amide motifs gives rise to intramolecular hydrogen bonding, for example between the amide moiety and the carbonyl groups of the perylene core. This

intramolecular hydrogen bonding can be encoded for through the use of an appropriate alkyl spacer, resulting in a kinetic trap which can be used to suppress self-nucleation, allowing for seeded growth of these PDIs to more closely approximate living polymerisation.[63] Amide-bearing PDIs have also been used to prepare supramolecular triblock copolymers (ABA), using a seed of vinyl-functionalised PDI as the core, which was then elongated through the addition of non-vinyl functionalised PDI unimer.[64]

Like cooperative growth, anticooperative growth in PDIs can also be encoded for on the molecular level. Since anticooperative growth favours nucleation over growth kinetics, a common means to encode for anticooperative growth in PDIs is to use sterically demanding substituents, which successively hinder aggregation as PDI supramolecular polymers grow. An extreme example of this utilises PDIs with asymmetric imide-substituted 2,5-dodecyloxyphenyl and 2,5-di-*tert*-butylphenyl groups; these sterically demanding moieties halted aggregation at the dimer stage.[65] Self-assembly of these PDIs at high concentrations resulted in a mixture of 10% unimers and 90% dimers. Thus, extremely anticooperative PDIs (which do not aggregate beyond an *n*-mer) could be used to create *n*-mer with a high degree of length control, though this method is only suitable for small aggregates.

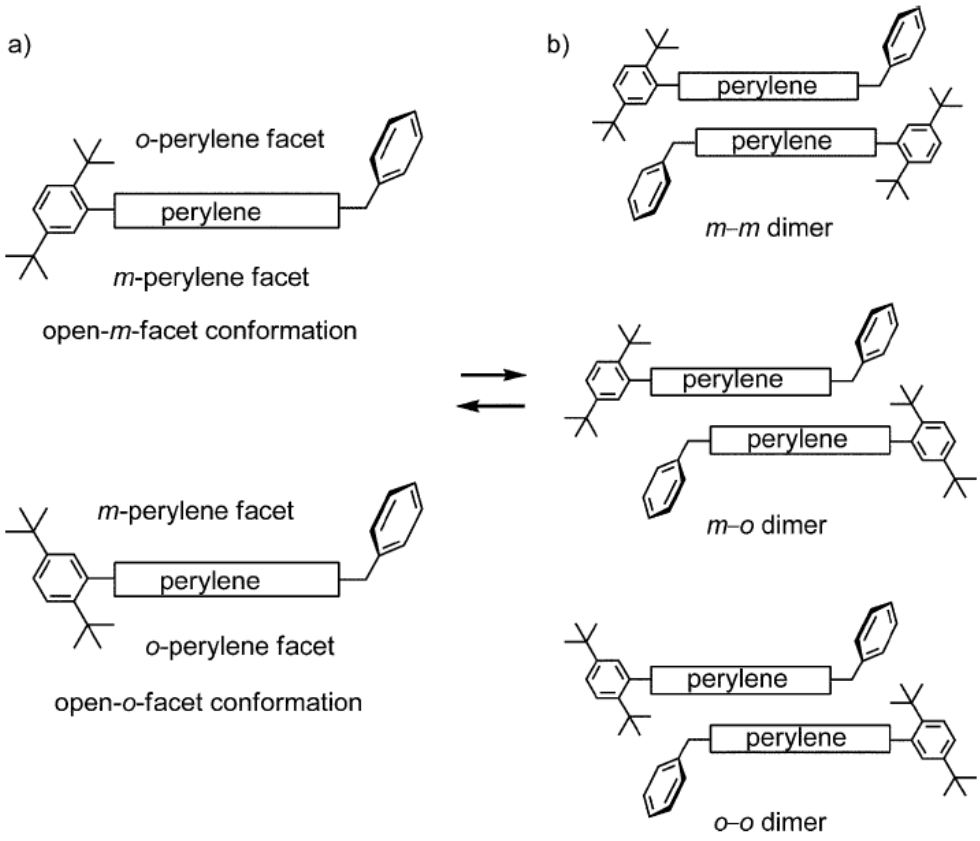

Figure 15 *An example of extreme anticooperativity -* ***a)*** *these substituted PDIs have two conformational minima (m, with an open* m-*perylene facet, and* o*, with an open* o*-perylene facet), and* ***b)*** *can dimerise in a range of conformations (*m-m, m-o, *or* o-o*), but each of these dimers does not have a sterically accessible facet to allow for further polymerisation.*[65]

This principle of extreme anticooperative self-assembly (i.e. growth halting at the dimer level) has also been employed to control larger PDI aggregates through multistage self-assembly. For example, by utilising an asymmetric PDI (imide substituted with a 2,5-dodecyloxyphenyl and a 2,5-dodecyloxyphenyl-substituted L-alanine derivative), the Würthner group created a molecule whose self-assembly is initially driven by hydrogen bonding from the L-alanine amide, complementing the perylene core's π-stacking to form hydrogen-bonded dimers.[15] Due to the steric demand of the bulky 2,5-dodecyloxyphenyl groups, these dimers cannot adopt a conformation that allows for further growth via complementary hydrogen bonding, limiting further growth. At high concentrations, these dimers then assemble via π-stacking without the aid of hydrogen bonding from the amide moieties. Thus, linear π-stacked aggregates are formed at high concentrations, with 84% of these aggregates

being even-numbered. Since this second self-assembly step is not anticooperative, extended even-numbered aggregates could be formed. Thus, anticooperative self-assembly can be used to control the length of large aggregates in multistage self-assemblies, in this case not by controlling dispersity, but by favouring even-numbered aggregates.

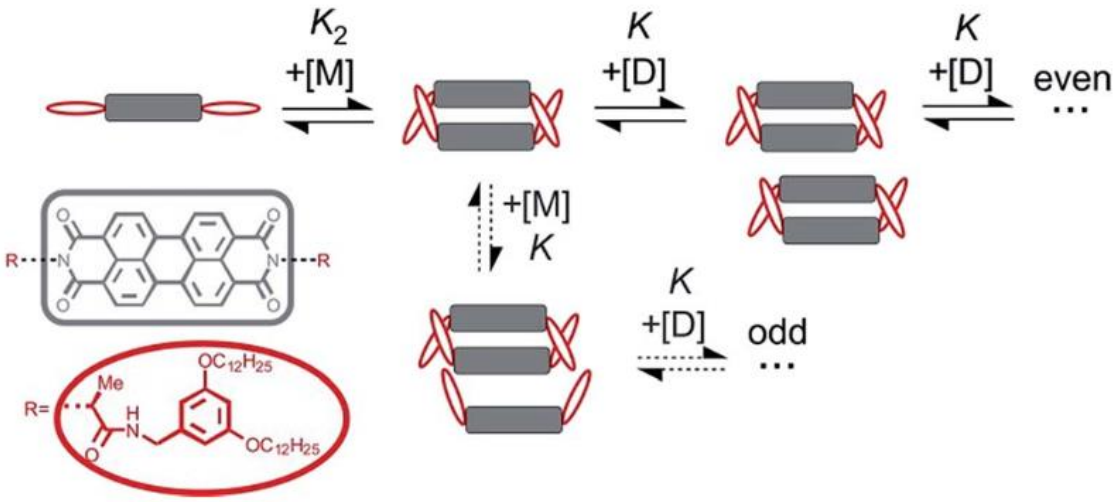

Figure 16 *A schematic illustration of the self-assembly of the asymmetric PDI investigated by the Würthner group. High values for the association constants* K_2 *and* $K_{+[D]}$ *favour the formation of even-numbered aggregates.*

1.4 Properties and Electronic Applications of Poly(aniline)s and Tetra(aniline)

One of the first conductive polymers discovered and most extensively researched, poly(aniline) (PANI) was first reported in 1834, and examined further in 1862, where its acid-base and redox-responsive optical properties were noted alongside its insolubility.[66] As with perylene, poly(aniline) was first utilised as a commercial dye (Aniline Black) before its discovery as a viable candidate for organic electronic materials due to its stability and ease of manufacture.[67] The polymer can occur in three distinct oxidation states, defined by the ratio of benzenoid to quinoid units contained within. These states are the fully benzenoid, unoxidized leucoemeraldine base (LEB), the half-oxidised emeraldine base (EB) state, and the fully quinoid, oxidised pernigraniline base (PB). Each oxidation state has its own characteristic spectroscopic signature, and UV/Vis spectroscopy can be used to readily discriminate between oxidation states. In fact, redox-dependent UV/Vis spectroscopy was used to confirm the presence of only three oxidation states of PANI: the spectroscopic signatures obtained from partially oxidised PANI contained three isosbestic points (nonvariable with respect to oxidant concentration), showing that only three oxidation states existed.[68]

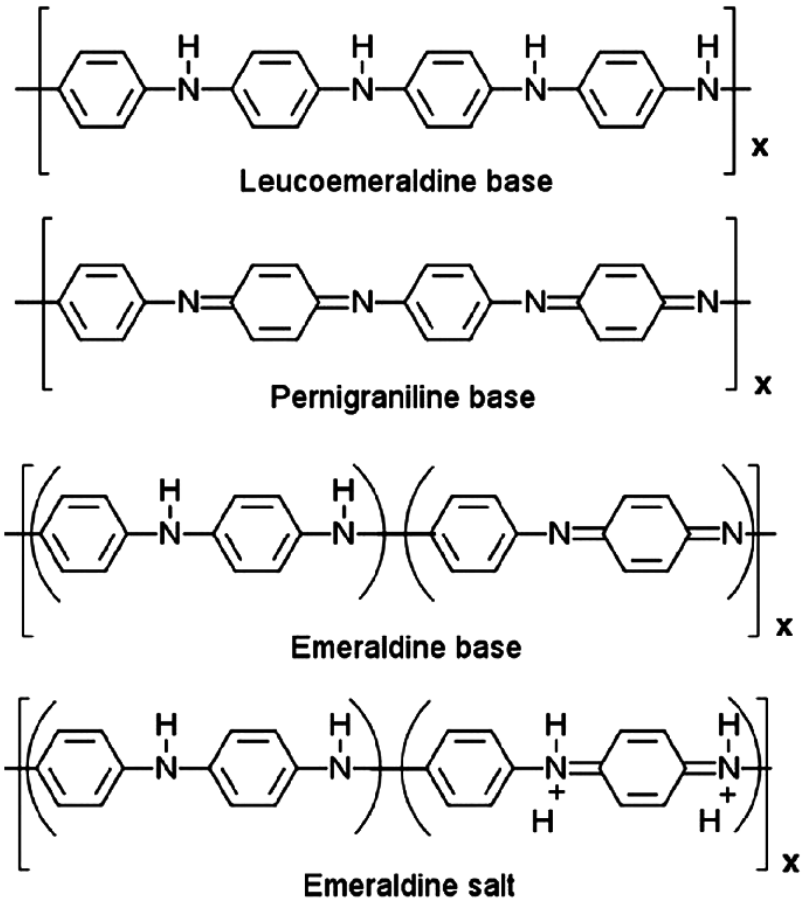

Figure 17 *The three different oxidation states of poly(aniline), and its fourth, acid-doped emeraldine salt state.*[69]

Of particular interest is the half-oxidised emeraldine base (EB) oxidation state, which can be reversibly acid-doped to the conductive emeraldine salt (ES) state.[70] The ES state, the only conductive state of PANI, can be tuned via doping and dedoping to create high-performance organic conductors (up to 10^2 S cm^{-1}) and semiconductors.[71] This conductivity, discovered by Nobel Laureate Alan MacDiarmid, sparked renewed interest in the polymer, and during the 1980s PANI chemistry became a key area of research in the growing field of conductive polymers.[72] Since then, PANI has been used in a range of electronic applications - bulk supercapacitors,[73] organic field effect transistors (OFETs)[74] and organic light emitting diodes (OLEDs).[75] However, the electronic performance of these devices has often been hampered by defects and polymer coiling, disrupting the π-conjugation intrinsic to the electronic properties of ES state PANI and giving rise to poorly ordered, noncrystalline domains which hamper intermolecular charge transfer.[76] With some predictions placing the potential conductivity of PANI at

10^5 S, comparable to that of copper, optimisation of PANI conductivity has received a great deal of attention to attempt to reach such levels.[77]

To investigate and tune the electronic performance of PANI, reproducible and pure samples need to be synthesised; this is a challenging feat for extended polymers. However, the structure of aniline oligomers (commonly n=4, 8, 16, 32) can be precisely synthesised, allowing monodisperse oligomers to be synthesised, their conformations and coiling to be studied, and number of defects reduced in comparison to PANI.[78] Studies of ES state octo(aniline) reveal that short-chain oligo(aniline)s have comparable conductivity to PANI; this suggests that charge transport within aniline polymers occurs via an inter-chain process.[79] Thus, understanding and controlling the packing of aniline polymers and improving their crystallinity may be the key to realising the electronic potential of this class of molecules. Controlled packing is a difficult feat to achieve with polydisperse PANI, but oligo(aniline)s provide a means to create finely controlled nanostructures to optimise charge transport.

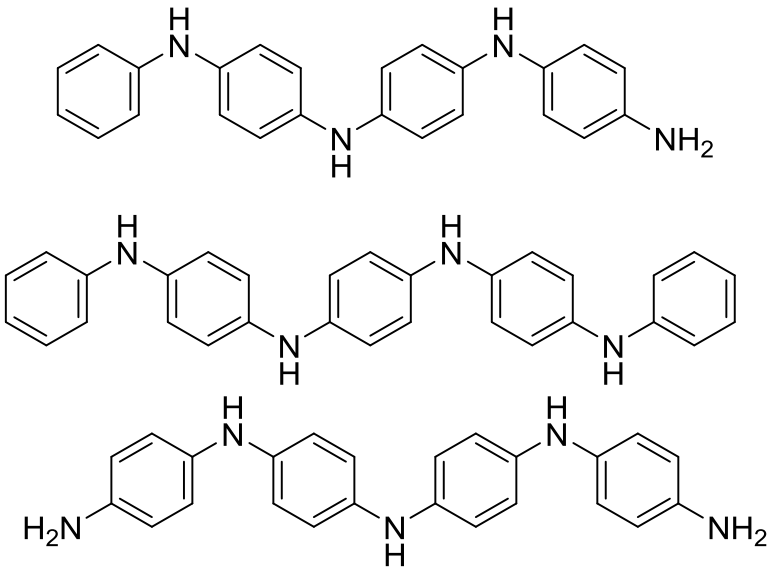

Figure 18 *Three forms of the oligo(aniline) TANI; Ph/NH_2 end-capped, Ph/Ph end-capped, and NH_2/NH_2 end-capped.*

The shortest oligomer of PANI which exhibits LEB, EB and PB oxidation states is tetra(aniline) (TANI), shown in **Figure 18.** As such, it is the most facile oligo(aniline) to prepare via a series of coupling reactions (a common method to create monodisperse heteroatomic oligomers)[80] and process (due to its high solubility). This combination of factors makes TANI easy to prepare, derivatise and graft, either to other molecules, polymers or material surfaces, making this oligomer an ideal candidate to create highly ordered nanostructures. Through investigating how the electronic properties of TANI are affected by tuning its nanostructure, a clear understanding of its emergent conductive behaviour can be garnered. Grasping how inter-chain, inter-domain and bulk conductivities vary in controlled TANI assemblies could lead to design principles to optimise oligo(aniline) and PANI conductivity in both nanoscale and bulk materials.[81]

1.5 Sensing Applications of Poly(aniline)s

Facile, reversible access to the conductive ES state via protonation/deprotonation reactions allows for chemically switchable conductivity of poly(anilines) and oligo(anilines), and as such this class of molecules is an excellent candidate for bulk or nanoscale chemiresistors (electroactive chemical sensors). PANI has been investigated for use in sensing of gas-phase ammonia,[82] hydrogen sulphide[83] and hydrogen chloride.[84] Furthermore, the unique optical properties of the LEB, EB and ES states allow for colorimetric detection of chemical changes, for example the doping–dedoping of hydrogen chloride.[85]

PANI chemiresistors and colorimetric sensors are not limited to acid-base reactions, however. The switchable redox chemistry from the LEB to EB (or ES) state has led to the development of PANI-based sensors for the detection of gas-phase and solution-phase redox reagents, such as hydrazine,[84] ammonium chloroimidate, Trolox (a derivative of Vitamin E)[86] and ascorbic acid (Vitamin C).[87] This redox chemistry has also been exploited in biological settings, for example, PANI intercalated graphite oxide electrodes have been used to monitor DNA hybridisation and distinguish between single and double-stranded DNA.[88]

Early sensors, created from bulk (poly)aniline, suffered from the challenge of limited processability (particularly in deposition and templating), and as such nanoscale alternatives, such as colloidal suspensions and nanofibers were developed to enable straightforward deposition and templating of PANI.[89] These approaches to PANI-based sensors also led to a marked improvement in sensitivity and performance by enhancing surface area. For example, PANI nanowires created by the Kaner group had a 19-fold improved response for ammonia sensing compared to bulk PANI sensors.[90] Thus, controlling the nanostructure of PANI is key to improving its performance in sensing applications.

1.6 PDI-TANI - Enhanced Functionality and New Opportunities?

Two major challenges exist within poly(aniline) chemistry: highly ordered crystalline domains are required to improve the conductivity of PANI, and the fabrication of nanostructured PANI-based is required to improve the molecule's surface area and thus its sensing capabilities. Meanwhile, PDIs are prized for their strong, highly ordered, readily controlled π-stacking and their ability to form 1D supramolecular polymers or structured porous 2D and 3D materials. Thus, a unimer consisting of a PDI scaffold decorated with TANI moieties is an attractive choice to create multifunctional supramolecular polymers, improving the performance of ES-state TANI as a conductor and sensor, and bestowing new functionality from the π-stacked perylene core. Furthermore, the same methods used to control the growth of PDI supramolecular polymers can be translated to controlling the dimensions of a PDI-TANI supramolecular polymer; for example, the incorporation of amide moieties into this PDI-TANI molecule could encode for cooperative growth by enabling macrodipole formation. To date, no literature exists where PDI imide substituents control growth and bestow additional functionality. Thus, the creation and controlled polymerisation of a PDI-TANI unimer would be an important proof of concept, probing the limits of perylene supramolecular chemistry and opening new horizons to design multifunctional supramolecular polymers for optical, sensing and electronic applications.

The dual functionality of a PDI-TANI unimer also opens up new applications that extend beyond those of individual PDI and TANI aggregates. As discussed in **Section 1.2**, PDIs can be either p- or n- doped, and as such, a PDI-TANI molecule could be doped to create molecular p-n heterojunctions for use in molecular photovoltaics.[91] The symmetric imide substitution of two TANI moieties, followed by the appropriate doping, could also be used to create p-n-p heterojunctions, the key component in bipolar junction transistors, which are used for logic gates and signal processing in analogue circuits.[92] The commercial impact of a functioning PDI-TANI p-n-p heterojunction is immediately apparent; organic p-n-p heterojunctions have already been commercially employed in analogue audio processing units

where they are prized for their versatility, able to emulate the tonality of classic tube-amplifiers or create new nonlinear signal distortions.[93]

Of the range of PDIs discussed in **Section 1.3**, the amide-substituted derivative explored by the Würthner group shows most promise for a PDI-TANI unimer. This molecule is already encoded for cooperative growth with its amide substituents, and for living polymerisation through the use of an ethyl spacer which allows for an intramolecularly hydrogen-bonded, kinetically trapped conformation. This design has been used to create low-dispersity, one-dimensional supramolecular polymers, control their growth via living polymerisation (i.e. by modulating seed and unimer ratios), and in creating supramolecular block copolymers. As such, using this design as a basis for a PDI-TANI unimer could allow for fine length control, and thus careful tuning of electronic, optical and sensing properties, as well as provide means to incorporate PDI-TANI into larger polymeric architectures (such as supramolecular block copolymers) and fabricate nanoscale-ordered devices. Another advantage of the Würthner group's design is that it relies on the presence of substituted aryl groups to impart solvophilicity to the PDI - these aryl groups can be replaced with TANI moieties, which, in the ES state, can be doped with appropriate acids to achieve a similar effect.

2. Aim and Objectives

The aim of this project is to create a length-controlled, novel supramolecular polymer consisting of PDI-TANI unimers, whereby aggregation behaviour and the optoelectronic properties could be encoded for at the molecular level.

This aim would be achieved through the following objectives:

1) The synthesis of a novel unimer bearing both PDI and TANI moieties, termed **PDI-2-TANI** (see **Figure 19**). This design was chosen due the promising seeded growth behaviour of its non-TANI analogue, investigated by the Würthner and Faul groups (see **Section 1.6**).

2) Investigation of the aggregation behaviour of **PDI-2-TANI**, with the aim of creating one-dimensional supramolecular polymers via a cooperative growth mechanism.

3) Trials of seeded growth to achieve length control over **PDI-2-TANI** supramolecular polymers by altering seed:unimer ratios.

4) Doping of **PDI-2-TANI** to create **PDI-2-TANI-ES**, an electroactive derivative whose aggregation behaviour, optical and electronic properties could be studied and compared to literature results for other self-assembled TANI-based materials.

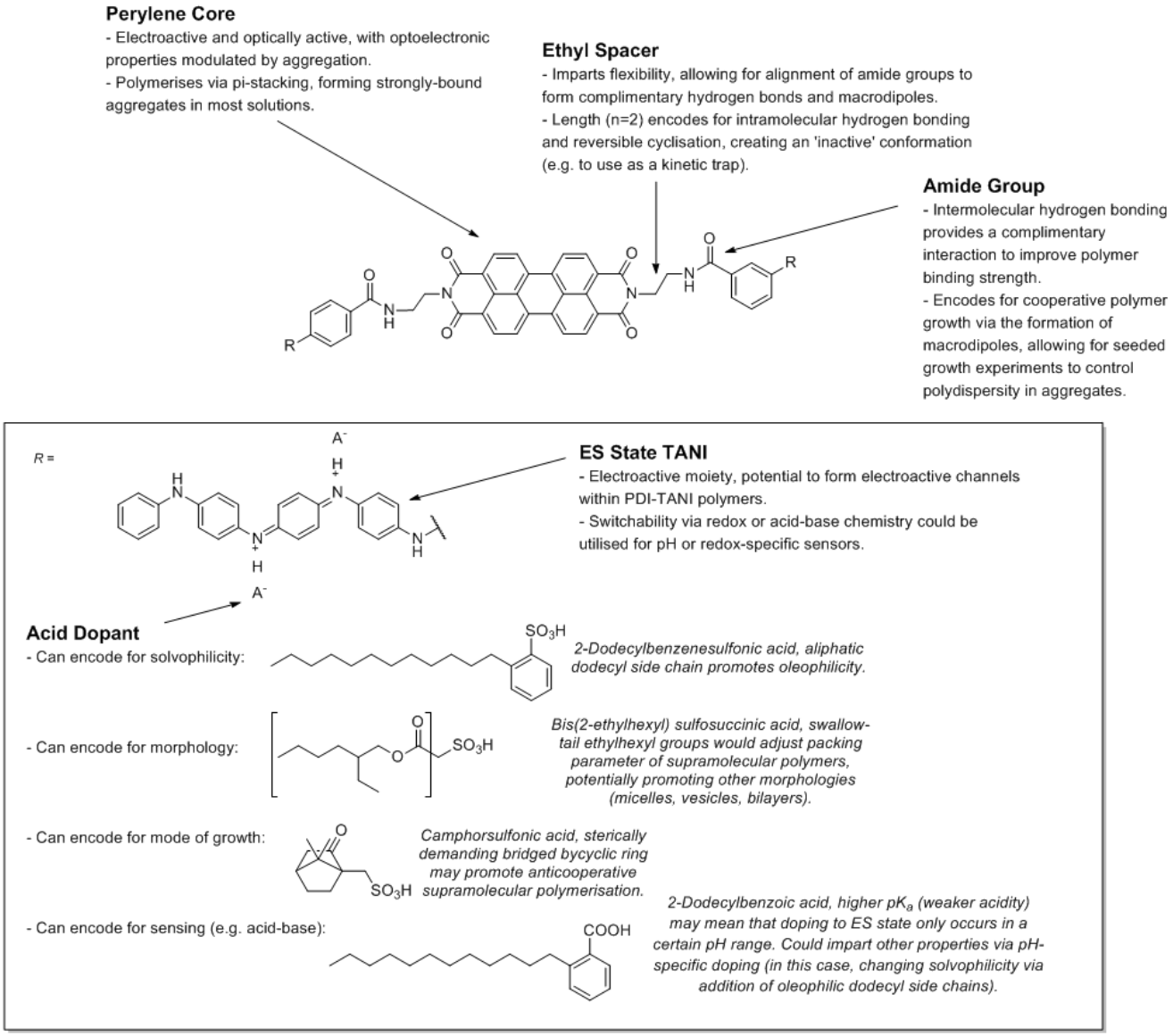

Figure 19 *The design of* ***PDI-2-TANI*** *in its ES-State form, showing the design principles employed (see* ***Section 1.3****,* ***Section 1.6****) and potential acid dopants to modulate self-assembly properties.*

3. Synthesis and Discussion

3.1 TANI - Synthetic Pathway

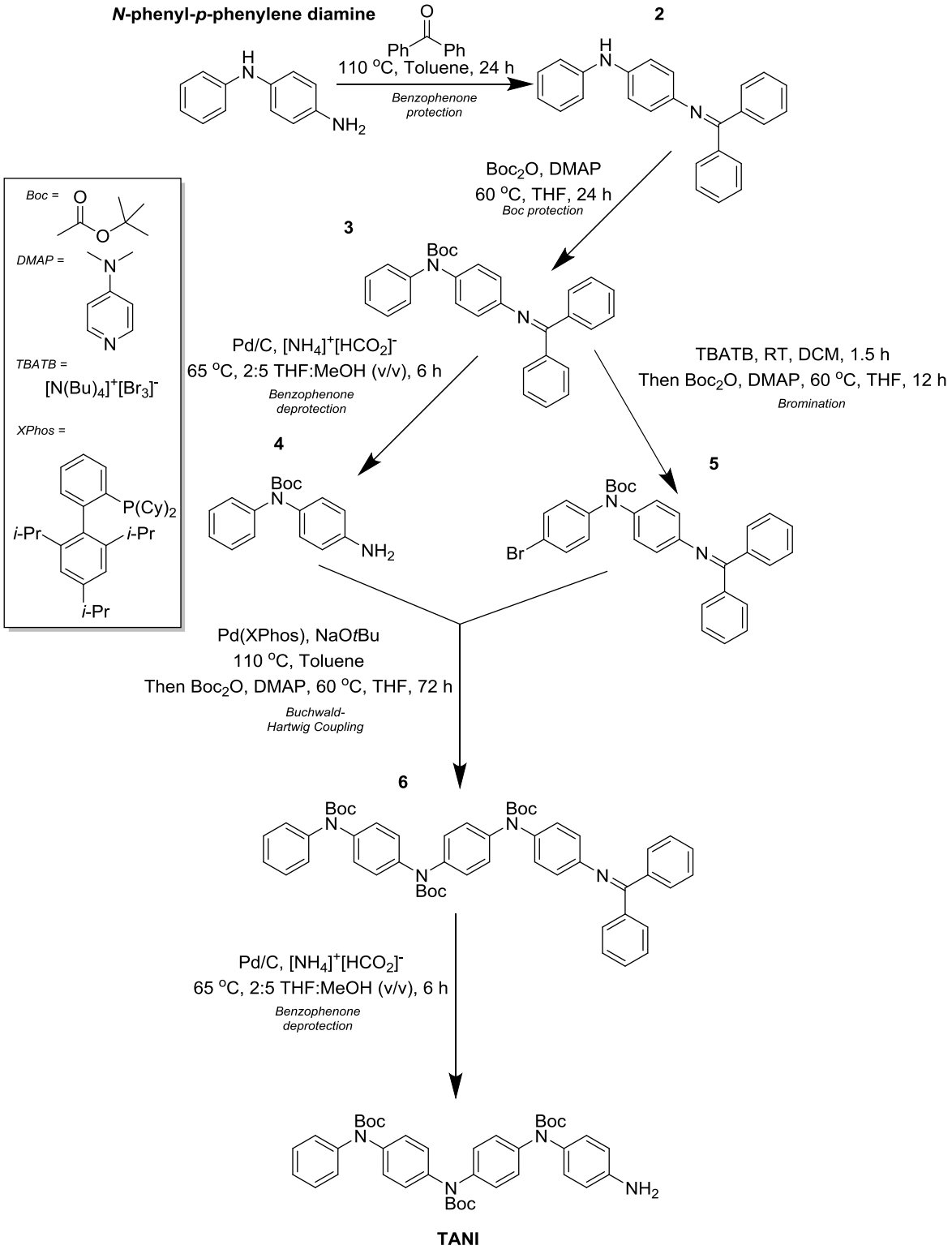

Scheme 1 *The synthesis of* ***TANI****, adapted from Chen and Benicewitz' procedure by the Faul group.*[94]

Coupling reactions are a common method for preparing monodisperse heterochain oligomers, allowing these oligomers to be constructed monomer-by-monomer. For example, oligo(thiophene)s are prepared via Stille or Kumada coupling,[95,96] and Suzuki coupling has been used to produce phenylene, pyrimidine and thiophene oligomers, as well as alternating and block co-oligomers.[97,98] Buchwald-Hartwig cross-coupling was chosen to prepare phenyl-amine capped tetra(aniline) (**TANI**) - a well-established method for synthesising monodisperse oligo(anilines) pioneered by the Buchwald group themselves to synthesise both symmetric and asymmetric oligo(anilines) up to *n*=16.[80]

The Buchwald group's synthesis proceeds via the coupling of an aniline derivative with a *p*-brominated, amine-protected aniline, the former acting as the capped terminus and the latter acting as a monomer for monodirectional chain growth. Buchwald-Hartwig cross-coupling (discussed in depth in **Section 3.1.5**) then selectively couples the unprotected aniline NH_2 with the *p*-bromine of the protected aniline, creating a di(aniline) with a protected NH_2 terminus. Before this terminus can be deprotected and coupled with further *p* brominated NH_2 protected aniline, *tert*-butyl carbamate (Boc) protection is required for the secondary amine formed during the initial coupling. Boc protection serves several major purposes. Firstly, it prevents any unwanted coupling between the secondary amine and future brominated substituents, which would result in chain branching. Secondly, it protects the aniline oligomer from oxidation, a process which even at room temperature, readily converts oligo(anilines) to quinolene and imine-containing pernigraniline (which occurs at the dimer scale) or emeraldine (at the tetramer scale) bases (see **Section 1.4** for more details). Finally, it greatly improves the solubility of aniline oligomers in both polar and nonpolar organic solvents, allowing oligo(anilines) to be easily purified, processed, and used in further syntheses. The two protecting groups, Boc and the group used to protect the NH_2 terminus, must be orthogonal, allowing for

deprotection of the primary amine to add further monomer units without risking Boc deprotection and oxidation of the oligo(aniline).

The synthesis used in this project revolves around the same principles, though it has been adapted to produce **TANI** in a single Buchwald-Hartwig cross-coupling, using the commercially available dianiline *N*-phenyl-*p*-phenylene diamine. This procedure was initially utilised by Chen and Benicewicz[94] to produce **TANI** to graft to poly(methacrylamide) and has been optimised and refined by the Faul group. Shown in **Scheme 1**, the route involves the synthesis of two dianilines, one bearing a benzophenone-protected NH_2 terminus and *p*-bromine, and the other bearing an unprotected primary amine. Both dianilines have Boc-protected secondary amines, ensuring selective Buchwald-Hartwig coupling with only the primary amine, facile processing and preventing oxidation of the **TANI** formed. Whilst benzophenone groups are selective for primary amines,[99] Boc groups readily protect both primary and secondary amines.[100] Thus, to produce a Boc-protected dianiline with a free NH_2 terminus, benzophenone protection must be carried out first, followed by Boc protection and then a benzophenone deprotection.

Since the synthesis of **TANI** is established (i.e. no new novel reactions are employed), and the NMRs obtained for this section correspond closely to literature results, detailed NMR assignments and elucidation are not discussed in these sections. Please see the relevant experimental sections (**Section 7.1.1** to **7.1.6**) for full NMR assignments and comparison to literature results.

3.1.1 Synthesis of 2

As mentioned in **Section 3.1**, benzophenone protection is ideal for the synthesis of **TANI** owing to its selectivity for primary amines and its orthogonality with Boc protecting groups. The benzophenone imine protecting group is formed via nucleophilic attack of a primary amine, and subsequent proton transfer and elimination of water yields the protected amine (**Scheme 2**). This reaction can be promoted through acid catalysis or through performing the reaction at high temperatures. However, since the reaction is reversible, utilising an aqueous acidic solution would result in lower yields, and as such dry toluene was chosen as a solvent. The anhydrous conditions improve the yield of **2**, and the high boiling point of toluene (110 ^{o}C) allows the reaction to be carried out under reflux at high temperatures. Filtration with THF to remove unreacted *N*-phenyl-*p*-phenylene diamine and traces of water, and subsequent recrystallisation from methanol yields **2** in excellent yield (88%).[94] The efficacy of this reaction was confirmed in this project, with **2** synthesised by this procedure and obtained in yields of 79%. The purity of **2** was confirmed by ^{1}H NMR (**Appendix A1**).

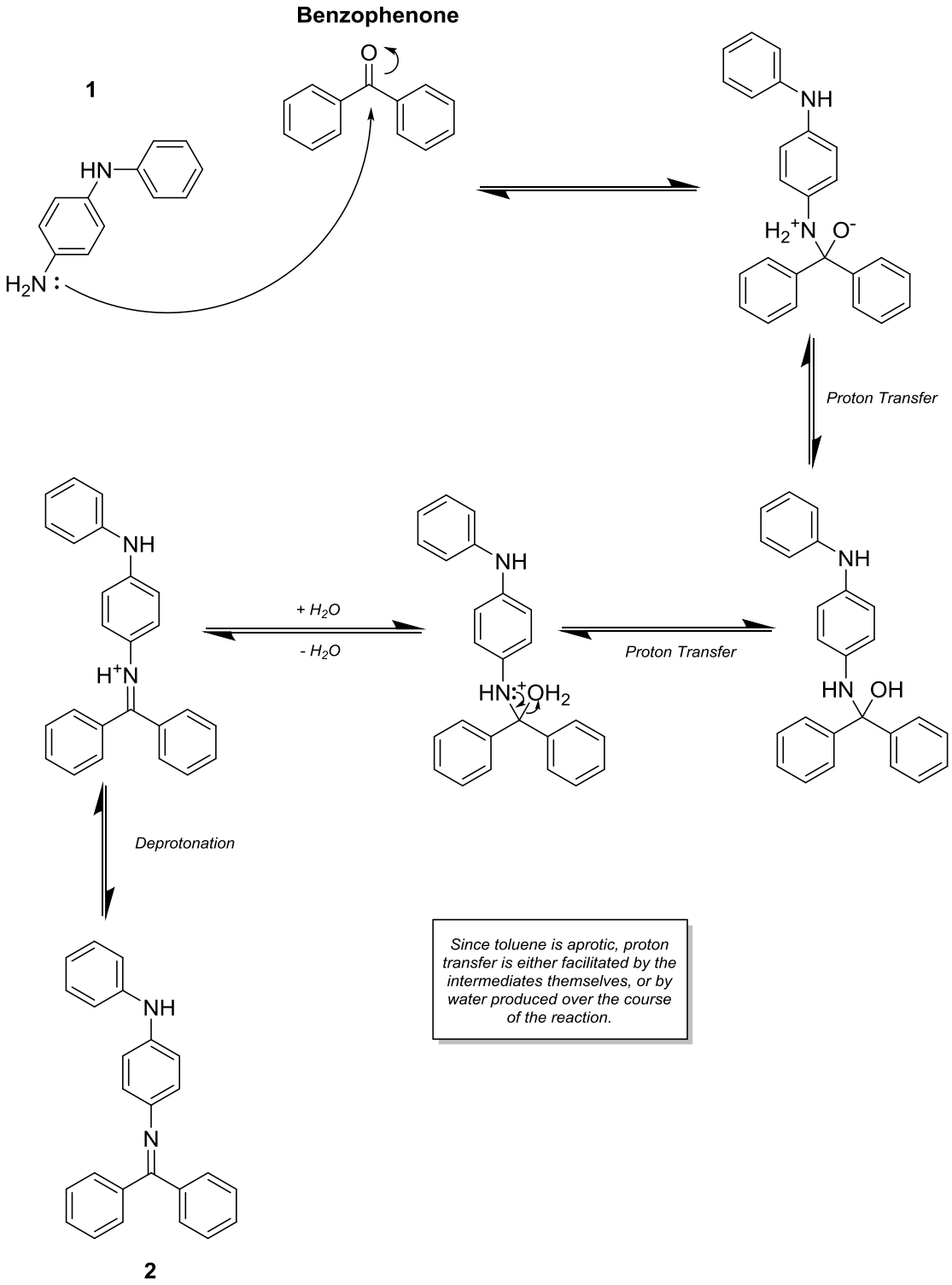

Scheme 2 *Mechanism of benzophenone protection of* N*-phenyl-*p*-phenylene diamine, yielding* ***2****.*

3.1.2 Synthesis of 3

The orthogonal protecting group to the benzophenone, *tert*-butyl carbamate (Boc) was utilised to protect the secondary amines present in **2**. Boc groups have several advantages over other amine protecting groups - they readily protect secondary amines, provide *tert*-butyls and carbamate groups which are highly solvophilic for nonpolar and polar organic solvents respectively, and are stable to nucleophiles and bases but are easily cleaved by strong acids or heat.[100] They are typically prepared using di-*tert*-butyl dicarbonate (Boc anhydride) and a base, and proceed via nucleophilic attack of one of the Boc anhydride's carbonyl moieties, yielding a protonated carbamate and *tert*-butyl carbonate (**Scheme 3**).[101] The base serves as a proton scavenger, deprotonating the carbamate to yield the Boc protecting group and facilitating proton transfer in *tert*-butyl carbonate, forming the deprotonated CO_2^- leaving group and yielding *tert*-butanol and carbon dioxide.

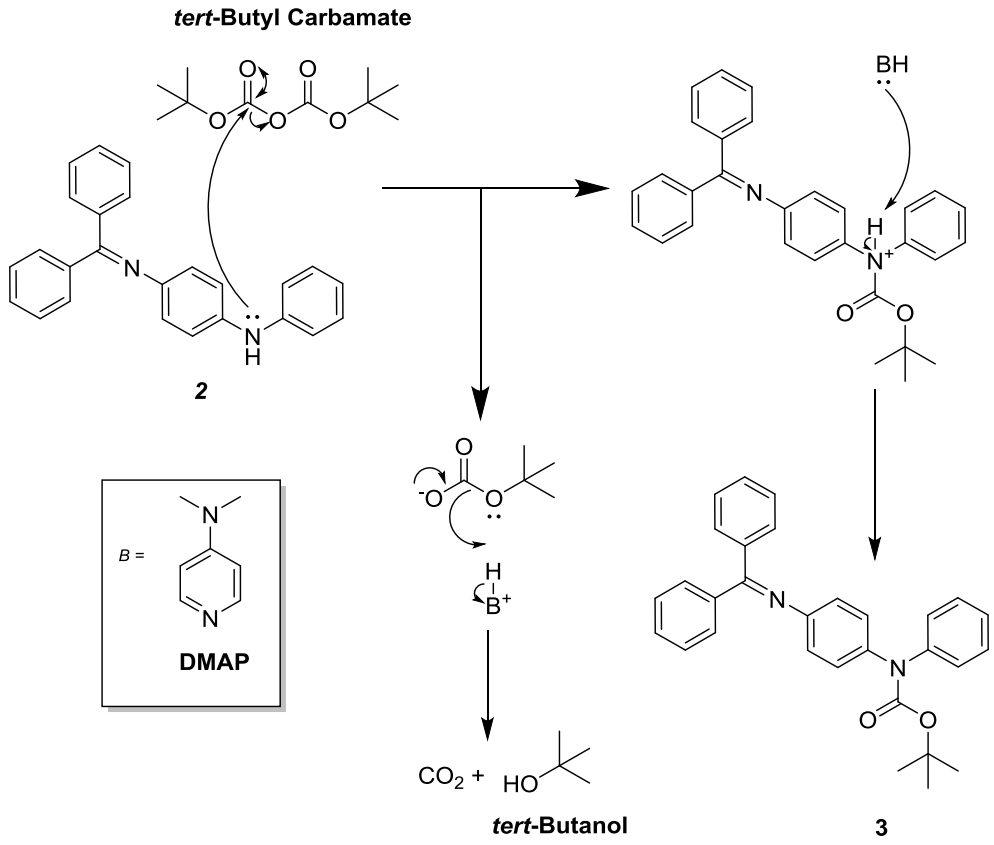

Scheme 3 *Mechanism of Boc protection of* ***2****, yielding* ***3****.*

For this reaction, mild conditions were employed - refluxed tetrahydrofuran (THF) was utilised as the solvent, and dimethylaminopyridine (DMAP) was used a suitable base. The THF also served as the crystallisation solvent, being mixed with ethanol to create a 1:2 (v/v) THF:ethanol solution. Since Boc protection only yields ethanol-soluble *tert*-butanol as a side product (*tert*-butyl carbonate readily decomposes), this ethanol recrystallisation was sufficient to isolate **3** in good yields (75%), with its purity confirmed by ^{1}H NMR (**Appendix A2**). These yields are lower than the 95% obtained Chen and Benicewicz' procedure,[94] which utilised a recrystallisation solvent of ethyl acetate and hexane, but given the large quantities of **2** obtained earlier in the project, this slight depression of yield was acceptable.

3.1.3 Synthesis of 4

To achieve selective protection of the secondary amine of *N*-phenyl-*p*-phenylene diamine, deprotection of the benzophenone imine of **3** was required. Whilst deprotection can be achieved by using strong acids such as hydrochloric acid,[102] this method does not preserve the orthogonality of the benzophenone and Boc protecting groups, since Boc groups are also readily cleaved by this route. However, reduction of the benzophenone imine to the primary amine, via transfer hydrogenation, using ammonium formate as a source of hydrogen and a palladium catalyst (palladium on carbon), selectively deprotects the benzophenone imine. Since the H_2/Pd system acts as a strong reducing agent, it allows for full reduction of the benzophenone imine - full reduction would not be achieved with milder agents such as sodium borohydride which yield secondary amines from benzophenone imine.[103] An advantage of using ammonium formate as a source of hydrogen is that it readily decomposes in the presence of a palladium catalyst, and its decomposition byproducts are carbon monoxide and ammonia (**Scheme 4**).[104] Thus, hydrogen from the decomposition will be readily absorbed onto the palladium surface, whilst carbon monoxide and ammonia will escape the reaction system as gases and will not be present in the final mixture.

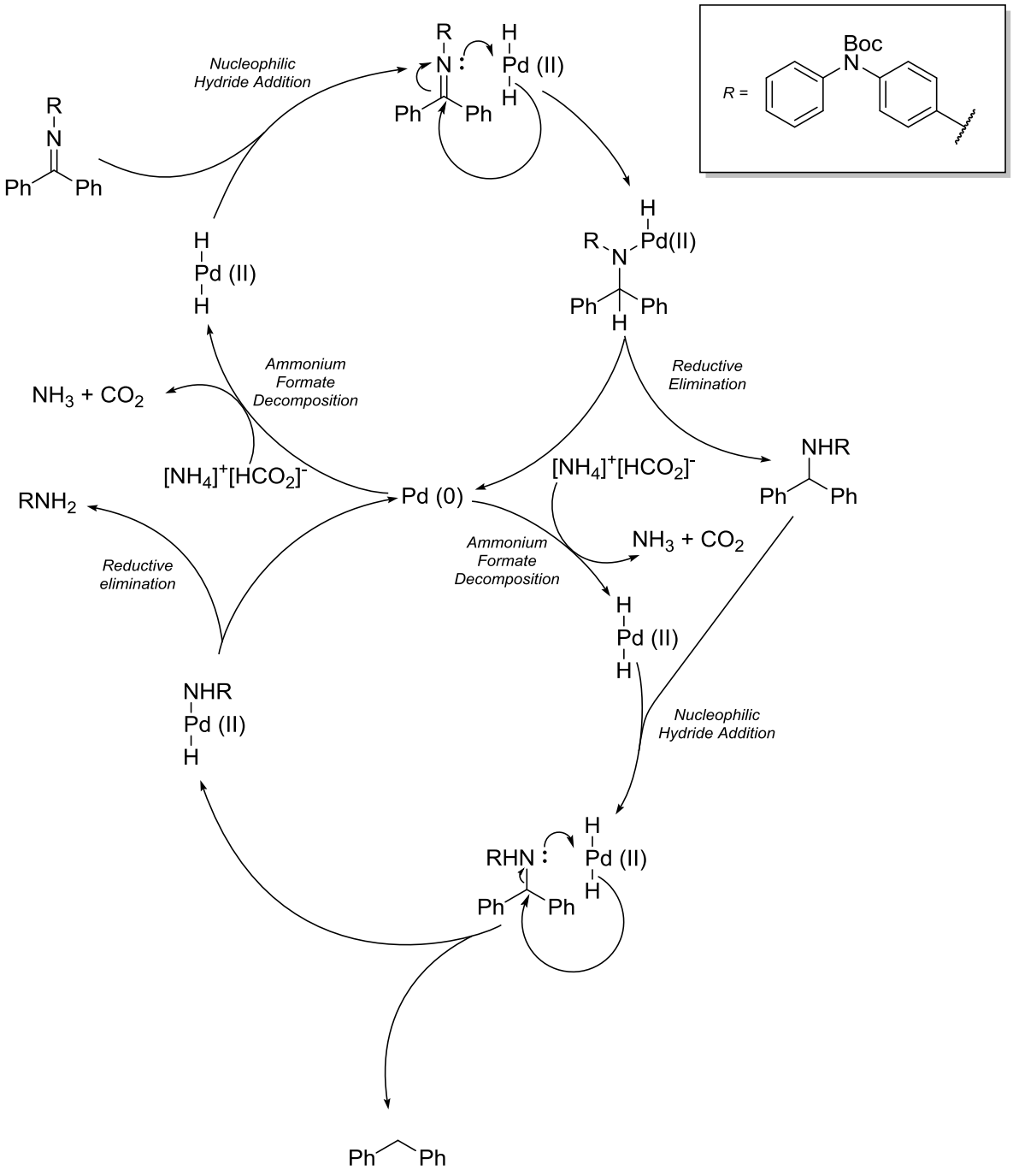

Scheme 4 *A proposed mechanism for the hydrogenation of* ***3*** *on a palladium catalyst to yield* ***4****. To explicitly clarify the steps in this mechanism and redox changes of the Pd centre, it is portrayed in the same format as solution-phase mechanisms - in reality, these reactions would occur via adsorption to sites on the surface of the heterogeneous Pd/C catalyst.*

Whilst the full mechanism for benzophenone deprotection via reduction was not found in literature, a mechanism can be postulated from the well-studied reduction of imines to secondary amines.[105] Transfer hydrogenation facilitates the formation of the oxidised [H_2Pd(II)] species from the Pd(0)

catalyst, enabling a nucleophilic hydride attack at the imine of **3**. Subsequent reductive elimination yields a tertiary amine (**Scheme 4**), which can then undergo a second hydrogenation due to the low electron density of the $NCPh_2$ carbon. Purification of **4** with dichloromethane and hexane washes to remove any diphenylmethane biproduct yielded **4** in quantitative yields (98%, compared to Chen and Benicewicz' 96%)[94], with its purity confirmed by ^1H NMR (**Appendix A3**).

3.1.4 Synthesis of 5

Tetra-*n*-butylammonium tribromide (TBATB) was used to achieve selective *p*-bromination of doubly protected *N*-phenyl-*p*-phenylene diamine **3** (**Scheme 5**). TBATB is a commonly used brominating agent for alkenes, alkynes and aromatics, prized for its excellent (>90%) yields under mild conditions.[106] In the context of aromatic systems, it selectively brominates the *para* position to an electron donating group, such as an aromatic amine.[107] As such, it is an excellent reagent for the synthesis of **5** due to its high yield, regioselectivity and its non-interference with the benzophenone and Boc protecting groups.

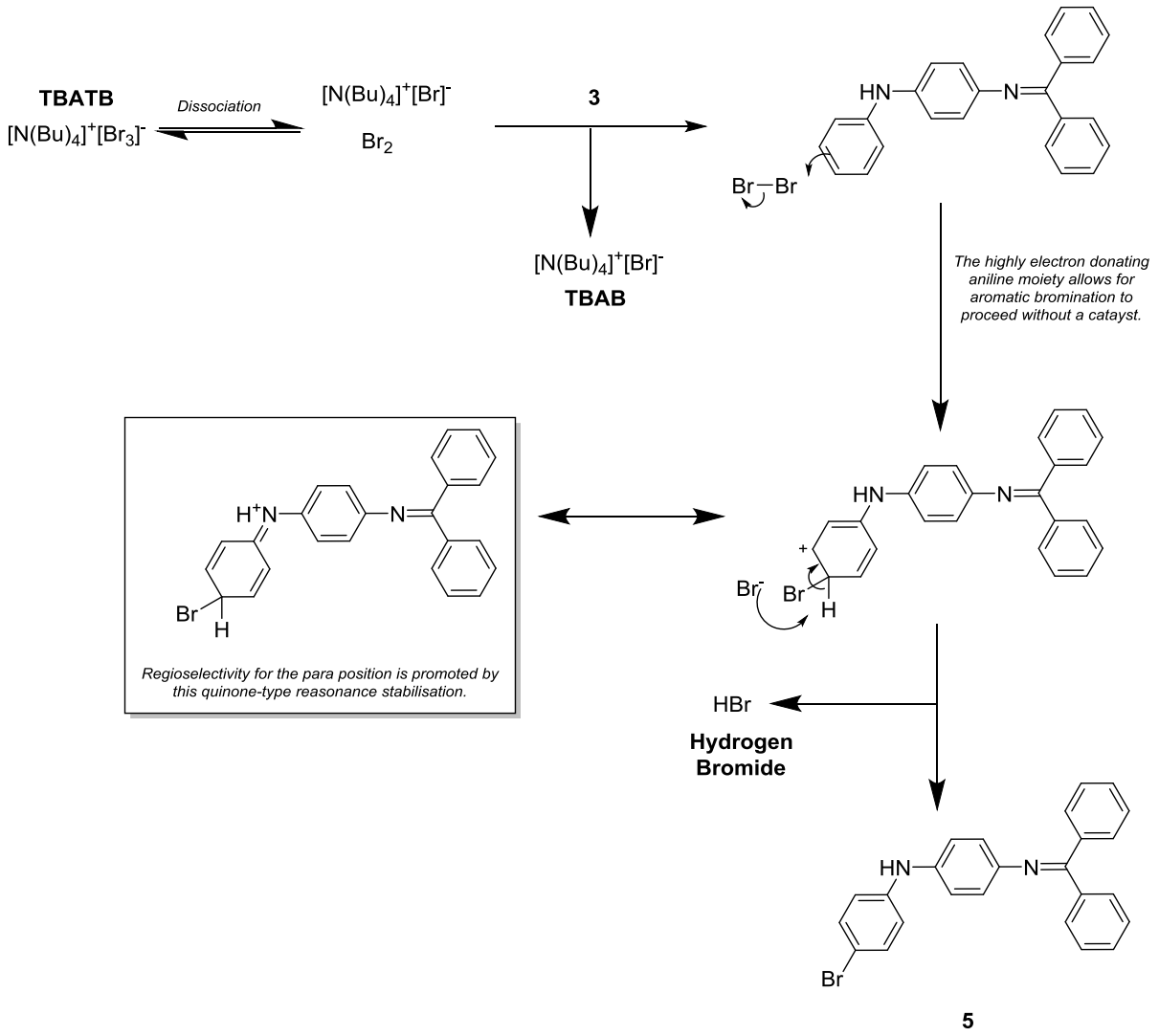

Scheme 5 *Mechanism of* p*-bromination of* ***3*** *by TBAB, yielding* ***5***.[108]

TBATB functions as source of bromine[108], which, via electrophilic aromatic substitution, yields **5**, TBAB and hydrogen bromide (see **Scheme 5**).[109] Regioselectivity for the *para* position is provided by the presence of the secondary amine, a strong electron donating group. Sodium sulphite is used for the purification procedure to remove any traces of molecular bromine, and hydrogen bromide is removed via water washes. The product was then reacted with di-*tert*-butyl dicarbonate and DMAP to ensure Boc protection - this is due to the fact that, despite the reaction being carried out at room temperature, the production of any hydrobromic acid from HBr and trace amounts of water may create an acidic environment where the Boc groups are labile. Finally, pouring into a cold 1:2 (v/v)

THF:ethanol mixture removes TBAB to yield **5** in fair yields (65%, compared to Chen and Benicewicz' yields of 88%).[94] Purity of **5** was confirmed by ^{1}H NMR (**Appendix A4**).

3.1.5 Synthesis of 6

With two dianilines, **4** and **5**, appropriately protected and brominated, Buchwald-Hartwig coupling can now be performed to create **6**, tetra(aniline) protected with Boc groups at its secondary amines, and a benzophenone group protecting its primary amine cap. Buchwald-Hartwig cross-coupling utilises a palladium catalyst, which can be substituted with a range of different ligands to improve its solubility, selectivity and catalytic activity. Contemporary research into ligand development primarily revolves around the utilisation of a few key coordinating motifs; *N*-heterocyclic carbenes, cyclopentadienes, diamines, pyridines, and phosphines.[110] In the case of Buchwald-Hartwig coupling, phosphines, particularly dialkylbiaryl phosphines, are prized as catalytic ligands due to their steric bulk and strong electron donor ability. The steric bulk of this ligands favours the formation of a highly-reactive [L_1Pd(0)] complex with a free active site which greatly improves reactivity compared to a disubstituted [L_2Pd(0)] complex. Furthermore, the biaryl system helps to promote reductive elimination and catalyst regeneration, improving catalytic turnover and thus promoting the reaction rate.[111] Chen and Benicewicz utilised the dialkylbiaryl phosphine XPhos in their methodology for synthesising **TANI**, but since their publication, the more active BrettPhos ligand has been developed (**Figure 20**).[112] BrettPhos has the additional advantage of being selective for primary amines,[113] though in the context of the synthesis of **TANI**, this does not preclude pre-coupling Boc-protection (which is also required to improve processibility and prevent oxidation of **TANI**).

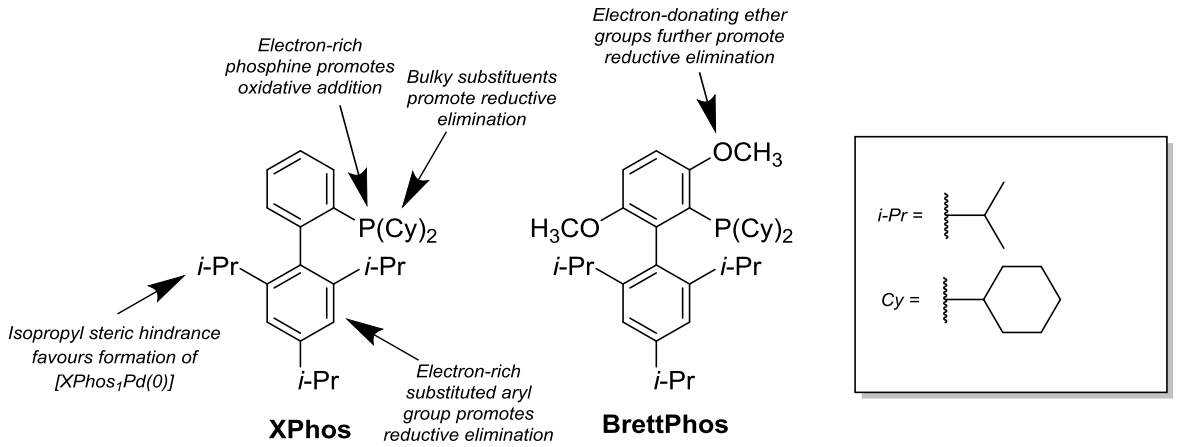

Figure 20 *The structural features of two dialkylbiaryl phosphines, XPhos and BrettPhos.*[114]

Despite the higher activity of BrettPhos, XPhos was chosen to be the catalytic system utilised in the synthesis of **6** as the methodology for utilising this ligand in the synthesis of **TANI** is already established. However, for industrial applications, use of a BrettPhos-based catalytic system is a promising route to optimisation. The catalytic system is synthesised in-situ from bis(dibenzylideneacetone)palladium(0) [$Pd(dba)_2$], which is readily substituted by XPhos to form the active [$XPhos_1Pd(0)$] catalyst. This active catalyst then undergoes oxidative addition with an aryl bromide, in this case **5**. Coordination of **4** and its subsequent *N*-deprotonation by the strong base sodium *tert*-butoxide (NaO*t*Bu) then facilitates a reductive elimination to form **6** and regenerate the [$XPhos_1Pd(0)$] catalyst.

After two days of refluxing in toluene at 110 °C, the product mixture was purified with dichloromethane and water washes, before being reacted with di-*tert*-butyl dicarbonate and DMAP to ensure Boc protection. A second Boc protection is necessary due to the Boc group's lability at these high temperatures, and as such this Boc reprotection ensures that **6** is produced in high yields (see **Section 3.1**). After a final wash with methanol, **6** was obtained in fair yields of 61% (compared to Chen and Benicewicz' yield of 63%),[94] with its purity confirmed by ^{1}H NMR (**Appendix A5**).

3.1.6 Synthesis of TANI

The final stage of the synthesis involved the benzophenone deprotection of **6** to yield the NH_2 terminus, which could then be used in further reactions to incorporate it into **PDI-2-TANI** (see **Section 3.2**). This was achieved using the same method as the synthesis of **4**, using the H_2/Pd system discussed in **Section 3.1.3** and following the same mechanism shown in **Scheme 4**. Filtration with DCM to isolate the product mixture from the palladium catalyst, and subsequent immersion and filtration in hexane to isolate **TANI**, produced **TANI** in excellent yields (89%). A direct comparison to the yields of Chen and Benicewicz' procedure cannot be made for this stage - benzophenone deprotection and **TANI** functionalisation were performed in the same step. However, given the high yields of **4** from the dianiline benzophenone deprotection (see **Section 3.1.3**), it is expected that this synthesis has excellent to quantitative yields. The purity of **TANI** was confirmed by ^{1}H NMR (**Appendix A6**).

3.2 Synthesis of PDI-2-TANI - First Pathway

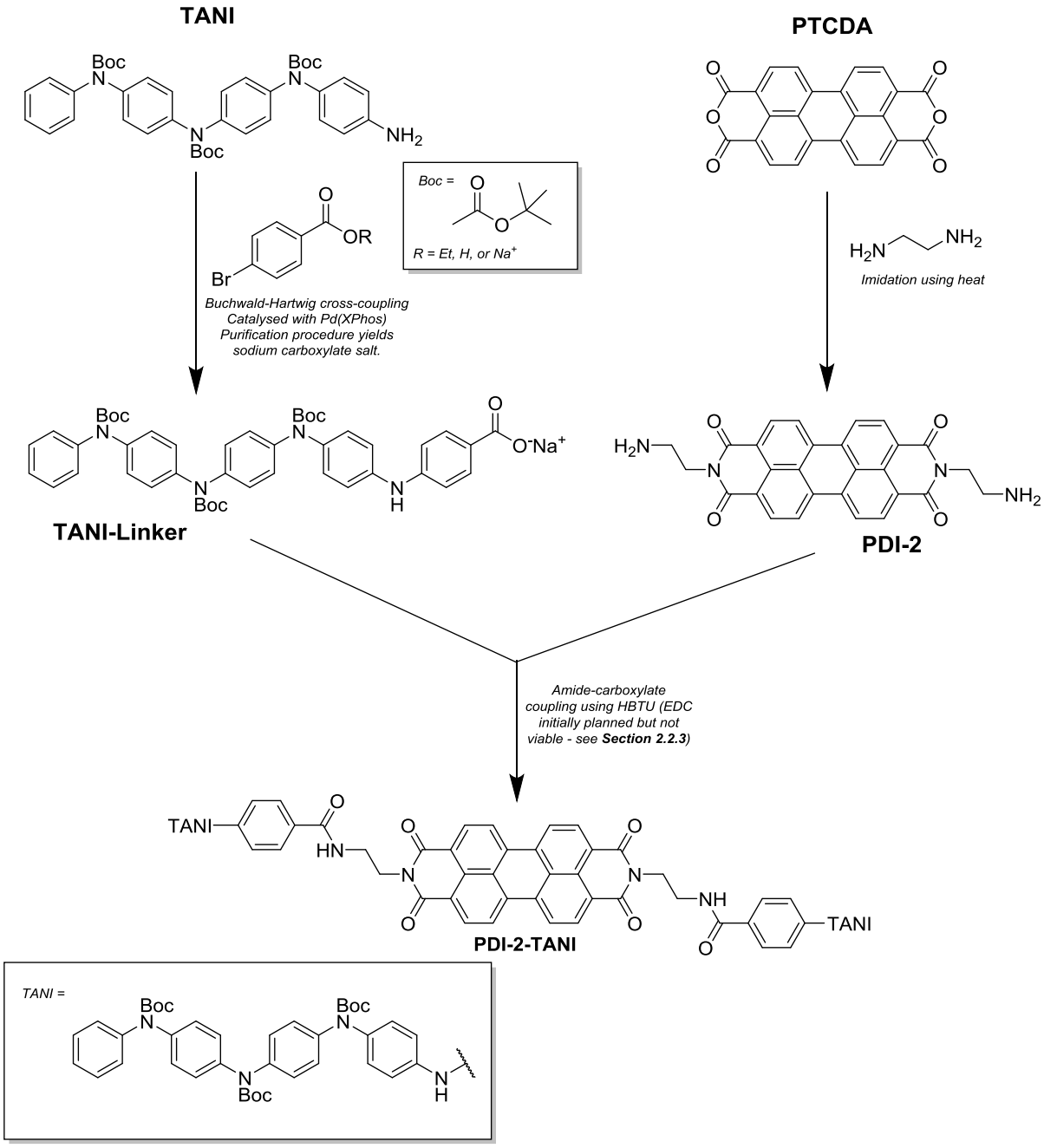

Scheme 6 *The initial synthetic route used to prepare* ***PDI-2-TANI.***

Alongside the synthesis of **TANI** discussed in **Section 3.1**, the other established synthesis used in this project is the synthesis of **PDI-2** (discussed in **Section 3.2.1**), a PDI derivative with two aminoethyl imide substituents. Thus, the planned synthetic route to **PDI-2-TANI** revolves around derivatising and

coupling **TANI** and **PDI-2** (**Scheme 6**). Carboxylic acid–amine coupling is an attractive choice for this step; several methods exist to perform this in high yield, such as carbodiimide couplings, uronium couplings and amine acylation. Further modification of **PDI-2** is not required for these procedures, but functionalisation of **TANI** with a carboxylic acid moiety is necessary.

Given that the synthesis of **PDI-2-TANI** from **TANI** revolves around coupling and imidation reactions, it is highly modular - the order of reactions can be changed to optimise yield and processability, or to minimise any undesirable side reactions (notably the possibility of Boc deprotection of **TANI**). For example, another synthetic pathway is trialled in **Section 3.3**, planned around the conservation of **TANI**, the only reagent which is not commercially available. This synthesis revolves around the derivatisation of **TANI** to create **TANI-Linker**, performed with a Buchwald-Hartwig coupling with a 4-bromobenzoic acid derivative as discussed in **Section 3.2.2**. Then, **TANI-Linker** is coupled with **PDI-2** to create the decoupled product, **PDI-2-TANI**, using hexafluorophosphate benzotriazole tetramethyl uronium (HBTU) coupling discussed in **Section 3.2.3**.

The initial scope of the project called for subsequent Boc deprotection, oxidation and acid-doping of **PDI-2-TANI** to create the conductive emeraldine salt form, **PDI-2-TANI-ES**. However, due to the low yields of **PDI-2-TANI** from HBTU coupling (discussed in **Section 3.2.3**), this procedure was not viable. Instead, the findings from this synthetic pathway, and that pathway discussed in **Section 3.3**, provide the means to optimise a high-yield synthesis of **PDI-2-TANI** for future projects involving the self-assembly and optoelectronic properties of **PDI-2-TANI-ES** (see **Section 4.3**).

3.2.1 Synthesis of PDI-2

The synthesis of **PDI-2** was adapted from the Würthner group[62] by another Faul Group member, Henry Symons. The original synthesis pioneered by the Würthner group was itself based upon an earlier naphthalene diimide imidation,[115] both using an *N*-(2-aminoethyl)-benzamide derivative (**Scheme 7**). The synthesis involves the condensation reaction of perylene tetracarboxylic dianhydride (PTCDA) with a primary amine and has a wide scope which encompasses most alkyl and aryl amines.[43,116] These syntheses are often carried out using zinc acetate as a catalyst and molten imidazole as a suitable solvent for both PTCDA and zinc acetate. However, Henry Symons' adaptation did not employ a catalyst and utilised refluxed toluene as a solvent. Whilst this procedure led to suppressed yields (68%, as opposed to 95%), the commercial availability and low cost of PTCDA and ethylene diamine made this reaction viable.

Toluene was chosen as a suitable solvent since it is selective for ethylene diamine and has a lower melting point than imidazole (-95 ^{o}C vs. 91 ^{o}C). Thus, purification procedures can be carried out at room temperature, and filtration of the reaction mixture will remove any unreacted ethylene diamine. Isolation of **PDI-2** is straightforward - like many PDIs without solubilising groups, **PDI-2** is highly insoluble, whilst PTCDA can be treated with strong aqueous base (in this case, 5 M potassium hydroxide) and hydrolysed to water-soluble perylene tetracarboxylic acid. Since ethylene diamine is also water-soluble,[117] any traces of unreacted ethylene diamine will also be removed with this aqueous wash.

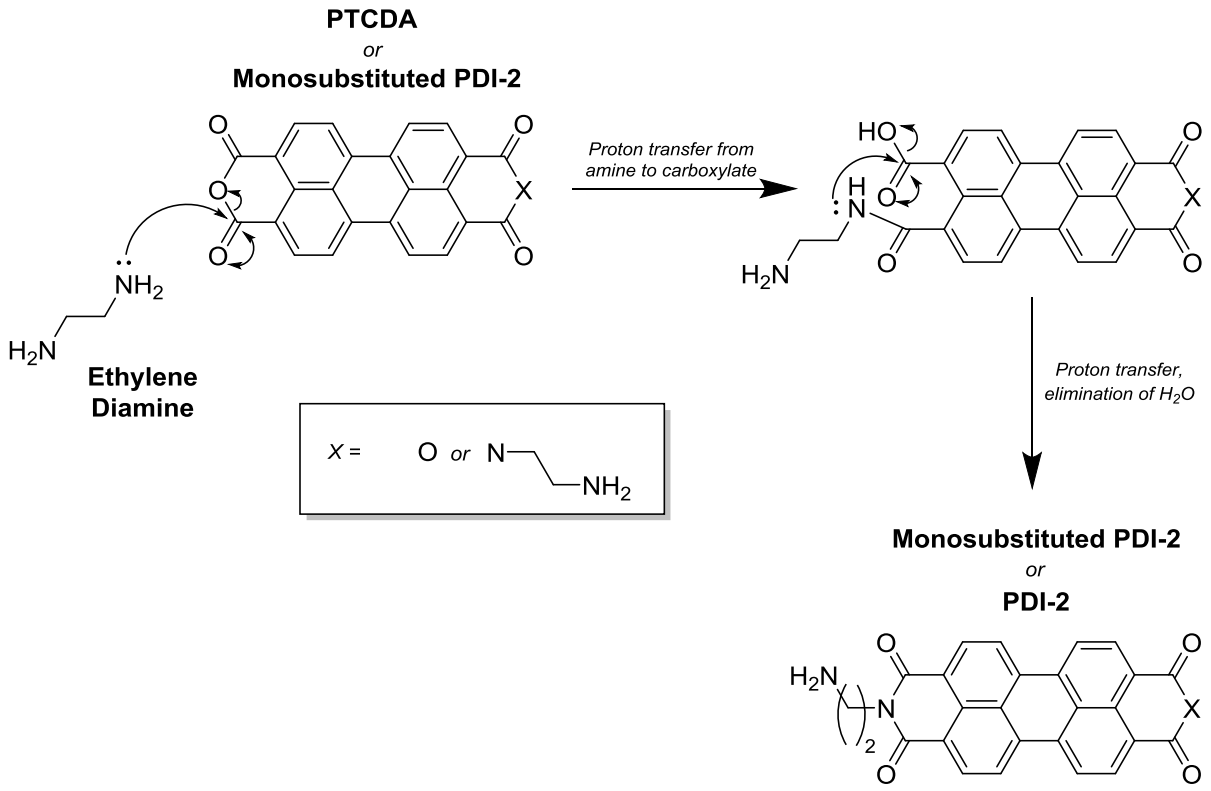

Scheme 7 *The imidation of PTCDA to form monosubstituted* ***PDI-2****, and of monosubstituted* ***PDI-2*** *to form the final product,* ***PDI-2****.*

As expected, the synthesis and purification procedure yielded **PDI-2**, a dark purple solid, in fair yields of 55%. However, due to the insolubility of this product, NMR analysis was unviable - ^{1}H NMR in DMSO did not yield any characteristic perylene or aminoethyl signals, signalling the absence of any PTCDA or perylene tetracarboxylic acid, but it did not confirm the formation of **PDI-2**. For this same reason, ESI and MALDI mass spectrometry were not able to confirm the purity of the product. To confirm the absence of PTCDA or perylene tetracarboxylic acid, a sample of the solid was crushed with a pestle and mortar before the resulting powder was immersed in 5 M potassium hydroxide. This aqueous solution was then observed using long-wave UV light - unlike a reference of dissolved perylene tetracarboxylic acid, this sample did not fluoresce at 365 nm, confirming that the only perylene compounds present in the reaction mixture must be **PDI-2**, which does not fluoresce due to its insolubility.

3.2.2 Synthesis of TANI-Linker

As discussed in (**Section 3.2**), the conversion of **TANI** to a carboxylic acid derivative was ideal for a later coupling reaction with **PDI-2** to produce **PDI-2-TANI** due to the range of reactions available to produce amides from amines and carboxylic acids. Direct conversion of the **TANI** amine terminus (the fourth aniline unit) to a carboxylic acid would diminish the conjugation length of the **TANI** moiety in the emeraldine base and salt forms and preclude full oxidation to the PB state.[78] As a result, to preserve this fourth aniline unit in **TANI-Linker**, it was decided that the amine terminus would be Buchwald-Hartwig coupled with a 4-bromobenzoic acid derivative, creating an asymmetric, carboxylic acid functionalised phenyl/phenyl-capped **TANI**. This moiety would retain the conjugation length, and therefore the optoelectronic properties of **TANI**, but be available for further functionalisation via the COOH terminus. Since **TANI** is protected at its secondary amine sites by Boc groups, Buchwald-Hartwig coupling could be employed to selectively couple **TANI**'s amine terminus, precluding the generation of other Buchwald-Hartwig coupled side products.

The initial choice of 4-bromobenzoic acid derivative was methyl 4-bromobenzoate, due to its ready availability and the advantage of protecting the carboxylic acid moiety by esterification. Previous reports of Buchwald-Hartwig coupling reactions involving methyl 2-bromobenzoate and methyl 3-bromobenzoate resulted in excellent yields (80-88%)[118] and it was expected that **TANI-Linker** would be obtained in similar yields. The reaction was carried out in THF, a suitable solvent for both methyl 4-bromobenzoate and **TANI**; several literature reports note successful Buchwald-Hartwig couplings in similar ethers such as dioxane and dimethoxyethane.[119,120] As in **Section 3.1.5**, XPhos was chosen as a suitable ligand system for Buchwald-Hartwig coupling. The reaction proceeds in an analogous mechanism to that in **Section 3.1.5** (**Scheme 7**). The reaction was run at low temperatures (55 ^{o}C) due to the low boiling point of THF (66 ^{o}C) and also to ensure no deprotection of the thermally labile Boc groups in **TANI**. Initial palladium catalyst loading was 2 mol% (compared to **TANI**).

TLC was used to monitor the reaction as it progressed over the course of 6 days. At the end of this timespan, significant amounts of **TANI** and methyl 4-bromobenzoate were still found by TLC testing. These observations hinted at two problems with the reaction setup. Firstly, the low temperatures used greatly suppressed the rate of Buchwald-Hartwig coupling, a reaction which is normally performed for 2-48 hours using refluxed toluene, dioxane or dimethoxyethane (i.e. at temperatures of 90-110 ^{o}C).[119,120] Secondly, because of the long reaction time, it may be possible that traces of oxygen or other reactive contaminants have poisoned the palladium catalyst, explaining the lack of product production after the fourth day of reaction. Despite this, purification of the product mixture by THF washes and column chromatography yielded **TANI-Linker** (a light brown crystal) in a poor yield of 38%.

TANI-Linker was analysed using ^{1}H NMR (**Figure 21**), where the appearance of downshifted aryl hydrogen peaks at 7.96 (**1**) and 7.30 ppm (**2**) indicated the presence of a benzoate moiety. The coupling of this moiety was confirmed by the appearance of a downshifted singlet at 6.16 ppm (**4**), corresponding to the lone hydrogen on the amine group formed during coupling. However, there were no signals corresponding to the methyl groups from the benzoate moiety, which should present at a sharp (3H integral) singlet at around 3.9 ppm.[121] ESI-MS (**Figure 22**) confirmed the production of **TANI-Linker** in its hydrolysed carboxylate sodium salt form; Whilst the reaction was performed under anhydrous conditions, the purification procedure involved washing with aqueous sodium hydroxide, accounting for conversion of **TANI-Linker** to its sodium carboxylate salt form.

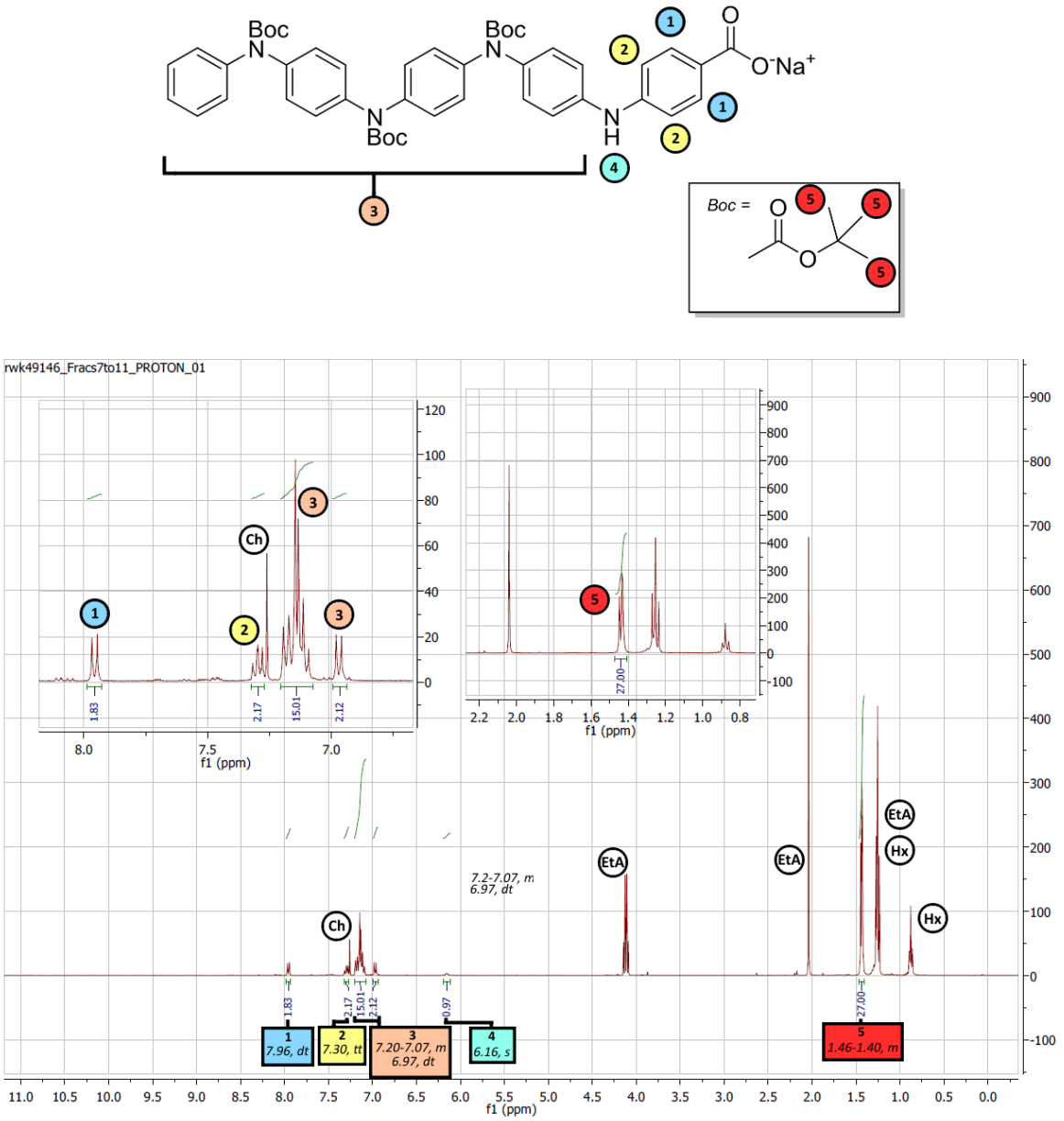

Figure 21 *The [1]H NMR spectrum of* ***TANI-Linker*** *after purification via column chromatography, with peaks assigned to its carboxylate salt form. Impurities are notated as follows: Ch = chloroform, EtA = ethyl acetate, Hx = hexane.*

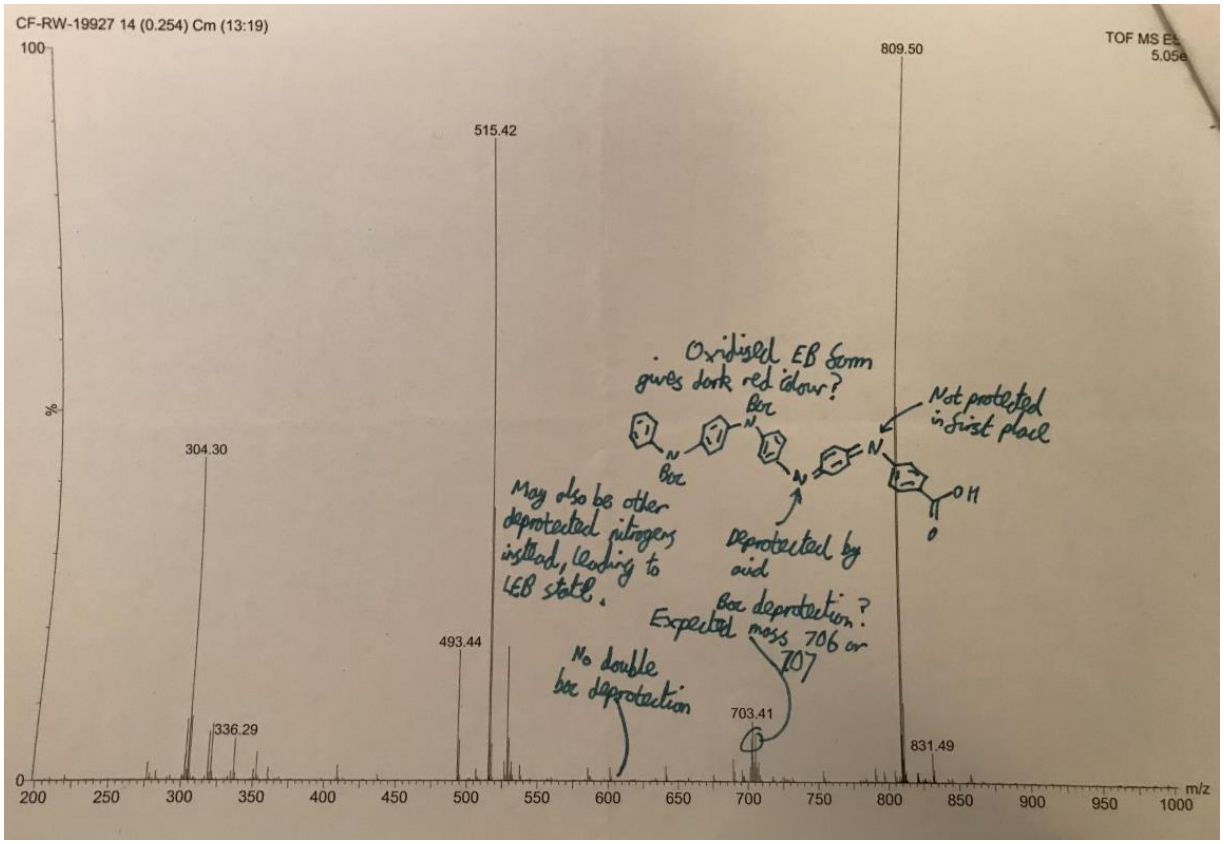

Figure 22 *The ESI-MS of* ***TANI-Linker.*** *The peak at* m/z *809.5 corresponds to the hydrolysed carboxylate sodium salt form. A cluster of peaks between* m/z *700-710 may indicate a single Boc deprotection - this, combined with the unprotected nitrogen involved in the Buchwald-Hartwig coupling, may have led to oxidation, explaining the red-brown colour and low purity of the initial* ***TANI-Linker*** *sample.*

To optimise the synthesis of **TANI-Linker**, a second Buchwald-Hartwig cross-coupling reaction was trialled, using a fivefold excess of 4-bromobenzoic acid (in lieu of methyl 4-bromobenzoate) and a catalyst loading of 10 mol%. This was predicted to offset the low temperatures used in the reaction and ensure that sufficient catalyst remained after any poisoning by trace oxygen. TLC confirmed completion of the reaction after 3 days, however the large excess of 4-bromobenzoic acid prohibited separation by column due to tailing of this fraction. Instead, 5 M aqueous sodium hydroxide was used to facilitate conversion of 4-bromobenzoic acid to its water-soluble sodium 4-bromobenzoate salt. This led to a slightly suppressed yield of 33% (compared to the initial procedure's 38%), but ^{1}H NMR analysis revealed that this deep red product was Boc deprotected and oxidised (**Appendix A7**). This was likely due to the very high catalyst loading - Buchwald-Hartwig cross-coupling is exothermic[122] and

the reaction was carried out at 55 °C, so excess heat generation may have heated the reaction mixture enough to facilitate Boc deprotection.

The results of this trial optimisation led to the establishment of a final, optimised protocol involving a fivefold excess of 4-bromobenzoic acid and a lower catalyst loading of 5 mol%. The reaction was also run at a slightly lower temperature - 50 °C - to ensure that Boc deprotection did not occur. The reaction was performed for 3 days, and the product was purified using THF washes and immersion and washing with 5 M aqueous sodium hydroxide, yielding a cream-coloured solid. ^{1}H NMR (**Appendix A8**) confirmed that this solid contained pure, Boc-protected **TANI-Linker** sodium carboxylate salt in a yield of 68%.

3.2.3 Synthesis of PDI-2-TANI

Whilst the initial synthetic scheme called for EDC coupling between **TANI-Linker** and **PDI-2**, the carboxylate salt form of **TANI-Linker** obtained in **Section 3.2.2** made this reaction unviable. Carbodiimide coupling requires a protic environment to activate the carbodiimide and form the reactive O-acylisourea leaving group via nucleophilic attack (see **Section 3.3.1** for full mechanism).[123] Normally, this protic environment is provided by dissociation of the carboxylic acid, but the **TANI-Linker** carboxylate salt is aprotic. Furthermore, since the **TANI-Linker** carboxylate salt is Boc-protected, carbodiimide coupling could not be carried out in an acidic environment: kinetic studies have shown that EDC coupling is optimal at pH 3.5-4.5.[124] At this pH range, even at room temperature, the Boc protecting group may be labile.[100] The issue of lability also prevents pre-acdification of the **TANI-Linker** carboxylate salt to convert it to its carboxylic acid form, **TANI-Linker**.

Whilst carbodiimide coupling was not suitable for the synthesis of **PDI-2-TANI**, an example of direct coupling between carboxylate salts and amines existed in literature. HBTU, a uronium coupling reagent normally utilised for peptide synthesis, was found to be highly effective in amidation reactions involving these two products, producing fair to quantitative yields (>61 %) with a range of lithium and sodium carboxylate salts.[125] The scope of couplings included amines and carboxylate salts bearing aliphatic, aromatic, cyclic and halogenated moieties, illustrating the versatility of this new procedure. Furthermore, whilst lithium carboxylate salts required a two-step addition (HBTU, then Hünig's base) to ensure completion of the reaction, sodium carboxylate salts could be amidated in high yields in a one-pot reaction. Importantly, HBTU coupling could be carried out at room temperature, minimising any risk of Boc deprotection. The findings from this procedure indicated that HBTU coupling was the ideal synthesis to creating **PDI-2-TANI** in high yield.

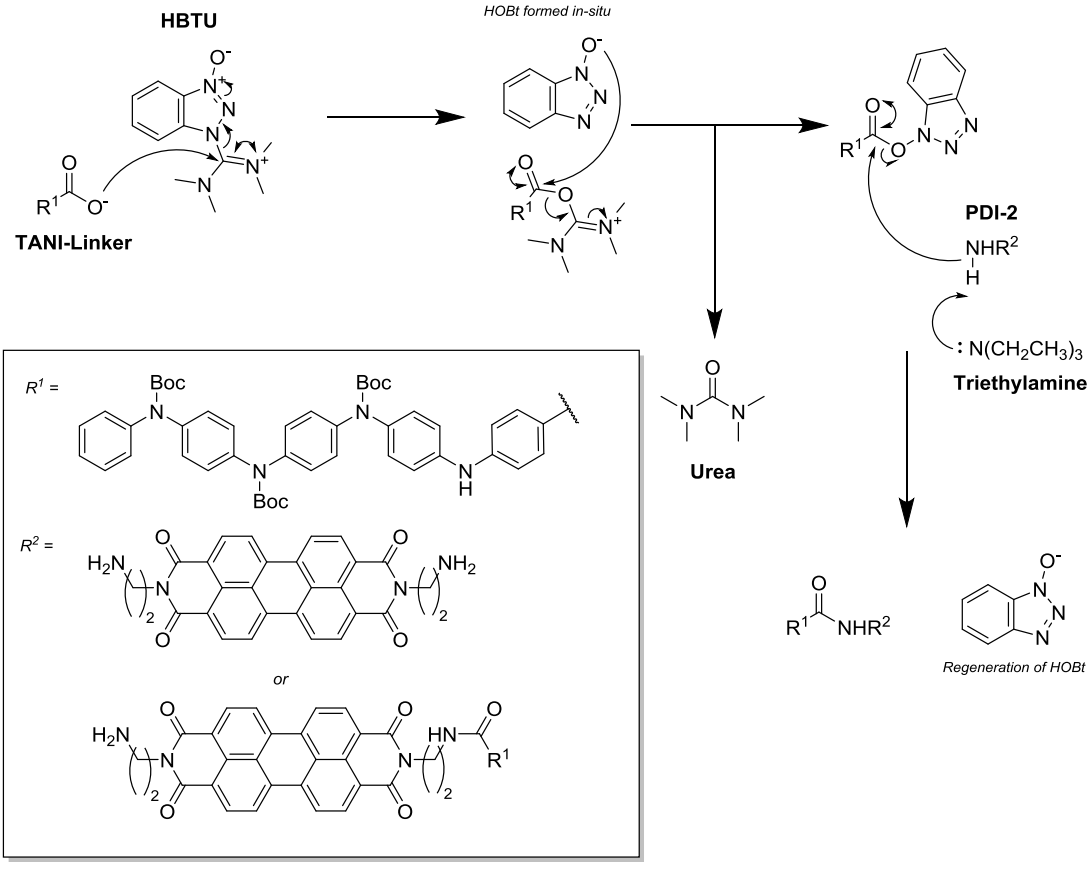

Scheme 8 *The mechanism for HBTU-mediated coupling of* ***TANI-Linker*** *(in its carboxylate salt form) and* ***PDI-2*** *to form* ***PDI-2-TANI****.*

In a similar manner to carbodiimides (discussed in **Section 3.3.1**), HBTU improves amidation kinetics by converting the carboxylic acid (or carboxylate) to an activated species, in this case a hydroxybenzotriazole (HOBt) leaving group (**Scheme 8**).[126] This conversion is initiated by nucleophilic attack of the carboxylate anion, which forms a C-C bond between the carboxylate and HBTU iminium moiety, producing an ester. The resulting rearrangement eliminates the deprotonated HOBt moiety, producing HOBt which acts as a nucleophile, attacking the newly formed ester to yield the HOBt ester and a urea byproduct. A third nucleophilic attack between the amine and the HOBt ester yields the desired amide, regenerating deprotonated HOBt. Thus, HBTU serves the dual purpose of activating the carboxylate via esterification and producing catalytic HOBt which further activates the carboxylate and accelerates the amide coupling.

The HBTU coupling procedure was adapted to utilise DMSO as a solvent, maximising the limited solubility of **PDI-2**. DMSO has been used with HBTU in solid-phase peptide synthesis[127] and a method of HBTU coupling in DMSO has been patented for use in solution-phase organic chemistry to create benzamides.[128] As such, this solvent is a suitable candidate for HBTU coupling. Since the resulting **PDI-2-TANI** is expected to have limited water solubility, aqueous washes were chosen to remove DMSO before further purification commenced. As such, another adaptation was made - instead of Hünig's base, triethylamine was selected as the base for the reaction due to its higher miscibility in water and immiscibility in apolar organic solvents. This would minimise any triethylamine contamination of the purified product.

The reaction was carried out at room temperature for 12 hours to ensure completion before aqueous washes were employed to dilute the product mixture for DMSO removal. This yielded a pink solution, indicative of a dissolved PDI derivative. Partitioning this aqueous/DMSO mixture with DCM yielded a clear, colourless aqueous fraction and a highly fluorescent DCM fraction which was salmon red, but

dark green in sunlight. Fluorescence was confirmed by irradiation with long-wave UV light (365 nm), thought to be due to the presence of **PDI-2-TANI**. **PDI-2** does not fluoresce at this wavelength, due to its strong aggregation in DCM quenching fluorescence (see **Section 1.2**), and **TANI-Linker** does not fluoresce either in DCM.

TLC in 5:6 ethyl acetate:hexane yielded four main fractions including a highly mobile (R_f 0.86), deep red-coloured fraction which fluoresces at 365 nm with a long non-fluorescent tail, indicative of **PDI-2-TANI** and a colourless R_f = 0.57 fraction corresponding to **TANI-Linker** (**Figure 23a**). The third and fourth fractions were deep red and non-fluorescent, with R_f values of 0.25 and 0 respectively, tentatively proposed as monocoupled **PDI-2-TANI** and uncoupled **PDI-2** respectively. Column chromatography isolated these fractions successfully (**Figure 23b**) with a low yield of 23%, and ^{1}H NMR confirmed the **PDI-2-TANI** (**Figure 24**) and **TANI-Linker** fractions. Interestingly, the third fraction studied (R_f = 0.25) exhibited a ^{1}H NMR signal indicative of **PDI-2-TANI**, with the integrals of the TANI aromatic system and Boc protecting groups more closely matching the spectrum of di-coupled product, instead of the mono-coupled product initially expected. Furthermore, TLC testing of the R_f = 0.86 **PDI-2-TANI** fraction yielded a new fraction at R_f = 0.25 (**Figure 23c**). This second fraction regenerated even after a second column separation was used to isolate the R_f 0.86 fraction from the R_f = 0.25 fraction. Again, the yield from this second column was low - around 20%.

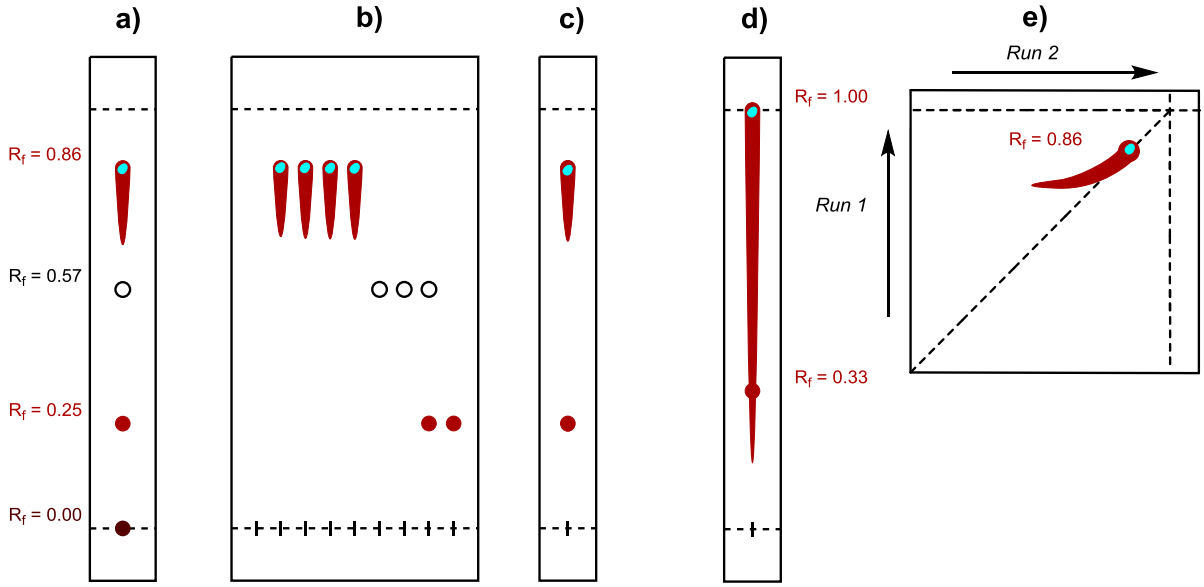

Figure 23 a) *TLC of product mixture, performed in 5:6 (v/v) ethyl acetate:hexane* ***b)*** *TLC of fractions obtained from silica gel column chromatography, performed in 5:6 (v/v) ethyl acetate:hexane* ***c)*** *TLC of the isolated and combined R_f = 0.86 fractions, showing regeneration of the R_f = 0.25 spot, performed in 5:6 (v/v) ethyl acetate:hexane* ***d)*** *TLC of the R_f = 0.86 fraction isolated from* ***2c*** *via silica gel column chromatography, performed in 1:10:90 (v/v/v) triethylamine:methanol:ethyl acetate* ***e)*** *2D TLC of the R_f = 0.86 fraction isolated from* ***b****. Colours indicate their colour under ambient light, with teal colouration at R_f = 0.86 representing fluorescence under long-wave ultraviolet light.*

Whilst PDIs are sometimes purified by column chromatography, this behaviour was not noted in any literature sources. Boc deprotection and oxidation of **PDI-2-TANI,** yielding this second fraction at R_f 0.25, was ruled out by ^{1}H NMR, which did not indicate significant Boc deprotection or subsequent oxidation of the TANI moieties. Furthermore, two-dimensional TLC showed that whilst the initial fluorescent fraction at R_f 0.86 did not degrade, the tail of this fraction underwent a significant change in mobility (**Figure 23e**). The fact that the tail of the Rf 0.86 fraction was not fluorescent when irradiated with 365 nm UV light, and that its mobility changed over the course of TLC indicated that the tail was **PDI-2-TANI** in its aggregated form, and that aggregation of **PDI-2-TANI** occurred during chromatography. This in-situ aggregation also explains the low recovery yields from column chromatography. The regeneration of the R_f 0.25 fraction, which did not fluoresce at 365 nm UV light, indicates that this fraction is probably an aggregate of **PDI-2-TANI** which showed significantly less mobility than either the solvated molecule or the aggregation mode of the R_f 0.86 tail.

Whilst the yields from this procedure were low (20 %), analysis of the other fractions obtained confirmed that HBTU coupling was in fact an effective reaction to produce **PDI-2-TANI** in high yield, and that the low recovery of **PDI-2-TANI** was due to the method of purification. Recovery of unreacted **TANI-Linker** from the column yielded amounts corresponding to the excess of this reagent used in the coupling reaction (2.3x with respect to **PDI-2**, i.e. a stoichiometric excess of 0.3x). No unreacted **PDI-2** was recovered from the reaction mixture, and no fractions corresponding to mono-coupled PDI were found, confirming that the HBTU coupling resulted in excellent to quantitative yields (>90%). As such, optimisation of this reaction called for separation of the product mixture via other means than column chromatography. Crystallisation was trialled as a potential route, given that **PDI-2-TANI** aggregates in ethyl acetate but does not aggregate in ethyl acetate or water. This procedure would allow for removal of DMSO, HBTU and urea side product via aqueous washes and isolation of the **PDI-2-TANI** from **TANI-Linker** by crystallisation in ethyl acetate (which **TANI-Linker** is partially soluble in). **PDI-2-TANI** should form an extended network in ethyl acetate due to the strong aggregation in ethyl acetate, a behaviour seen in the analogous amide-PDI gels of the Würthner group. However, due to the small quantity of reagents available at this point in the project, the scale of the reaction was too small to yield a solution that could be concentrated to gelation.

^{1}H NMR (**Figure 24**) was used to confirm the structure of **PDI-2-TANI**, with the presence of the perylene core hydrogens (**7**), the TANI aryl groups (**1, 2** and **3**), and the TANI's Boc methyl groups (**5**) providing strong evidence for the formation of disubstituted **PDI-2-TANI**. However, the integral for **2** was higher than expected (see **Table 1**), probably due to some overlap with the $CHCl_3$ solvent peak, and the integral for **3** was lower than expected, thought to be due to a longer relaxation time for these aryl hydrogens leading to a suppressed signal. There was also some ambiguity in assigning peaks for the aryl hydrogens at **1** - whilst a doublet peak was found 8.02 ppm, consistent with that of **TANI-Linker** (see **Section 3.2.2**), a second doublet peak was found at 7.57 ppm. Later in the project (**Section 3.4.3**)

it is postulated that **PDI-2-TANI** undergoes intramolecular hydrogen bonding; hydrogen bonding has been shown to cause a slight (0.1-0.2 ppm) upfield shift the aryl hydrogens of bemnzamide,[129] so it may be that this 7.57 ppm peak is a result of an intramolecularly hydrogen-bonded conformation of **PDI-2-TANI**. Peaks corresponding to the secondary amine groups (**4**) and amide (**9**) were also not found, thought to be due to hydrogen-deuterium exchange with the deuterated chloroform solvent. Whilst one ethyl linker bonding environment at **6** can be identified and reliably assigned due to its splitting pattern and similar chemical shift to other PDIs with ethyl linkers,[130] the other bonding environment, with an expected triplet signal at around 2.9 ppm (the chemical shift for the *N*-methyl hydrogens in *N*-methylbenzamide)[131] was not found. Significant impurities were also noted due to the use of a cotton wool plug during column chromatography. Signals corresponding to H-grease (0.75-1.5 ppm) and silicone grease (0.07 ppm) persisted even after washing the NMR sample with hexane,[132] but these signals do not mask any signals from **PDI-2-TANI** and thus do not interfere with the analysis.

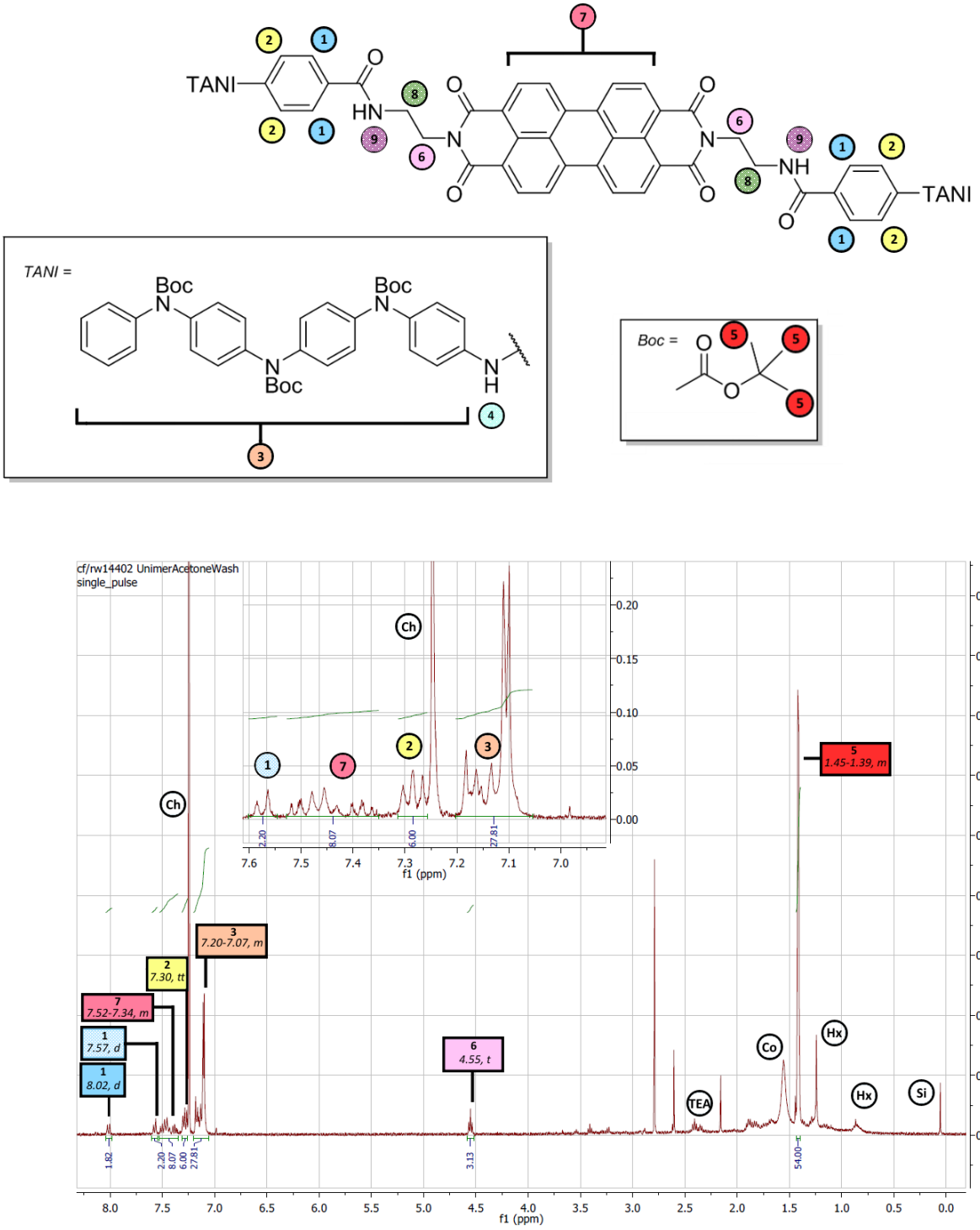

Figure 24 *The ^{1}H NMR spectrum of* ***PDI-2-TANI****, with peaks assigned. Peaks corresponding to hydrogen environments* ***4, 8*** *and* ***9*** *were not found, and thus these are shaded instead of fully coloured. One peak at 7.57 ppm has been ambiguously identified as belonging to protons in environment* ***1****, and this has been shaded. Impurities are notated as follows: Ch = chloroform, EtA = ethyl acetate, Hx = hexane or H grease, Si = silicone grease, Co = cotton wool, TEA = triethylamine.*

Proton Environment	Expected Integral (H)	Actual Integral (H)
1	4	4.02
2	4	6.00
3	34	27.81
4	2	Not Found
5	54	54 (Reference)
6	4	3.13
7	8	8.07
8	4	Not Found
9	2	Not Found

Table 1 *Comparison of expected and experimental (actual) integrals of signals found during* ^{1}H *NMR for* ***PDI-2-TANI****.*

PDI-2-TANI was also analysed using ESI-MS (**Figure 25**), yielding two significant peaks at mass-charge ratios (*m/z*) of 1012 and 2024 (calculated average isotopic mass: 2013). The peak at *m/z* 1012 is the base peak, whilst the *m/z* 2024 peak has a relative abundance of 12%, the heaviest ion peak. It is hypothesised that these two peaks are linked; due to the two secondary amines on **PDI-2-TANI**, the molecule is able to undergo double-ionisation (e.g. to form an $[M+2H]^{2+}$ peak). Whilst the *m/z* 2024 peak at does not correspond to the expected $[M+H]^{+}$ peak of *m/z* 2013.8, it has a gaussian-like distribution of peaks (**Figure 26**) which deviate by integer *m/z* values up to ±4, indicating that this is an isotopic distribution of a large molecule. Given that the reactants involved only contained hydrogen, carbon, nitrogen and oxygen, and that out of these four candidates, carbon has the highest isotopic variance (due to ^{13}C's relative abundance of 1.1%), this distribution must indicate a large, carbon-based compound, beyond the size of **PDI-2** or **TANI-Linker**. Comparing this distribution to calculated distributions (see **Figure 27** and **Table 2**), the distribution around the *m/z* 2024 peak more closely resembles a larger aggregate rather than a single **PDI-2-TANI** molecule. Thus, it may be that

the *m/z* 2024 peak (and by extension, the *m/z* 1012 peak) may correspond to an aggregate of ionised **PDI-2-TANI** molecules, which, due to their strong π-stacking, did not disaggregate during ESI-MS. Charged aggregates of **PDI-2-TANI** may also explain the discrepancy from the expected $[M+H]^+$ mass of 2013; the excess mass may be due to heavier ions (e.g. sodium, potassium) present in some of the **PDI-2-TANI** molecules within an aggregate. For example, the calculated mass-charge ratios of $[2M+H+Na]^{2+}$ and $[2M+3H+Na]^{4+}$ **PDI-2-TANI** aggregates are 2025 and 2013 respectively, closely corresponding to the experimental peaks observed.

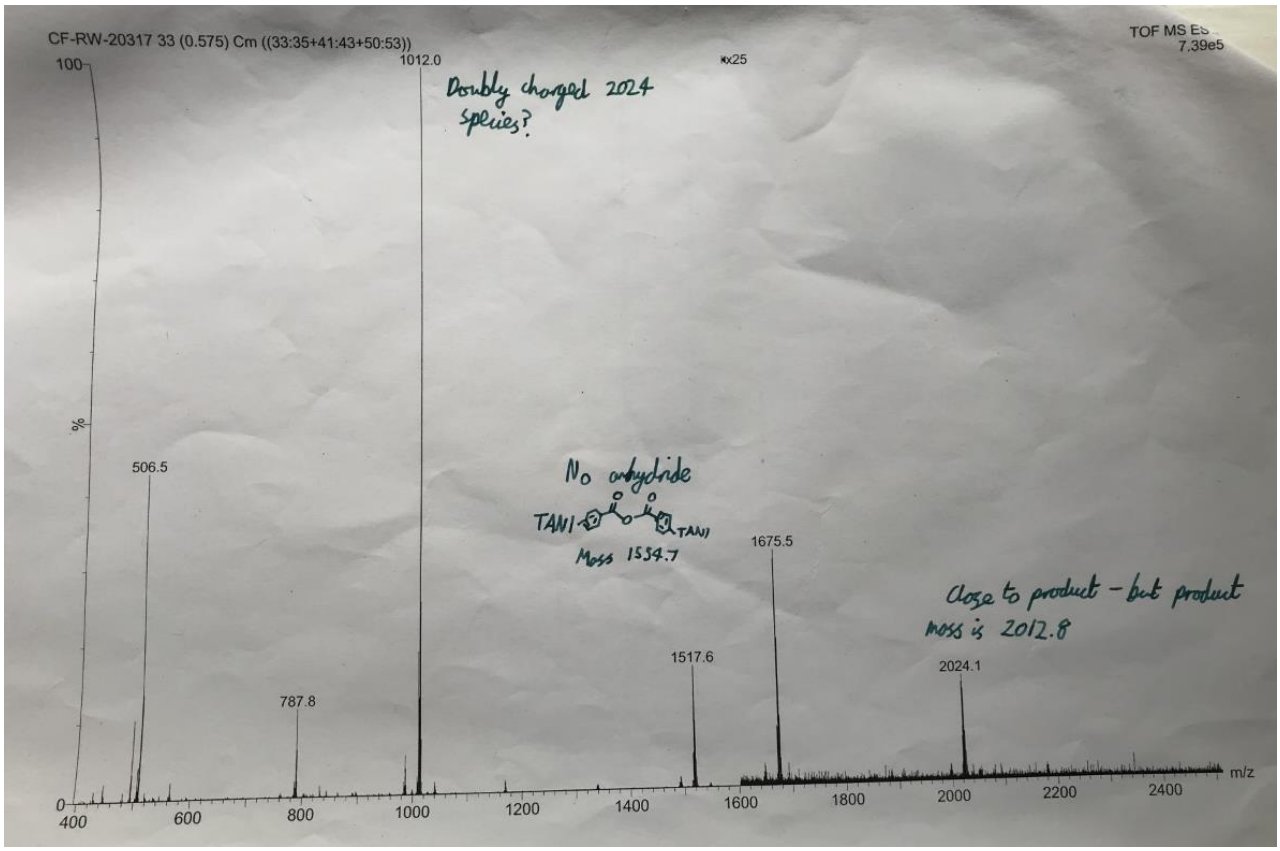

Figure 25 *The ESI-MS spectrum for* ***PDI-2-TANI****.*

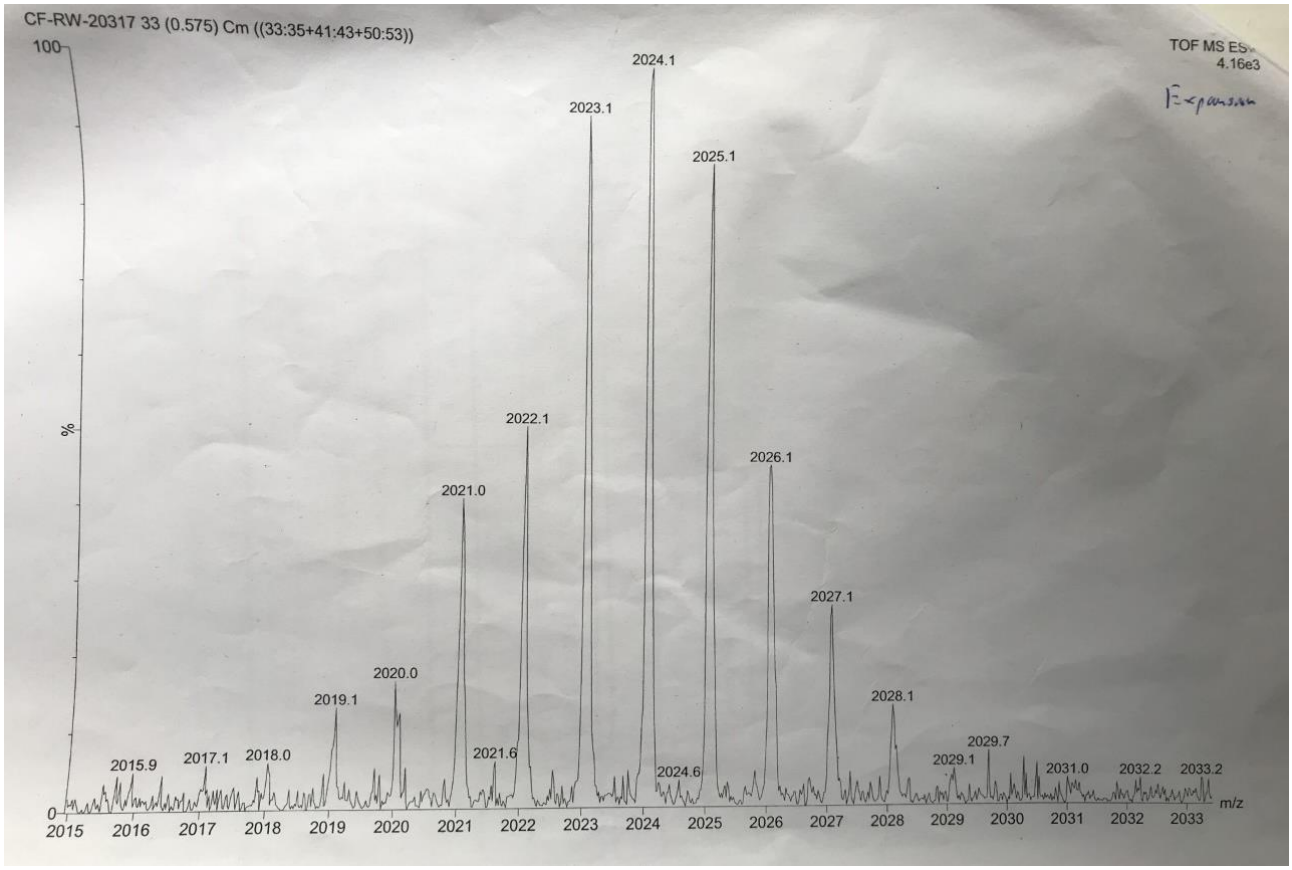

Figure 26 *Expansion of the ESI-MS spectrum for* ***PDI-2-TANI****, showing the isotopic distribution of the peaks around* m/z *2024.*

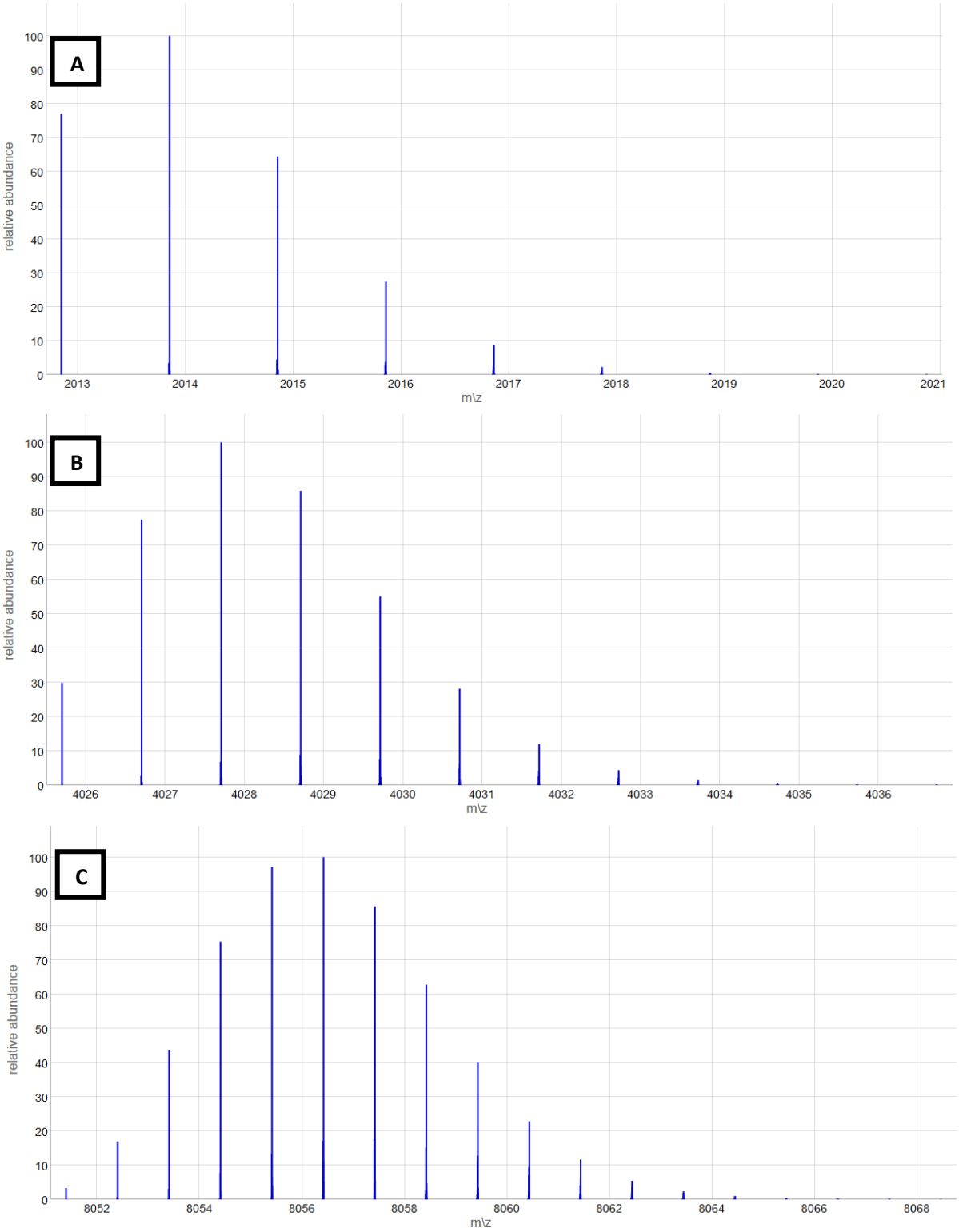

Figure 27 *Calculated isotopic distributions of* ***a)*** *a* ***PDI-2-TANI*** *unimer* $[M+H]^+$, ***b)*** *dimer* $[2M+H]^+$ *and* ***c)*** *tetramer* $[4M+H]^+$.[133]

	Relative Peak Intensities in ESI-MS (%)				
	BP - 2 *m/z*	**BP - 1 *m/z***	**Base Peak (BP)**	**BP + 1 *m/z***	**BP + 2 *m/z***
PDI-2-TANI Unimer	N/A	77	100	64	28
PDI-2-TANI Dimer	30	78	100	86	55
PDI-2-TANI Tetramer	75	97	100	86	63
Experimental Spectrum	51	93	100	85	45

Table 2 *Comparisons of relative peak intensities for ions of* ***PDI-2-TANI****, from* ***Figure 26*** *and* ***Figure 27.***

3.3 Alternative Synthesis of PDI-2-TANI

Due to the low yields obtained from the purification process of Boc-protected **PDI-2-TANI** described in **Section 3.2.3**, an alternative synthesis route to the unimer was trialled. Since the route from **TANI** to **PDI-2-TANI** consists of a linear series of couplings, the synthetic route shows a remarkable modularity, whereby couplings of **TANI**, PTCDA, ethylene diamine and 4-bromobenzoic acid could be performed in any order to achieve the desired product. This alternative synthesis route was designed with the conservation of **TANI** in mind, the only product which was not commercially available and required a lengthy synthesis to produce. As such, this new synthesis scheme required the unimer was built up from its three other component parts - starting with coupling of ethylene diamine to 4-bromobenzoic acid to create the amide **2-Linker**, which was then used to imidate PTCDA to create **PDI-2-Linker**. **PDI-2-Linker** could then be reacted with **TANI** through a double Buchwald-Hartwig coupling to yield **PDI-2-TANI**. A further advantage of this synthetic scheme is that since **TANI** is only utilised for the final Buchwald-Hartwig coupling, the preceding reactions and purifications can be carried out at high (>60 ^{o}C) temperatures or acidic conditions (pH<4) if required, as Boc deprotection of these intermediate products was no longer an issue.

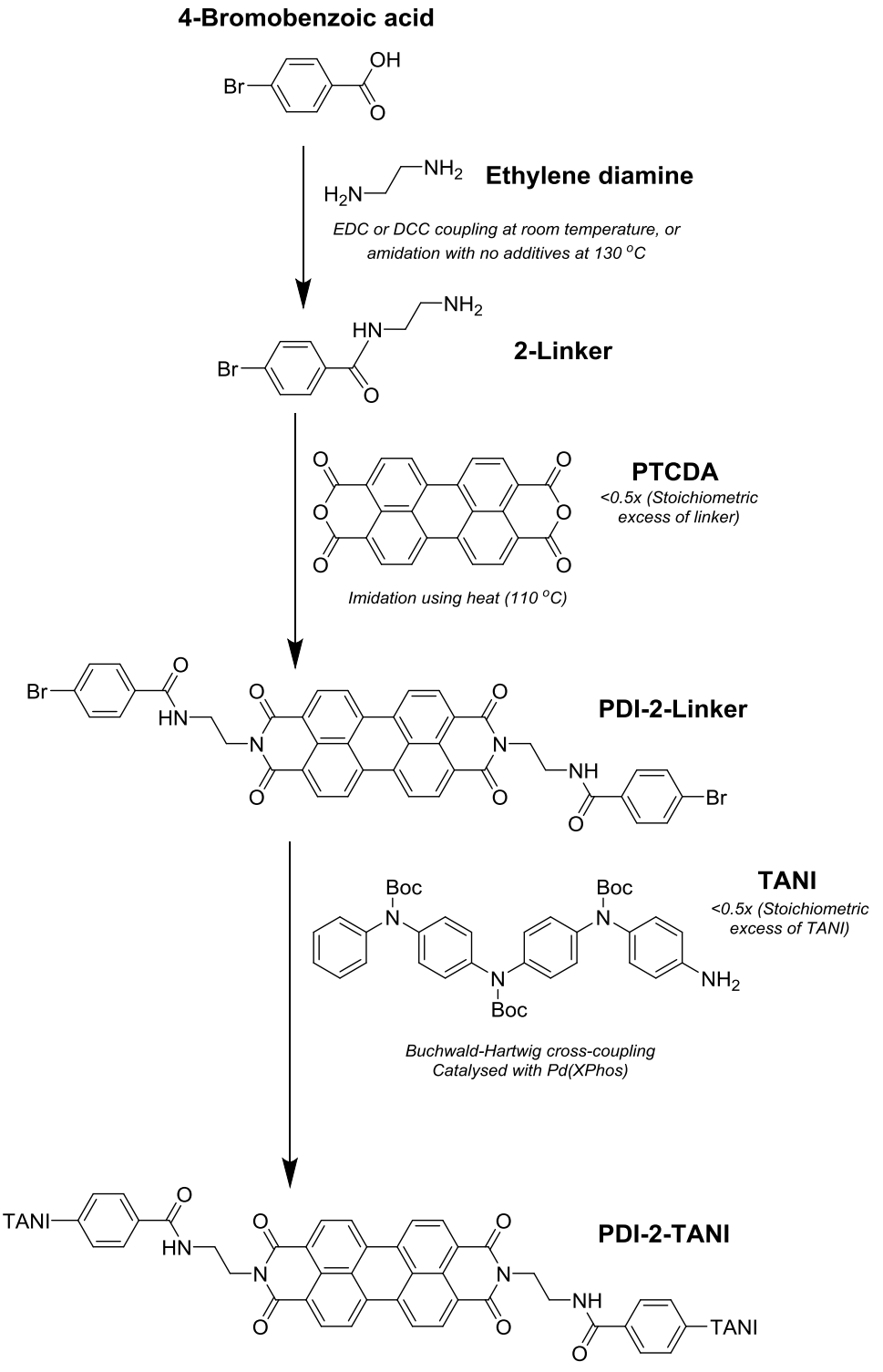

Scheme 9 *The alternative synthetic route used to prepare* ***PDI-2-TANI.***

The ordering of the first two reactions shown in **Scheme 9** was chosen with the aim of simplifying purification procedures throughout the synthetic scheme. Whilst an alternative synthesis involving

the coupling of **PDI-2** (created earlier in the project) with 4-bromobenzoic acid could also be performed to create **PDI-2-Linker** this was avoided due to concerns about separating **PDI-2-Linker** (predicted to be highly insoluble) from unreacted **PDI-2** (which exhibits almost complete insolubility in most solvent systems). However, the synthesis of **PDI-2-Linker** from PTCDA and **2-Linker** is more straightforward to purify, requiring strong base to hydrolyse unreacted PTCDA and form the water-soluble perylenetetracarboxylic acid. Due to time restrictions, the scope of this project does not examine the final Buchwald-Hartwig cross-coupling to form **PDI-2-TANI** - instead, the syntheses of **2-Linker** and **PDI-2-Linker** are examined.

3.3.1 Synthesis of 2-Linker

Three separate syntheses were trialled for *N*-(2-aminoethyl)-4-bromobenzamide (**2-Linker**), the first two using the carbodiimides EDC and DCC as coupling reagents, and the third using high temperature in a procedure adapted from Rafii et. al.[134] In all reactions, a fourfold excess of ethylene diamine was used to minimise formation of the unwanted N,N'-1,2-Ethanediylbis(4-bromobenzamide) double-coupled side product.

Using carbodiimides as coupling reagents was an attractive choice for amide formation. They convert the 4-bromobenzoic acid's COOH group to an *O*-acylisourea, an excellent leaving group which promotes nucleophilic attack on the 4-bromobenzoic acid's carbonyl moiety (**Scheme 10**). The formation of the O-acylisourea proceeds via a proton transfer from the COOH group to one of the carbodiimide's imide nitrogens. This now-protonated nitrogen then acts as an electron sink for the nucleophilic COO^-, allowing it to attack the imide carbon. The resulting O-acylisourea then acts as a leaving group, forming an *N*-substituted urea via a concerted rearrangement and proton transfer from the nucleophilic amine as the amine attacks the adjacent carbonyl moiety. From a practical perspective, this means that carbodiimide reagents allow for carboxylate-amine coupling reactions to

progress under milder conditions (for example, at room temperature). However, the formation of various side products, including the urea and *N*-acylurea (formed by the rearrangement of O-acylisourea) can pose difficulties with purification. Whilst a third side product, an acid anhydride, can be formed via nucleophilic attack of unreacted carboxylic acids with the O-acylisourea, this acid anhydride readily reacts with nucleophiles to yield the desired amide and regenerate the carboxylic acid (**Scheme 11**).

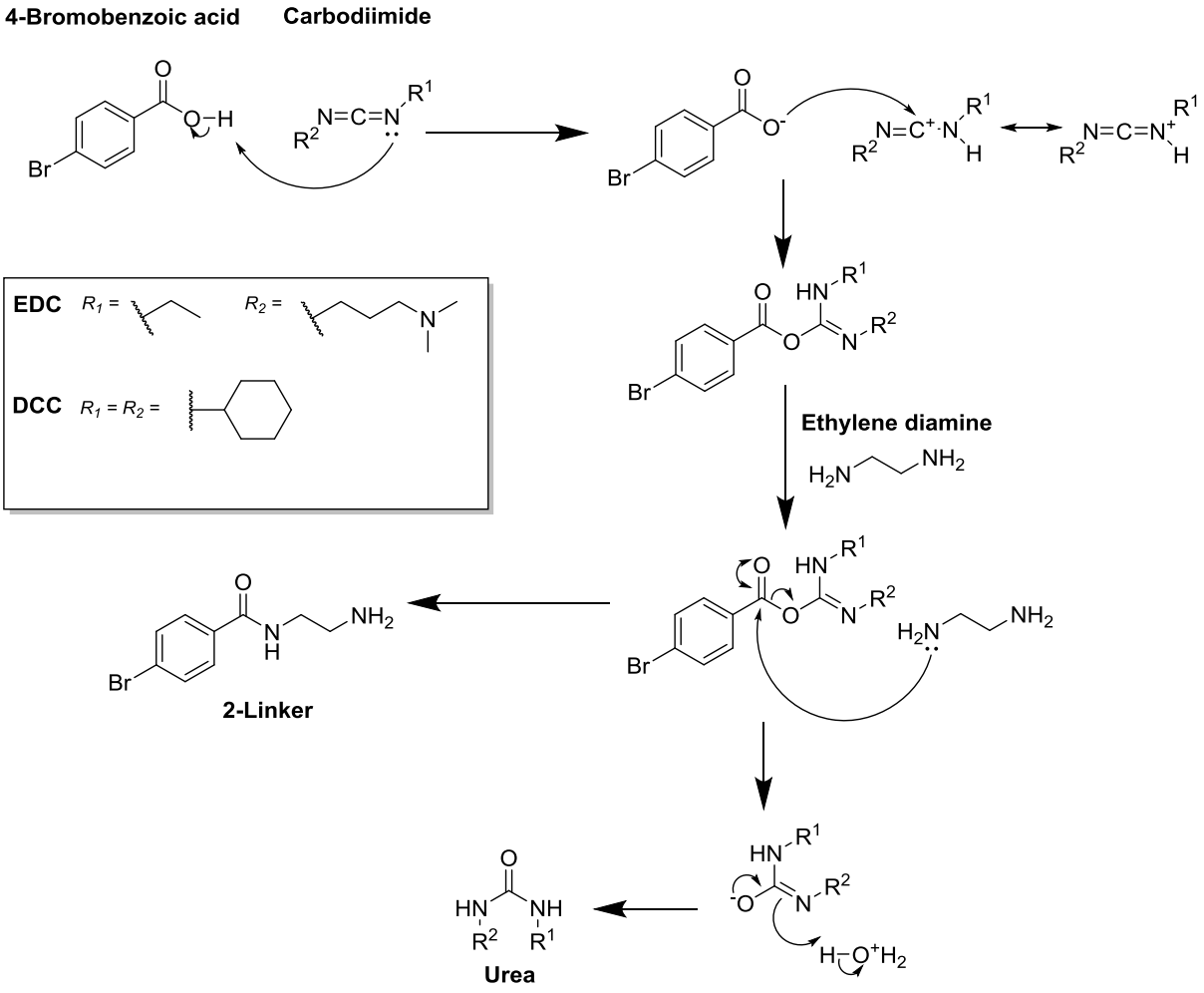

Scheme 10 *Mechanism of carbodiimide coupling between 4-bromobenzoic acid and ethylene diamine to form* ***2-Linker****.*

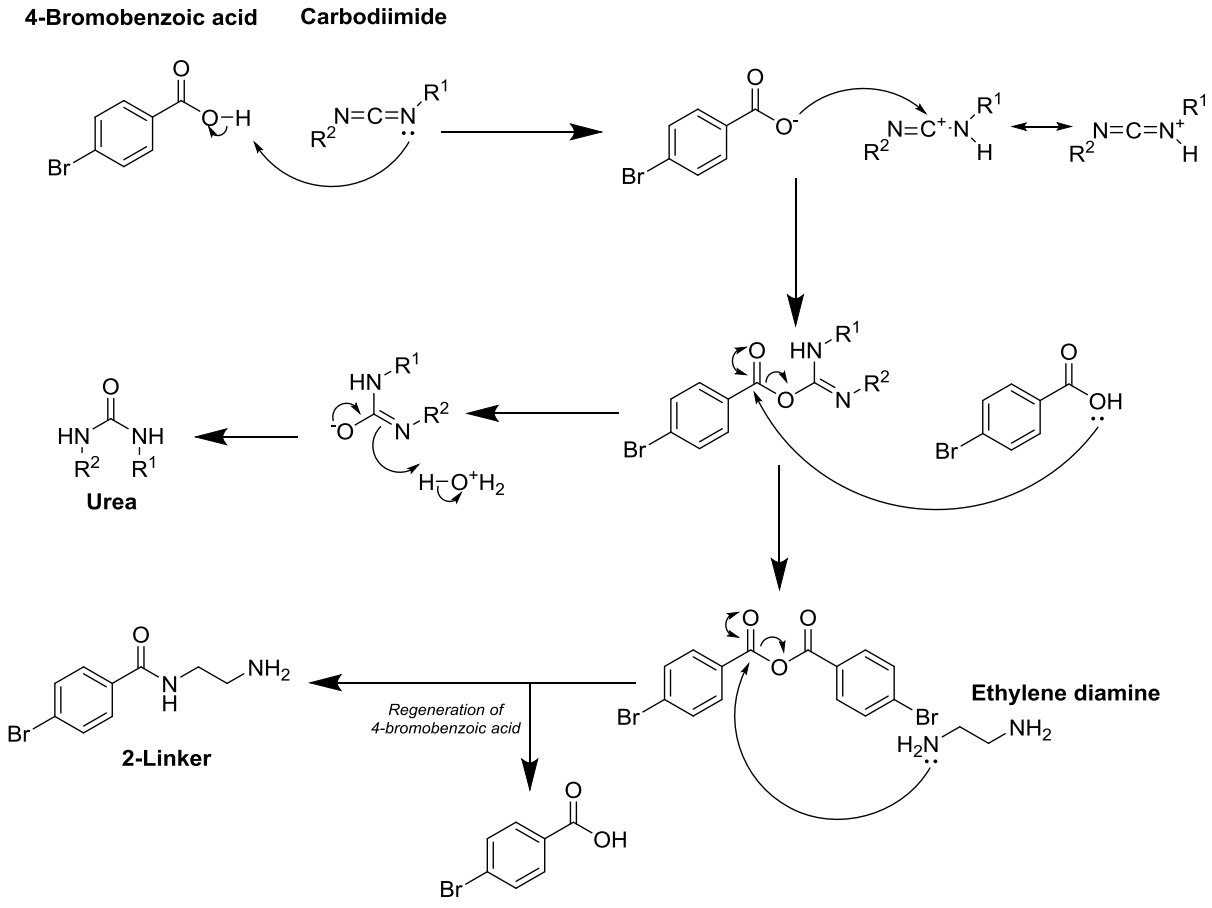

Scheme 11 *The alternative 'side reaction' anhydride mechanism for the carbodiimide coupling between 4-bromobenzoic acid and ethylene diamine to form* ***2-Linker****.*

EDC coupling was originally chosen due to the excellent water solubility of EDC and its corresponding urea side product. This allows for both impurities in the final product mixture, alongside unreacted ethylene diamine, to be easily removed via a water wash. However, through trialling purification procedures it was revealed that **2-Linker** showed pH-dependent solubility in water - whilst it was mildly soluble in basic solutions, it was highly soluble in acidic solutions due to the protonation of **2-Linker**'s free amine. As a result, 5 M NaOH was used to retain **2-Linker** and simultaneously remove ethylene diamine, EDC and its urea, as well as 4-bromobenzoic acid (which is soluble in basic solution as it forms a water-soluble deprotonated salt). However, yields of **2-Linker** were still low (15%), and ^{1}H NMR confirmed that significant trace amounts of EDC Urea were still present in the purified product (**Appendix A9**)**.** Separation of the EDC Urea from the product mixture was not possible using solvent

washes: water, aqueous HCl, methanol, ethanol, and ethyl acetate were trialled to separate these two polar compounds, but none yielded pure **2-Linker**.

Rather than continuing to purify the low yields of the EDC mixture, it was decided that trialling a DCC coupling would be a more effective use of time, as DCC and its corresponding urea are water-insoluble - thus, a 1 M aqueous HCl wash could be used to isolate the product and ethylene diamine from the other components within the product mixture. To separate ethylene diamine from the product mixture, toluene was chosen as a selective solvent for the ethylene diamine. A 5M NaOH wash was used to remove trace amounts of 4-bromobenzoic acid by precipitating the product. However, ^{1}H NMR analysis of the product confirmed that it still contained significant traces of DCC and its corresponding urea (**Appendix A10**), which persisted even after HCl washes (to precipitate the DCC) and DCM washes (to precipitate the product).

Whilst EDC and DCC couplings were unsuccessful in obtaining pure **2-Linker**, the synthesis used by Rafii et. al.[134] to produce *N*-(2-aminoethyl)-4-bromobenzamide (**2-Linker**) offered a promising route to obtain the pure product. Rather than using a coupling agent such as a carbodiimide (and a solvent suitable for both reagents and the carbodiimide), this synthesis utilised ethyl 4-bromobenzoate and ethylene diamine (**Scheme 12**). Ethylene diamine played two roles in this reaction - it was used to amidate ethyl bromobenzoate in a direct nucleophilic attack to produce **2-Linker** and was used as a solvent. Refluxing the reaction at 130 ^{o}C (the boiling point of ethylene diamine) allowed the reaction to be completed after 30 minutes whereupon the product mixture was concentrated under vacuum to remove ethylene diamine. Water washes were then used to remove traces of ethylene diamine and ethanol side product, and a 1M HCl wash used to isolate the *N*-protonated *N*-(2-aminoethyl)-4-bromobenzamide hydrochloride salt (**2-Linker.HCl**) from any unreacted ethyl 4-bromobenzoate.

Recrystallisation from 1:1 ethanol:diethyl ether was then used to ensure a pure product, which was neutralised in 1 M NaOH solution to precipitate **2-Linker**.

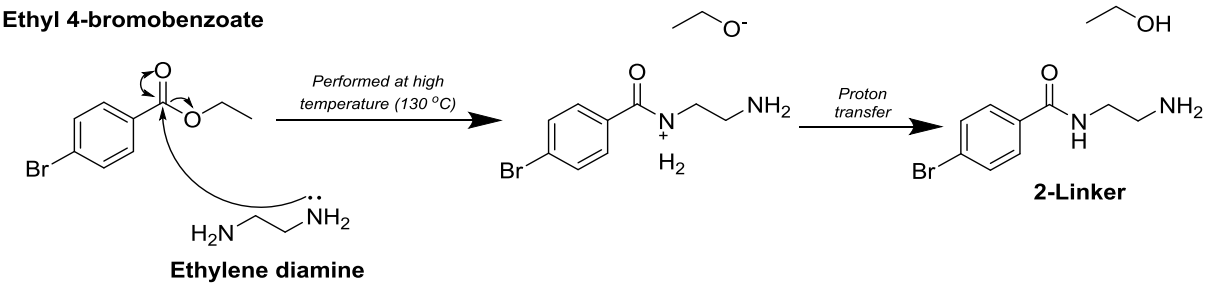

Scheme 12 *The direct amidation of ethyl 4-bromobenzoate with ethylene diamine, performed by Rafii et. al.*

This synthesis was trialled, substituting the ethyl 4-bromobenzoate used in literature for readily available methyl 4-bromobenzoate, and pure **2-Linker** was obtained, however the yield was minimal (0.5%, compared to the literature yield of 50%). This was partly due to the initial water washes to remove ethylene diamine, which also removed large quantities of **2-Linker**. Another possible factor could be the formation of methanol as a side product from methyl 4-bromobenzoate; this is more polar than the ethanol side product produced in the literature procedure and may have enhanced solvation of **2-Linker**, facilitating its removal during water washes. However, concentration of the product mixture under vacuum would have removed most traces of methanol alongside the less volatile ethylene diamine.

The purification procedure was modified and optimised to minimise the use of water. A toluene wash was used to remove ethylene diamine instead of water, and the protonation-deprotonation reaction to form **2-Linker.HCl** was modified to a single basic 5 M sodium hydroxide immersion and wash. This basic immersion was used to convert methyl 4-bromobenzoate to the water-soluble sodium bromobenzoate salt, via nucleophilic attack of hydroxide followed by deprotonation in the strongly

basic environment. This revised procedure produced **2-Linker** in a higher yield of 24%. This was lower than the cited literature yield of 40%, but given the speed of the reaction and purification, and ease of availability of ethylene diamine and methyl 4-bromobenzoate, it was sufficient for this project. ^{1}H NMR (**Figure 28**) confirmed the formation of **2-Linker** in high purity. Further work to optimise this reaction should focus on minimising the use of water washes, for example by using a more selective solvent to isolate **2-Linker** from excess ethyl 4-bromobenzoate.

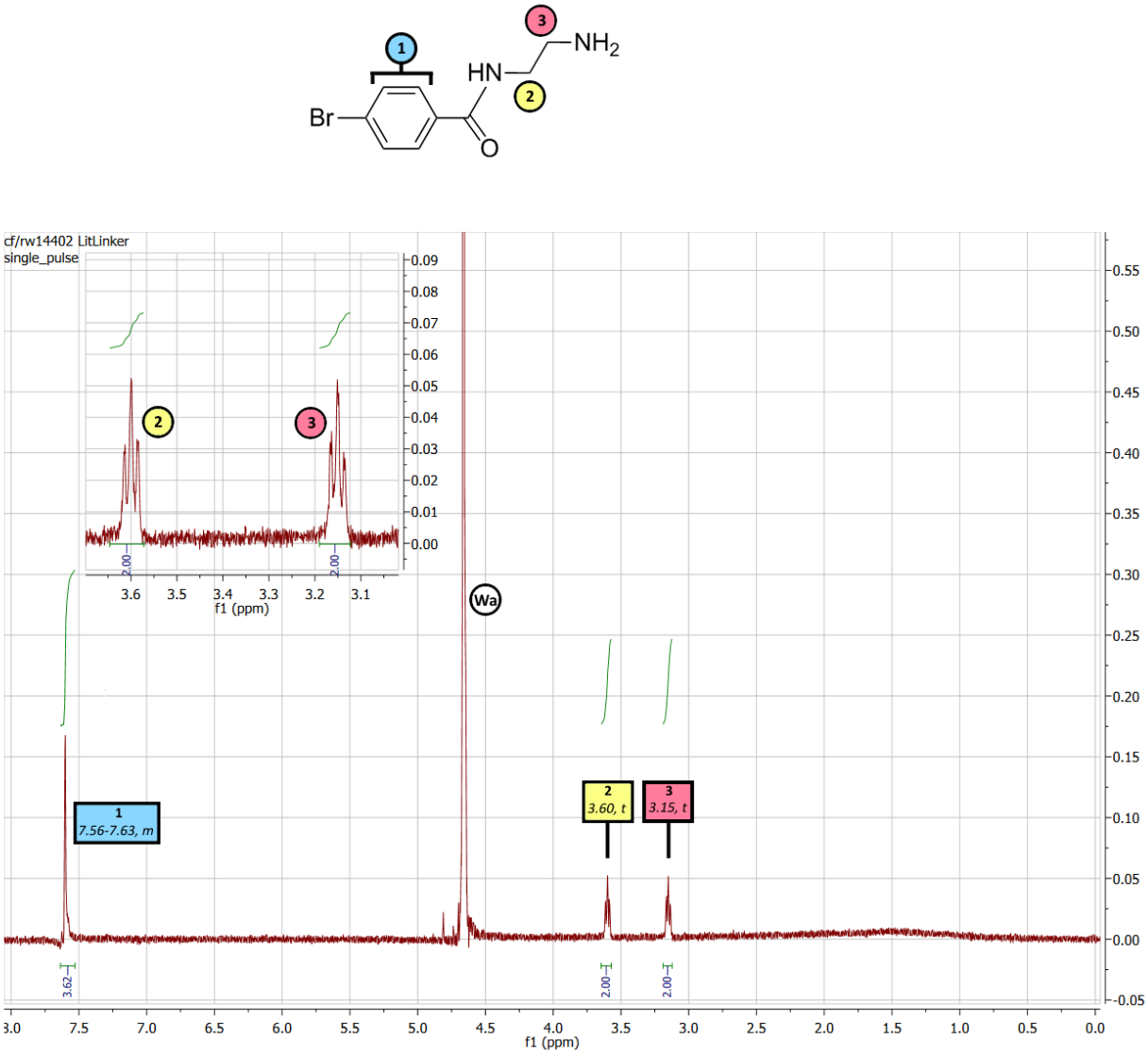

Figure 28 *The ^{1}H NMR spectrum of* ***2-Linker****, with peaks assigned. Impurities are notated as follows: Wa = HDO.*

3.3.2 Synthesis of PDI-2-Linker

To synthesise **PDI-2-Linker**, PTCDA was imidised using **2-Linker** (see **Section 3.2.1** for mechanism). Since **2-Linker** was purified to remove any ethylene diamine and methanol, and the aprotic solvent toluene was used for imidation, no unwanted side reactions were expected from direct imidation. However, the low yields of other perylene imidation reactions trialled in other stages of the project meant that significant excesses of PTCDA and **2-Linker** were expected. PTCDA can undergo two imidation reactions, and singularly imidated PTCDA (i.e. perylene monoimide) was undesirable and difficult to remove (as discussed earlier in **Section 3.2.3**, column chromatography of perylene compounds led to low yield recovery). As such, **2-Linker** was used in a stoichiometric ratio of 4:1 relative to PTCDA (i.e. a twofold excess for the formation of the PDI) to minimise any monoimide product.

The reaction mixture was refluxed for 24 hours - TLC was attempted to monitor the reaction's progress, but aggregation of perylene compounds on the TLC plate prevented any conclusive results. Toluene was removed via rotary evaporation to yield a solid product, which was immersed into 5 M aqueous potassium hydroxide to hydrolyse any remaining PTCDA to the water-soluble perylene tetracarboxylic acid. This yielded a yellow solution, characteristic of dissolved **2-Linker**, which after a minute changed colour to deep brown as PTCDA was produced. Filtration of this solution yielded a black solid, which was washed with aqueous 1 M HCl to remove unreacted **2-Linker** and yield **PDI-2-Linker**. This product was highly insoluble in water and chloroform, so ^{1}H NMR analysis required solution in D_6-DMSO, which confirmed the purity of **PDI-2-Linker** (8% yield).

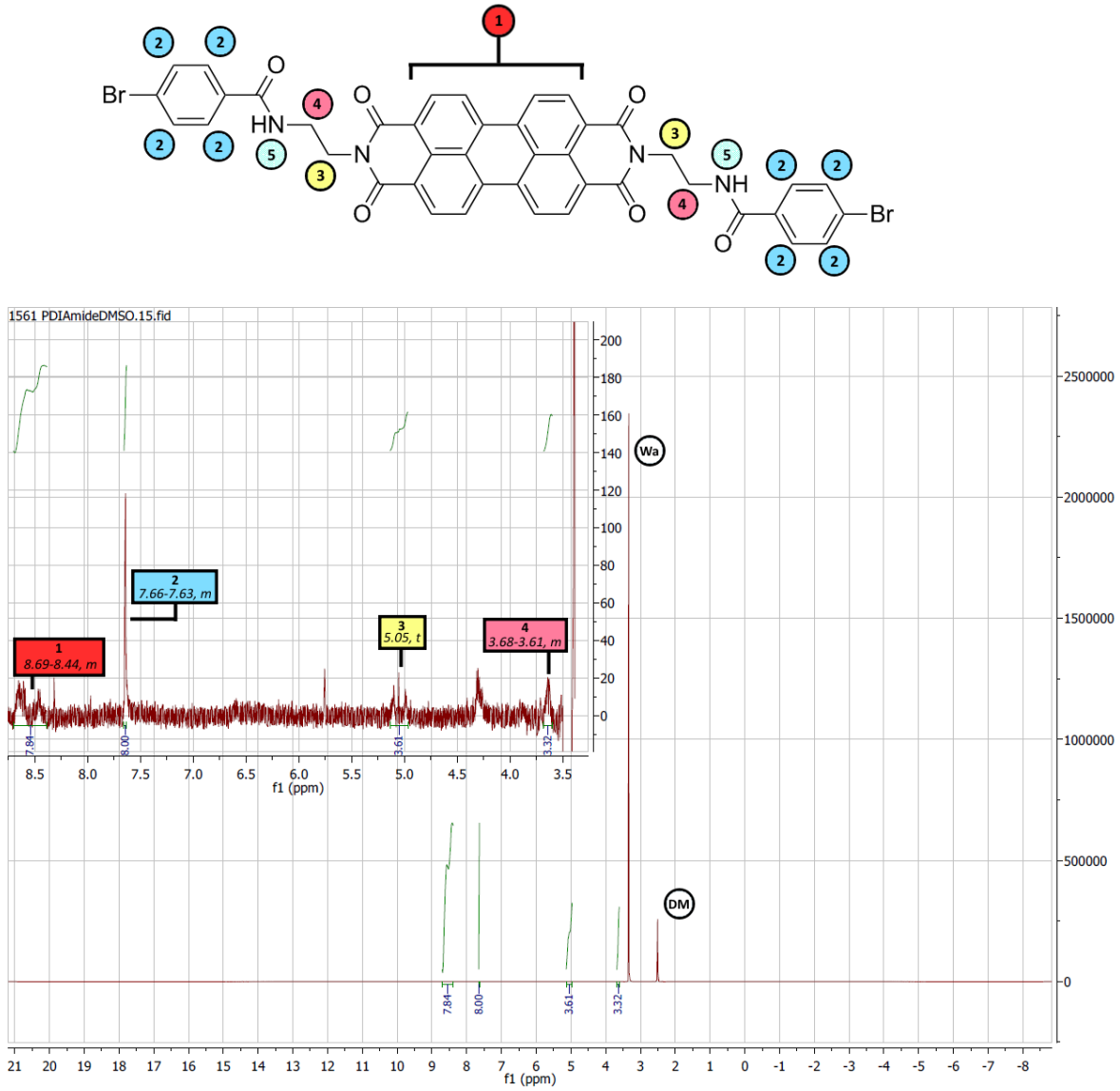

Figure 29 *The ^{1}H NMR spectrum of* ***PDI-2-Linker****, with peaks assigned. Peaks corresponding to hydrogen environment* ***5*** *were not found, and thus this environment is shaded instead of fully coloured in the assignment. Impurities are notated as follows: Wa = HDO, DM = DMSO.*

3.4 Self-Assembly of PDI-2-TANI

Due to the low yields of **PDI-2-TANI** obtained in **Section 3.2.3** precluding oxidation and acid-doping to the desired species **PDI-2-TANI-ES**, the self-assembly experiments discussed hereon focus solely on **PDI-2-TANI**. Whilst the results from this section may give a rough indication as to the nature of self-assembly for **PDI-2-TANI-ES**, the differing intermolecular forces between the two species will have profound effects on their aggregation behaviour. These differing intermolecular forces will arise in **PDI-2-TANI-ES** due to the absence of sterically demanding, organic-soluble Boc groups, the introduction of ionic, acid-doped nitrogen atoms and the electron delocalisation and resulting planarity of tetra(aniline) moieties. As a result, **PDI-2-TANI-ES** may have differing solubilities, aggregate binding strengths and modes of aggregation. However, these factors are predicted to be easily modulated by the wide scope of acid dopants that could be used to create **PDI-2-TANI-ES** (see **Section 5**). As such, the self-assembly of **PDI-2-TANI** serves as a proof of concept that this species can undergo supramolecular polymerisation and add credence to the viability of further research into the self-assembly of **PDI-2-TANI-ES**.

Studies of the self-assembly of **PDI-2-TANI** utilised two solvents - chloroform, in which **PDI-2-TANI** was highly soluble, and ethyl acetate, which readily promoted aggregation of the species. This solvent system was viable over a wide range of concentrations - at room temperature, **PDI-2-TANI** was readily soluble in chloroform in concentrations up to 6×10^{-4} M, whilst it aggregated strongly at this concentration in ethyl acetate (**Figure 30**). When studied using concentration-dependent UV/Vis in **Section 3.4.2**, ethyl acetate promoted aggregation of **PDI-2-TANI** in concentrations as low as 6×10^{-6} M. UV/Vis spectroscopy was used to monitor the aggregation of **PDI-2-TANI** - as discussed in **Section 1.2**, this method is ideal, as both the 0-0, 0-1 and 0-2 electronic transitions of PDIs exhibit peaks in the UV-Visible region.[135] Aggregation of PDIs cause a quenching of the 0-0 electronic transition, and the appearance of a new aggregate peak at higher wavelengths indicative of π-stacking between perylene

cores. In this case, the 0-0 peak exhibited a maximum absorbance at 520 nm, with the aggregate peak visible for **PDI-2-TANI** in ethyl acetate as a shoulder between 540-560 nm. These results corresponded with observations using long-wave (365 nm) ultraviolet light - strong fluorescence was seen at 6 x 10^{-3} M for the chloroform-dissolved **PDI-2-TANI**, but this fluorescence was quenched at this concentration when the sample was dissolved in ethyl acetate, indicating that aggregation occurred in ethyl acetate but not in chloroform.

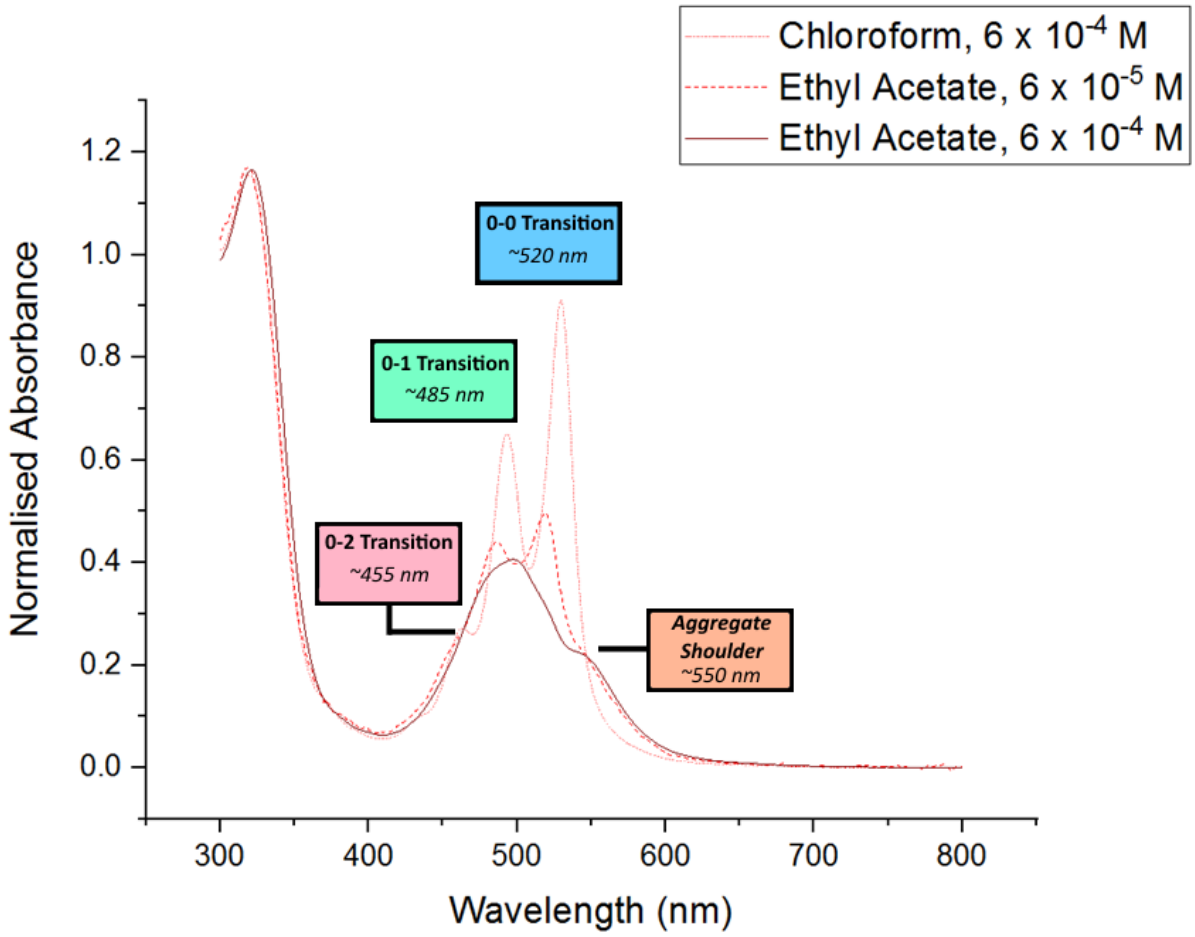

Figure 30 *UV/Vis spectra of preliminary samples of* ***PDI-2-TANI*** *in chloroform and ethyl acetate. Absorbances have been normalised to the peak at 320 nm. Peaks corresponding to the 0-0, 0-1 and 0-2 transitions of* ***PDI-2-TANI*** *are found at 520 nm, 485 nm, and 455 nm respectively.*[135]

To elucidate the structures of the aggregates observed in ethyl acetate, transmission electron microscopy (TEM) was used. TEM was carried out using drop-cast samples of **PDI-2-TANI** on carbon-film coated TEM grids, prepared from 6 x 10^{-4} M and 6 x 10^{-5} M solutions in ethyl acetate. Since these samples were prepared from solid **PDI-2-TANI**, these were pre-heated at 60 ^{o}C for 5 minutes to promote disaggregation of the extended solid structure (the macroscale powder particles) and then aged for 3 hours at room temperature to form nanoscale and mesoscale aggregates. **Figure 31** shows a striking difference between the two samples, with the 6 x 10^{-4} M sample forming large, irregular fibrous bundles ranging from approximately 200-2000 nm in length and width (**Figure 31a, 31b**), whilst the 6 x 10^{-5} M sample formed small anisotropic bundles of several aligned fibres, approximately 100-300 nm in length and <50 nm in width (**Figure 31c**), alongside irregular vesicle-like structures ranging from 50-200 nm in diameter (**Figure 31d**). Fibre widths within these bundles appear to be consistent, with widths at both concentrations judged to be around 4-6 nm. These values are consistent with literature citations for PDIs in X-ray crystallography (around 3-5 nm)[136–138] - thus it is likely that each fibre corresponds to a supramolecular polymer of **PDI-2-TANI**. Further images of these aggregates can be found in **Appendices B1-B8**.

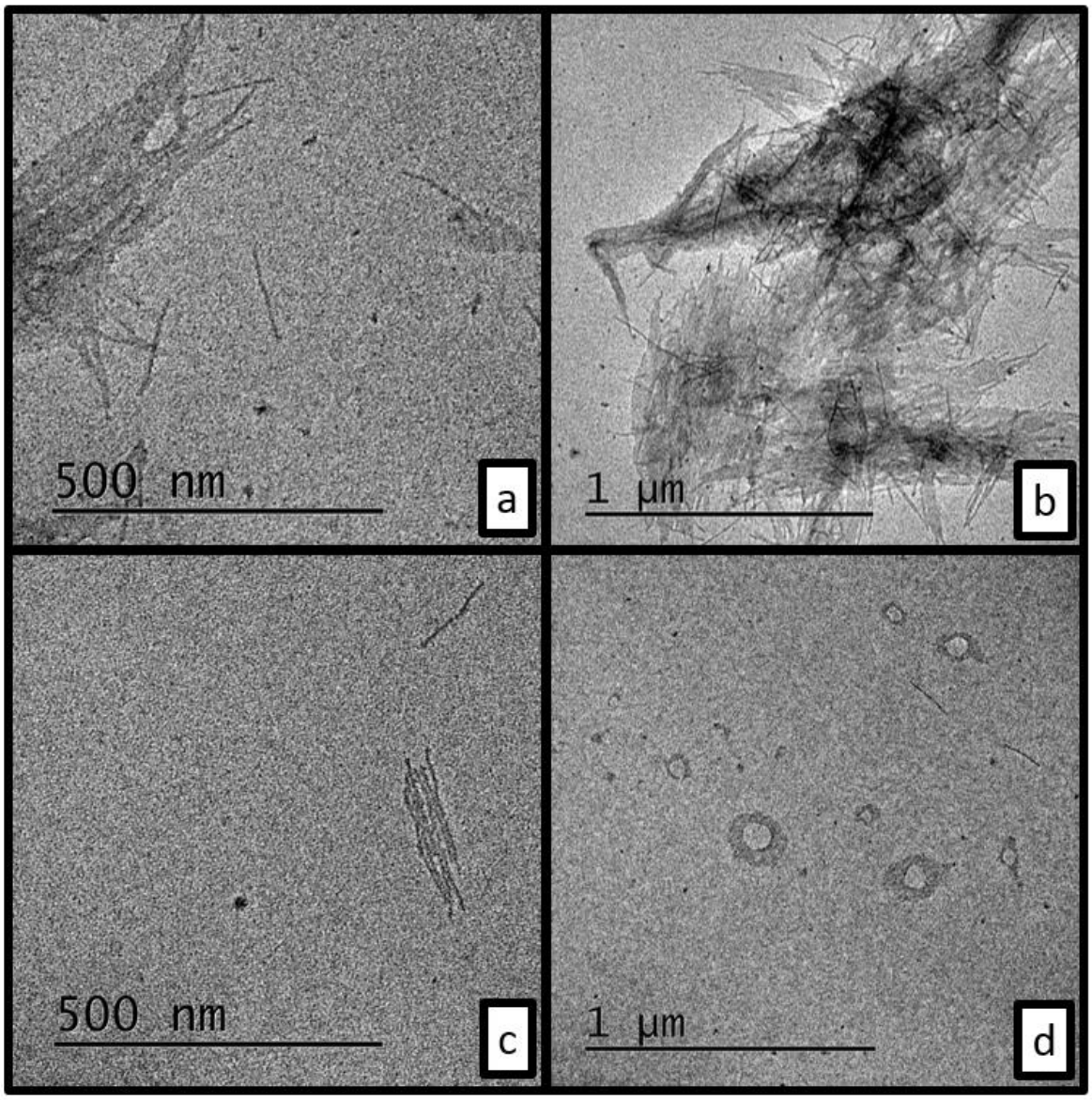

Figure 31 *TEM images of* ***PDI-2-TANI*** *aggregates dispersed in ethyl acetate after heating and cooling, at concentrations of* ***a, b)*** *6 x 10^{-4} M and* ***c, d)*** *6 x 10^{-5} M. Note the irregular vesicle-like structures formed in* ***c)*** *and* ***d)*** *at a 6 x 10^{-5} M concentration.*

Both samples contained populations of solitary fibres (those which do not constitute bundles) - of the 37 fibres observed via TEM at 6 x 10^{-5} M, 16 (43%) were observed as solitary fibres. At 6 x 10^{-4} M, only 12 solitary fibres were observed. Given that the sample at 6 x 10^{-4} M contained several large, irregular aggregates, each consisting of hundreds or thousands of fibres, a rough order-of-magnitude estimate would place the percentage of solitary aggregates at less than 1%. Thus, it is evident that fibre bundles are the preferred morphology for these **PDI-2-TANI** molecules, and that at high concentrations of **PDI-**

2-TANI, these fibre bundles will predominate. This may be due to the fact that these bundles are fragments of a highly ordered, extended solid structure of **PDI-2-TANI**, and at higher concentrations larger fragments are preserved after heating. However, it may also be that these bundles form in-situ from small seed fragments and dissolved unimer, with favourable lateral interactions between fibres promoting the formation of large fibre bundles in a thermal self-seeding process. Some evidence for this second hypothesis can be seen in the large fibre bundles at 6 x 10^{-4} M, whose edges contain many fibres and small bundles which are partly incorporated into the structure (see **Figure 32**).

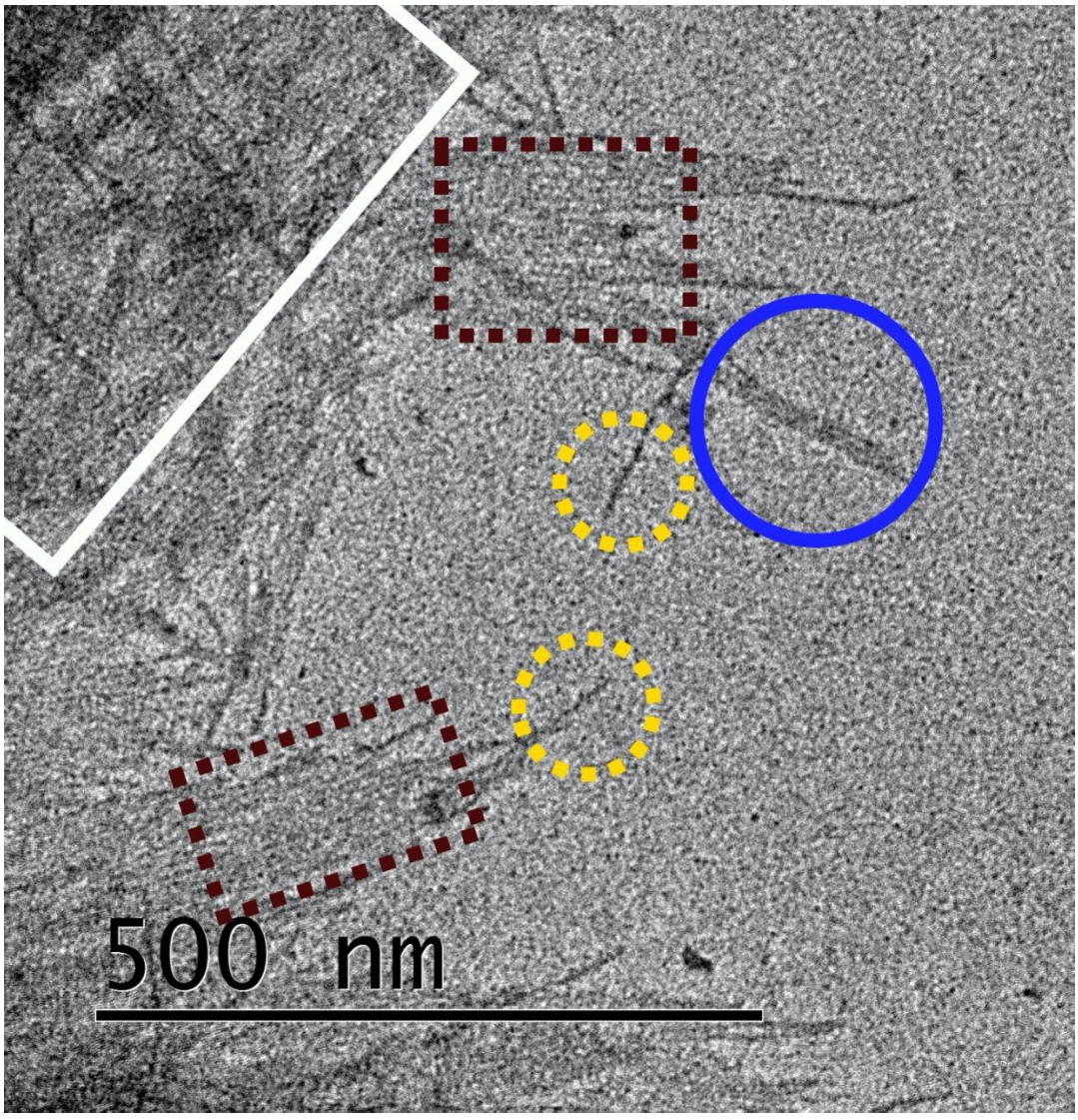

Figure 32 *Different morphologies observed within an extended fibrous bundle of **PDI-2-TANI** in ethyl acetate (6 x 10^{-4} M), visualised by TEM. Yellow dashed circles: partially incorporated 'dangling' fibres. Blue filled circle: a small fibre bundle, similar in scale to those observed at 6 x 10^{-5} M. Brown dashed squares: larger fibre bundles, larger than those observed at 6 x 10^{-5} M, but still anisotropic and two-dimensional (one layer of **PDI-2-TANI**). White filled square: The extended aggregate, comprising of several fibre bundles in multiple, differently aligned layers, with no overall anisotropy.*

Due to the size and complexity of the extended structures present in drop-cast samples of **PDI-2-TANI** at 6 x 10^{-4} M, accurate measurements of fibre lengths could not be carried out. However, the small, single-layer aggregates at 6 x 10^{-5} M, along with the several solitary fibres observed, were suitable for accurate measurement. Length measurements of the 37 supramolecular polymers observed at 6 x 10^{-5} M yielded a narrow distribution, with a number-average aggregate length L_n of 166 nm and a length-average aggregate length L_L of 181 nm, corresponding to a length dispersity ($Đ$, equal to L_L/L_n) of 1.09 (see **Figure 33**). Despite the small sample size, this very low dispersity is very promising for controlled growth experiments. Literature $Đ$ values for seeded and living growth of supramolecular polymers range between 1.1-1.4,[57,58,64] similar to or higher than this experimental value of 1.09. One possible explanation for this low dispersity may be due to the vesicle-like structures formed at this concentration (**Figure 31d**) - since these vesicles were not observed at 6 x 10^{-4} M (**Figure 31a, 31b**), it is possible that these structures are off-pathway aggregates. As the unimer solution was cooled from 60 ^{o}C, it may be that self-seeding behaviour took place, with these off-pathway aggregates providing a metastable source of **PDI-2-TANI**, preventing further seed formation at low temperatures and providing the conditions for a living growth process (see **Scheme 13**). This hypothesis is reinforced by TEM imaging of the 6 x 10^{-4} M solution after room temperature ageing for 2 days, whereupon these vesicle-like structures were absent.

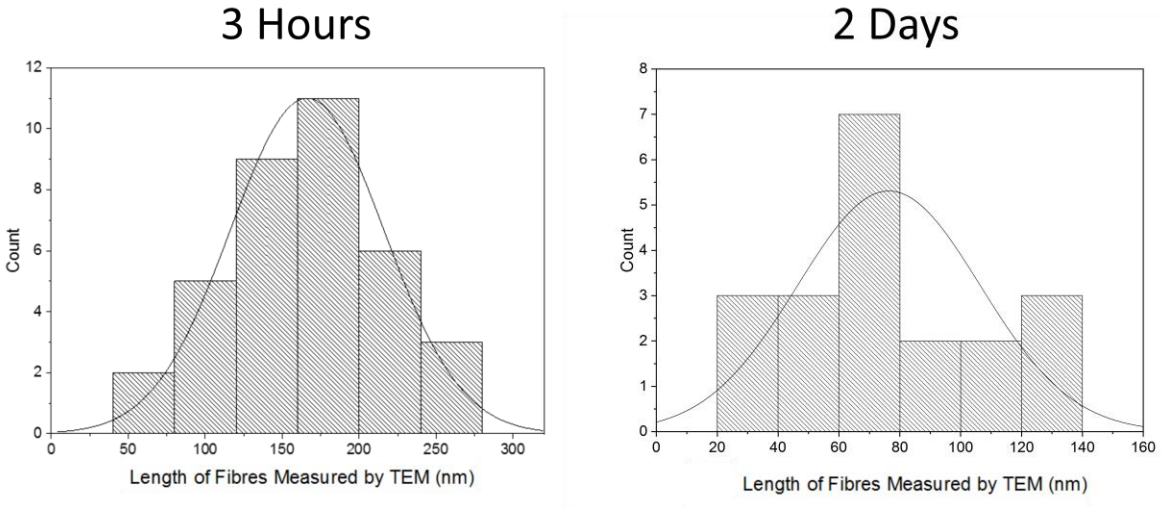

L_n = 166 nm	L_n = 76 nm
L_L = 181 nm	L_L = 87 nm
$Đ$ = 1.09	$Đ$ = 1.15

$$Đ = \frac{\bar{L}_L}{\bar{L}_n} \qquad \bar{L}_n = \frac{\sum i\ N_i L_i}{\sum i\ N_i} \qquad \bar{L}_L = \frac{\sum i\ N_i L_i^2}{\sum i\ N_i L_i}$$

Figure 33 *Fibre length histograms, averages and dispersities for thermally self-seeded* ***PDI-2-TANI*** *in ethyl acetate at 6 x 10^{-5} M. The dispersity Đ is calculated through a number-average (mean) length L_n, and a length-average length L_L, where N_i refers to the number of fibres of length L_i.* [139] *Raw data for these histograms can be found in* ***Appendices B10*** *and* ***B11****.*

Alongside the loss of vesicle-like structures, this room temperature 2-day aged solution contained smaller, more irregular bundles of fibres. Analysis of a sample of 20 discrete supramolecular polymers from these TEM images revealed a significant drop in L_n to 76 nm, and a slightly higher $Đ$ of 1.15. Both the drop in length and increase in $Đ$ indicate that the supramolecular polymers themselves are metastable and degrade as they age - however, they still retain a low dispersity. As such, ageing the solution may be a viable method to precisely control the length of **PDI-2-TANI** supramolecular polymers, but the loss of order within bundles of these polymers provides an additional challenge to isolate and process ordered supramolecular polymers obtained by this method. The appearance of a

film morphology in this 2-day aged solution implies that films may be the thermodynamically stable state in solution, and thus the morphology that the supramolecular polymers convert to.

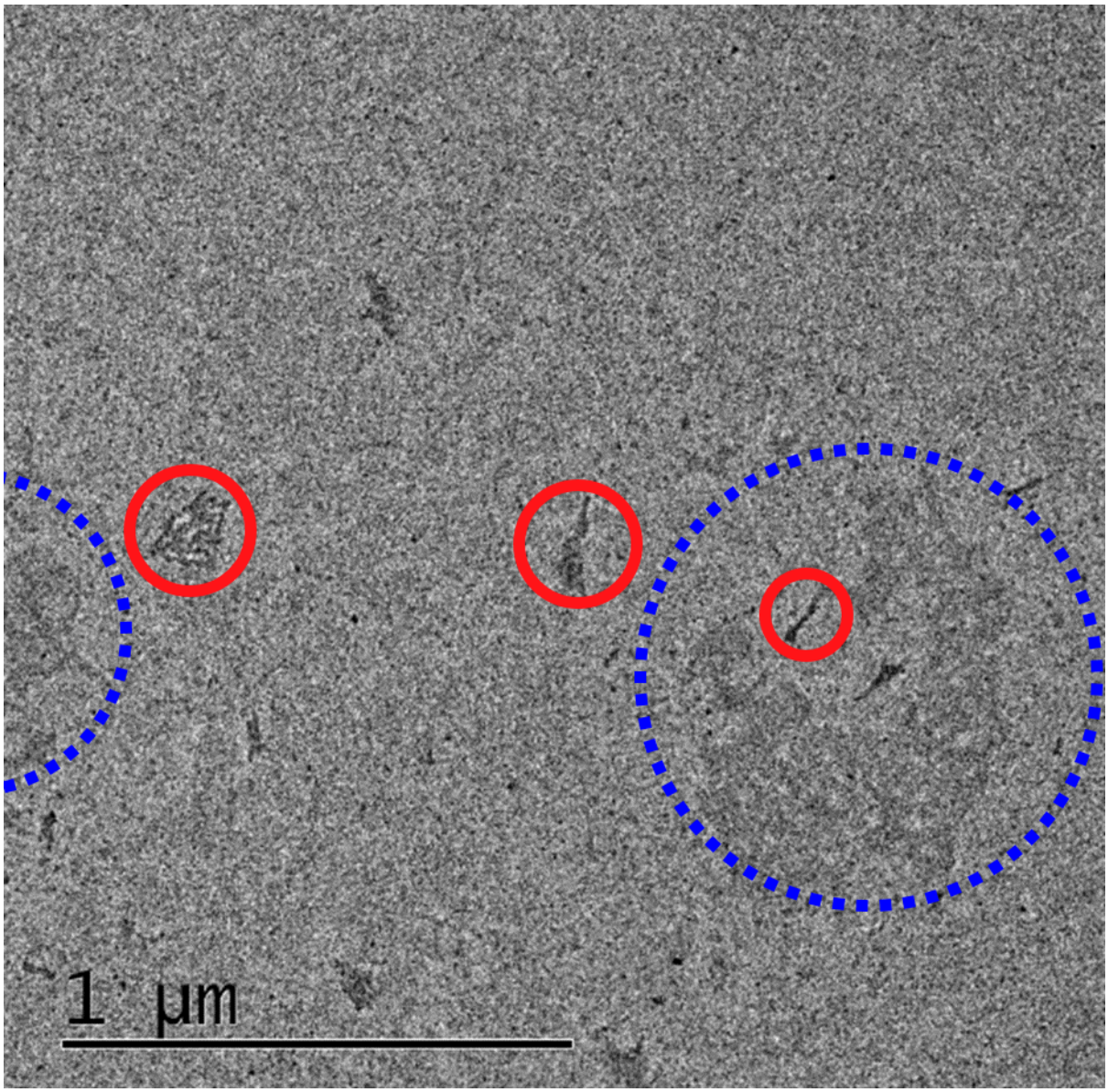

Figure 34 *TEM images of* ***PDI-2-TANI*** *aggregates dispersed in 6 x 10^{-5} M ethyl acetate after thermal self-seeding and being aged for two days. Red solid circles: small, irregular fibre bundles of* ***PDI-2-TANI****. Blue dashed circles: larger, low-contrast film aggregates.*

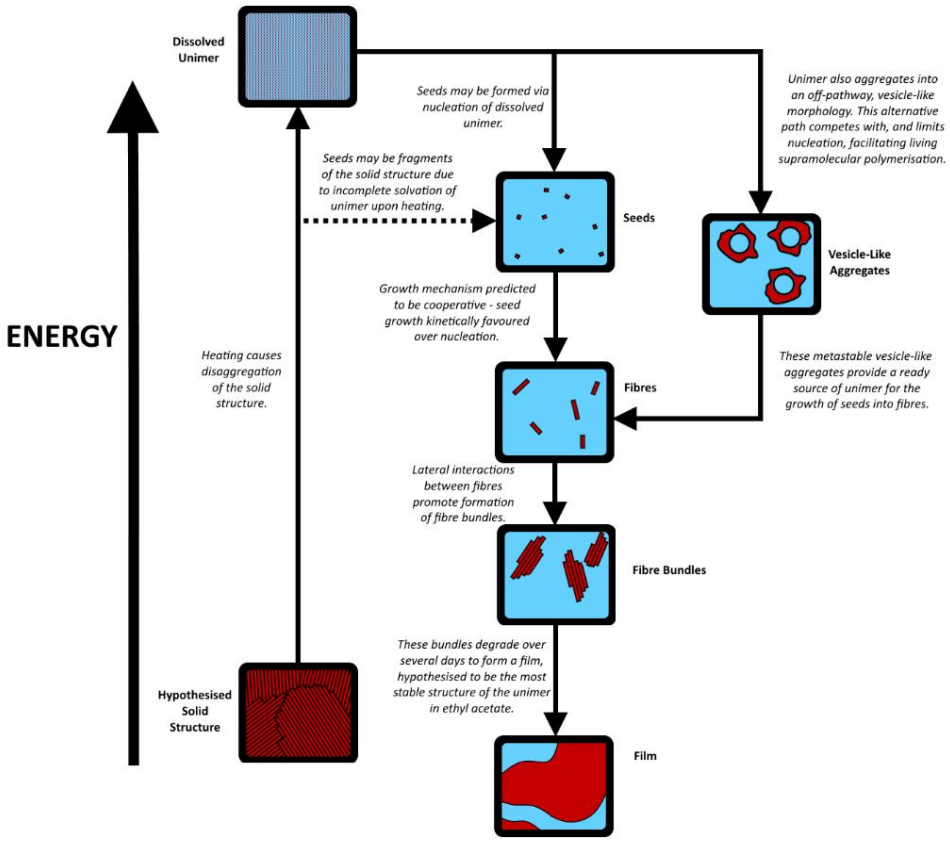

Scheme 13 *Proposed pathways for the thermal self-seeding of* ***PDI-2-TANI*** *in ethyl acetate.*

From these results, a tentative energy landscape for the thermal self-seeding of **PDI-2-TANI** in ethyl acetate can be proposed (**Scheme 13**). A highly ordered, π-stacked solid-state morphology exists in solution at room temperature, confirmed by UV/Vis spectroscopy in **Figure 30**. Heating this solution results in fragmentation of the structure, resulting in several small seeds and free unimer solution. As this solution cools and ages, these seeds form highly monodisperse fibres (**Figure 33**), which in turn readily aggregate to fibrous bundles (**Figure 32**). This low dispersity may be explained by a cooperative growth mechanism and a fixed amount of seeds from the initial heating process - as such this process is termed thermal self-seeding. Low dispersity is also preserved by a kinetically favoured, off-pathway vesicle-like aggregate (**Figure 31d**) which readily forms from free unimer solution, which acts as a source of unimer for the fibres to grow. The fibres themselves are metastable, and after a few days these degrade into the stable film morphology (**Figure 34**).

3.4.1 Temperature-Dependent UV/Vis Spectroscopy

To elucidate the mechanism of self-assembly of **PDI-2-TANI** aggregates in ethyl acetate, temperature-dependent UV/Vis spectroscopy was used. By recording the absorbance of the aggregate shoulder, or the 0-0 transition at 520 nm, the degree of aggregation at different temperatures can be found and fitted to either an isodesmic or cooperative model of growth. Initial temperature-dependent UV/Vis spectroscopy experiments utilised a concentration of 6 x 10^{-5} M, with heating and cooling curves taken at 5 °C intervals (**Figure 35**). Due to the low boiling point of ethyl acetate and the risk of thermal degradation via Boc-group deprotection, temperature-dependent UV/Vis spectroscopy experiments were limited to a maximum temperature of 60 °C. The minimum bound for these studies was either 25 °C (room temperature), or 15 °C (the lowest temperature accessible using the water-cooled UV/Vis spectrometer).

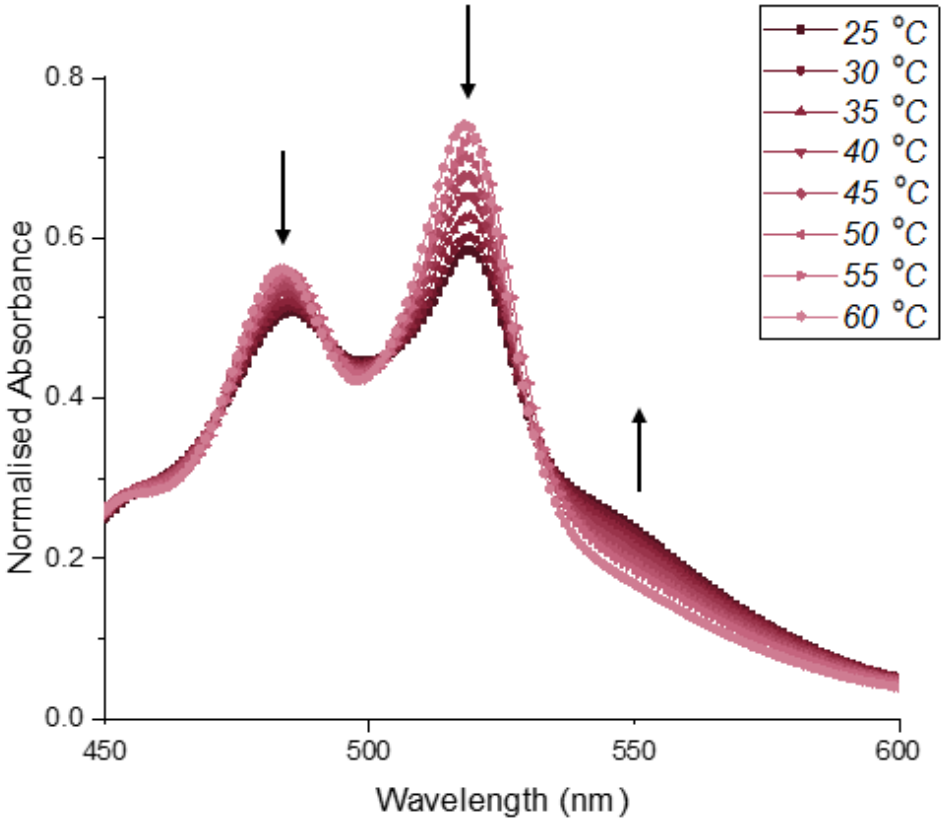

Figure 35 *Temperature-dependent UV/Vis spectra of* ***PDI-2-TANI*** *at a concentration of 6 x 10^{-5} M. Darker lines correspond to the unimer at lower temperature (i.e. higher degrees of aggregation). Arrows indicate the trend in absorption intensity with decreasing temperature.*

To fit the data from these US/Vis spectra to either an isodesmic or cooperative fitting model, values for the degree of aggregation α need to be obtained for each temperature step to create a plot of T vs. α. Since the 0-0 peak and the aggregate shoulder overlap, peak deconvolution was utilised to isolate the aggregate shoulder as an individual peak, from which its area could be used to calculate α (see **Figure 36**). However, using the Origin software's peak deconvolution tool gave a large range of results for the same data set, even when the same peak fitting algorithm (inverse polynomial) with the same number of iterations were used. This range of results corresponded to an error of up to ±25%, making values of α from peak deconvolutions unviable for a conclusive plot of T vs. α.

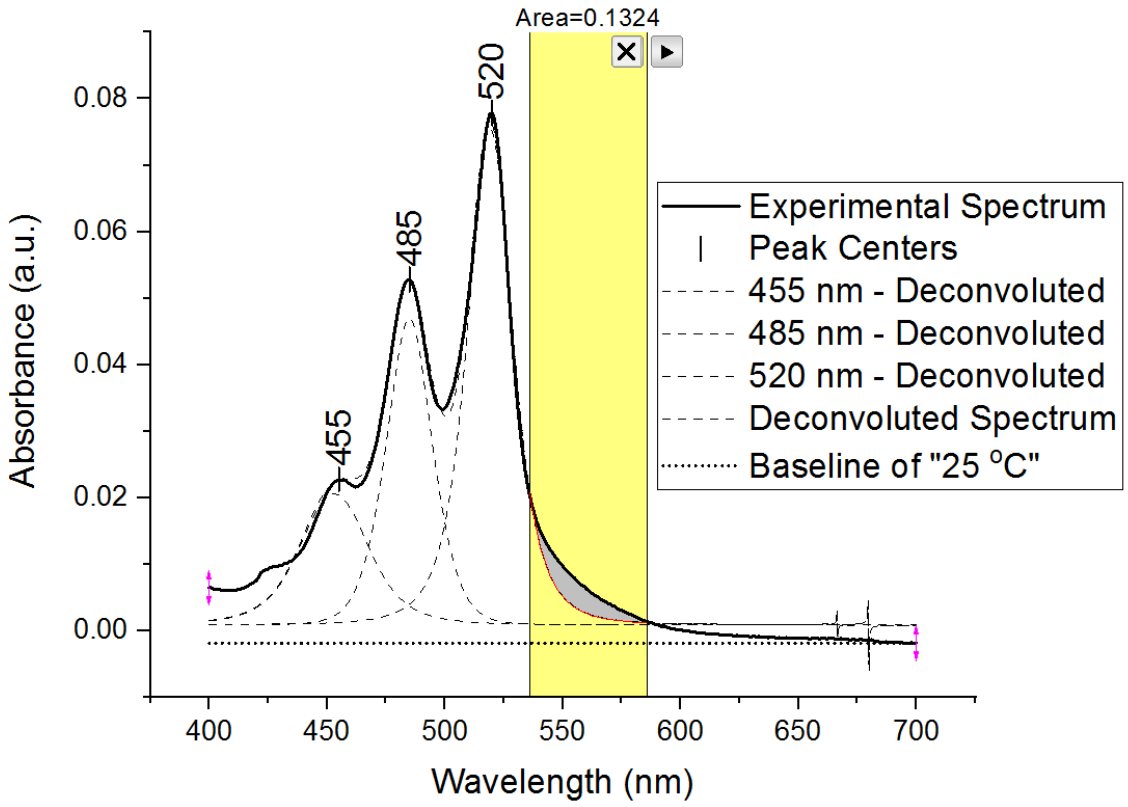

Figure 36 *An example of peak deconvolution performed on* ***PDI-2-TANI*** *at 3 x 10^{-5} M (discussed later). Three major peaks - 520 nm, 485 nm, 455 nm, corresponding to the 0-0, 0-1 and 0-2 transitions respectively were chosen for deconvolution, with the discrepancy between the 520 nm peak and the aggregate shoulder integrated to obtain an area for the aggregate shoulder. Using the same number of iterations of inverse polynomial fitting, other results for this peak area were 0.1657 and 0.1918.*

Instead, peak maxima were chosen to calculate α - this method introduced some systematic error as peaks overlapped, but this error could be minimised by using the intensity of the 0-0 transition peak at 520 nm to find α. Using the 0-0 transition peak should provide accurate data, because isodesmic and cooperative growth mechanisms deviate most significantly at low values of α, where the 0-0 transition peak is high-intensity and the aggregate shoulder is low-intensity. As such, measurements of the aggregate shoulder would give very large systematic errors at low α, whilst measuring the 0-0 transition peak at would only yield marginal increases in α from the low-intensity aggregate shoulder.

Whilst this method could be used to create a plot of *T* vs. α, it is evident from the raw data from UV/Vis spectroscopy that this 15-60 ^{o}C temperature range was insufficient to promote full aggregation (α=1) or disaggregation (α=0) of **PDI-2-TANI** in ethyl acetate. At 60 ^{o}C, a significant aggregate 'shoulder' was still visible at 550 nm, and at 15 ^{o}C, this peak was significantly lower than the aggregate peak seen at 6 x 10^{-4} M in **Section 3.4**, even when normalising these spectra for concentration. Without spectra available for α=0 or α=1, it is impossible to judge which range of α these values correspond to, and as such a plot of *T* vs. the 0-0 transition peak intensity (proportional to 1-α) was created in **Figure 37**. The plot fitted closely to a straight line - this could correspond to regions of either an isodesmic or cooperative model and thus temperature-dependent UV/Vis spectra are inconclusive at this concentration.

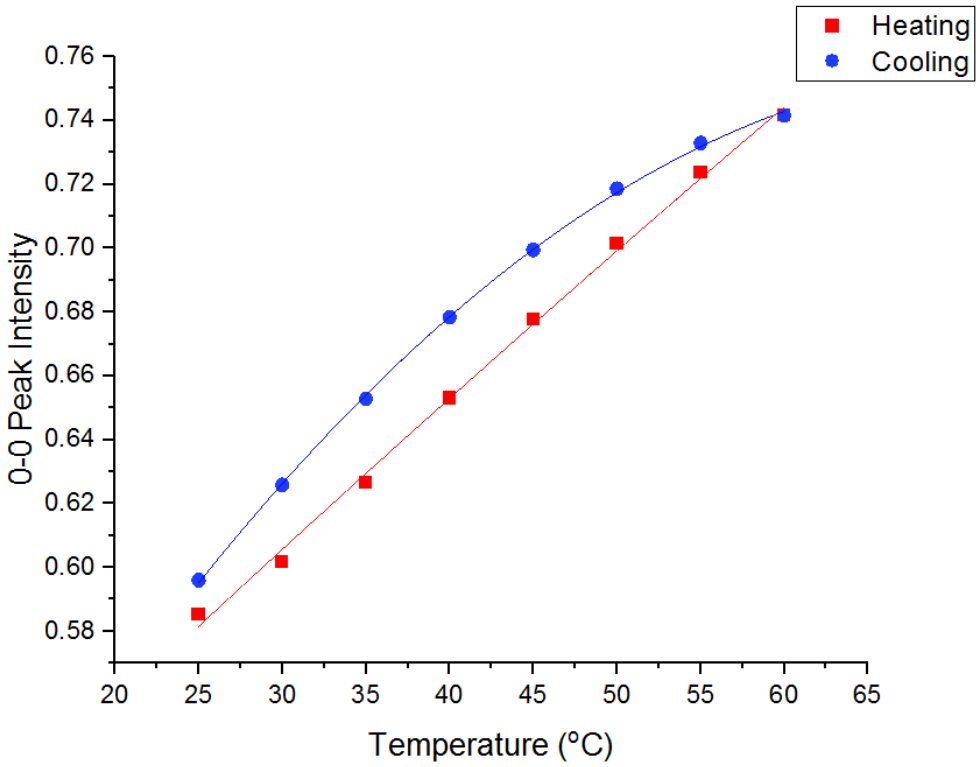

Figure 37 *Plot of temperature vs. 0-0 transition peak intensity using peak maxima obtained from temperature-dependent UV/Vis spectra of 6 x 10^{-5} M* ***PDI-2-TANI****.*

However, two important features were noted from the UV/Vis spectra: a bathochromic shift of the aggregate peak in **Figure 35** indicated that **PDI-2-TANI** formed an H-aggregate in ethyl acetate, and significant thermal hysteresis upon cooling in **Figure 37** indicates that there is some kinetic lag between cooling from high temperatures and formation of π-stacked **PDI-2-TANI** supramolecular polymers. The cause of this kinetic lag is thought to be due to the off-pathway vesicle-like aggregates discussed in **Section 2.4**.

To gain conclusive data for the self-assembly mechanism of **PDI-2-TANI** in ethyl acetate, a solution of 3 x 10^{-5} M was prepared for temperature-dependent UV/Vis spectroscopy. It was thought that this lower concentration be sufficiently disaggregated at 60 °C to elucidate a plot of *T* vs. α for low values of α. Whilst this would not allow a temperature for α=1 to be found and thus still preclude accurate

fitting of cooperative and isodesmic models, it was hoped that the shape of the fitting curve could be qualitatively attributed to either isodesmic or cooperative growth. However, even at this concentration, full disaggregation was not observed - at 60 °C, concordant results for the 0-0 peak were not obtained (**Figure 38**), showing that full disaggregation would only occur at higher temperatures which would risk thermal degradation of **PDI-2-TANI**. As such, the data range for this plot is too narrow to conclude whether isodesmic or cooperative growth is likely.

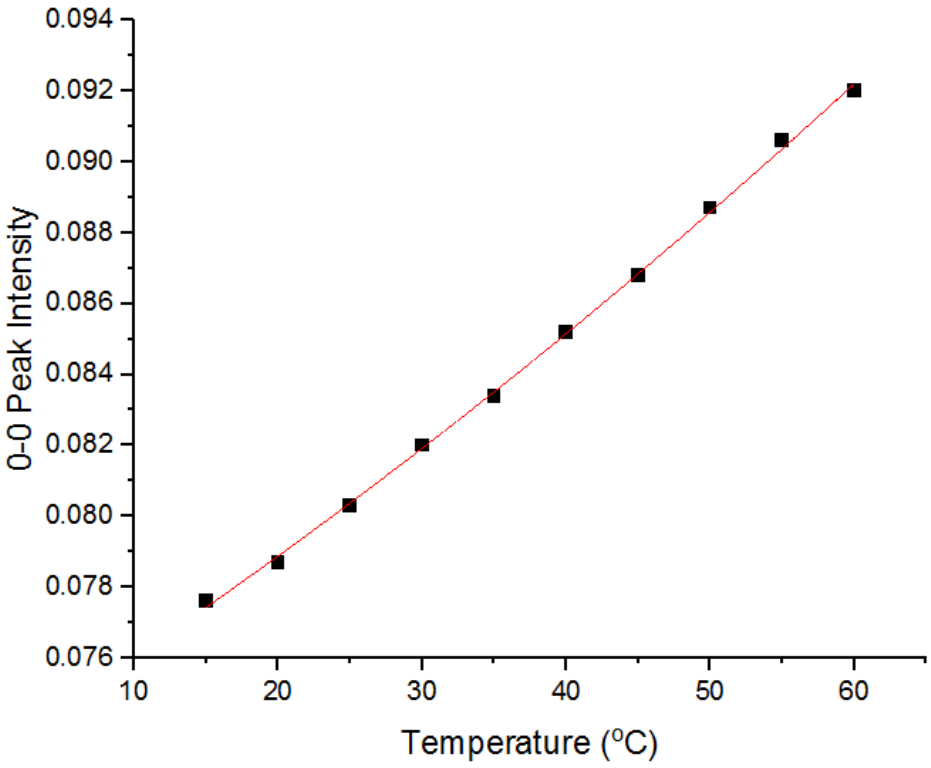

Figure 38 *Plot of temperature vs. unimer peak intensity using peak maxima obtained from temperature-dependent UV/Vis spectra of 3 x* 10^{-5} *M* ***PDI-2-TANI****.*

3.4.2 Concentration-Dependent UV/Vis Spectroscopy

With temperature-dependent UV/Vis spectroscopy giving inconclusive results for the mode of growth of **PDI-2-TANI** in ethyl acetate due to the limited temperature range available, concentration-dependent UV/Vis spectroscopy was trialled as an alternative. Unlike temperature-dependent UV/Vis spectroscopy, the range of spectra obtained via this method was only limited by the resolution of the UV/Vis spectrometer and accuracy of baseline correction, and for these reasons a lower bound was set at 2 x 10^{-6} M was set. Solutions of **PDI-2-TANI** in ethyl acetate were prepared in concentrations ranging from 2 x 10^{-6} M to 6 x 10^{-4} M from a 2 x 10^{-6} M stock which was heated at 60 ^{o}C for 5 minutes to encourage thermal self-seeding, and then left to cool for 3 hours before being analysed by UV/Vis spectroscopy. The temperature-dependent UV/Vis spectra in **Section 3.4.1** contained isosbestic points at wavelengths of 471, 497 and 503 nm, and as such these concentration-dependent UV/Vis spectra could be normalised according to these points to account for the effect of concentration on spectrum intensity. Being closest to the 0-0 transition at 520 nm, the 503 nm isosbestic point as chosen to normalise these spectra, resulting in **Figure 39**. From the 0-0 transitions in **Figure 39**, a plot of normalised intensity (proportional to 1-α) vs. $\log_{10}$ [**PDI-2-TANI**] could then be plotted (**Figure 12**), as discussed in **Section 3.4.1**. A logarithmic scale for concentration was chosen as it yields analogous results to the linear temperature scales used in temperature-dependent UV/Vis spectra - this scale was used by the Würthner group to yield sigmoidal plots for isodesmic growth models.[15]

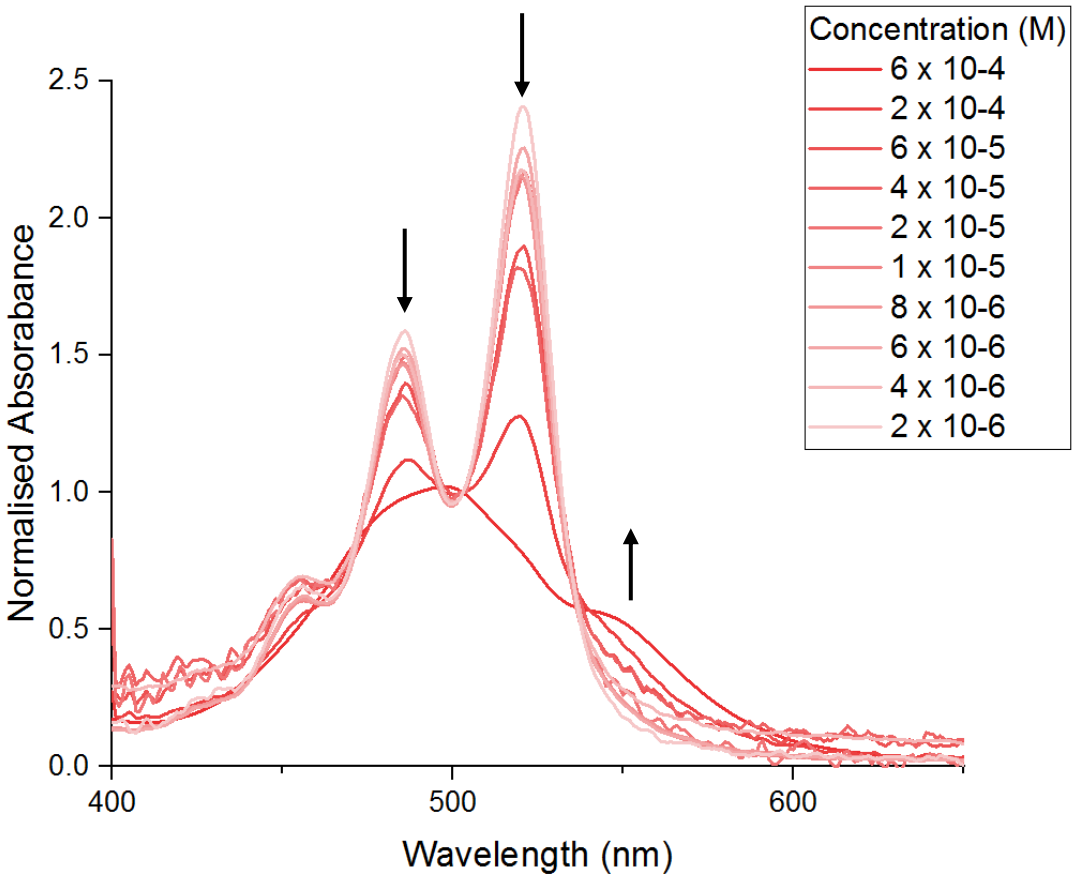

Figure 39 *Isosbestic normalised UV/Vis spectra of* ***PDI-2-TANI*** *at various concentrations. Arrows indicate the trend in absorption intensity with increasing concentration.*

Whilst this concentration range was not large enough to gain data for α=1 and α=0 and thus mathematically fit to isodesmic or cooperative models, a large enough data range was collected to qualitatively examine the concentration-dependent aggregation behaviour of thermally self-seeded **PDI-2-TANI**. With no clear critical aggregation concentration (which would be represented by a sudden drop in 0-0 peak intensity as aggregation occurred) visible in **Figure 40**, it is likely that the growth mechanism is isodesmic. As such, the smooth curve in **Figure 40** is likely to be part of a sigmoidal curve, characteristic of an isodesmic growth model.

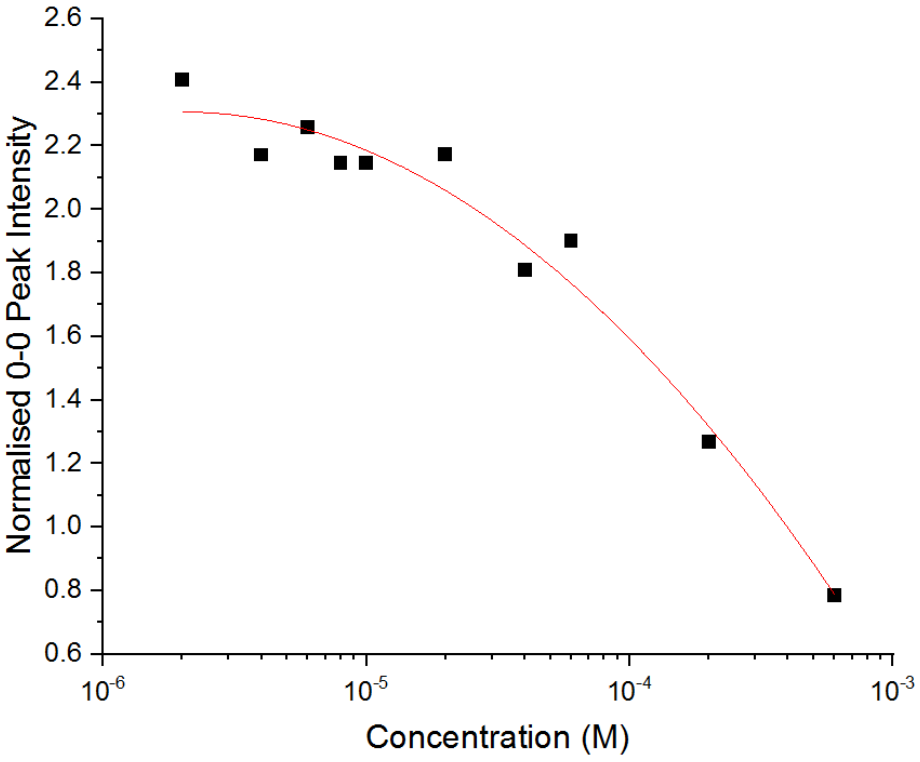

Figure 40 *Plot of concentration vs. normalised 0-0 peak intensity using peak maxima obtained from concentration-dependent UV/Vis spectra of thermally self-seeded* ***PDI-2-TANI****.*

3.4.3 Seeded Growth Via Sonication

Seeded growth experiments were trialled to confirm the growth mechanism of **PDI-2-TANI** (which appeared from results in **Section 3.4.2** to be isodesmic) and evaluate the unimer's potential for living supramolecular polymerisation (which would prove the initial expectation of cooperative growth). These experiments consisted of adding a fixed ratio of **PDI-2-TANI** seeds, prepared through sonication of solid **PDI-2-TANI** in ethyl acetate for 5 minutes. It was thought that since the seeds described in thermal self-seeding (**Section 3.4**) are fragments of a fibrous solid structure, sonication of solid **PDI-2-TANI** would obtain the same fibrous morphology as thermal self-seeding. Chloroform-dissolved **PDI-2-TANI** was then added as a source non-aggregated unimer. The high solubility of **PDI-2-TANI** in chloroform allows it to remain disaggregated at concentrations as high as 3 x 10^{-3} M, meaning that seeded growth experiments could be carried out at 6 x 10^{-5} M with a 1:50 (v/v) chloroform:ethyl

acetate mixture, closely approximating the pure ethyl acetate solution used in **Section 3.4, 3.4.1** and **3.4.2**. These solutions were then left to age for 3 hours for seeded growth to occur.

Seeded growth experiments utilising this method produced no discernible fibres - instead, TEM revealed the assembly of irregular assemblies in the drop-cast solutions of both seeds and the 1:1 seed:unimer ratio solution (see **Figure 41b, 41c** respectively, and **Appendices B12-B16**). Whilst the small change in solvent quality from the addition of chloroform may have had an effect on the assemblies of the mixed solutions, it is evident from the morphology of the seeds that sonication of room-temperature **PDI-2-TANI** in ethyl acetate could not produce suitable seeds for the growth of fibres. These results bring into question whether the ordered fibres formed from thermal self-seeding are fragments of the solid-state structure of **PDI-2-TANI**, as proposed in **Section 3.4**. TEM images of dispersed **PDI-2-TANI** in ethyl acetate before sonication (**Figure 41a**) revealed that this is not the case - ordered fibrous assemblies were not seen and instead films and irregular vesicle-like assemblies predominated.

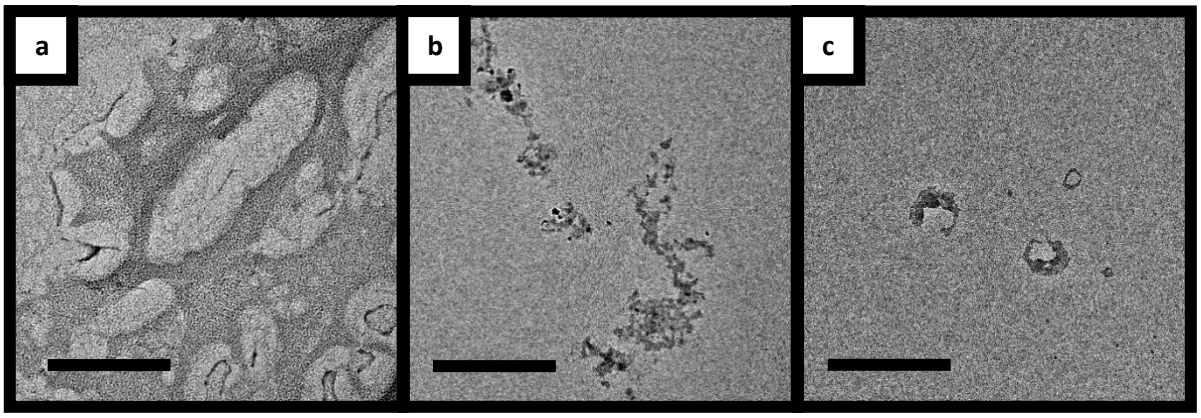

Figure 41 *Morphologies of* ***PDI-2-TANI*** *obtained via seeded growth at room temperature, in 1:50 (v/v) chloroform:ethyl acetate. Viewed are* ***a)*** *pre-sonicated* ***PDI-2-TANI b) PDI-2-TANI*** *after sonication for 5 minutes, and* ***c)*** *seeded growth of* ***PDI-2-TANI*** *using a 1:1 seed:unimer ratio. Scale bars are 500 nm.*

The absence of ordered fibrous assemblies for the pre-sonicated **PDI-2-TANI** implies that the fibres obtained from thermal self-seeding behaviour in **Section 3.4** are formed in-situ rather than being fragments of solid **PDI-2-TANI**. Given that these fibres are metastable, it appears that these fibres are in fact out-of-equilibrium self-assemblies, requiring heat to form. The thermodynamically stable state of **PDI-2-TANI** in ethyl acetate is a film - this was seen in both the thermally self-seeded **PDI-2-TANI** in **Section 3.4** and in the pre-sonicated unimer in **Figure 41a**. Furthermore, from the preliminary UV/Vis spectrum of dissolved **PDI-2-TANI** in ethyl acetate in **Section 3.4**, it is evident that this film morphology contains strong π-π interactions and exhibits a sharp aggregate peak, ruling out the possibility that this film is simply unaggregated unimer. As such, this film aggregate is the preferred mode of aggregation for **PDI-2-TANI** in ethyl acetate, with the fibre and vesicle-like morphologies viewed in **Section 3.4** only accessed via the heating-cooling process of thermal self-seeding.

One plausible explanation for this behaviour may be that the conformational energy minimum of **PDI-2-TANI** results in intramolecular hydrogen bonding between amide nitrogen and imide carbonyl moieties, a phenomenon noted in an analogous PDI by the Würthner group.[63] Their findings noted that intramolecular hydrogen bonding and subsequent folding of their PDI unimer was enthalpically favourable but entropically unfavourable, resulting in this folded conformation occurring within a limited temperature range. In their work, folding of the PDI resulted in no π-stacking, but **PDI-2-TANI** as a dissolved solid, in its film morphology, exhibits strong π-stacking. However, since these films do not have any long-range anisotropy like the fibres in **Section 3.4**, it is evident that extended π-stacking (i.e. the formation of a π-stacked supramolecular polymer) does not occur. Thus, a conformational change in **PDI-2-TANI** from a folded to an extended state drives supramolecular polymerisation and the formation of extended π-stacked fibres, whilst the folded **PDI-2-TANI** forms π-stacked films, possibly containing inactive **PDI-2-TANI** dimers (**Scheme 14**).

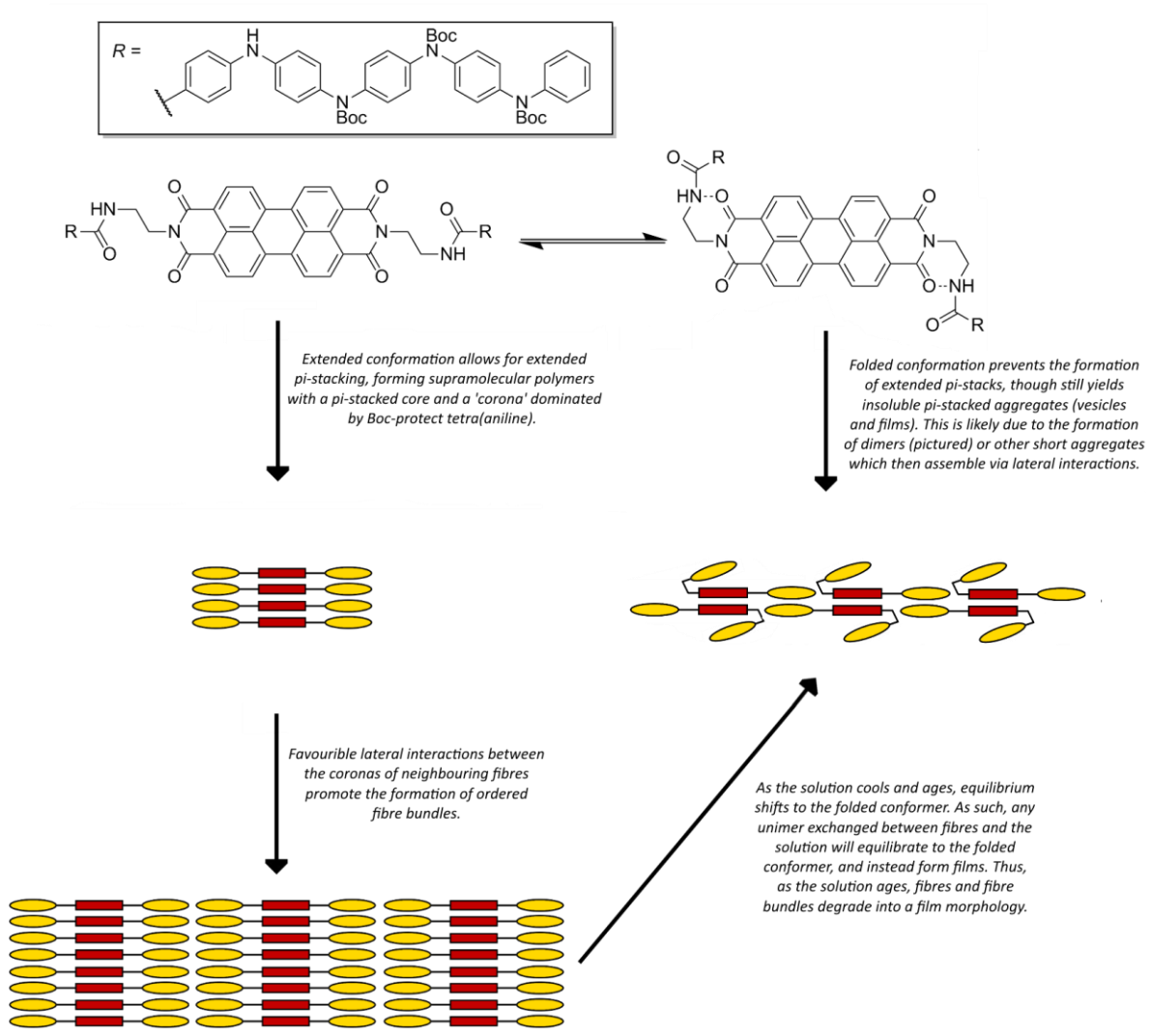

Scheme 14 *Diagram showing how fibre and film morphologies may arise from the conformation of* ***PDI-2-TANI****.*

This hypothesis would explain why the π-stacked fibres viewed in **Section 3.4** can only be accessed through thermal self-seeding - a large activation energy is required to break these intramolecular hydrogen bonds and change conformation, thus dissolving the stable film morphology and instead promoting supramolecular polymerisation of metastable ordered fibres. Inside these fibres, the extended conformation of **PDI-2-TANI** creates an ordered π-stacked perylene core and an extensive tetra(aniline) corona with several hydrophobic Boc groups, promoting a second stage of self-assembly, fibre bundling, to optimise lateral interactions between the coronas of fibres. As these fibre bundles then cool and age at room temperature, they then degrade to the film morphology as **PDI-2-TANI**

molecules revert back to the folded state. This reversion may be due to unimer exchange - as unimer is expelled from the fibres during exchange, it undergoes a conformational change to the folded state in the ethyl acetate solution, 'deactivating' it and preventing its reincorporation into the fibres. As such, this folded unimer then aggregates to generate the stable film morphology.

Regarding the vesicle-like assemblies viewed in **Figure 41a**, these were more disordered than those seen in **Section 3.4**, ranging from 30 nm to over 400 nm in diameter and often only partially formed. Interestingly, these vesicle morphologies, whilst absent after sonication, re-form upon addition of unimer solution, as seen in **Figure 41c**. The rapid regeneration of this morphology confirms that the vesicle-like structures viewed in pre-sonicated **PDI-2-TANI** (**Figure 41a**) are an intermediate, metastable aggregate, readily forming in-situ from dissolved unimer before the film morphology. It also shows that this aggregate is not part of the thermal self-seeding pathway as it can be accessed at room temperature through sonication and the addition of chloroform-dissolved unimer. Thus, the vesicle-like structures may arise from dissolved, folded conformation unimer, as opposed to the extended conformation unimer which gives rise to ordered fibres. Their appearance after thermal self-seeding (in **Section 3.4**) may be ascribed to the fact that the thermal self-seeding process does not eliminate populations of folded conformation **PDI-2-TANI**, it only shifts the equilibrium towards extended conformation **PDI-2-TANI**.

If this theory is correct and extended π-stacking of **PDI-2-TANI** only occurs at high temperatures it also brings into question the validity of temperature-dependent and concentration-dependent UV/Vis spectroscopy (**Section 3.4.1** and **Section 3.4.2**). Temperature-dependent UV/Vis spectroscopy would be unviable for probing the growth mechanism of **PDI-2-TANI**, as supramolecular polymerisation to form fibres requires a critical temperature to form enough open-conformation unimer, otherwise films form. Since both fibres and films contain π-stacked **PDI-2-TANI** and exhibit aggregate peaks, this

critical point would be indistinguishable using spectroscopic techniques (e.g. UV/Vis spectroscopy or fluorescence quenching). However, utilising concentration-dependent UV/Vis spectroscopy at high temperature (i.e. 60 ^{o}C) may be viable to probe the self-assembly of fibres in isolation, since at these temperatures extended conformation **PDI-2-TANI** would predominate.

With the growth mechanism of **PDI-2-TANI** undetermined, and vesicle-like assemblies ruled out as a probable source of inactive unimer for a living growth process, the low dispersities for fibres of **PDI-2-TANI** must still be accounted for. However, this hypothesis of extended and folded conformation unimer provides a promising route to living supramolecular polymerisation of **PDI-2-TANI**, bearing a striking resemblance to Aida's work on the living polymerisation of substituted corranulenes. These corranulenes self-assembled via a cooperative mechanism, with folded, inactive unimers that could not undergo seeding but could add to existing fibres by extending their conformation.

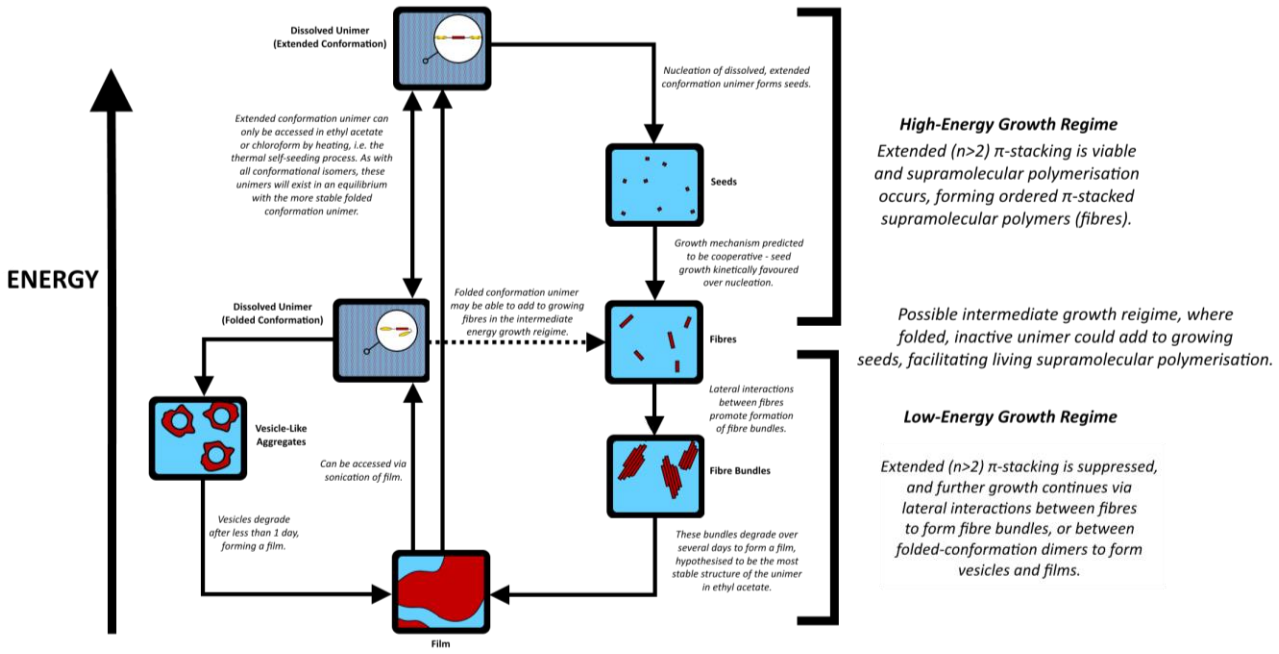

Scheme 15 *A revised energy pathway diagram, illustrating the path-dependence of the morphologies observed, and highlighting three main growth regimes occurring at different temperatures.*

A similar process could be governing the growth of **PDI-2-TANI** fibres, with three main growth regimes outlined (**Scheme 15**). The first is a high-energy regime, accessible via thermal self-seeding, where extended-conformation **PDI-2-TANI** predominates, favouring the formation of π-stacked fibre seeds. The second is a low-energy regime where **PDI-2-TANI** adopts a folded conformation, suppressing extended π-stacking, so lateral interactions lead to the formation of vesicles, films, and the bundling of any fibres formed in the high-energy regime. Finally, a hypothesised intermediate-energy regime may exist - a timeframe during the cooling period of thermal self-seeding where folded conformation **PDI-2-TANI** can overcome a kinetic barrier to add to existing seeds and fibres, but is not energetic enough to form solvated open-conformation **PDI-2-TANI** to create new seeds. A key part of this hypothesis is the assumption that cooperative growth does occur in the high-energy regime, thus the addition of closed-conformation **PDI-2-TANI** to growing fibres is kinetically favourable to self-nucleation. However, this hypothesis would explain how thermal self-seeding affords such low dispersities for fibres, and why it is required in the first place to initiate supramolecular polymerisation as opposed to film formation.

3.4.4 Seeded Growth Via Thermal Self-Seeding

As discussed in **Section 3.4.3**, thermal self-seeding is required to access the fibrous morphology whereby **PDI-2-TANI** assembles into supramolecular polymers. As such, a new method of seeded growth was developed - seeds would be prepared and aged using the same heating-cooling and 3-hour ageing method discussed in **Section 3.4** before being aged for 2 days and then sonicated for 5 minutes. Unimer solution would then be added to these sonicated seeds to promote growth. Form **Section 3.4.3**, it was postulated that the **PDI-2-TANI** unimer needed to be in an extended conformation to form extended π-stacks - as such, this unimer solution needs to be pre-heated in ethyl acetate. This method is viable due to the cooling hysteresis found in **Section 3.4.1** - if a 60 ^{o}C ethyl acetate solution of **PDI-2-TANI** is added immediately, the predominant morphology found within the solution should be dissolved, extended conformation unimer. Seed formation within this unimer solution should be minimal, preserving the conditions for living growth. Seed:unimer ratios of 1:1, 1:3 and 1:5 were trialled, and the solutions were left to age for another 3 hours after mixing. This time should be sufficient for unimer to be incorporated into the fibrous seeds, whilst minimising degradation of the metastable fibres formed.

As expected, TEM revealed the formation of fibrous aggregates for the thermally self-seeded solution, concordant with the results from **Section 3.4**. Irregular vesicle-like aggregates were largely absent from the mixture, and a large film with 50-200 nm pores was found similar to the stable morphology observed in the aged solution in **Section 3.4** and the non-thermally self-seeded solution in **Section 3.4.3**. These results closely correlate with those for the aged solution in **Section 3.4**, where vesicle-like aggregates were absent and a large film was noted. This film persisted after sonication and seeded growth, and was seen in all TEMs for this process, confirming that it is the most stable morphology. Furthermore, the film grew during the seeded growth process - whilst it was present as discrete several-micron sized films in the aged and sonicated solutions, it became a continuous film, present

throughout the substrate for 1:1, 1:3 and 1:5 seed:unimer ratios, implying that the majority of **PDI-2-TANI** unimer incorporated itself into the film rather than into fibres.

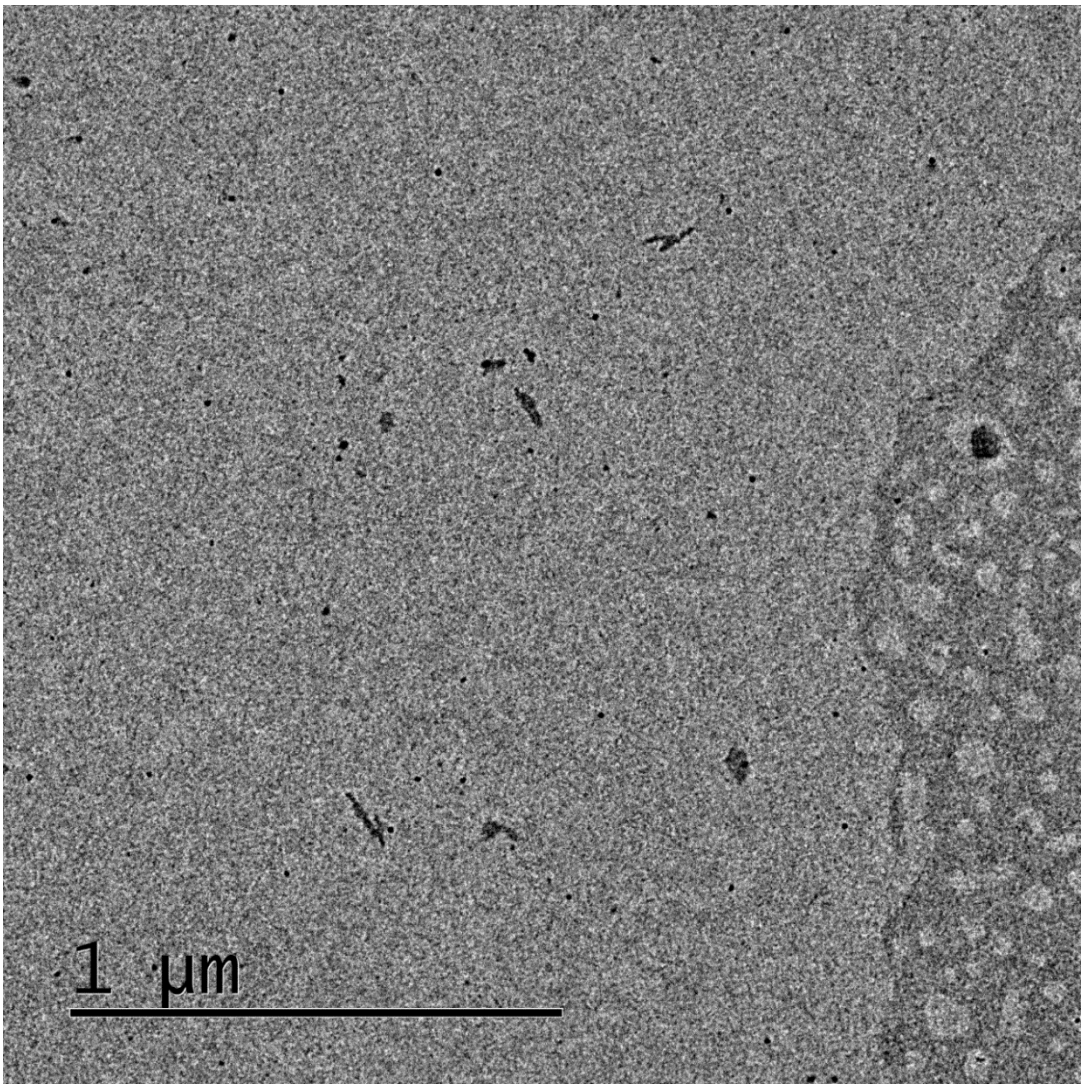

Figure 42 *TEM images of* ***PDI-2-TANI*** *seeds formed via thermal self-seeding, ageing for 2 days and sonication, showing the coexistence of small seeds and film.*

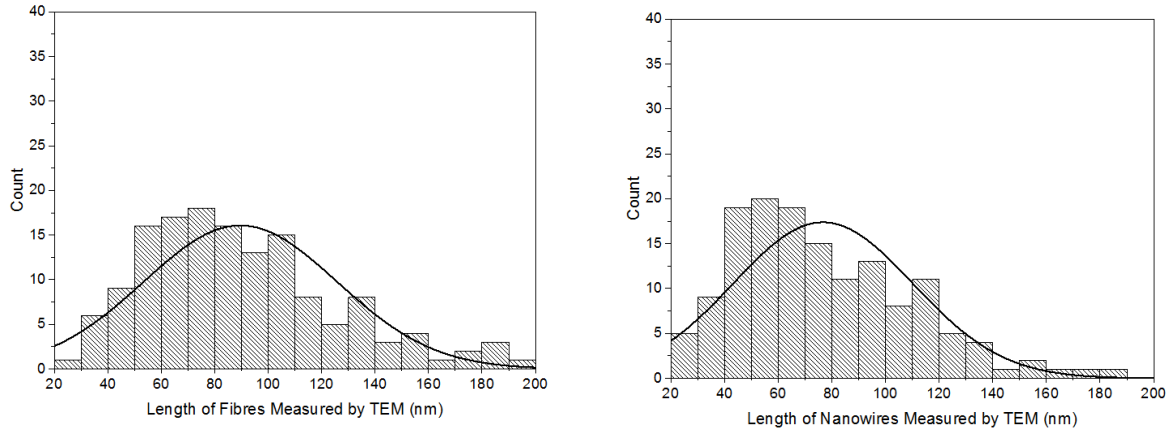

Figure 43 *Fibre length histograms for thermally self-seeded and 2-day aged* ***PDI-2-TANI*** *before sonication (left) and after sonication (right). Raw data for these histograms can be found in* ***Appendices B20*** *and* ***B26****.*

Despite the presence of the film, several large populations of fibres were observed with clear seeded growth behaviour (**Appendices B17-B20**). From 146 recorded fibres lengths after thermal self-seeding, the average length L_n was 90 nm with a $Đ$ of 1.16, corresponding closely to the 2-day aged solution in **Section 3.4** and confirming the reproducibility of those results. 101 fibre lengths recorded via TEM after sonication of this solution (**Figure 42**, **Figure 43**, **Appendices B22-B25**) revealed a drop in L_n to 69 nm, and low dispersity preserved - $Đ$ was 1.17. When a 1:1 equivalent of hot unimer solution was added, a marked increase in fibre length was noted - L_n rose to 211 nm, and an increase in dispersity was noted, with $Đ$ equal to 1.29 (**Figure 45**). This increase in dispersity was expected - whilst the lag time for thermal-self seeding would prevent most spontaneous aggregation, the formation of new aggregates in the unimer solution could not be ruled out. Furthermore, the addition of fresh unimer solution at 60 ^{o}C may have heated up the 1:1 mixture enough to promote some disaggregation. Nevertheless, a $Đ$ value of 1.29 is still comparable to literature values for living supramolecular polymerisation experiments.[57,58,64] Importantly, the low dispersity and increase in L_n gives credence to the hypothesis that these fibres undergo cooperative self-assembly, as discussed in **Section 3.4.2**.

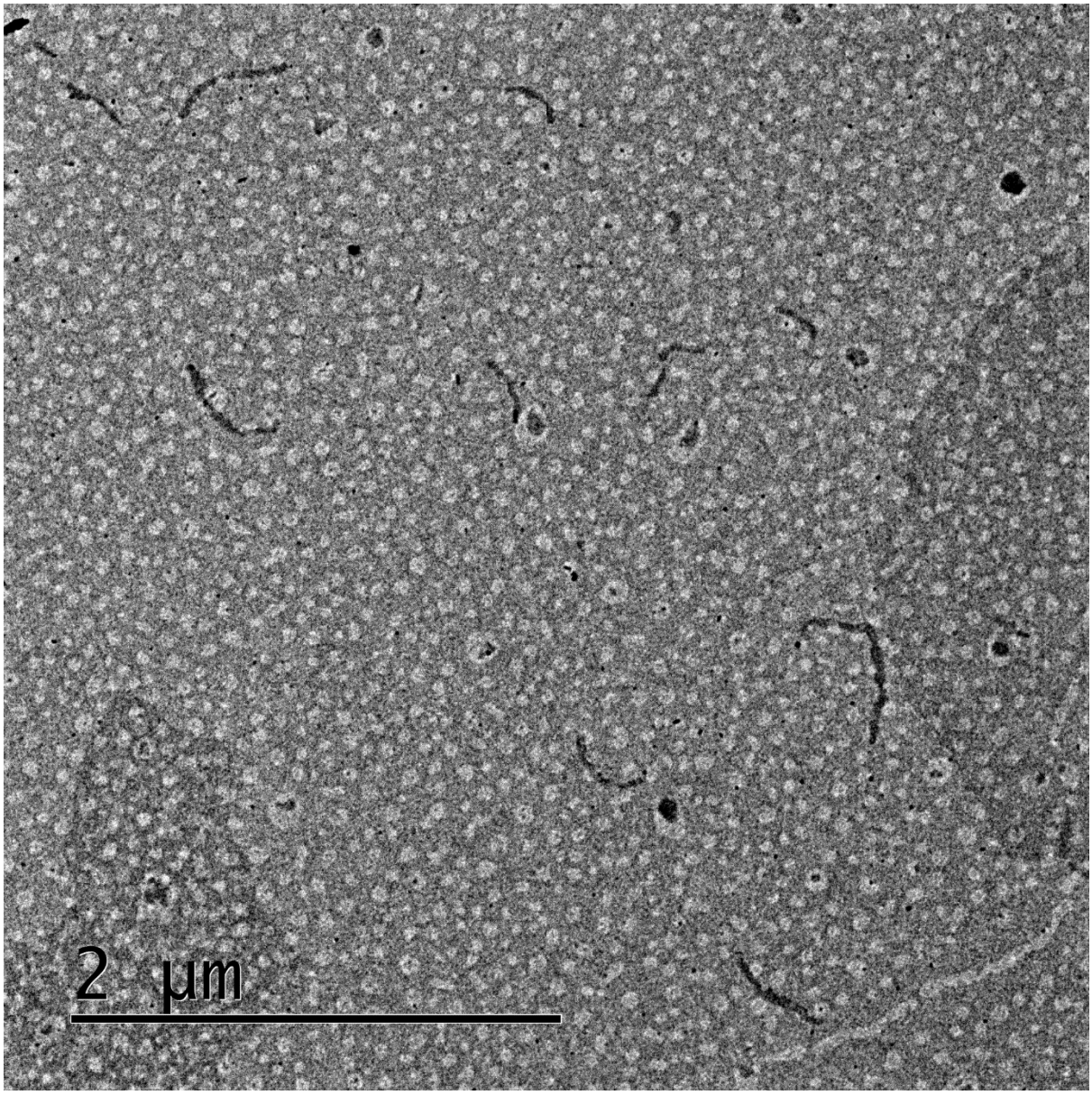

Figure 44 *TEM image of seeded growth* ***PDI-2-TANI*** *aggregates formed using a 1:1 ratio of seeds to unimer, alongside an extensive film.*

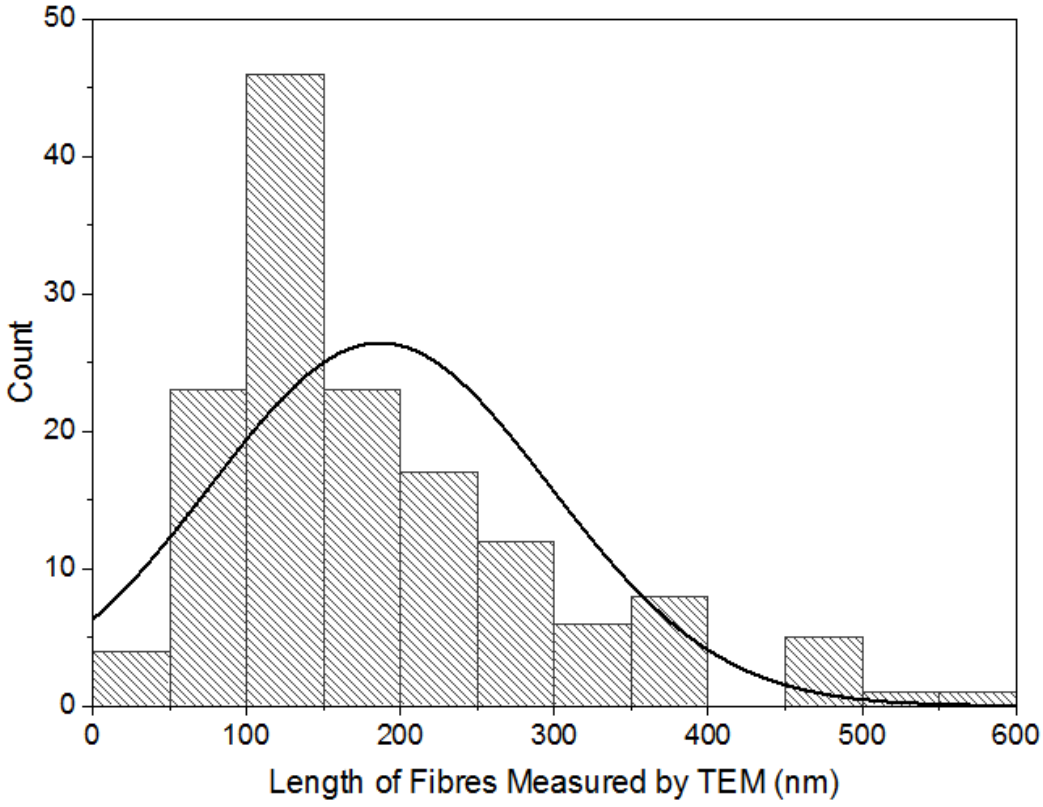

Figure 45 *Fibre length histogram for 1:1 seed:unimer ratio* ***PDI-2-TANI*** *in ethyl acetate, after ageing for 3 hours. Raw data for this histogram can be found in* ***Appendix B31****.*

For the 1:1 solution, a marked change in the morphology of these fibres is evident - the width of these fibres increased from 4-5 nm (corresponding to a single unimer width) to 10-15 nm, and the majority of these fibres exhibited a highly irregular, curved morphology (**Figure 44**, **Appendices B27-B30**), in stark contrast to the ordered fibre bundles observed in **Section 3.4**. This morphology suggested that these fibre aggregates are not bundles of supramolecular polymers with anisotropic π-stacking persisting throughout each aggregate - instead, these are probably irregular clusters consisting of many supramolecular polymers much shorter than the fibre length L_n of 211 nm (**Figure 46**). If conformational change does drive supramolecular polymerisation, as discussed in **Section 3.4.3**, then these irregular fibres may be due to the inactivation of seeds. The seed solution was aged for 2 days at room temperature before sonication - this would be ample time for the supramolecular polymers within to deactivate as their chain ends revert to a folded conformation and self-cap. This self-capping

would prevent further π-stacking, but not inhibit the lateral interactions which bind adjacent supramolecular polymers together into fibre bundles. Thus, the addition of new unimer solution would not grow the existing supramolecular polymers through π-stacking - instead, lateral interactions promote the self-assembly of extended, disordered fibres seen in **Figure 44**. As such, the three growth regimes postulated in **Section 3.4.3** do not only rely on the conformation of dissolved unimer and whether it is 'active' (extended) or 'inactive' (folded), but they also rely on the conformation of the fibre chain ends - whether those are active or not.

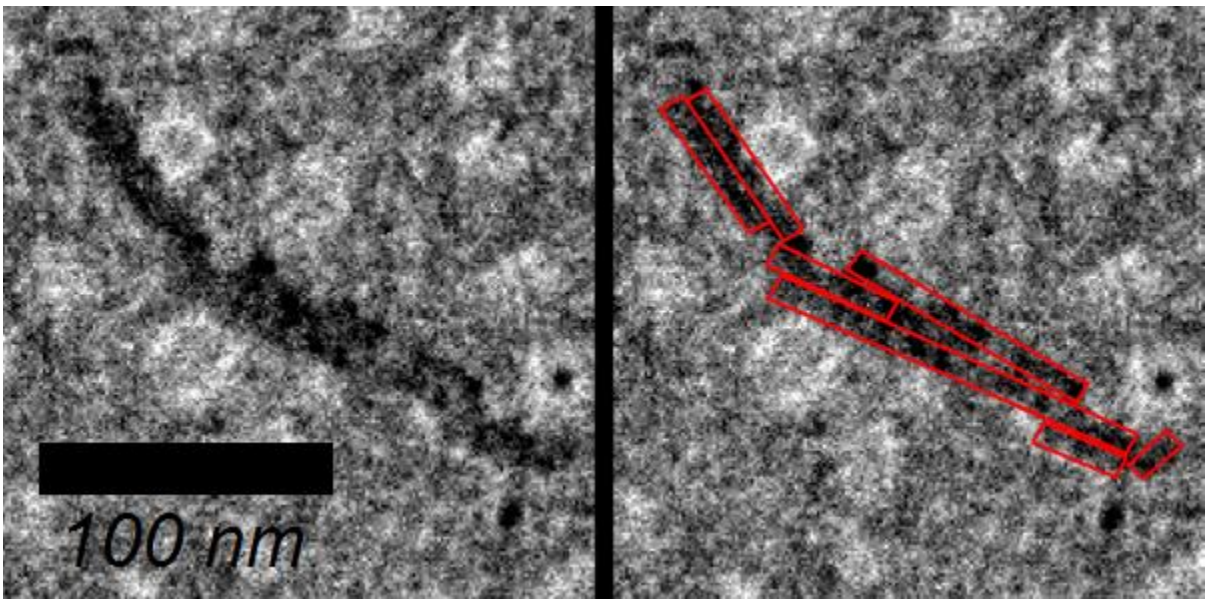

Figure 46 *One of the fibres obtained from a 1:1 seed:unimer ratio, visualised via TEM (left), showing the possible internal structure consisting of disordered fibres (right).*

Unlike the 1:1 solution, the 1:3 solution contained a bimodal population of 40-150 nm aggregates, similar in dimensions to those created by thermal self-seeding, and several large aggregates from around 170-600 nm (**Figure 47**, **Appendices B32** and **B33**). These large aggregates are distinguished by two features - their large width (a consistent 25-35 nm) and their relatively high contrast compared to those in the seed and 1:1 solutions (**Figure 48**). Thicker aggregates cause an increased contrast in TEM (this was seen in the multi-layered aggregates in **Section 3.4**),[140] and thus the contrast of these

large fibres implies that they consist of many layers of **PDI-2-TANI**. The darkness of these fibres precludes any elucidation from TEM of their internal structure, though given that they are highly curved, it is expected that their internal structure consists of many disordered **PDI-2-TANI** supramolecular polymers, similar to those postulated for the 1:1 solution. The 8 large aggregates measured had an L_n of 306 nm and a low $Đ$ of 1.19, though with such a small sample size, the relevance of this calculated dispersity is statistically questionable. The smaller aggregates measured had an L_n of 63 nm, comparable to that of the seed solution, but their high $Đ$ of 1.39 (compared to 1.20 for the seeds) indicates that these fibres are unlikely to be seeds.

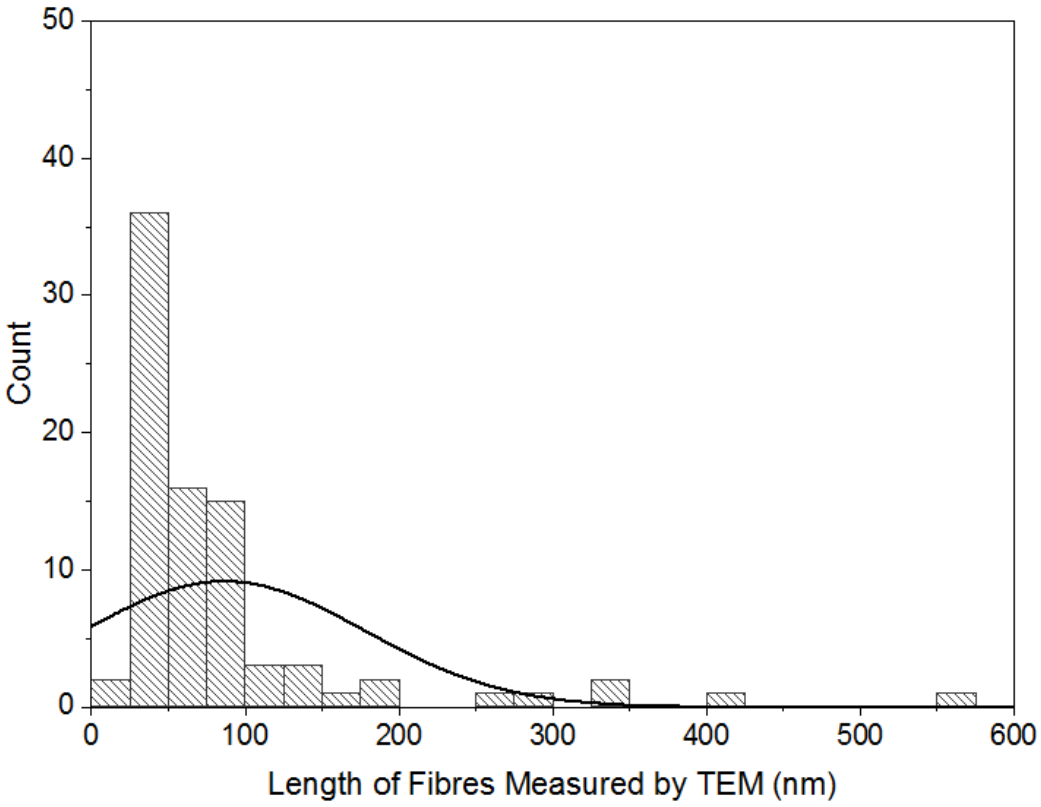

Figure 47 *Fibre length histogram for 1:3 seed:unimer ratio* ***PDI-2-TANI*** *in ethyl acetate, after ageing for 3 hours. Raw data for this histogram can be found in* ***Appendix B34****.*

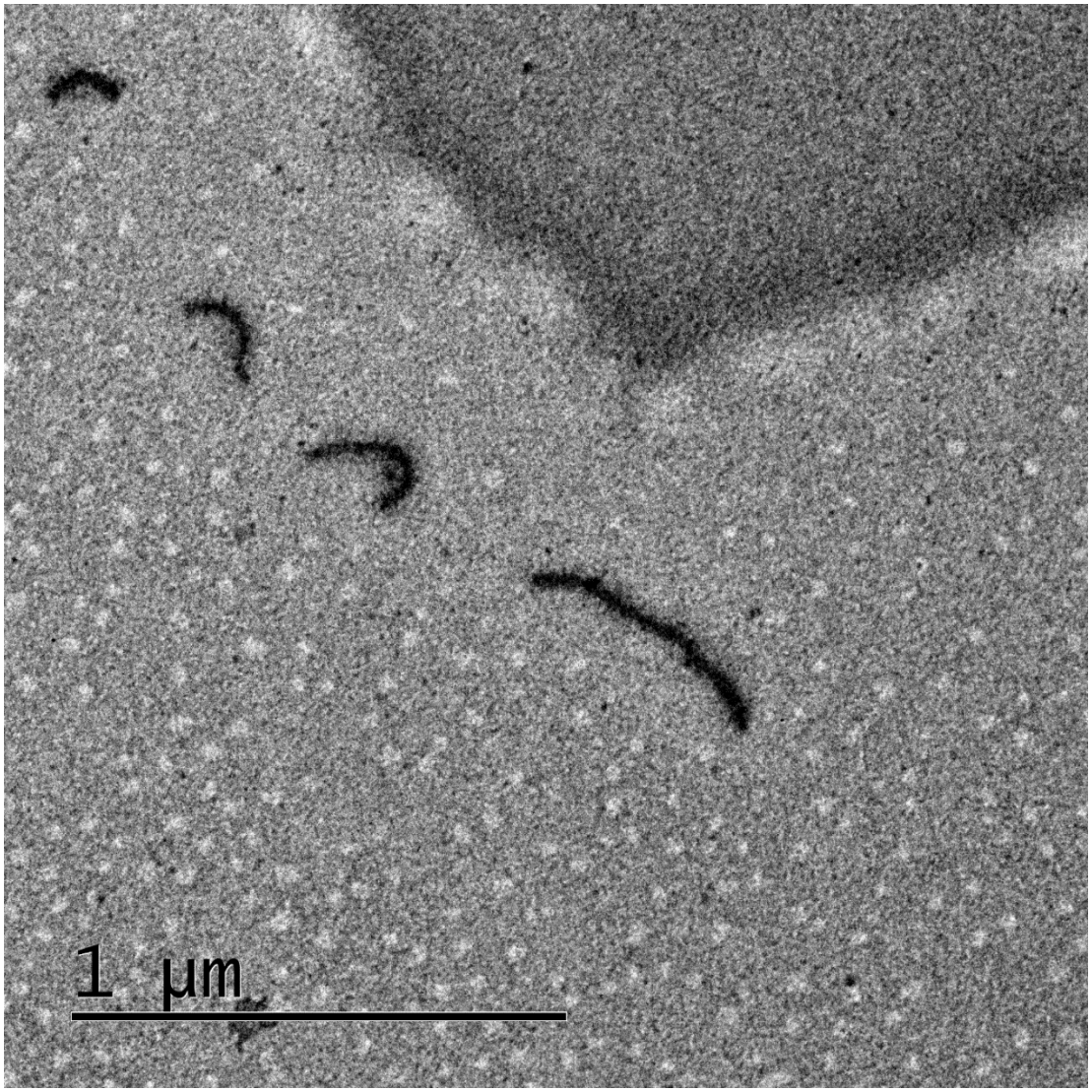

Figure 48 *TEM image of seeded growth* ***PDI-2-TANI*** *aggregates formed using a 1:3 ratio of seeds to unimer. The dark fibrous structures correspond to extended aggregates of* ***PDI-2-TANI****.*

Two hypotheses are put forward for the presence of small aggregates in the 1:3 solution and the rise of a bimodal population of fibres - thermal self-seeding occurring in the unimer solution or the disaggregation of large fibres. Since these small aggregates were not present as a discrete population in the 1:1 solution, have a significantly higher *Đ* compared to the thermally self-seeded fibres in **Section 3.4** (1.39 vs. 1.09), and mostly occur in the 1:3 solution in closely packed clusters surrounded by films (see **Figure 49**), it is more likely that these aggregates are remnants of large fibres. If these fibres are primarily held together by irregular lateral interactions, the relative weakness of these

interactions (compared to the ordered, π-stacked fibre bundles seen in **Section 3.4**) would make these fibres relatively fragile. Thus, the appearance of clusters of small aggregates may be the remains of large fibres which fragmented during drop-casting on the TEM grids.

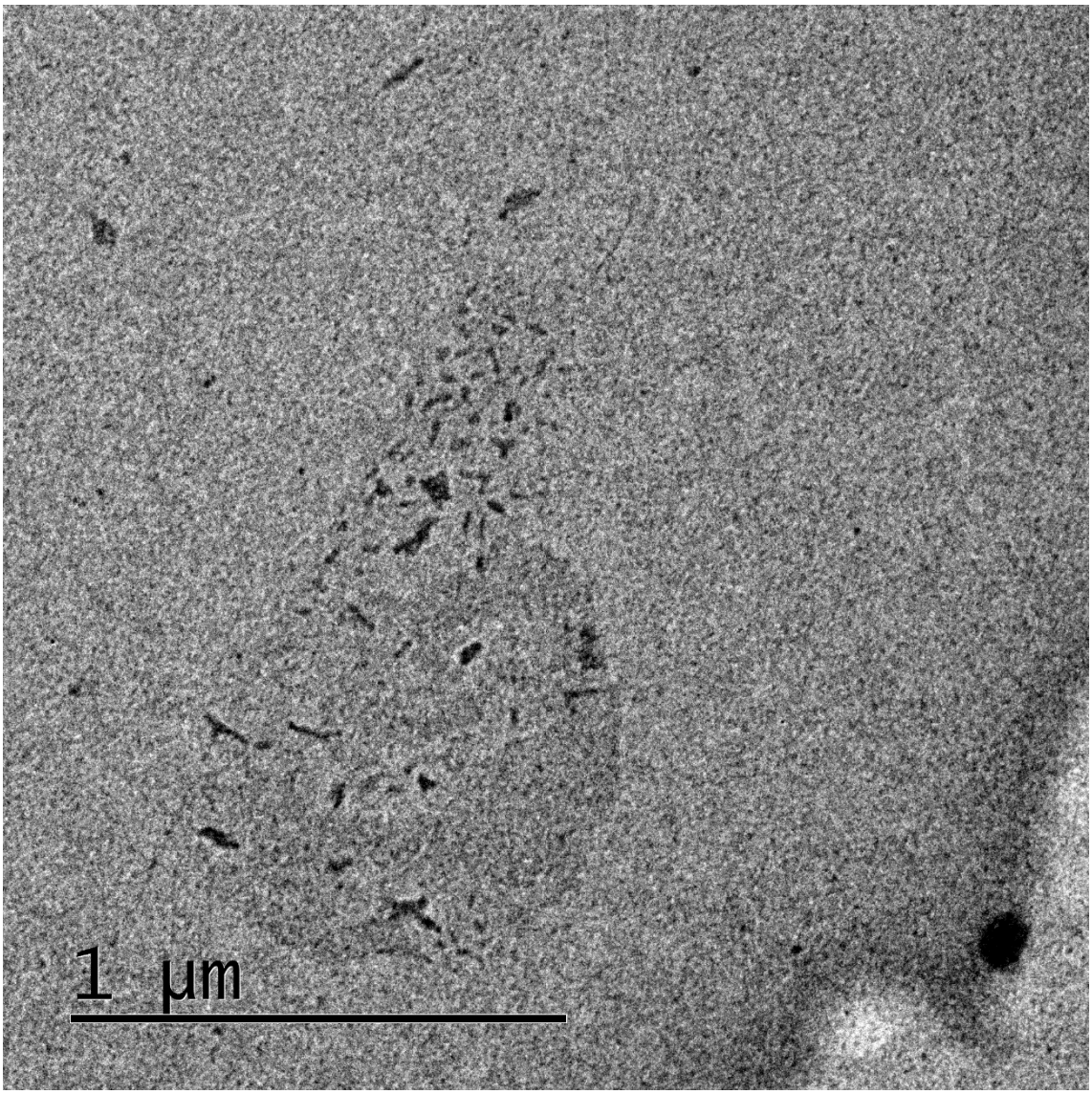

Figure 49 *A cluster of small (<100 nm) aggregates formed via during seeded growth (1:3 seed:unimer ratio). Note the darker region around these aggregates, which corresponds to a film.*

TEM imaging of the 1:5 solution revealed an extensive film which pervaded throughout the TEM grid, with very few fibrous aggregates which were either solitary fibres or small bundles (**Appendices B35-**

B38). Several of these bundles existed at the fringes of this film or were partially incorporated into the film. It may be that the high proportion of unimer favoured rapid growth of the film, and reincorporation of any fibres into this stable film morphology prevented the formation of extended fibrous aggregates.

4. Conclusions

The initial aim of the project was to design and carry out a synthesis of a tetra(aniline)-functionalised PDI capable of undergoing living supramolecular polymerisation. Using research conducted by the Würthner group to establish a set of rational design principles, **PDI-2-TANI** was designed to aggregate via a cooperative growth mechanism, allowing for seeded growth of π-stacked supramolecular polymers (**Section 1.6**, **Section 2**). It was envisioned that through the addition of fixed ratios of dissolved unimer and pre-formed seeds, the length of **PDI-2-TANI** polymers could be carefully controlled via a living process where the addition of unimer to existing seeds was kinetically favoured.

Through Buchwald-Hartwig cross-coupling of Boc-protected, phenyl-amine capped tetra(aniline) (**TANI**) (synthesised in **Section 3.1**) with methyl 4-bromobenzoate, an asymmetric sodium carboxylate salt derivative of phenyl-phenyl capped **TANI** was obtained (**Section 3.2.2**). This derivative could then be coupled with a symmetric aminoethyl PDI via HBTU coupling (**Section 3.2.3**), to yield the Boc-protected species **PDI-2-TANI**. Whilst the syntheses proceeded with good to qualitative yields, purification protocols had to be optimised several times to recover pure products in high yields. Notably, the column purification of Boc-protected **PDI-2-TANI** following HBTU coupling only gave a 20% recovery despite near quantitative conversion of **PDI-2** and **TANI-Linker** to **PDI-2-TANI**. The difficulties in optimising the purification procedure of this final step led to milligram-scale yields of **PDI-2-TANI**, precluding further Boc deprotection, oxidation and acid-doping synthesis steps to obtain **PDI-2-TANI** in its conductive emeraldine salt form (**PDI-2-TANI-ES**).

The self-assembly of **PDI-2-TANI** was examined in ethyl acetate and monitored via TEM and UV/Vis spectroscopy. Heating at 60 ^{o}C and cooling to room temperature yielded bundles of defined fibres, with each fibre around 50-250 nm long and 4-6 nm wide, corresponding to a supramolecular polymer

of **PDI-2-TANI** (**Section 3.4**). These fibres had very low length dispersities of 1.09-1.15, indicating some form of seeded growth behaviour, termed thermal self-seeding. However, these fibres were found to be out-of-equilibrium assemblies, as they degraded to a π-stacked film morphology. Attempts to access this fibre morphology via changing solvent quality from chloroform (a good solvent **PDI-2-TANI**) to ethyl acetate were unsuccessful, yielding only π-stacked films (**Section 3.4.3**). This suggested that the heating-cooling process formed fibres in-situ from the equilibrium film morphology of **PDI-2-TANI**, probably by allowing **PDI-2-TANI** unimers to 'activate' by undergoing a conformational change whereupon extended π-stacking and supramolecular polymerisation could take place. The in-situ activation of unimer and formation of a fixed number of seeds at high temperatures, combined with a medium-temperature regime where growth of these fibres progressed without further nucleation, may explain the low dispersities obtained from thermal self-seeding, as this process would constitute living growth.

A major caveat of this theory was that it relied upon the assumption of cooperative growth of these fibres, which was rationalised by the design of **PDI-2-TANI**. However, in an attempt to elucidate the method of growth, temperature-dependent UV/Vis spectra (**Section 3.4.1**) were inconclusive, and concentration-dependent UV/Vis spectra hinted at isodesmic growth (**Section 3.4.2**). The validity of these concentration-dependent UV/Vis spectra was questionable as these experiments were performed at room temperature, whilst the formation of fibres only happened at high temperature - thus, it was rationalised that concentration-dependent UV/Vis spectroscopy in fact probed the growth mechanism of the π-stacked film morphology. Temperature-dependent UV/Vis spectroscopy indicated a significant kinetic lag between cooling and aggregation, and as such seeded growth experiments were trialled using sonicated aged fibres (as seeds) and freshly heated **PDI-2-TANI** (disaggregated, but 'activated' unimer) (**Section 3.4.4**). These experiments demonstrated clear seeded growth behaviour, whereupon an increase in seed:unimer ratio obtained low-dispersity populations

of fibres with mean lengths of 211 nm (1:1 ratio) or 306 nm (1:3 ratio), significantly longer than the 69 nm mean length of fibre seeds. Upon seeded growth via this method, there was a marginal increase in *Đ* from 1.09 to 1.19 (1:3 ratio) and 1.29 (1:1 ratio). However, the curved, irregular morphology of these larger fibres, and their increase in width, hinted that these were not π-stacked throughout their entire length, but were in fact irregular aggregates of smaller π-stacked polymers. This behaviour could be explained by the earlier theory that the activation of unimers, via a thermally-induced conformational change, was required: whilst the unimer was heated and activated, the aged seeds, which were at room temperature, may have self-capped, limiting their ability to π-stack.

5. Future Work

One of the key limitations of this project has been the low yield of **PDI-2-TANI** obtained from the current synthesis, and whilst an alternative synthesis has been explored (**Section 3.3)**, time constraints have prevented its completion to yield **PDI-2-TANI** in high yields. Follow-up work has already been undertaken to explore this alternative synthesis towards **PDI-2-TANI**, with the aim of producing it in sufficient quantities to oxidise and dope it to create a class of doped **PDI-2-TANI-ES** molecules. Obtaining **PDI-2-TANI-ES** allows for the optical, sensing and electronic properties of these molecules to be elucidated and compared to other TANI aggregates. In **Section 1.6** and **Section 2**, it was stated that the initial rationale for the project was to improve the conductivity of TANI and its sensitivity in chemiresistive or optical sensors. By obtaining the Boc deprotected, oxidised and doped **PDI-2-TANI-ES**, the semiconductive properties of the TANI moieties may then be probed, alongside its optoelectronic responses to redox reactions (e.g. by reducing to **PDI-2-TANI-LEB**) and its acid-base reactions (via dedoping to form **PDI-2-TANI-EB**). Furthermore, varying the acid dopant to form the TANI ES state would yield a range of different **PDI-2-TANI-ES** molecules, with their self-assembly properties (morphology, mode of growth, solvophilicity) affected by the acid dopant used. This would make **PDI-2-TANI-ES** very versatile as a unimer; like other tetra(aniline) derivatives, its aggregates could be modified simply through dedoping and re-doping with a different acid.[141]

The project has confirmed that the supramolecular polymerisation of **PDI-2-TANI** occurs as an out-of-equilibrium process and gives promising indications that this polymerisation occurs via a cooperative self-assembly mechanism. To confirm this mechanism, future growth experiments need to be carried out at high temperature to ensure that the unimer is activated and thus will undergo polymerisation, instead of reforming the equilibrium film morphology. Performing concentration-dependent UV/Vis spectroscopy at 60 ^{o}C should yield a growth profile for the fibres formed, and if this profile fits a cooperative growth mechanism, it would provide strong evidence for the proposed mechanism of

thermal self-seeding. Furthermore, seeded growth experiments should be performed at this temperature to ensure that the chain ends of **PDI-2-TANI** fibre seeds are active, leading to the formation of long π-stacked supramolecular polymers instead of the irregular fibres obtained in this project.

If this method of seeded growth can be used to control the length of ordered **PDI-2-TANI** polymers, these polymers could be converted in-situ to electroactive TANI-doped **PDI-2-TANI-ES**, or even a dual-doped **PDI-2-TANI-ES** with a doped perylene core. Whilst these molecules would have differing self-assembly properties to **PDI-2-TANI**, the fixing of **PDI-2-TANI** aggregates (e.g. via chemical crosslinking) could enable redox chemistry and doping to occur without a morphological change. This has already been explored in other PDI derivatives, whereby chemical crosslinking of PDI aggregates rendered them stable to changes in solvent conditions, temperature, and redox via cyclic voltammetry.[142] Thus, a future strategy to create electroactive, doped **PDI-2-TANI-ES** aggregates of controlled morphology may be to perform a living supramolecular polymerisation of a **PDI-2-TANI** derivative, followed by chemically crosslinking and then doping of the TANI and PDI moieties to suit various applications.

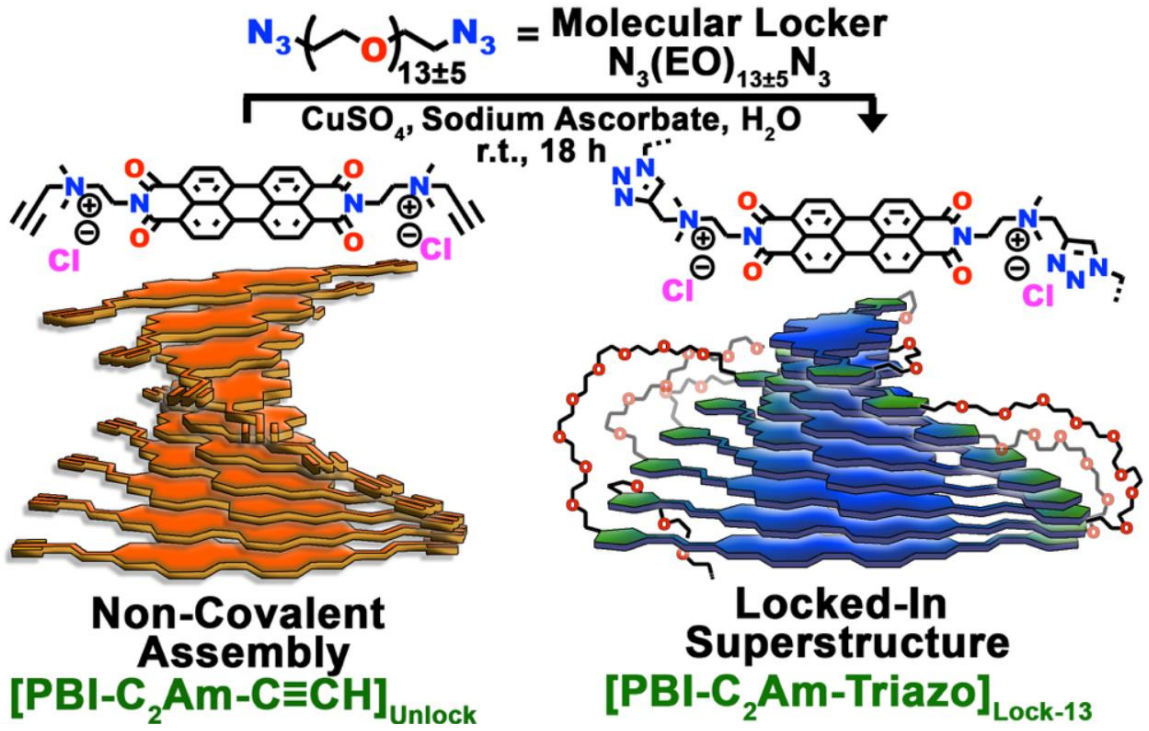

Figure 50 *An example of chemical crosslinking of PDI supramolecular polymers via a copper-catalysed cycloaddition, resulting in a 'locked-in' morphology which does not change with solvent, temperature or redox conditions.*[142]

Thermal self-seeding may be a viable new method to create out-of-equilibrium structures with low dispersity and could be applied beyond perylene chemistry to other cooperative, out-of-equilibrium aggregates. By controlling the cooling curve of a heated solution (e.g. via a Peltier stage), the kinetics of 'activation' (in the case of **PDI-2-TANI**, conformational change), nucleation and polymer growth, would all be controlled in a one-pot system. Since in cooperative systems, nucleation has a higher kinetic barrier than polymer growth, controlled cooling would have the same effect as modifying the seed:unimer ratio in traditional seeded growth experiments. Rapid cooling at higher temperatures would inhibit nucleation and thus limit the population of seeds formed; the high concentration of disaggregated, 'active' unimer remaining would then polymerise to create larger aggregates. Conversely, slow cooling at higher temperatures would maximise seed formation and minimise the amount of disaggregated, 'active' unimer available for growth, creating smaller aggregates. In the case of **PDI-2-TANI** rapid cooling during thermal-self seeding could lead to highly ordered supramolecular

polymers well below the 50 nm scale observed in this project. Structural fixing and doping could then lead to the formation of organic PNP bipolar junctions at the sub-10 nm scale, comparable to that of current commercial lithographic transistors.[143]

6. References

1 D. Garcia and H. W. Starkweather, *J. Polym. Sci. Polym. Phys. Ed.*, 1985, **23**, 537–555.

2 H. Liao, S. Liao, X. Tao, C. Liu and Y. Wang, *J. Mater. Chem. C*, 2018, **6**, 12992–12999.

3 H. Chen, X. Ma, S. Wu and H. Tian, *Angew. Chemie*, 2014, **126**, 14373–14376.

4 R.-F. Wang, H.-Q. Peng, P.-Z. Chen, L.-Y. Niu, J.-F. Gao, L.-Z. Wu, C.-H. Tung, Y.-Z. Chen and Q.-Z. Yang, *Adv. Funct. Mater.*, 2016, **26**, 5419–5425.

5 K. Petkau-Milroy and L. Brunsveld, *Org. Biomol. Chem.*, 2013, **11**, 219–232.

6 Z. Dong, Q. Luo and J. Liu, *Chem. Soc. Rev.*, 2012, **41**, 7890.

7 M. Bonchio, Z. Syrgiannis, M. Burian, N. Marino, E. Pizzolato, K. Dirian, F. Rigodanza, G. A. Volpato, G. La Ganga, N. Demitri, S. Berardi, H. Amenitsch, D. M. Guldi, S. Caramori, C. A. Bignozzi, A. Sartorel and M. Prato, *Nat. Chem.*, 2019, **11**, 146–153.

8 U. Michelsen and C. A. Hunter, *Angew. Chemie Int. Ed.*, 2000, **39**, 764–767.

9 F. Würthner, C. Thalacker, A. Sautter, W. Schärtl, W. Ibach and O. Hollricher, *Chem. - A Eur. J.*, 2000, **6**, 3871–3886.

10 M. Miyauchi, Y. Takashima, H. Yamaguchi and A. Harada, *J. Am. Chem. Soc.*, 2005, **127**, 2984–2989.

11 T. F. A. De Greef, M. M. J. Smulders, M. Wolffs, A. P. H. J. Schenning, R. P. Sijbesma and E. W. Meijer, *Chem. Rev.*, 2009, **109**, 5687–5754.

12 T. Haino, *Polym. J.*, 2019, **51**, 303–318.

13 M. Higuchi, *Metallo-Supramolecular Polymers*, Springer Japan, Tokyo, 2019.

14 R. F. Goldstein and L. Stryer, *Biophys. J.*, 1986, **50**, 583–599.

15 J. Gershberg, F. Fennel, T. H. Rehm, S. Lochbrunner and F. Würthner, *Chem. Sci.*, 2016, **7**, 1729–1737.

16 M. Greene, in *High Performance Pigments*, Wiley-VCH Verlag GmbH & Co. KGaA, Weinheim, FRG, pp. 249–261.

17 F. Zhang, Y. Ma, Y. Chi, H. Yu, Y. Li, T. Jiang, X. Wei and J. Shi, *Sci. Rep.*, 2018, **8**, 8208.

18 M. Sun, K. Müllen and M. Yin, *Chem. Soc. Rev.*, 2016, **45**, 1513–1528.

19 U. Avcıbaşı, H. Dinçalp, T. Ünak, Y. Yıldırım, N. Avcıbaşı, Y. Duman and S. Içli, *J. Radioanal. Nucl. Chem.*, 2007, **273**, 669–675.

20 W. E. Ford and P. V. Kamat, *J. Phys. Chem.*, 1987, **91**, 6373–6380.

21 E. Shirman, A. Ustinov, N. Ben-Shitrit, H. Weissman, M. A. Iron, R. Cohen and B. Rybtchinski, *J. Phys. Chem. B*, 2008, **112**, 8855–8858.

22 J. D. Yuen, M. Wang, J. Fan, D. Sheberla, M. Kemei, N. Banerji, M. Scarongella, S. Valouch, T. Pho, R. Kumar, E. C. Chesnut, M. Bendikov and F. Wudl, *J. Polym. Sci. Part A Polym. Chem.*, 2015, **53**, 287–293.

23 J. E. Anthony, A. Facchetti, M. Heeney, S. R. Marder and X. Zhan, *Adv. Mater.*, 2010, **22**, 3876–3892.

24 H. AKAMATU, H. INOKUCHI and Y. MATSUNAGA, *Nature*, 1954, **173**, 168–169.

25 F. Würthner, C. R. Saha-Möller, B. Fimmel, S. Ogi, P. Leowanawat and D. Schmidt, *Chem. Rev.*, 2016, **116**, 962–1052.

26 M. R. Battaglia, A. D. Buckingham and J. H. Williams, *Chem. Phys. Lett.*, 1981, **78**, 421–423.

27 C. R. Martinez and B. L. Iverson, *Chem. Sci.*, 2012, **3**, 2191.

28 M. Kasha, *Radiat. Res.*, 1963, **20**, 55.

29 F. Graser and E. Hädicke, *Liebigs Ann. der Chemie*, 1980, **1980**, 1994–2011.

30 H. Bronstein, C. B. Nielsen, B. C. Schroeder and I. McCulloch, *Nat. Rev. Chem.*, 2020, **4**, 66–77.

31 N. Lu, L. Li, D. Geng and M. Liu, *Org. Electron.*, 2018, **61**, 223–234.

32 J.-F. Chang, H. Sirringhaus, M. Giles, M. Heeney and I. McCulloch, *Phys. Rev. B*, 2007, **76**, 205204.

33 L. Wang and D. Beljonne, *J. Chem. Phys.*, 2013, **139**, 064316.

34 J. Idé, R. Méreau, L. Ducasse, F. Castet, Y. Olivier, N. Martinelli, J. Cornil and D. Beljonne, *J. Phys. Chem. B*, 2011, **115**, 5593–5603.

35 M. O'Neill and S. M. Kelly, *Adv. Mater.*, 2011, **23**, 566–584.

36 P. Würfel, *Physics of Solar Cells*, Wiley, 2005.

37 G. E. Arnaoutakis, Heriot-Watt University, 2015.

38 B. A. Gregg, J. Sprague and M. W. Peterson, *J. Phys. Chem. B*, 1997, **101**, 5362–5369.

39 O. V. Mikhnenko, P. W. M. Blom and T.-Q. Nguyen, *Energy Environ. Sci.*, 2015, **8**, 1867–1888.

40 Y. V. Aulin, K. M. Felter, D. D. Günbas, R. K. Dubey, W. F. Jager and F. C. Grozema, *Chempluschem*, 2018, **83**, 230–238.

41 C. S. Solanki and G. Beaucarne, *Energy Sustain. Dev.*, 2007, **11**, 17–23.

42 N. J. Hestand and F. C. Spano, *Chem. Rev.*, 2018, **118**, 7069–7163.

43 F. Würthner, *Chem. Commun.*, 2004, **4**, 1564–1579.

44 D. P. Hoffman, S. Y. Leblebici, A. M. Schwartzberg and R. A. Mathies, *J. Phys. Chem. Lett.*, 2015, **6**, 2919–2923.

45 S. Yagai, T. Seki, T. Karatsu, A. Kitamura and F. Würthner, *Angew. Chemie Int. Ed.*, 2008, **47**,

3367–3371.

46 C. Huang, S. Barlow and S. R. Marder, *J. Org. Chem.*, 2011, **76**, 2386–2407.

47 Z. Wang, N. Zheng, W. Zhang, H. Yan, Z. Xie, Y. Ma, F. Huang and Y. Cao, *Adv. Energy Mater.*, 2017, **7**, 1700232.

48 K. Nagarajan, A. R. Mallia, V. S. Reddy and M. Hariharan, *J. Phys. Chem. C*, 2016, **120**, 8443–8450.

49 T. Fukui, S. Kawai, S. Fujinuma, Y. Matsushita, T. Yasuda, T. Sakurai, S. Seki, M. Takeuchi and K. Sugiyasu, *Nat. Chem.*, 2017, **9**, 493–499.

50 S. Ogi, K. Sugiyasu, S. Manna, S. Samitsu and M. Takeuchi, *Nat. Chem.*, 2014, **6**, 188–195.

51 B. F. P. Edwards and B. D. Sykes, *Biochemistry*, 1981, **20**, 4193–4198.

52 V. K. Ravi, T. Swain, N. Chandra and R. Swaminathan, *PLoS One*, 2014, **9**, e87256.

53 K. M. Skillman, C. I. Ma, D. H. Fremont, K. Diraviyam, J. A. Cooper, D. Sept and L. D. Sibley, *Nat. Commun.*, 2013, **4**, 2285.

54 A. Sekhar and J. B. Udgaonkar, *Biochemistry*, 2011, **50**, 805–819.

55 G. Echue, G. C. Lloyd-Jones and C. F. J. Faul, *Chem. - A Eur. J.*, 2015, **21**, 5118–5128.

56 J. Kumar, H. Tsumatori, J. Yuasa, T. Kawai and T. Nakashima, *Angew. Chemie - Int. Ed.*, 2015, **54**, 5943–5947.

57 J. Kang, D. Miyajima, T. Mori, Y. Inoue, Y. Itoh and T. Aida, *Science (80-.).*, 2015, **347**, 646–651.

58 X. Wang, G. Guerin, H. Wang, Y. Wang, I. Manners and M. A. Winnik, *Science (80-.).*, 2007, **317**, 644–647.

59 M. E. Robinson, D. J. Lunn, A. Nazemi, G. R. Whittell, L. De Cola and I. Manners, *Chem.*

Commun., 2015, **51**, 15921–15924.

60 F. He, T. Gädt, I. Manners and M. A. Winnik, *J. Am. Chem. Soc.*, 2011, **133**, 9095–9103.

61 C. Kulkarni, K. K. Bejagam, S. P. Senanayak, K. S. Narayan, S. Balasubramanian and S. J. George, *J. Am. Chem. Soc.*, 2015, **137**, 3924–3932.

62 X. Q. Li, V. Stepanenko, Z. Chen, P. Prins, L. D. A. Siebbeles and F. Würthner, *Chem. Commun.*, 2006, 3871–3873.

63 S. Ogi, V. Stepanenko, K. Sugiyasu, M. Takeuchi and F. Würthner, *J. Am. Chem. Soc.*, 2015, **137**, 3300–3307.

64 C. Jarrett-Wilkins, X. He, H. E. Symons, R. L. Harniman, C. F. J. Faul and I. Manners, *Chem. - A Eur. J.*, 2018, **24**, 15556–15565.

65 C. Shao, M. Grüne, M. Stolte and F. Würthner, *Chem. - A Eur. J.*, 2012, **18**, 13665–13677.

66 H. Letheby, *J. Chem. Soc.*, 1862, **15**, 161–163.

67 W. J. Feast, J. Tsibouklis, K. L. Pouwer, L. Groenendaal and E. W. Meijer, *Polymer (Guildf).*, 1996, **37**, 5017–5047.

68 J. E. de Albuquerque, L. H. C. Mattoso, R. M. Faria, J. G. Masters and A. G. MacDiarmid, *Synth. Met.*, 2004, **146**, 1–10.

69 S. Rasmussen, *Substantia*, 2017, **1**, 99–109.

70 A. G. Green and A. E. Woodhead, *J. Chem. Soc., Trans.*, 1910, **97**, 2388–2403.

71 E. Llorens, E. Armelin, M. del Mar Pérez-Madrigal, L. del Valle, C. Alemán and J. Puiggalí, *Polymers (Basel).*, 2013, **5**, 1115–1157.

72 A. G. Macdiarmid, J. C. Chiang, A. F. Richter and A. J. Epstein, *Synth. Met.*, 1987, **18**, 285–290.

73 A. Eftekhari, L. Li and Y. Yang, *J. Power Sources*, 2017, **347**, 86–107.

74 K. Amer, S. Ebrahim, M. Feteha, M. Soliman and A. El-Shaer, in *2017 34th National Radio Science Conference (NRSC)*, IEEE, 2017, pp. 440–447.

75 J. Jang, J. Ha and K. Kim, *Thin Solid Films*, 2008, **516**, 3152–3156.

76 A. G. MacDiarmid and A. J. Epstein, *Synth. Met.*, 1994, **65**, 103–116.

77 R. S. Kohlman, A. Zibold, D. B. Tanner, G. G. Ihas, T. Ishiguro, Y. G. Min, A. G. MacDiarmid and A. J. Epstein, *Phys. Rev. Lett.*, 1997, **78**, 3915–3918.

78 A. G. MacDiarmid, Y. Zhou and J. Feng, *Synth. Met.*, 1999, **100**, 131–140.

79 F. L. Lu, F. Wudl, M. Nowak and A. J. Heeger, *J. Am. Chem. Soc.*, 1986, **108**, 8311–8313.

80 J. P. Sadighi, R. A. Singer and S. L. Buchwald, *J. Am. Chem. Soc.*, 1998, **120**, 4960–4976.

81 A. G. MacDiarmid, *Synth. Met.*, 1997, **84**, 27–34.

82 S. K. Dhawan, D. Kumar, M. K. Ram, S. Chandra and D. C. Trivedi, *Sensors Actuators B Chem.*, 1997, **40**, 99–103.

83 L.-Y. Yang and W.-B. Liau, *Mater. Chem. Phys.*, 2009, **115**, 28–32.

84 S. Virji, J. Huang, R. B. Kaner and B. H. Weiller, *Nano Lett.*, 2004, **4**, 491–496.

85 B. T. E. Thornton, A. Harrison, A. L. Pham, C. E. Castano and C. Tang, *ACS Omega*, 2018, **3**, 3587–3591.

86 V. V. Abalyaeva and O. N. Efimov, *Russ. J. Electrochem.*, 2005, **41**, 1180–1184.

87 M. Porcel-Valenzuela, J. Ballesta-Claver, I. de Orbe-Payá, F. Montilla and L. F. Capitan-Vallvey, *J. Electroanal. Chem.*, 2015, **738**, 162–169.

88 J. WU, *Sensors Actuators B Chem.*, 2005, **104**, 43–49.

89 K. CROWLEY, A. MORRIN, A. HERNANDEZ, E. OMALLEY, P. WHITTEN, G. WALLACE, M. SMYTH and A. KILLARD, *Talanta*, 2008, **77**, 710–717.

90 J. Huang, S. Virji, B. H. Weiller and R. B. Kaner, *J. Am. Chem. Soc.*, 2003, **125**, 314–315.

91 J.-F. Nierengarten, G. Hadziioannou and N. Armaroli, *Mater. Today*, 2001, **4**, 16–18.

92 J. Simon, F. Tournilhac and J. -J. André, *J. Appl. Phys.*, 1987, **62**, 3304–3307.

93 A. J. Bergren, L. Zeer-Wanklyn, M. Semple, N. Pekas, B. Szeto and R. L. McCreery, *J. Phys. Condens. Matter*, 2016, **28**, 094011.

94 R. Chen and B. C. Benicewicz, *Macromolecules*, 2003, **36**, 6333–6339.

95 M. M. M. Raposo, A. M. C. Fonseca and G. Kirsch, *Tetrahedron*, 2004, **60**, 4071–4078.

96 S. Tanaka, S. Tamba, D. Tanaka, A. Sugie and A. Mori, *J. Am. Chem. Soc.*, 2011, 16734–16737.

97 K. T. Wong, T. S. Hung, Y. Lin, C. C. Wu, G. H. Lee, S. M. Peng, C. H. Chou and Y. O. Su, *Org. Lett.*, 2002, **4**, 513–516.

98 S. Lightowler and M. Hird, *Chem. Mater.*, 2005, **17**, 5538–5549.

99 J. P. Wolfe, J. Åhman, J. P. Sadighi, R. A. Singer and S. L. Buchwald, *Tetrahedron Lett.*, 1997, **38**, 6367–6370.

100 T. W. Green and P. G. M. Wuts, in *Protective Groups in Organic Synthesis*, Wiley-Interscience, New York, 1991, p. 442.

101 V. V. Sureshbabu and N. Narendra, in *Amino Acids, Peptides and Proteins in Organic Chemistry*, Wiley-VCH Verlag GmbH & Co. KGaA, Weinheim, Germany, 2011, pp. 1–97.

102 T. Hvidt, W. A. Szarek and D. B. Maclean, *Can. J. Chem.*, 1988, **66**, 779–782.

103 J. H. Billman and A. C. Diesing, *J. Org. Chem.*, 1957, **22**, 1068–1070.

104 Z. Dobrovolná and L. Červený, *Res. Chem. Intermed.*, 2000, **26**, 489–497.

105 A. G. Becalski, W. R. Cullen, M. D. Fryzuk, B. R. James, G. J. Kang and S. J. Rettig, *Inorg. Chem.*, 1991, **30**, 5002–5008.

106 M. Fournier, F. Fournier and J. Berthelot, *Bull. des Sociétés Chim. Belges*, 1984, **93**, 157–158.

107 J. Berthelot, C. Guette, P.-L. Desbène, J.-J. Basselier, P. Chaquin and D. Masure, *Can. J. Chem.*, 1989, **67**, 2061–2066.

108 S. Hazarika, P. Gogoi and P. Barman, *RSC Adv.*, 2015, **5**, 25765–25767.

109 J. Berthelot, C. Guette, M. Essayegh, P. L. Desbene and J. J. Basselier, *Synth. Commun.*, 1986, **16**, 1641–1645.

110 K. M. Engle and J. Q. Yu, *J. Org. Chem.*, 2013, **78**, 8927–8955.

111 D. S. Surry and S. L. Buchwald, *Angew. Chemie - Int. Ed.*, 2008, **47**, 6338–6361.

112 B. P. Fors, D. A. Watson, M. R. Biscoe and S. L. Buchwald, *J. Am. Chem. Soc.*, 2008, **130**, 13552–13554.

113 D. Maiti, B. P. Fors, J. L. Henderson, Y. Nakamura and S. L. Buchwald, *Chem. Sci.*, 2011, **2**, 57–68.

114 D. S. Surry and S. L. Buchwald, *Chem. Sci.*, 2011, **2**, 27–50.

115 P. Mukhopadhyay, Y. Iwashita, M. Shirakawa, S. I. Kawano, N. Fujita and S. Shinkai, *Angew. Chemie - Int. Ed.*, 2006, **45**, 1592–1595.

116 C. Huang, S. Barlow and S. R. Marder, *J. Org. Chem.*, 2011, **76**, 2386–2407.

117 S. T. K. Riddick, J.A., W.B. Bunger, *Techniques of Chemistry 4th ed., Volume II. Organic Solvents.*, John Wiley and Sons., New York, 1985.

118 J. R. Martinelli, D. A. Watson, D. M. M. Freckmann, T. E. Barder and S. L. Buchwald, *J. Org. Chem.*, 2008, **73**, 7102–7107.

119 N. Marion, E. C. Ecarnot, O. Navarro, D. Amoroso, A. Bell and S. P. Nolan, *J. Org. Chem.*, 2006, **71**, 3816–3821.

120 G. D. Vo and J. F. Hartwig, *J. Am. Chem. Soc.*, 2009, **131**, 11049–11061.

121 Methyl Benzoate 1H NMR, ChemicalBook, https://www.chemicalbook.com/SpectrumEN_93-58-3_1hnmr.htm.

122 P. Yaseneva, P. Hodgson, J. Zakrzewski, S. Falß, R. E. Meadows and A. A. Lapkin, *React. Chem. Eng.*, 2016, **1**, 229–238.

123 S. Ficht, L. Röglin, M. Ziehe, D. Breyer and O. Seitz, *Synlett*, 2004, **2004**, 2525–2528.

124 N. Nakajima and Y. Ikada, *Bioconjug. Chem.*, 1995, **6**, 123–130.

125 J. D. Goodreid, P. A. Duspara, C. Bosch and R. A. Batey, *J. Org. Chem.*, 2014, **79**, 943–954.

126 E. Valeur and M. Bradley, *Chem. Soc. Rev.*, 2009, **38**, 606–631.

127 L. P. Miranda and P. F. Alewood, *Proc. Natl. Acad. Sci. U. S. A.*, 1999, **96**, 1181–1186.

128 WO 2010/035166, .

129 S. R. Chaudhari and N. Suryaprakash, *J. Mol. Struct.*, 2012, **1016**, 163–168.

130 F. Du, J. Tian, H. Wang, B. Liu, B. Jin and R. Bai, *Macromolecules*, 2012, **45**, 3086–3093.

131 N-Methylbenzamide 1H NMR, ChemicalBook, https://www.chemicalbook.com/SpectrumEN_613-93-4_1HNMR.htm.

132 G. R. Fulmer, A. J. M. Miller, N. H. Sherden, H. E. Gottlieb, A. Nudelman, B. M. Stoltz, J. E. Bercaw and K. I. Goldberg, *Organometallics*, 2010, **29**, 2176–2179.

133 M. Loos, C. Gerber, F. Corona, J. Hollender and H. Singer, *Anal. Chem.*, 2015, **87**, 5738–5744.

134 H. Rafii, S. Chalon, J.-E. Ombetta, Y. Frangin, L. Garreau, A.-M. Dognon, I. Lena, S. Bodard, M.-P. Vilar, J.-C. Besnard and D. Guilloteau, *Nucl. Med. Biol.*, 1995, **22**, 617–623.

135 Y. S. Ma, C. H. Wang, Y. J. Zhao, Y. Yu, C. X. Han, X. J. Qiu and Z. Shi, *Supramol. Chem.*, 2007, **19**, 141–149.

136 S. Tatemichi, M. Ichikawa, T. Koyama and Y. Taniguchi, *Appl. Phys. Lett.*, 2006, **89**, 112108.

137 K. Balakrishnan, A. Datar, T. Naddo, J. Huang, R. Oitker, M. Yen, J. Zhao and L. Zang, *J. Am. Chem. Soc.*, 2006, **128**, 7390–7398.

138 S.-G. Liu, G. Sui, R. A. Cormier, R. M. Leblanc and B. A. Gregg, *J. Phys. Chem. B*, 2002, **106**, 1307–1315.

139 F. T. WALL, *Science (80-.).*, 1954, **119**, 283–284.

140 C. B. Williams, David B., Carter, *Transmission Electron Microscopy*, Springer US, 2009.

141 W. Lyu, M. Alotaibi, O. A. Bell, K. Watanabe, R. Harniman, B. M. Mills, A. M. Seddon, S. E. Rogers, S. M. King, W. Yan and C. F. J. Faul, *Chem. Sci.*, 2018, **9**, 4392–4401.

142 A. Ashcraft, K. Liu, A. Mukhopadhyay, V. Paulino, C. Liu, B. Bernard, D. Husainy, T. Phan and J. Olivier, *Angew. Chemie Int. Ed.*, 2020, **59**, 7487–7493.

143 P. Raghavan, M. G. Bardon, D. Jang, P. Schuddinck, D. Yakimets, J. Ryckaert, A. Mercha, N. Horiguchi, N. Collaert, A. Mocuta, D. Mocuta, Z. Tokei, D. Verkest, A. Thean and A. Steegen, in *2015 IEEE Custom Integrated Circuits Conference (CICC)*, IEEE, 2015, pp. 1–5.

144 Faul Group Synthesis Wiki - Ph/NH2 TANI, https://wikis.bris.ac.uk/display/ISA/Oligoaniline+materials.

7. Experimental

All chemicals were purchased from Sigma-Aldrich, unless otherwise stated.

^{1}H NMR experiments were performed using either a 400 MHz Varian VNMR 400 or a Jeol ECS 400.

Mass spectrometry was performed using either a Thermo Scientific Orbitrap Elite (ESI-Orbitrap), or a Waters Synapt G2S (IMS-Q-TOF, nanospray ionisation).

TEM was performed using a Jeol 1400 TEM. Samples were drop-cast via a single drop (~10 µL) onto 300 mesh carbon-coated grids before being dried under high vacuum for 2 days prior to TEM imaging.

Room temperature UV-Vis spectroscopy was performed using a Shimadzu UV 2600 spectrophotometer, with either a 1 mm path length quartz cuvette (for >1 x 10^{-5} M samples) or a 1 cm path length quartz cuvette (for <1 x 10^{-5} M samples). Temperature-dependent UV/Vis spectroscopy was performed using a Lambda 35 spectrometer, fitted with a Perkin Elmer PTP 1 Peltier Temperature Programmer, using a 1 mm path length quartz cuvette.

Sonication was carried out using a SciMed UP100H ultrasonic processor, at 100% amplitude and 100% duty cycle.

7.1 TANI - Synthesis

7.1.1 Synthesis of 2

N-phenyl-*p*-phenylene diamine (27.68 g, 150 mmol) was added to a flask containing dried molecular sieves (114 g, 4 Å mesh size), before benzophenone (27.68 g, 166 mmol) was added. The flask was purged with nitrogen, and dry toluene (150 mL) added via syringe, before the mixture was refluxed under nitrogen for 24 hours. Afterwards, the mixture was cooled to room temperature and decanted from the dark grey stained molecular sieves. THF (2.5 L) was used to wash the molecular sieves until colourless. The THF and toluene fractions were combined and dried via rotary evaporation to yield a brown oil, which yielded a suspension of beige crystals upon the addition of methanol (300 mL). This suspension was filtered, and the methanol filtrate was concentrated to ~50 mL via rotary evaporation and filtered again. The resulting solids were combined and recrystallised from methanol to yield light beige crystals of **2** (79 % yield).

Experimental: ^{1}H NMR (400 MHz, $CDCl_3$) δ 7.75 (d, J = 7.1 Hz, 2H), 7.49 – 7.43 (m, 1H), 7.43 – 7.37 (m, 2H), 7.33 – 7.27 (m, 3H), 7.25 – 7.18 (m, 2H), 7.18 – 7.13 (m, 2H), 6.95 (d, J = 7.7 Hz, 2H), 6.91 – 6.83 (m, 3H), 6.69 (d, J = 8.7 Hz, 2H), 5.56 ppm (s, 1H)

Literature: ^{1}H NMR (400 MHz, $CDCl_3$) δ 7.75 (d, J = 7.1 Hz, 2H), 7.49 – 7.43 (m, 1H), 7.43 – 7.37 (m, 2H), 7.33 – 7.27 (m, 3H), 7.25 – 7.18 (m, 2H), 7.18 – 7.13 (m, 2H), 6.95 (d, J = 7.7 Hz, 2H), 6.91 – 6.83 (m, 3H), 6.69 (d, J = 8.7 Hz, 2H), 5.56 ppm (s, 1H)[144]

7.1.2 Synthesis of 3

To a flask containing **2** (7.50 g, 22.5 mmol), di-*tert*-butyl dicarbonate (5.82 g, 27 mmol) and dimethylaminopyridine (0.273 g, 4.5 mmol) were added, before the flask was purged with nitrogen. Dry THF (55 mL) was added, and the mixture was refluxed under nitrogen for 24 hours. After the reaction, the mixture was cooled to room temperature, and ethanol (100 mL) was added, before the mixture was cooled in a fridge (4 ^{o}C) for 14 hours, yielding pale yellow crystals of **3**. Filtration to isolate these crystals, followed by concentration of the filtrate via rotary evaporation to yield a second crop, led to a combined yield of 75%.

Experimental: ^{1}H NMR (400 MHz, $CDCl_3$) δ 7.73 (d, J = 7.0 Hz, 2H), 7.50 – 7.44 (m, 1H), 7.43 – 7.36 (m, 2H), 7.31 – 7.20 (m, 7H), 7.16 – 7.08 (m, 5H), 6.96 (d, J = 8.7 Hz, 2H), 6.67 (d, J = 8.6 Hz, 2H), 1.39 ppm (s, 8H)

Literature: ^{1}H NMR (400 MHz, $CDCl_3$) δ 7.74 (d, J = 7.0 Hz, 2H), 7.50 – 7.44 (m, 1H), 7.43 – 7.36 (m, 2H), 7.33 – 7.20 (m, 5H), 7.18 – 7.06 (m, 5H), 6.97 (d, J = 8.6 Hz, 2H), 6.67 (d, J = 8.6 Hz, 2H), 1.40 ppm (s, 9H)[144]

7.1.3 Synthesis of 4

To a flask containing ammonium formate (1.59 g, 25.4 mmol), **3** was added (1.00 g, 2.23 mmol) and palladium on carbon (10 % Pd by weight, 60 mg) before the flask was purged with nitrogen. Dry THF (10 mL) and dry methanol (25 mL) were added via syringe and the mixture was refluxed for 6 hours. The mixture was then cooled to room temperature and the solvent removed via rotary evaporation, with the remaining solid dissolved in DCM (50 mL) and filtered through a plug of celite. The filtrate

was then dried via rotary evaporation, and the cream-coloured solid was dissolved in 150 mL of *n*-hexane and filtered to yield **4** (98 % yield).

Experimental: ^{1}H NMR (400 MHz, $CDCl_3$) δ 7.36 – 7.14 (m, 7H), 7.11 (t, J = 7.1 Hz, 1H), 6.99 (dt, J = 8.2, 2.2 Hz, 2H), 6.61 (d, J = 8.2 Hz, 2H), 3.73 (s, 5H), 1.43 ppm (s, 10H)

Literature: ^{1}H NMR (400 MHz, $CDCl_3$) δ 7.29 – 7.20 (m, 4H), 7.11 (tt, J = 7.2, 1.5 Hz, 1H), 6.99 (dt, J = 8.6, 2.7 Hz, 2H), 6.61 (dt, J = 8.6, 2.7 Hz, 2H), 3.63 (s, 2H), 1.44 ppm (s, 9H)[144]

7.1.4 Synthesis of 5

To a flask containing **3** (500 mg, 1.11 mmol), DCM (10 mL) was added alongside TBATB (0.588 g, 1.22 mmol), and the mixture stirred at room temperature for 1 hour. Aqueous sodium sulphite (5 mL, 22 % *w/v*) was added and the mixture stirred for a further 30 minutes at room temperature. Aqueous sodium hydroxide (5 mL, 2 M) was then added, and the mixture was stirred for another 5 minutes before being left to separate, with the DCM phase retained and washed with deionised water (3 x 20 mL) before being dried using anhydrous magnesium sulphate and filtered. The resulting solution was dried using rotary evaporation, yielding dark red crystals. These crystals were then dissolved in dry THF (100 mL), and di-*tert*-butyl dicarbonate (0.226 g, 1.22 mmol) and dimethylaminopyridine (14 mg, 0.11 mmol) were added, before the flask was purged with nitrogen and refluxed under nitrogen for 12 hours. The mixture was then filtered, and the filtrate concentrated under rotary evaporation before being filtered again to yield a second crop of **4** as pale green crystals (65 % yield).

Experimental: ^{1}H NMR (400 MHz, $CDCl_3$) δ 7.74 (d, J = 7.4 Hz, 2H), 7.49 – 7.44 (m, 1H), 7.44 – 7.32 (m, 4H), 7.31 – 7.21 (m, 3H), 7.11 (dd, J = 6.4, 1.2 Hz, 2H), 7.02 (dt, J = 8.7, 2.8 Hz, 2H), 6.93 (dt, J = 8.4, 3.0 Hz, 2H), 6.68 (dt, J = 8.7, 2.6 Hz, 2H), 1.39 ppm (s, 9H)

Literature: ^{1}H NMR (400 MHz, $CDCl_3$) δ 7.74 (d, J = 7.7 Hz, 2H), 7.49 – 7.46 (m, 1H), 7.42 – 7.34 (m, 4H), 7.31 – 7.23 (m, 3H), 7.12 (dd, J = 7.6, 1.7 Hz, 2H), 7.02 (dt, J = 8.7, 2.6 Hz, 2H), 6.94 (dt, J = 8.6, 2.6 Hz, 2H), 6.68 (dt, J = 8.6, 2.6 Hz, 2H), 1.39 ppm (s, 9H)[144]

7.1.5 Synthesis of 6

4 (1.35 g, 4.76 mmol) and **5** (2.09 g, 3.96 mmol) g, were added to a pre-dried Schlenk tube, alongside $Pd(dba)_2$ (45 mg, 2 mol%), XPhos (40 mg, 2 mol%) and sodium *tert*-butoxide (0.86 g, 9.52 mmol). The mixture was purged with nitrogen, and dry toluene (40 mL) was added. The tube was sealed and heated at 110 ^{o}C for 2 days, before being cooled to room temperature and the reaction mixture filtered through celite, before the filtrate was dried via rotary evaporation. The resulting residue was taken up in DCM (100 mL) and washed with deionised water (3 x 100 mL) before being dried over anhydrous magnesium sulphate, filtered, and dried via rotary evaporation. To this residue, di-*tert*-butyl dicarbonate (1.27 g, 5.14 mmol) and dimethylaminopyridine (59 mg, 0.40 mmol) were added, before the mixture was taken up in dry THF (100 mL) and refluxed under nitrogen for 3 days. The resulting mixture was dried via rotary evaporation, and the residue was washed with methanol (2 x 10 mL) to yield **6** (61 % yield).

Experimental: ^{1}H NMR (400 MHz, $CDCl_3$): δ 7.70 (d, J = 7.1 Hz, 2H), 7.44 (t, J = 7.3 Hz, 1H), 7.36 (t, J = 7.2 Hz, 2H), 7.30-7.19 (m, 5H), 7.18-7.10 (m, 3H), 7.09 (s, 3H), 7.05 (s, 3H), 6.92 (dt, J = 8.7, 2.2 Hz, 2H), 6.64 (dt, J = 8.8 Hz, 2.5 Hz, 2H), 1.44-1.38 (m, 17H), 1.35 ppm (s, 9H)

Literature: ^{1}H NMR (400 MHz, $CDCl_3$): δ 7.74 (d, J = 7.2 Hz, 2H), 7.47 (t, J = 7.3 Hz, 1H), 7.40 (t, J = 7.3 Hz, 2H), 7.32-7.22 (m, 5H), 7.20-7.10 (m, 5H), 7.12 (s, 4H), 7.08 (s, 4H), 6.95 (dt, J = 8.7 Hz, 2.5 Hz, 2H), 6.66 (dt, J = 8.6 Hz, 2.6 Hz, 2H), 1.44 (s, 9H), 1.43 (s, 9H), 1.39 ppm (s, 9H)[144]

7.1.6 Synthesis of TANI

To a flask, ammonium formate (1.5 g, 24 mmol), **6** (2 g, 2.4 mmol), and Pd/C (51 mg, 10% Pd content) were added. The flask was purged with nitrogen, and dry THF (50 mL) and methanol (125 mL) were added, before the reaction mixture was refluxed under nitrogen for 18 hours. The mixture was then cooled down to room temperature, the solvent removed via rotary evaporation, and the resulting solid taken up in DCM (100 mL) and filtered through celite. The filtrate was then dried via rotary evaporation and the residue stirred in hexane (300 mL) for 1 hour. Filtration of this mixture yielded **TANI** as an off-white powder (89 %).

Experimental: ^{1}H NMR (400 MHz, $CDCl_3$): δ 7.33-7.28 (m, 3H), 7.20-7.04 (m, 5H), 6.96 (d, 8.0 Hz, 2 H), 6.61 (d, 8.9 Hz, 2H), 1.44-1.37 (m, 25 H)

7.2 - PDI-2-TANI - Synthesis

7.2.1 Synthesis of PDI-2

3,4,9,10-perylenetetracarboxylic acid dianhydride (PTCDA) (0.97 g, 2.47 mmol) was added to a flask containing 40 mL of toluene. To this suspension, ethylene diamine (1.7 mL, 25.6 mmol) was added, and the mixture refluxed for 16 hours. The resulting powder was filtered and washed with hot toluene, before being added to aqueous potassium hydroxide (40 mL, 5 M). This suspension was stirred for 6 hours, before being filtered and washed with water to yield **PDI-2** (64 % yield).

7.2.2 Synthesis of TANI-Linker

To a pre-dried flask, **TANI** (0.6 g, 0.9 mmol) was added, alongside a 4-bromobenzoic acid derivative (see **Table 3** for compounds and masses). Palladium(0) bis(dibenzylideneacetone) was added using catalyst loadings of either 2% (18 µmol), 5% (45 µmol), or 10% (90 µmol), alongside sodium *tert*-butoxide (0.6 g, 6.31 mmol). The flask was purged with nitrogen, and THF was added via syringe (10 mL). The mixture was then refluxed under nitrogen over several days, with reaction progress monitored via TLC using an elution of 5:6 (v/v) ethyl acetate:hexane. The reaction was then cooled to room temperature, filtered through celite, and the solvent removed via rotary evaporation.

	Ratio to TANI	Catalyst Loading (%)	Reaction Time (days)	Yield (%)	Notes
Methyl 4-bromobenzoate	1.2	2	6	38	Purified via method A.
4-bromobenzoic acid	5	10	3	33	Purified via method A, could not be isolated via column. Purified via method B to yield Boc-deprotected, oxidised product.
4-bromobenzoic acid	5	5	3	68	Purified via method B.

Table 3 *The reaction conditions used in the Buchwald-Hartwig couplings trialled for* ***TANI-Linker****.*

Two differing purification methods were trialled for this reaction:

Method A: The resulting residue was then dissolved in DCM (50 mL) and washed with deionised water (3 x 50 mL), before the DCM was removed via rotary evaporation. The resulting solid was then washed with sodium hydroxide (1 M, 60 mL). A column was then prepared silica gel, and the solid product was taken up in 10 mL of acetone before being dry-loaded onto silica gel (2 g). The dry-loaded product was added to the column, and eluted using a 5:6 (v/v) mixture of ethyl acetate:hexane, yielding **TANI-Linker**.

Method B: The resulting residue was then washed with THF (3 x 10 mL) and added to sodium hydroxide (5 M, 50 mL) and stirred for 10 minutes before being filtered, washed with sodium hydroxide (5 M, 3 x 10 mL) and deionised water (3 x 10 mL).

Methyl 4-bromobenzoate, Method A: ^{1}H NMR (400 MHz, $CDCl_3$) δ 7.95 (dt, J = 8.7, 1.7 Hz, 2H), 7.30 (tt, J = 7.4, 2.4 Hz, 2H), 7.20 – 7.07 (m, 15H), 6.97 (dt, J = 8.8, 1.8 Hz, 2H), 6.16 (s, 1H), 1.46-1.40 (m, 27 H), ESI-MS *m/z* 809.5 (M^+, 100%), 703.4 ($[M\text{-}Boc]^+$, 6)

4-bromobenzoic acid, Method A/B: ^{1}H NMR (400 MHz, $CDCl_3$) δ 7.82 (dt, J = 8.5 Hz, 2H), 7.57 (d, J = 8.8 Hz, 2H), 7.20 – 7.09 (m, 25H), 6.99-6.96 (m, 3H), 1.45-1.40 (m, 70 H)

4-bromobenzoic acid, Method B: ^{1}H NMR (400 MHz, $CDCl_3$) δ 7.44 (d, J = 8.3 Hz, 2H), 7.29 (t, J = 7.2 Hz, 2H), 7.20 – 7.05 (m, 13H), 1.44-1.40 (m, 31 H)

7.2.3 Synthesis of PDI-2-TANI

To a pre-dried flask, **TANI-Linker** (120 mg, 0.130 mmol) was added alongside HBTU (151 mg, 0.4 mmol). The flask was purged with nitrogen, before dry DMSO (5 mL) was added, and the resulting solution stirred at room temperature for 30 minutes. **PDI-2** (24 mg, 50 µmol), was then added to the mixture, alongside 30 µL (0.4 mmol) of triethylamine (TEA), and the reaction mixture was left for 16 h at room temperature. The mixture was then diluted with 50 mL of deionised water, before being partitioned with DCM (2 x 50 mL). These DCM fractions were combined and washed with 4 x 50 mL aliquots of deionised water, before being dried via rotary evaporation. A column was then prepared silica gel, and the solid product was taken up in 5 mL of DCM before being dry-loaded onto silica gel (2 g). The dry-loaded product was added to the column, and eluted using a 5:6 (v/v) mixture of ethyl acetate:hexane. Fractions were tested via TLC utilising a 5:6 (v/v) mixture of ethyl acetate:hexane, and the R_f = 0.86 fractions were collected. The regeneration of a spot at R_f = 0.25 meant that the R_f = 0.86 fractions were purified via column chromatography a second time; either using the same 5:6 (v/v) ethyl acetate:hexane elution, or a more polar 1:10:90 (v/v/v) TEA:methanol:ethyl acetate elution. These fractions were confirmed to be **PDI-2-TANI** (20 % yield).

^{1}H NMR (400 MHz, $CDCl_3$) δ 8.02 (d, J = 8.5 Hz, 2H), 7.57 (d, J = 8.4 Hz, 2H) 7.52-7.34 (m, 8H), 7.30 (tt, J = 7.9, 1.8 Hz, 6H), 7.20 – 7.07 (m, 28H), 4.55 (t, J = 6.3 Hz, 3H) 1.45-1.39 (m, 54 H)

7.3 - PDI-2-TANI - Alternative Synthesis

7.3.1 Synthesis of 2-Linker - EDC

To a dry flask, 4-bromobenzoic acid (5.02 g, 25 mmol) was added, alongside EDC.HCl (4.78 g, 25 mmol). The flask was purged with nitrogen and placed in an ice bath for 10 minutes, before dry ethanol (70 mL) was added alongside ethylene diamine (6.7 mL, 100 mmol) and the mixture left at room temperature for 14 hours under nitrogen. The mixture was then dried via rotary evaporation, and the resulting solid washed with deionised water (250 mL), before being dissolved in DCM (100 mL), then washed with aqueous NaOH (2 x 100 mL, 5 M). The resulting solution was then partitioned using aqueous HCl (100 mL, 1 M), and the aqueous fraction dried via rotary evaporation before being washed with aqueous NaOH (3 x 30 mL, 5M) to yield an impure mixture containing **2-Linker** and EDC urea (<15 % yield).

^{1}H NMR (400 MHz, D_2O) δ 7.65-7.49 (m, 4H), 3.60-3.53 (m, 3H), 3.12-3.05 (m, 2H)

7.3.2 Synthesis of 2-Linker - DCC

To a dry flask, 4-bromobenzoic acid (4.98 g, 25 mmol) was added, alongside DCC (5.15 g, 25 mmol). The flask was purged with nitrogen and placed in an ice bath for 10 minutes, before dry diethyl ether (100 mL) was added alongside ethylene diamine (6.7 mL, 100 mmol) and the mixture left at room temperature for 72 hours under nitrogen. The mixture was then filtered, with the resulting solid added to toluene (500 mL) and sonicated in a water bath for 1 hour before being filtered. The resulting solid was again added to toluene (500 mL) and sonicated in a water bath for 1 hour, before being filtered and washed with DCM (2 x 100 mL) before being washed with aqueous NaOH (2 x 100 mL, 5 M). The solid was then taken up in HCl (20 mL, 1 M) and the mixture filtered, with the filtrate neutralised using

NaOH (20 mL, 1 M) to precipitate the resulting solid, an impure mixture containing **2-Linker** and DCC urea (<10 % yield).

^{1}H NMR (400 MHz, D_2O) δ 7.61-7.55 (m, 4H), 3.52 (t, J = 6.0 Hz, 2H), 3.20 (t, J = 5.8 Hz, 2H)

7.3.3 Synthesis of 2-Linker - Direct Amidation

To a dry flask, methyl 4-bromobenzoate (2.19 g, 10 mmol) was added and the flask was purged with nitrogen. Ethylene diamine (6.6 mL, 100 mmol) was added via syringe and the mixture refluxed (at 132 ^{o}C) under nitrogen for 30 minutes.

Two differing purification methods were trialled for this reaction:

Method A: The resulting mixture was concentrated under vacuum, before being diluted with ethyl acetate (50 mL) and filtered. The filtrate was washed with deionised water (3 x 20 mL) and dried using rotary evaporation, before being added to HCl (10 mL, 1M) and filtered again. The filtrate was then dried using rotary evaporation and the resulting solid washed with a mixture of ethanol and toluene (20 mL, 50/50 (v/v)), before being recrystallised with ethanol and diethyl ether (1 mL, 50/50 (v/v)) to yield pure **2-Linker** (0.5 % yield).

Method B: The resulting mixture was concentrated under vacuum, before being diluted with toluene (500 mL) and sonicated in a water bath for 1 hour before being filtered. The resulting solid was again

added to toluene (500 mL) and sonicated in a water bath for 1 hour, before being filtered and the solid washed with NaOH (10 mL, 5 M) to yield pure **2-Linker** (24 % yield).

^{1}H NMR (400 MHz, D_2O) δ 7.63-7.56 (m, 4H), 3.60 (t, J = 5.9 Hz, 2H), 3.15 (t, J = 5.3 Hz, 2H)

7.3.4 Synthesis of PDI-2-Linker

2-Linker (0.140 g, 0.575 mmol) was added to a suspension of PTCDA (0.07 g, 0.175 mmol) in toluene (20 mL). This mixture was placed under reflux for 24 hours, and the resulting powder was filtered and washed with hot toluene. The solid was added to aqueous potassium hydroxide (5 M, 5 mL) and stirred at room temperature for 4 hours, before being filtered to yield a very fine black solid. This was then immersed in HCl (1 M, 20 mL), centrifuged for 5 minutes, and the yellow aqueous layer (indicative of **2-Linker**) decanted off to yield the solid. This process was repeated 6 times until the aqueous layer was colourless, yielding **PDI-2-Linker** (8 % yield).

^{1}H NMR (400 MHz, DMSO-d_6) δ 8.69-8.44 (m, 8H), 7.66-7.63 (m, 8H), 5.05 (t, J = 23 Hz, 4H), 3.68-3.61 (m, 3H)

8. Appendices

8.1 Appendix A - NMR and Mass Spectra

A1. ^{1}H NMR spectrum of **2**.

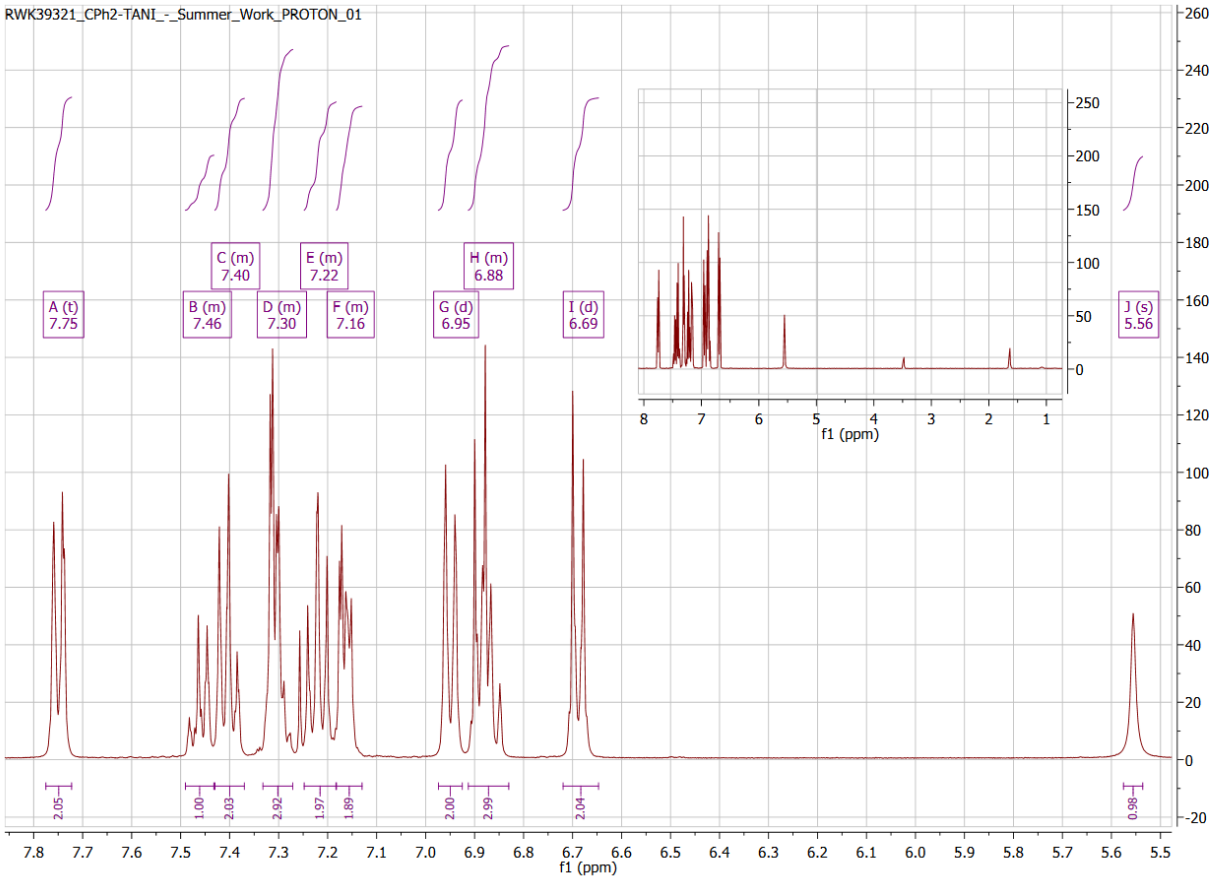

A2. ^{1}H NMR spectrum of **3**.

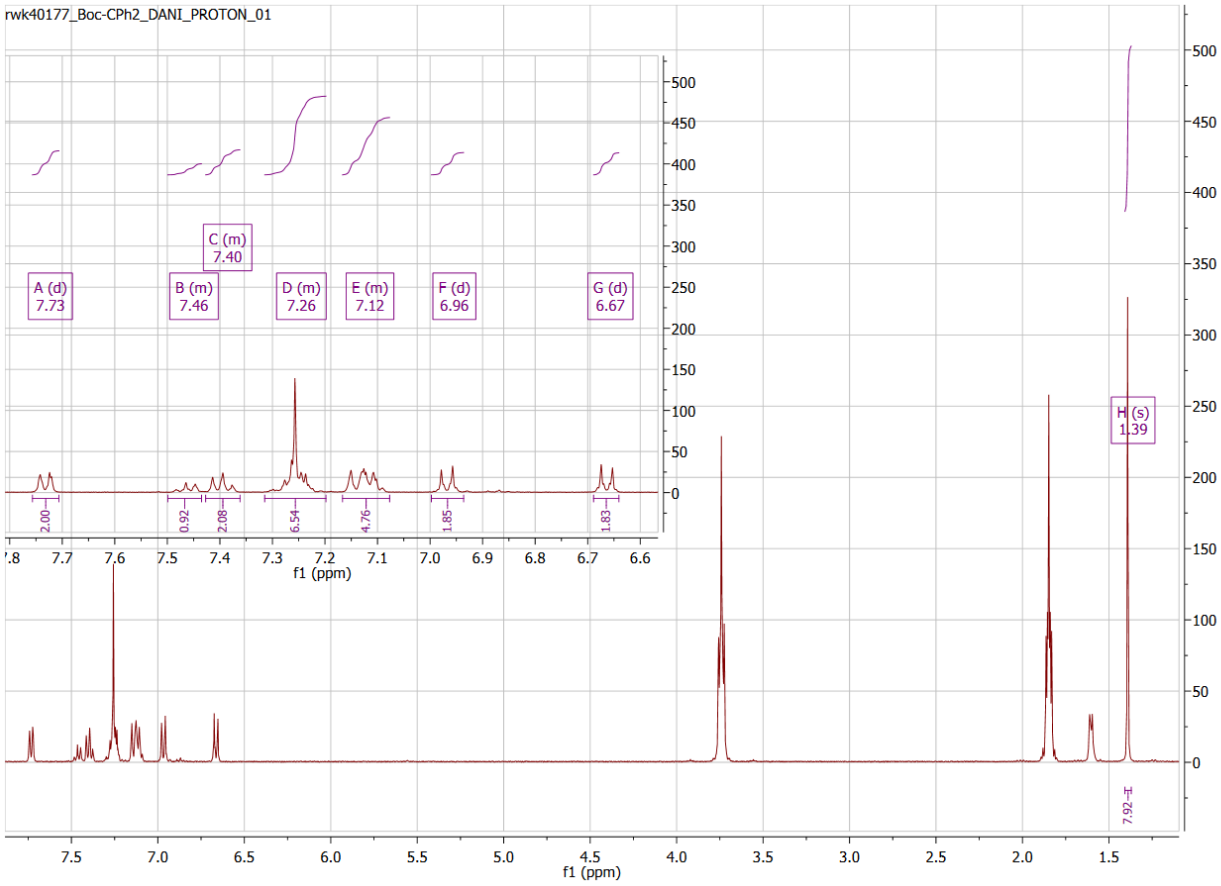

A3. ^{1}H NMR spectrum of **4**.

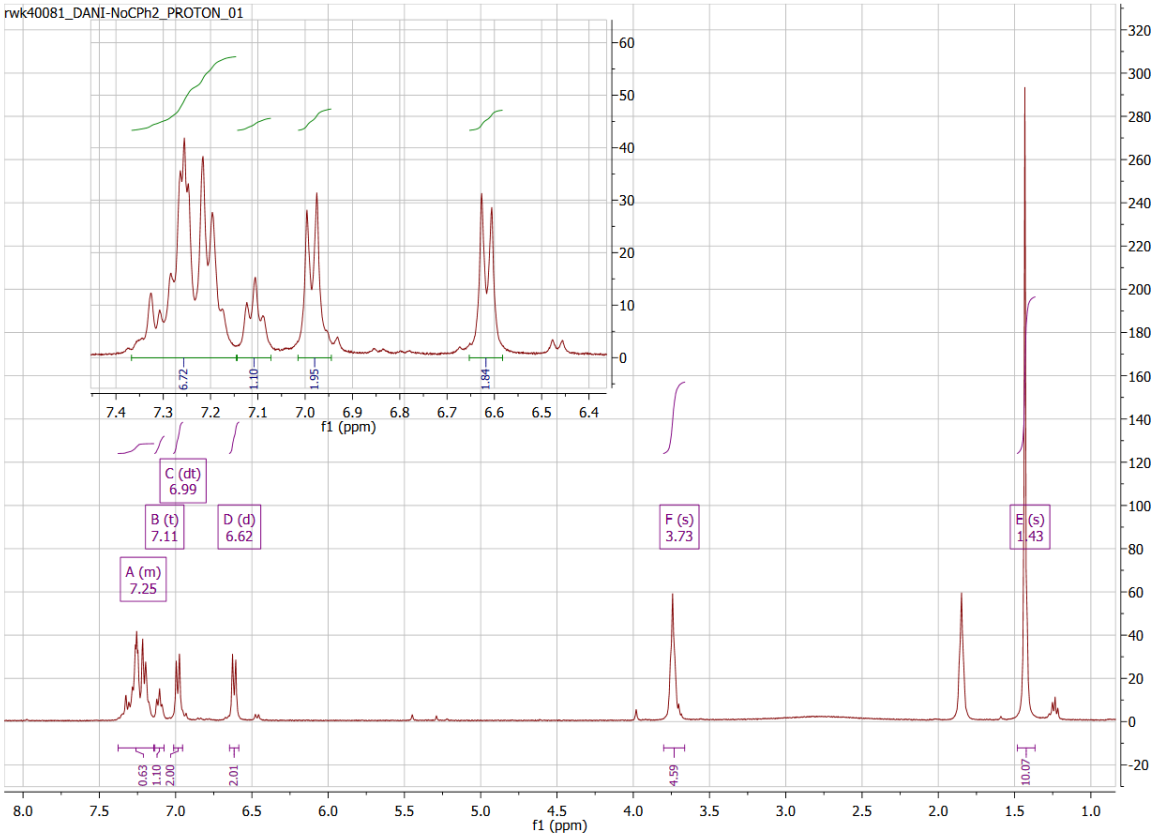

A4. ^{1}H NMR spectrum of **5**.

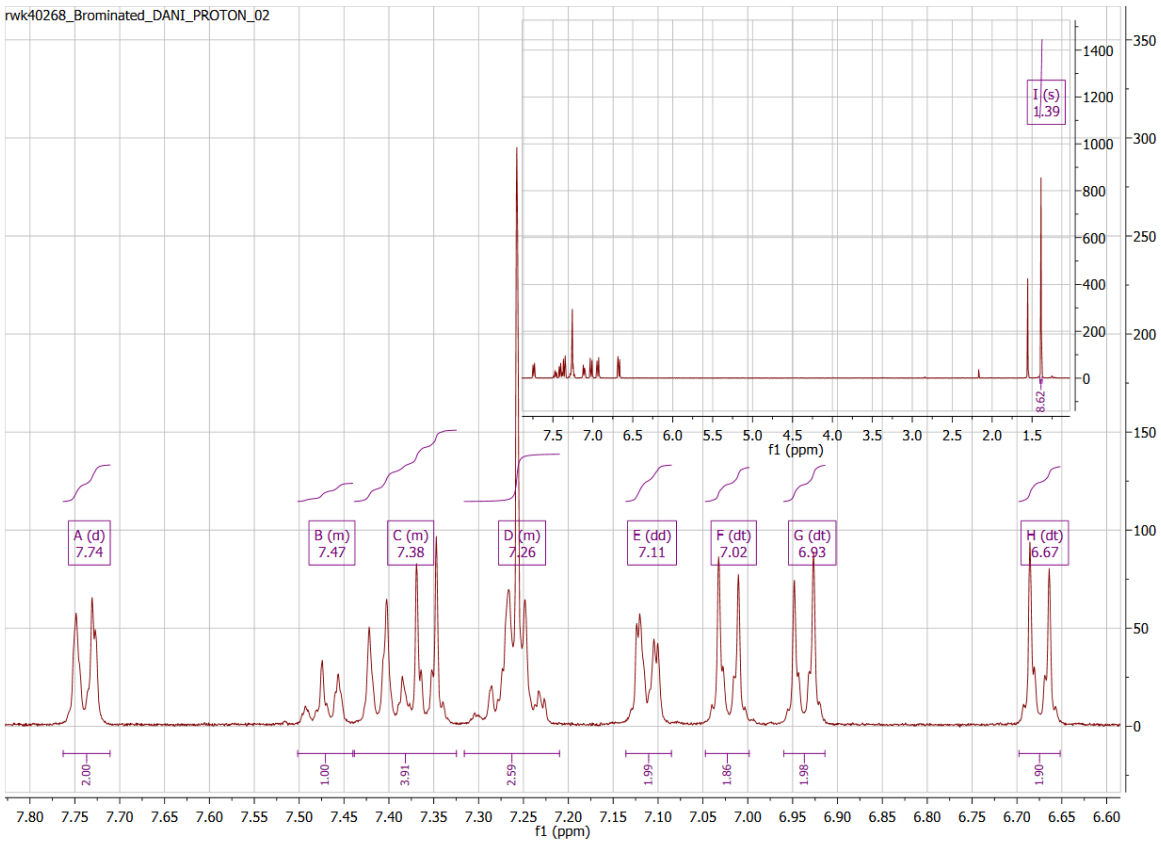

A5. ^{1}H NMR spectrum of **6**.

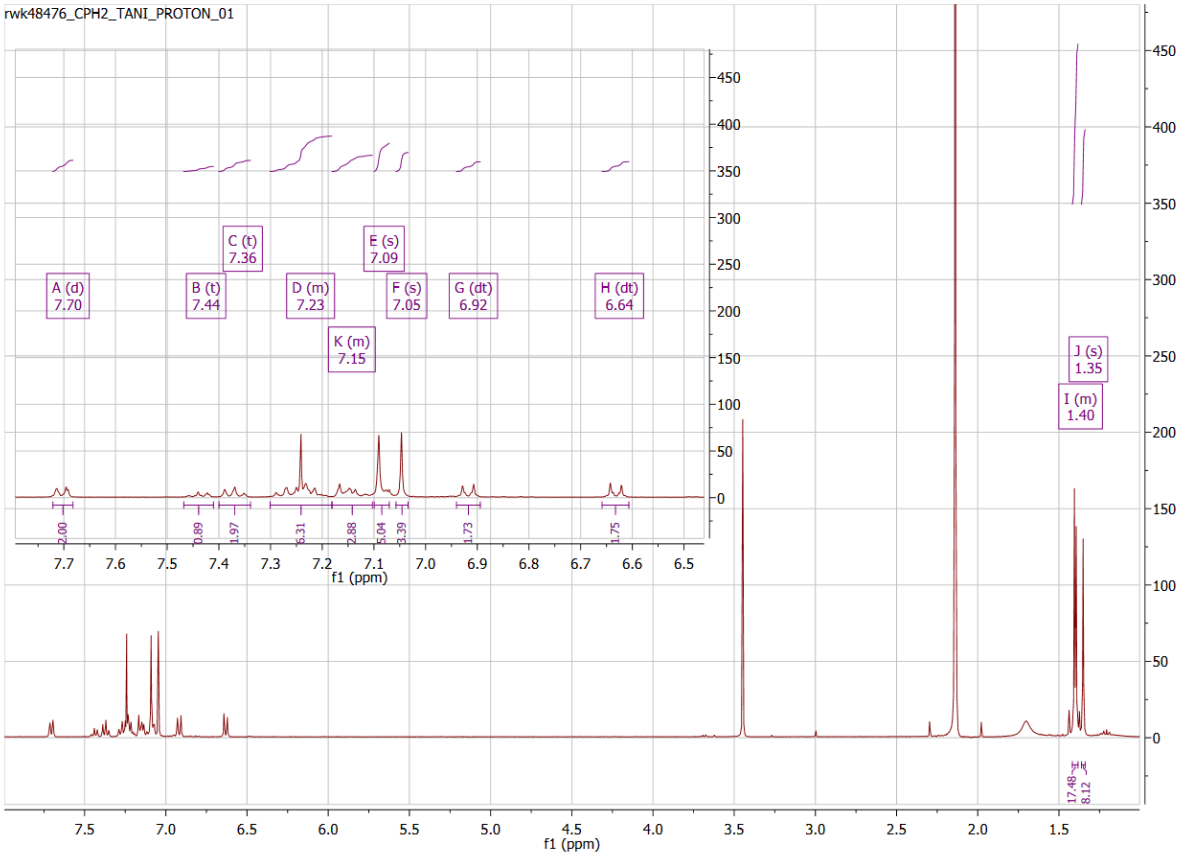

A6. ^{1}H NMR spectrum of **TANI**.

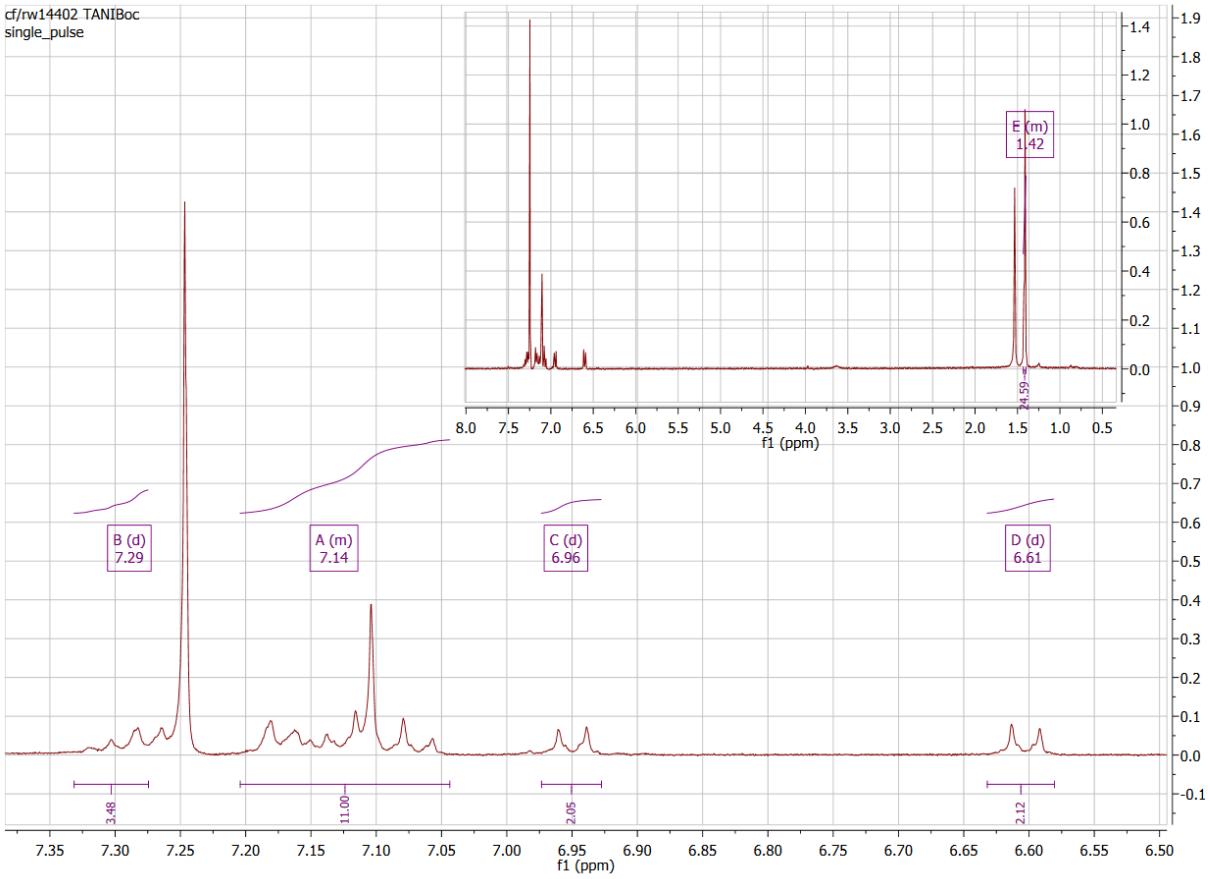

A7. ^{1}H NMR spectrum of **TANI-Linker**, prepared from bromobenzoic acid via purification method A, then method B.

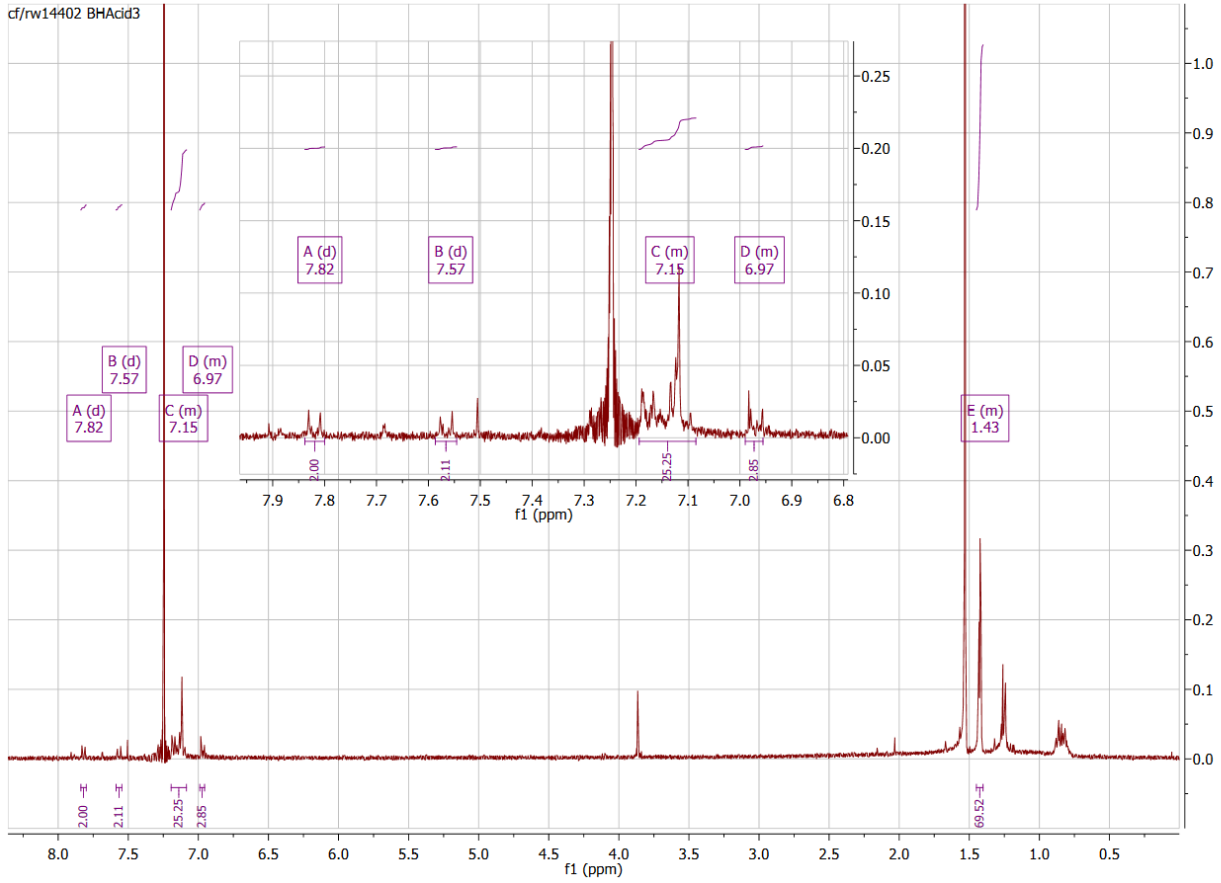

A8. ^{1}H NMR spectrum of **TANI-Linker**, prepared from bromobenzoic acid via purification method B.

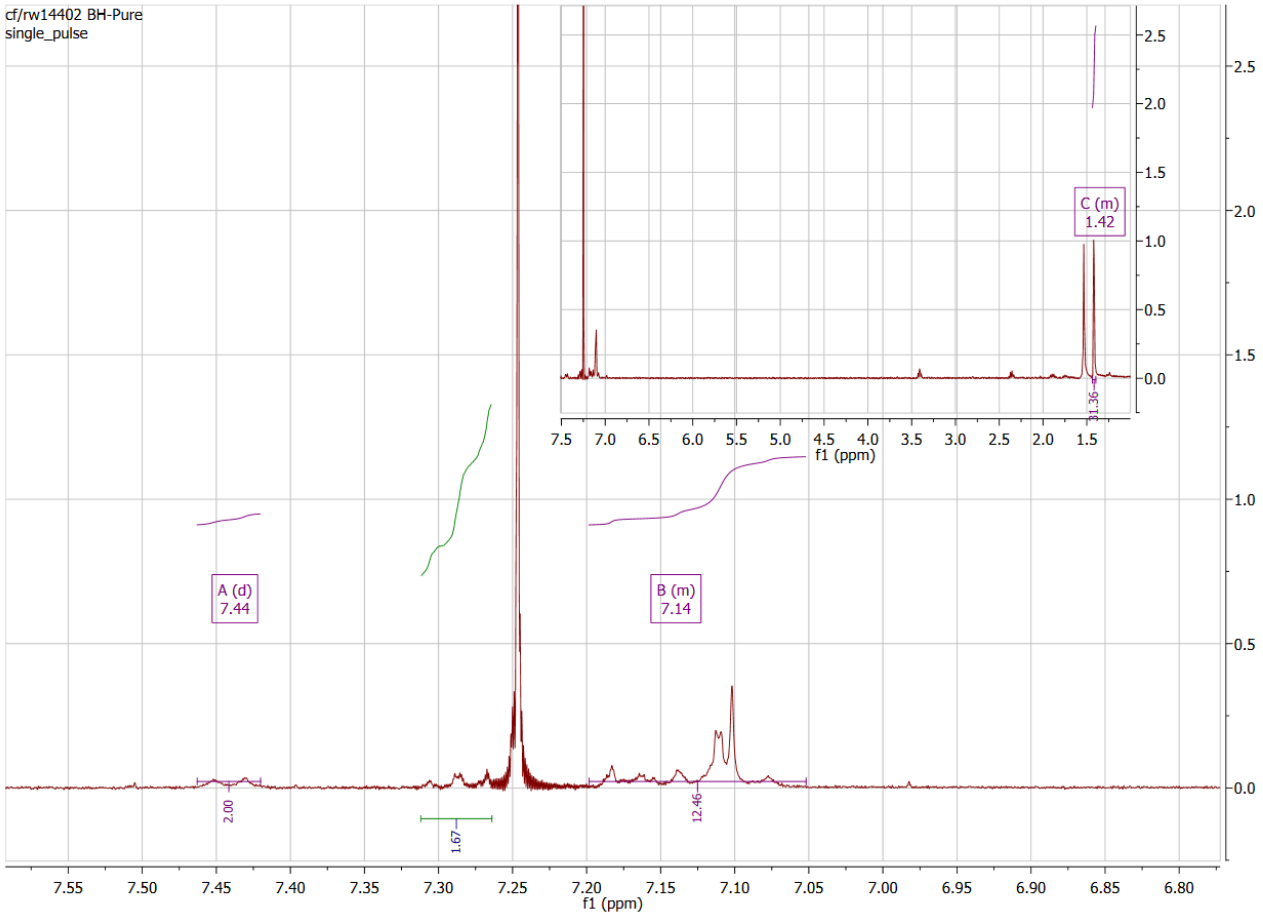

A9. ^{1}H NMR spectrum of **2-Linker**, prepared via EDC coupling.

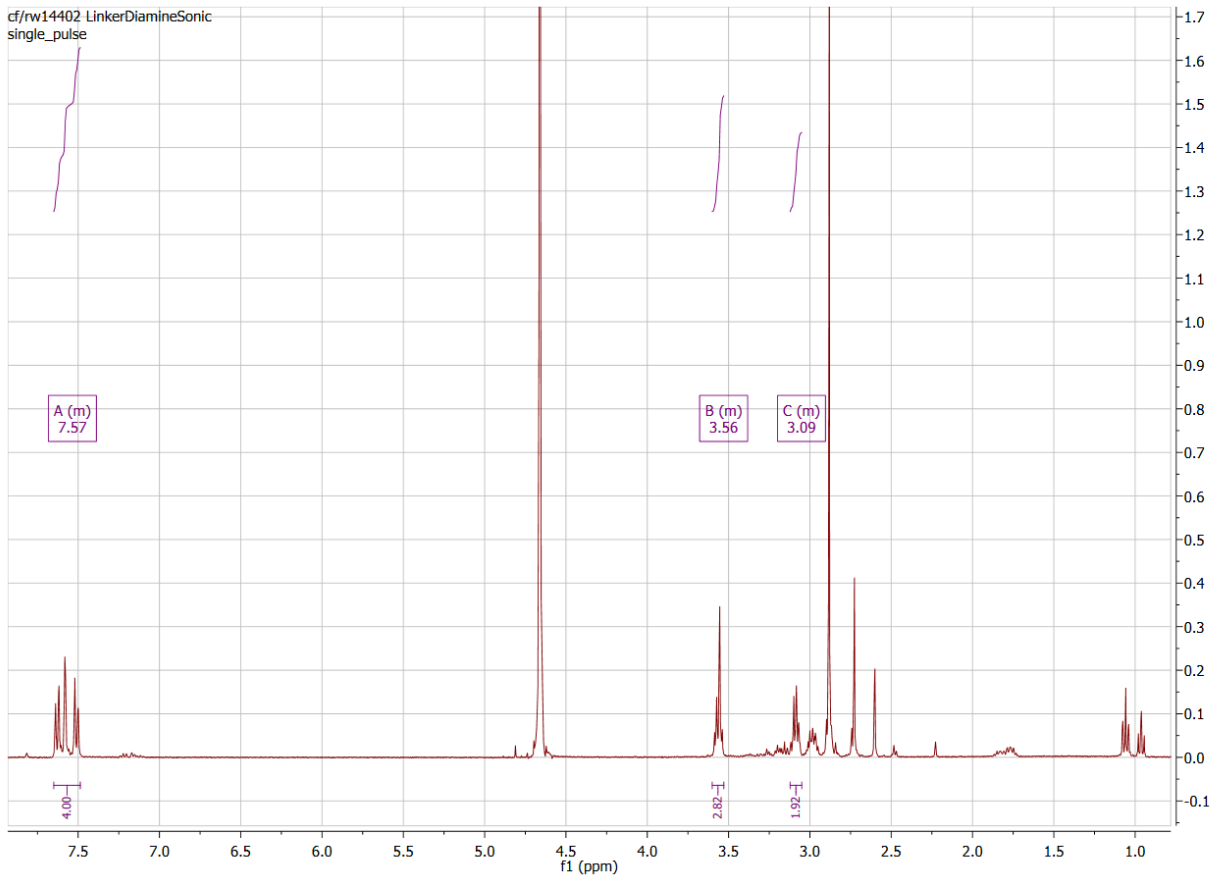

A10. ^{1}H NMR spectrum of **2-Linker**, prepared via DCC coupling.

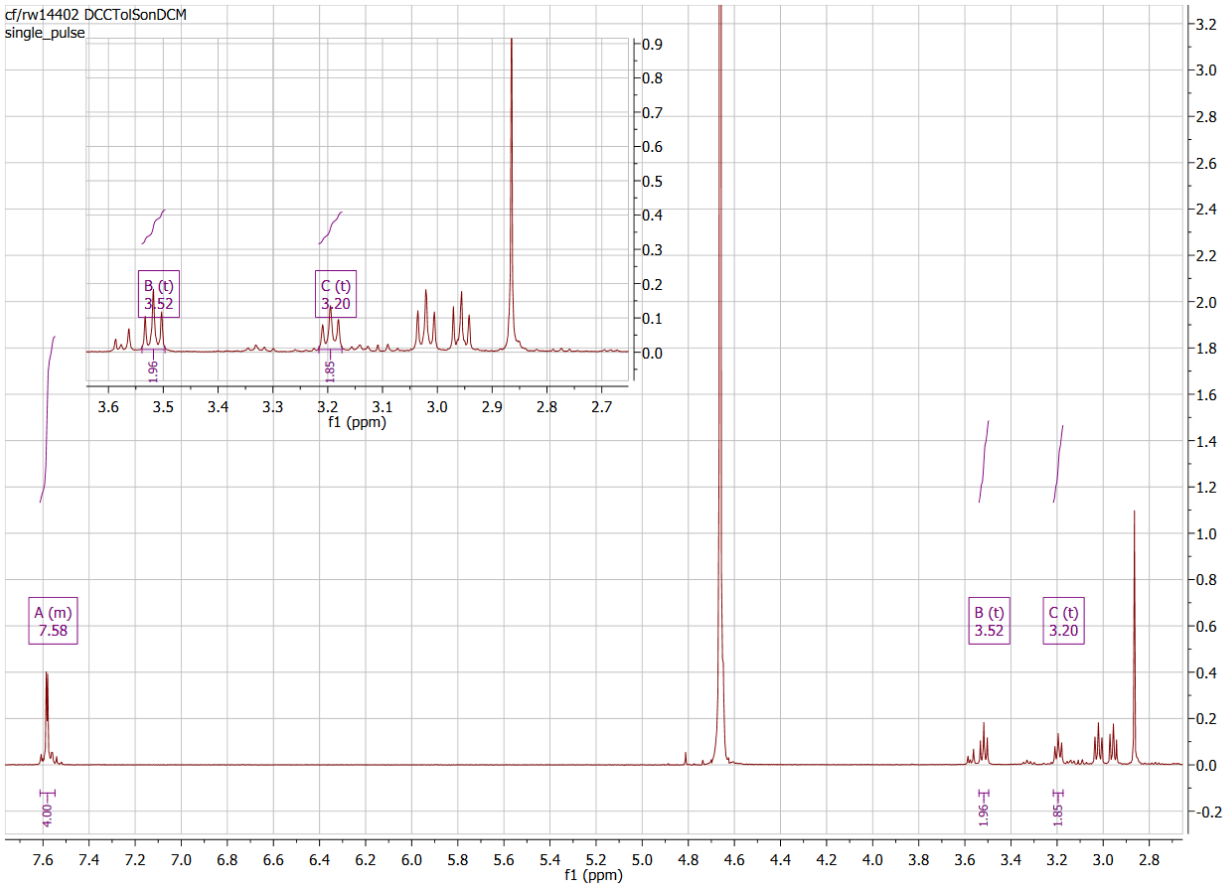

8.2 Appendix B - TEM Images

Due to the large number of TEM images used to calculate fibre lengths and their distributions, a representative selection of images has been chosen for each experiment. Tables of measured fibre lengths, also included in this section, provide the full set of raw data used to calculate distributions and dispersities in **Section 3.4**, **Section 3.4.3** and **Section 3.4.4**.

B1. TEM image of thermally self-seeded **PDI-2-TANI** in ethyl acetate - [**PDI-2-TANI**] = 6 x 10^{-4} M.

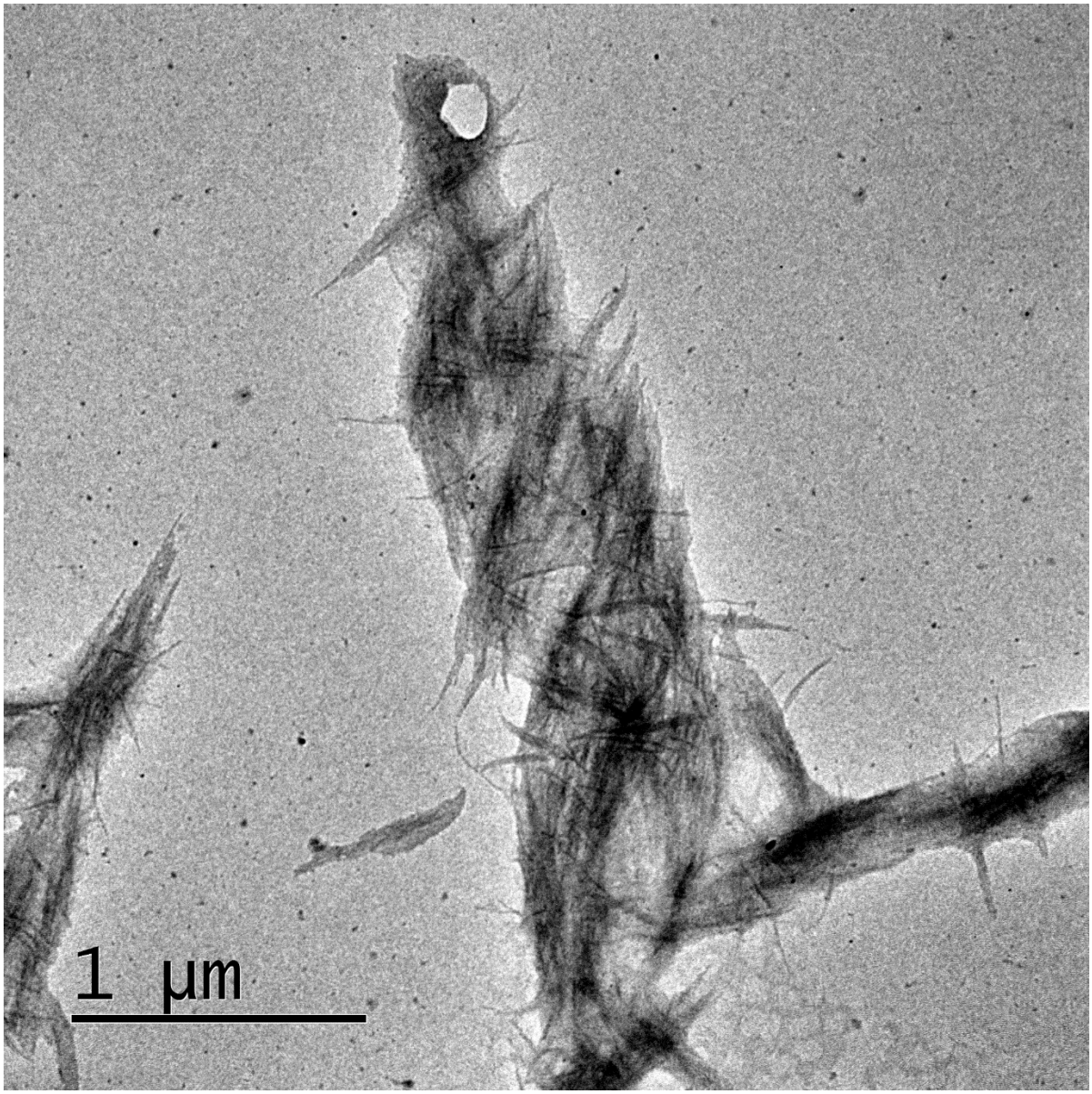

B2. TEM image of thermally self-seeded **PDI-2-TANI** in ethyl acetate - [**PDI-2-TANI**] = 6 x 10^{-4} M.

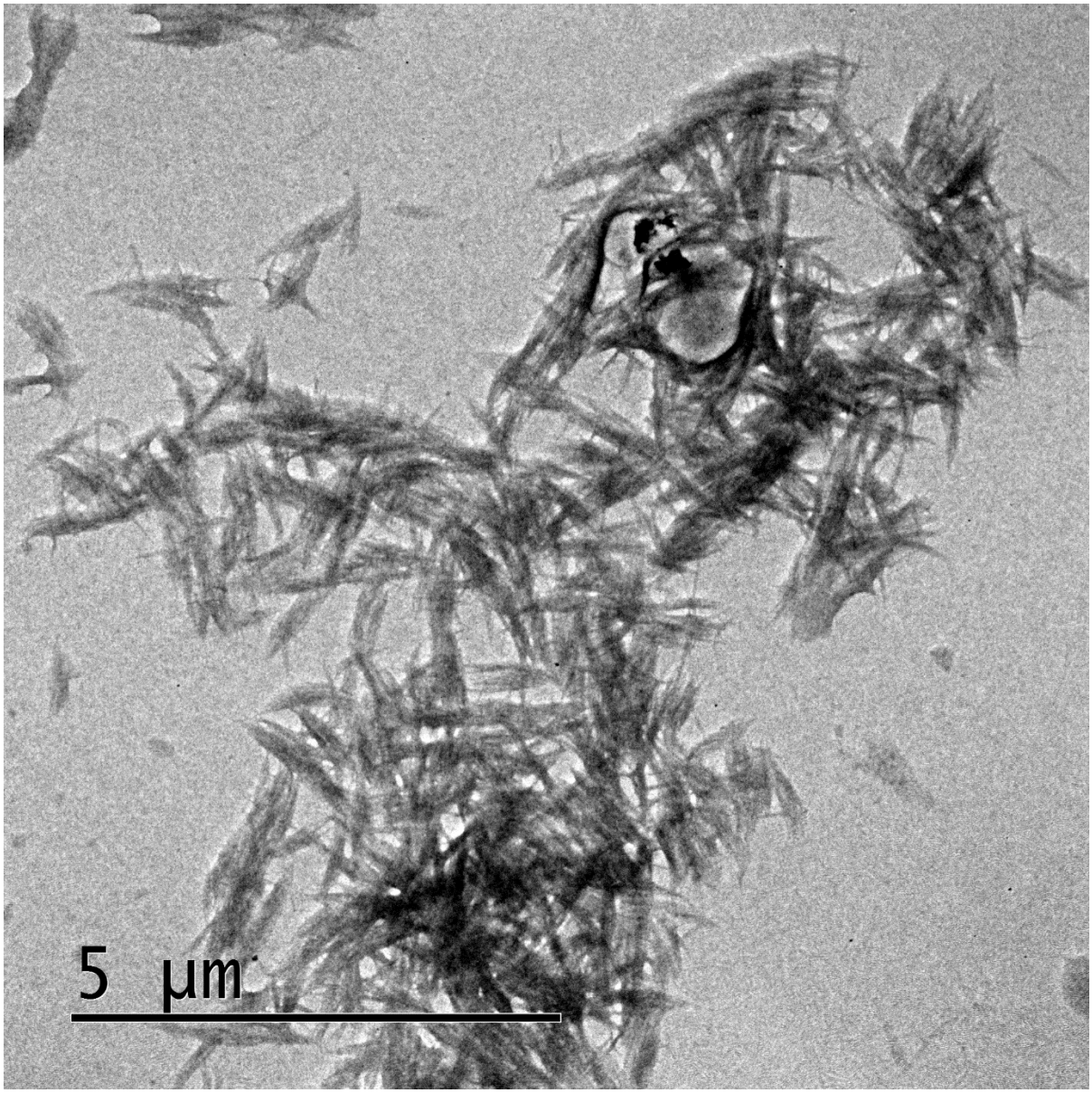

B3. TEM image of thermally self-seeded **PDI-2-TANI** in ethyl acetate - [**PDI-2-TANI**] = 6 x 10^{-4} M.

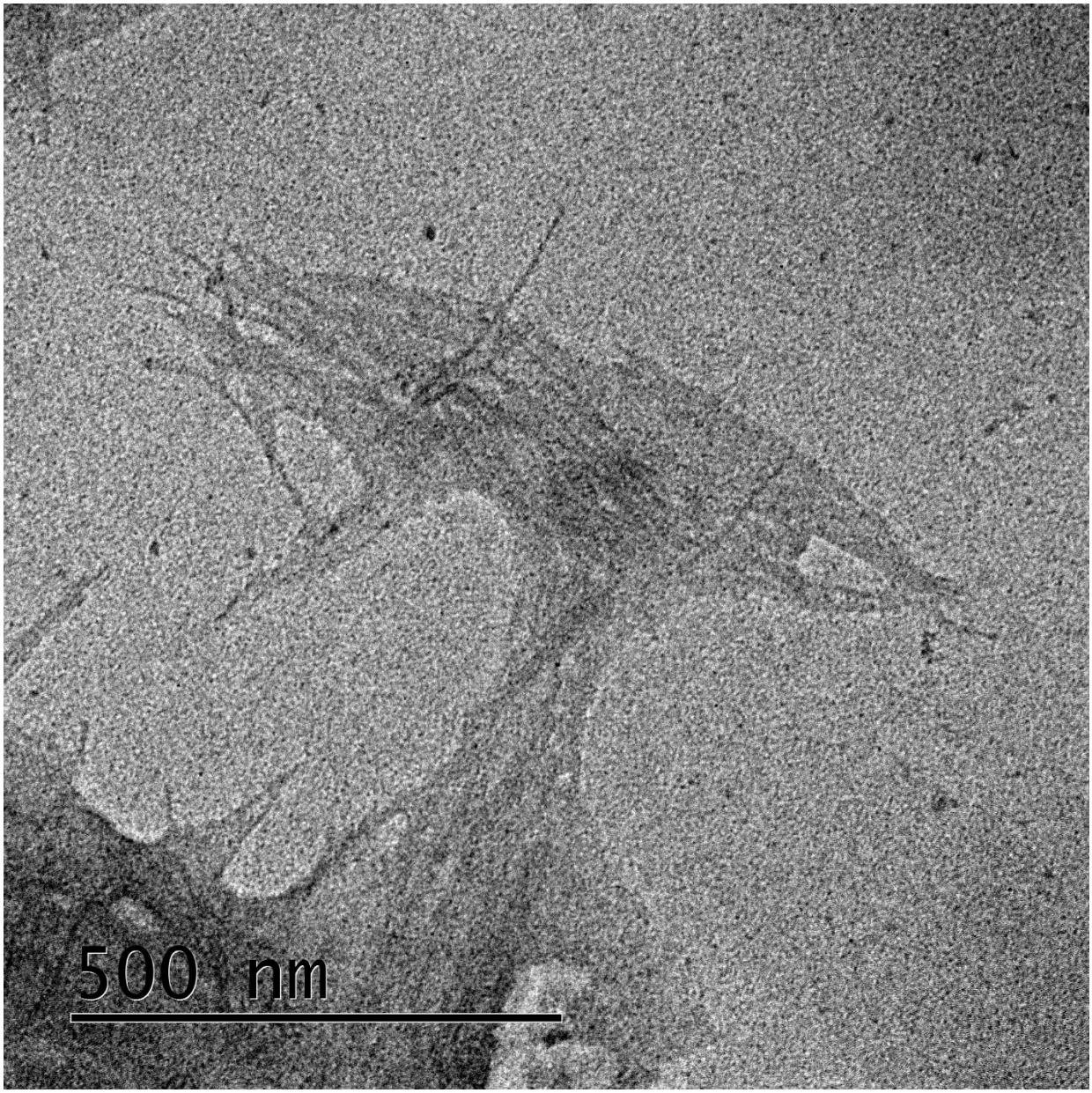

B4. TEM image of thermally self-seeded **PDI-2-TANI** in ethyl acetate - [**PDI-2-TANI**] = 6 x 10^{-4} M.

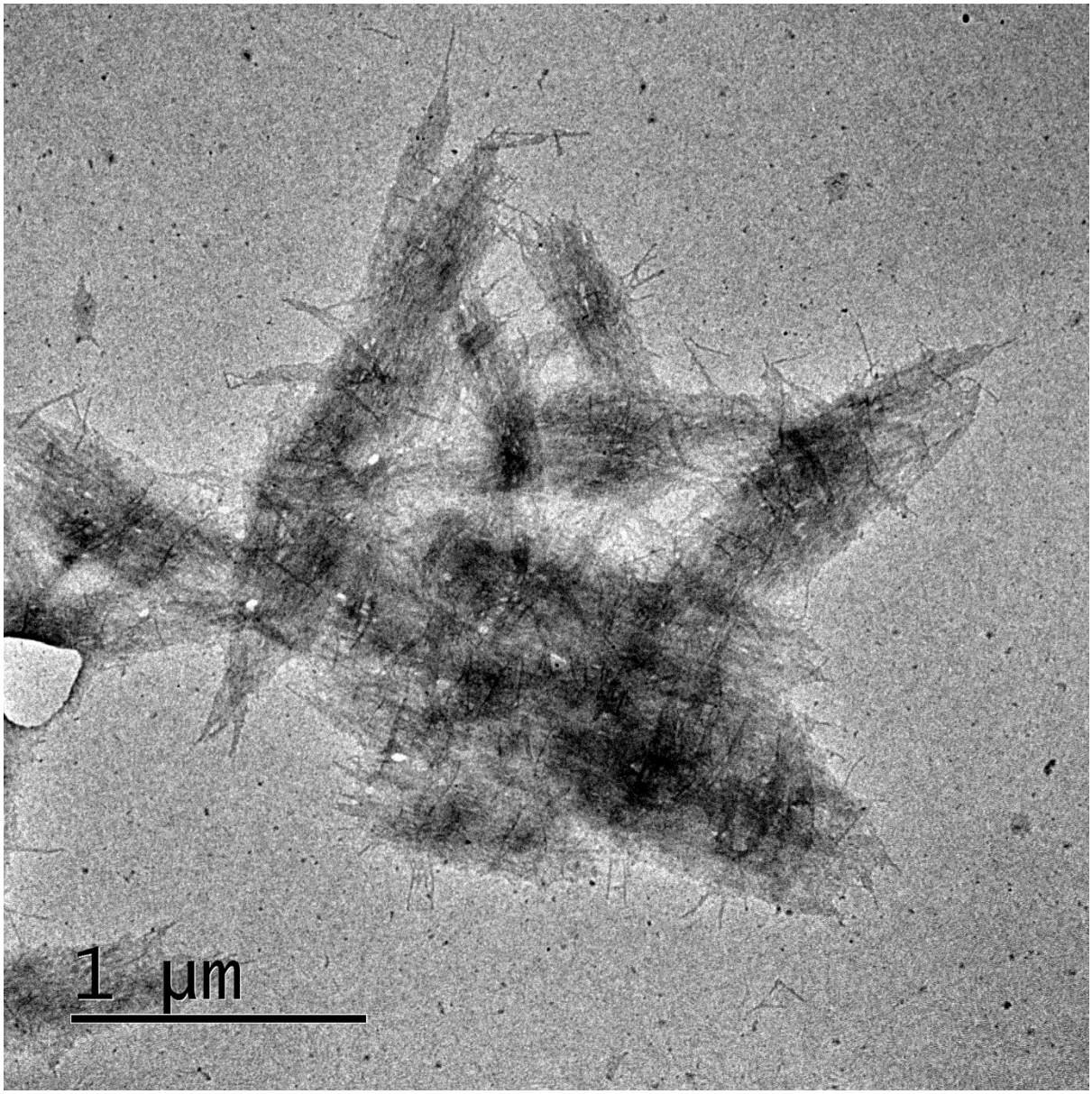

B5. TEM image of thermally self-seeded **PDI-2-TANI** in ethyl acetate - [**PDI-2-TANI**] = 6 x 10^{-5} M.

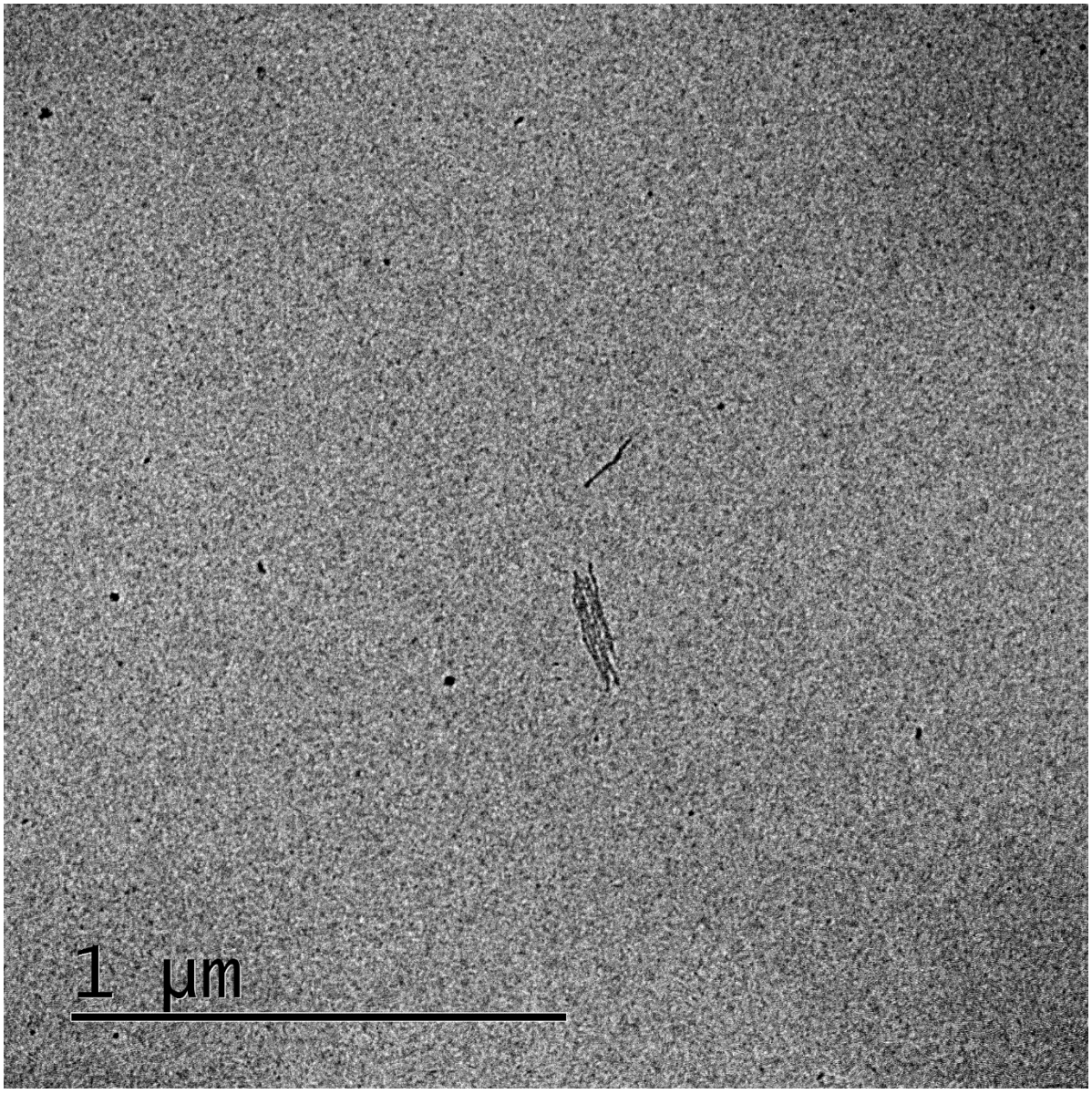

B6. TEM image of thermally self-seeded **PDI-2-TANI** in ethyl acetate - [**PDI-2-TANI**] = 6 x 10^{-5} M.

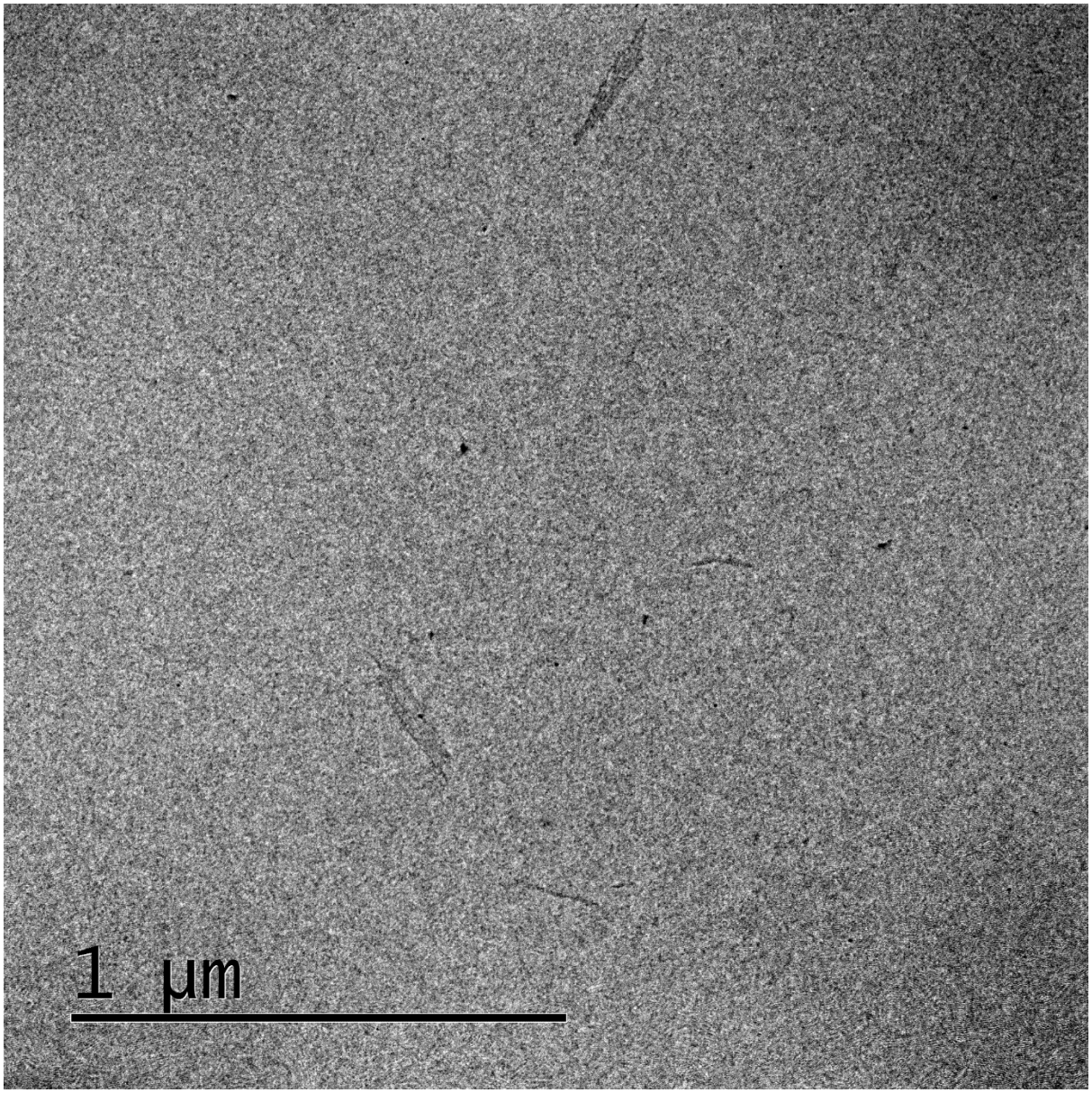

B7. TEM image of thermally self-seeded **PDI-2-TANI** in ethyl acetate - [**PDI-2-TANI**] = 6 x 10^{-5} M.

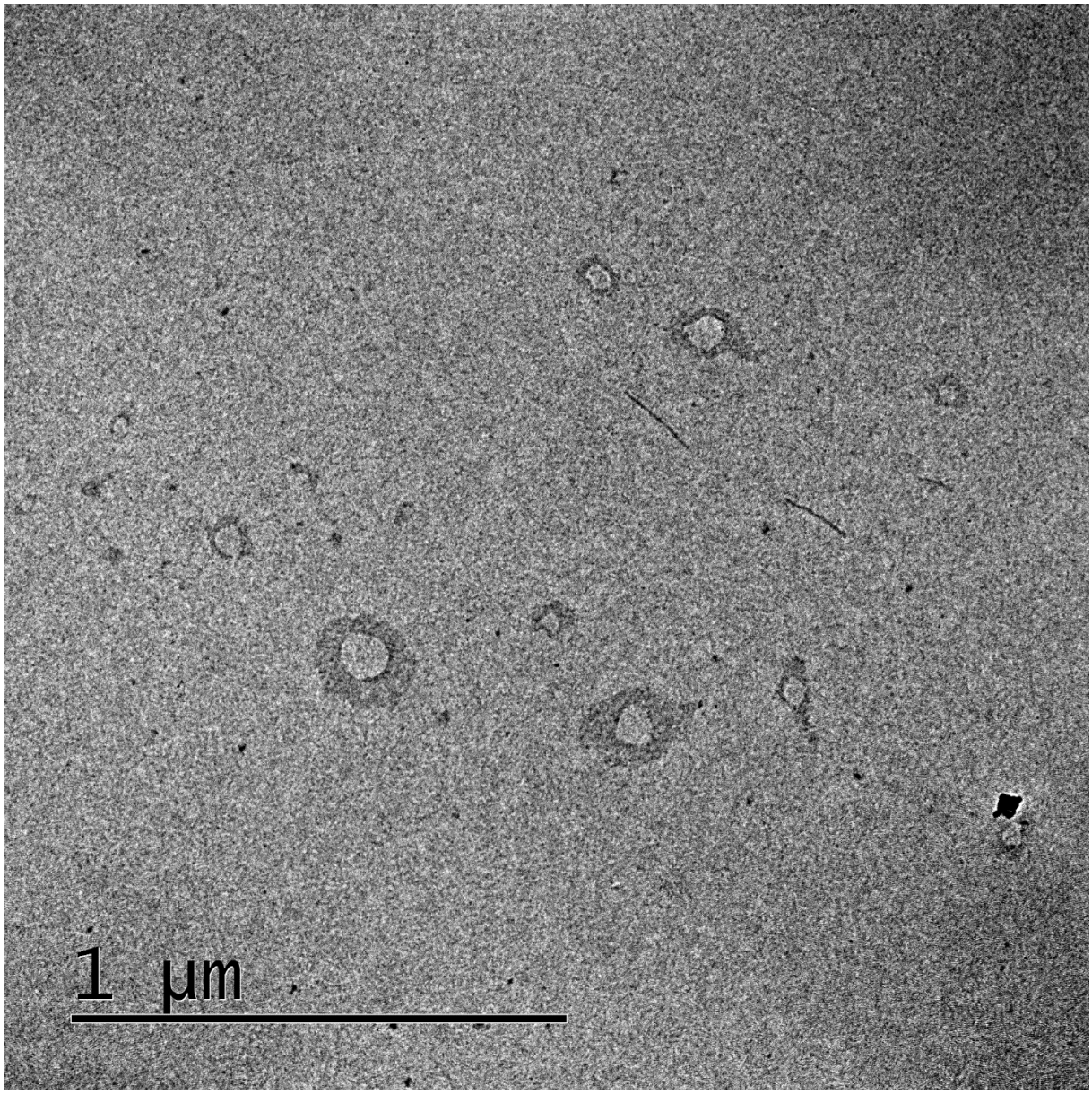

B8. TEM image of thermally self-seeded **PDI-2-TANI** in ethyl acetate - [**PDI-2-TANI**] = 6 x 10^{-5} M.

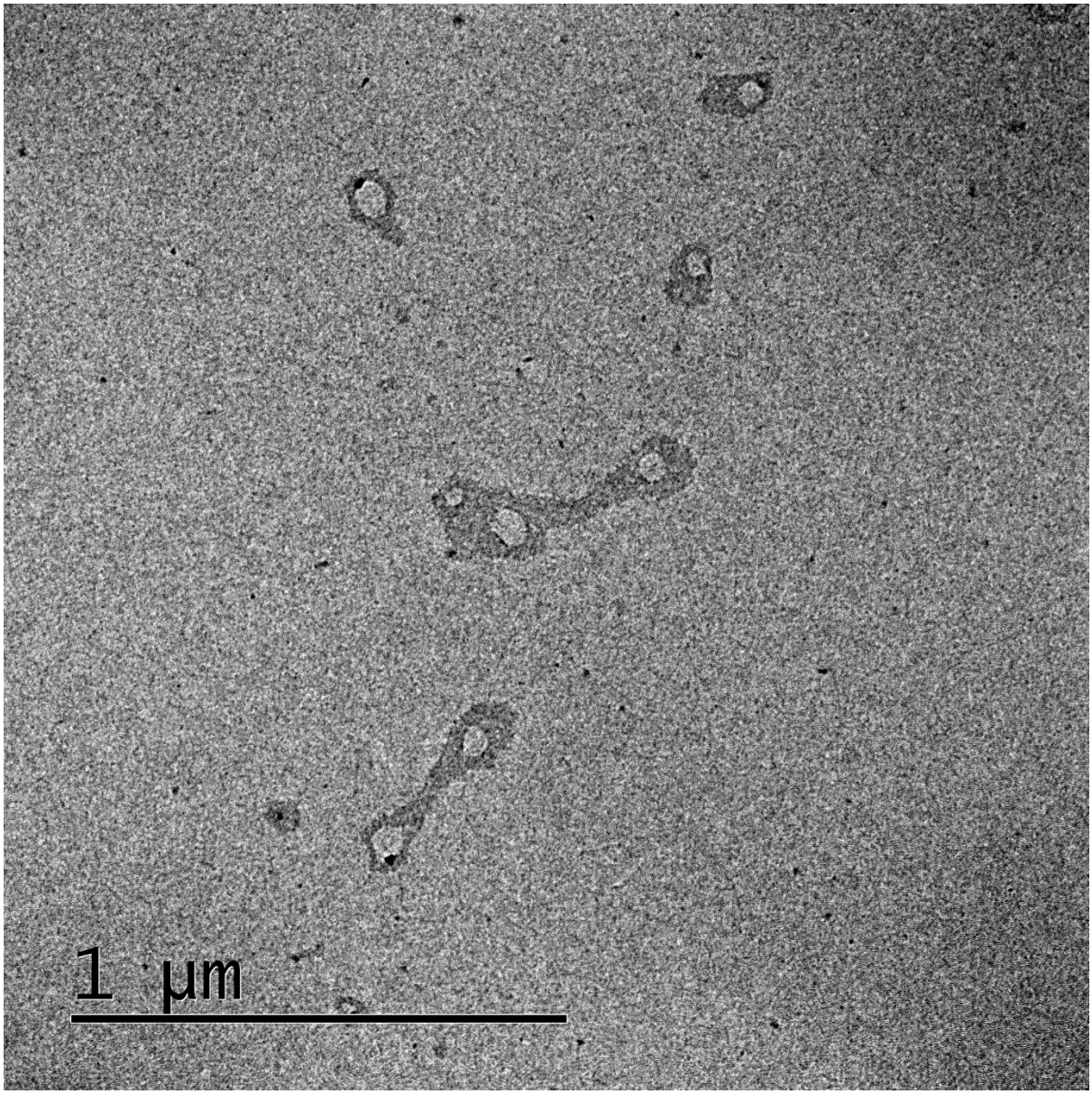

B9. TEM image of thermally self-seeded **PDI-2-TANI** in ethyl acetate, after 2 days of ageing at room temperature - [**PDI-2-TANI**] = 6 x 10^{-5} M.

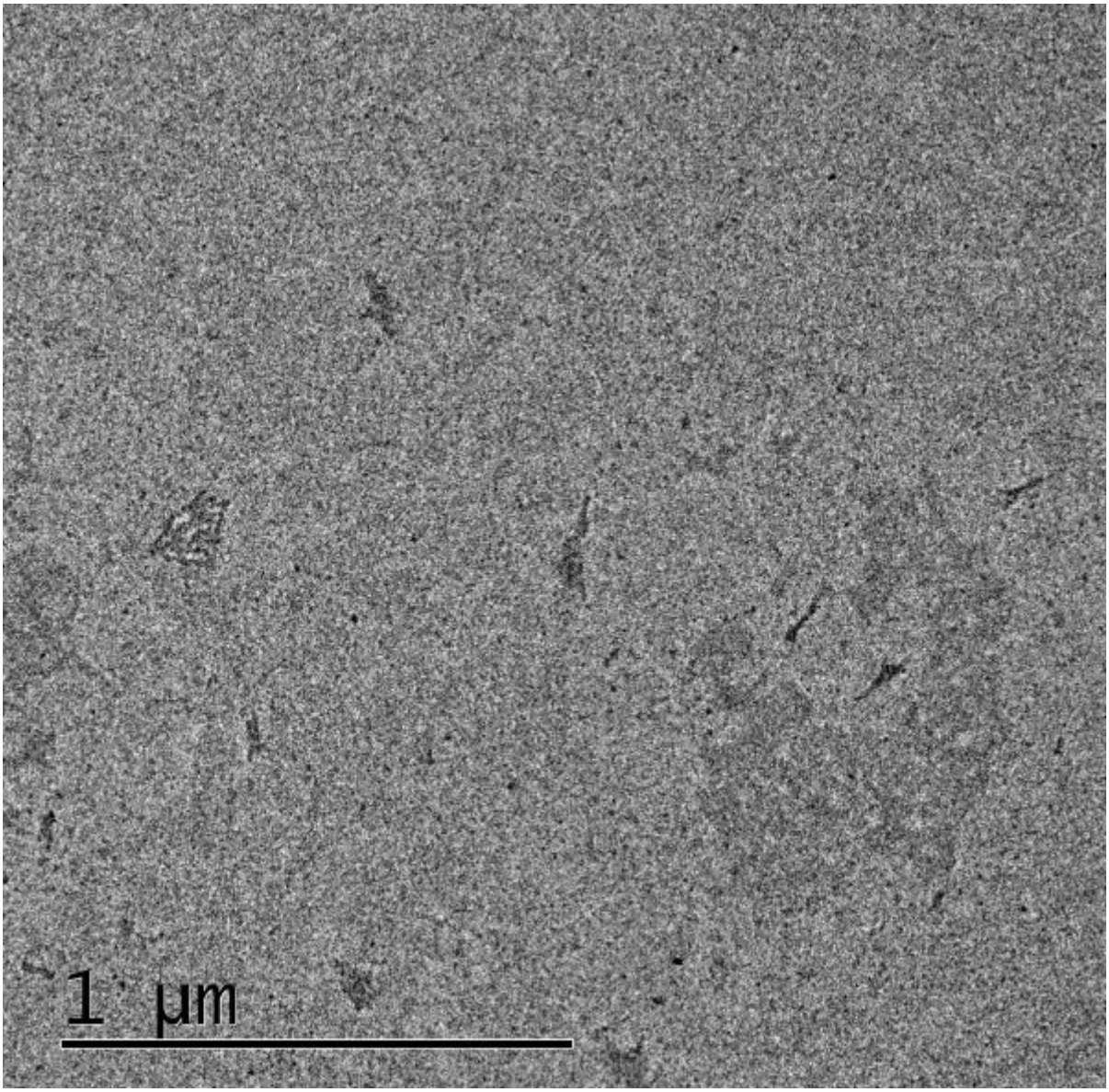

B10. Tabulated fibre lengths of thermally self-seeded **PDI-2-TANI** in ethyl acetate - [**PDI-2-TANI**] = 6 x 10^{-5} M.

Count	Fibre length *L* (nm)	L^2 (nm^2)
1	53	2777
2	70	4958
3	96	9255
4	101	10194
5	117	13598
6	117	13637
7	119	14274
8	125	15681
9	137	18683
10	138	19120
11	141	20015
12	143	20387
13	145	20918
14	153	23418
15	153	23477
16	156	24205
17	161	25882
18	162	26171
19	169	28460
20	169	28722
21	170	28834
22	173	29887
23	176	31073
24	176	31089
25	178	31745
26	188	35216
27	193	37247
28	213	45352
29	220	48368
30	232	53797
31	233	54305
32	238	56842
33	239	57315
34	241	58159
35	241	58164
36	245	60209

B11. Tabulated fibre lengths of thermally self-seeded **PDI-2-TANI** in ethyl acetate after 2 days of ageing at room temperature - [**PDI-2-TANI**] = 6 x 10^{-5} M.

Count	Fibre length *L* (nm)	L^2 (nm^2)
1	65	4251
2	52	2707
3	73	5305
4	73	5378
5	113	12684
6	76	5707
7	127	16233
8	124	15468
9	49	2390
10	36	1293
11	125	15742
12	69	4815
13	55	3001
14	81	6565
15	70	4869
16	108	11559
17	39	1547
18	28	758
19	86	7313
20	80	6351

B12. TEM image of **PDI-2-TANI** in ethyl acetate at room temperature prior to sonication - [**PDI-2-TANI**] = 6 x 10^{-5} M.

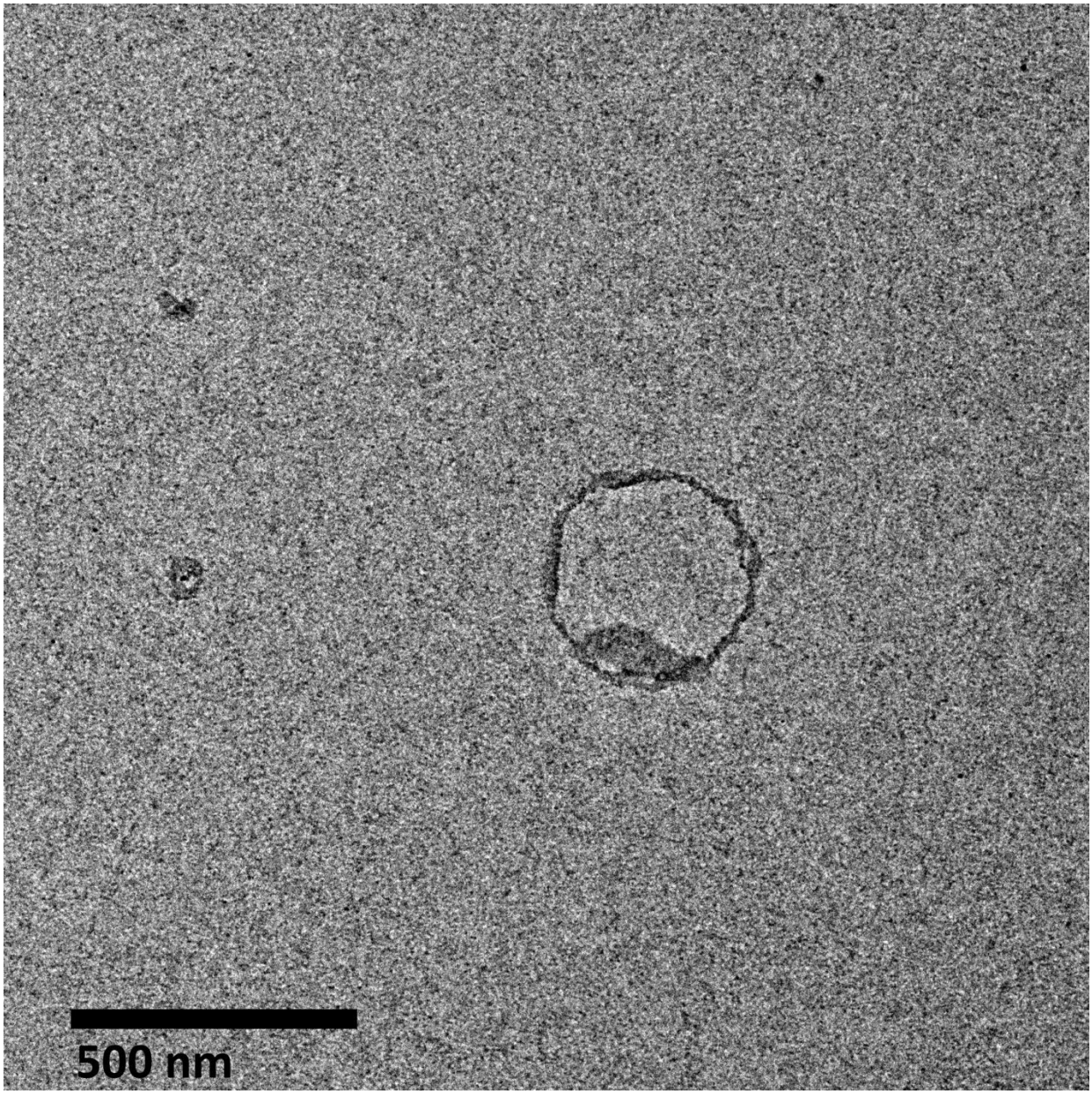

B13. TEM image of **PDI-2-TANI** in ethyl acetate at room temperature prior to sonication - [**PDI-2-TANI**] = 6 x 10^{-5} M.

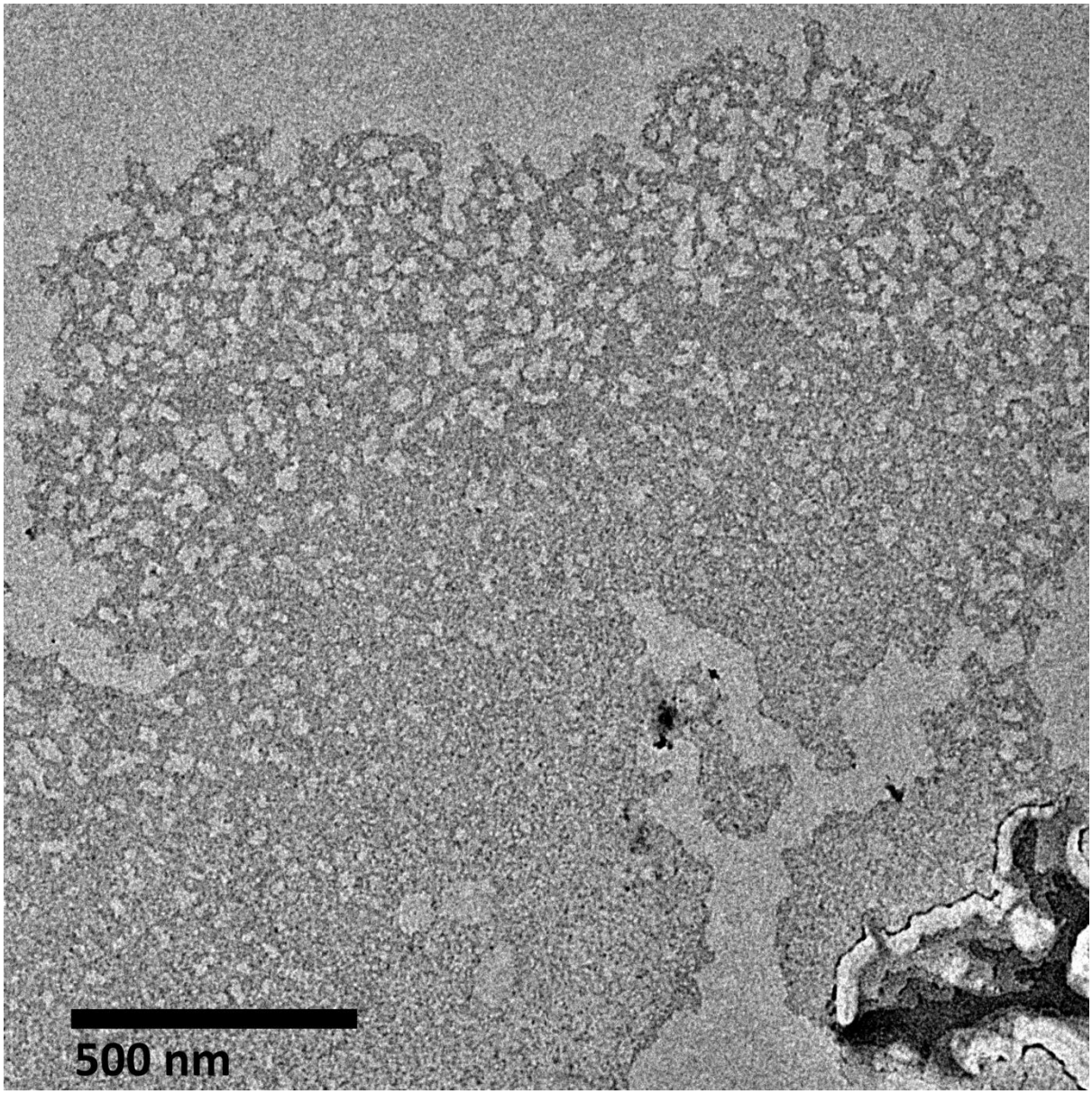

B14. TEM image of **PDI-2-TANI** in ethyl acetate at room temperature prior to sonication - [**PDI-2-TANI**] = 6 x 10^{-5} M.

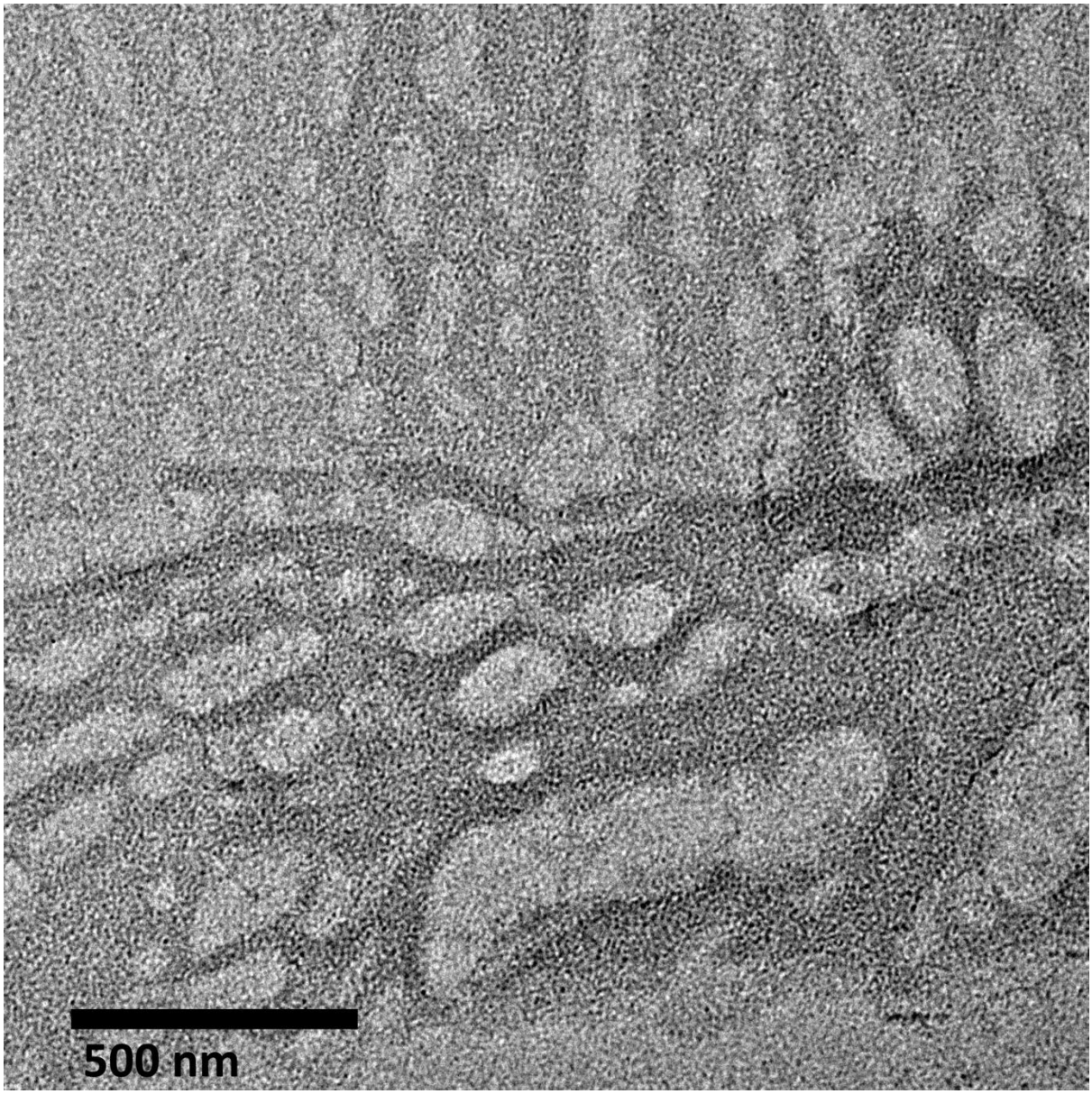

B15. TEM image of **PDI-2-TANI** in ethyl acetate at room temperature after sonication (**PDI-2-TANI** seeds) - [**PDI-2-TANI**] = 6 x 10^{-5} M.

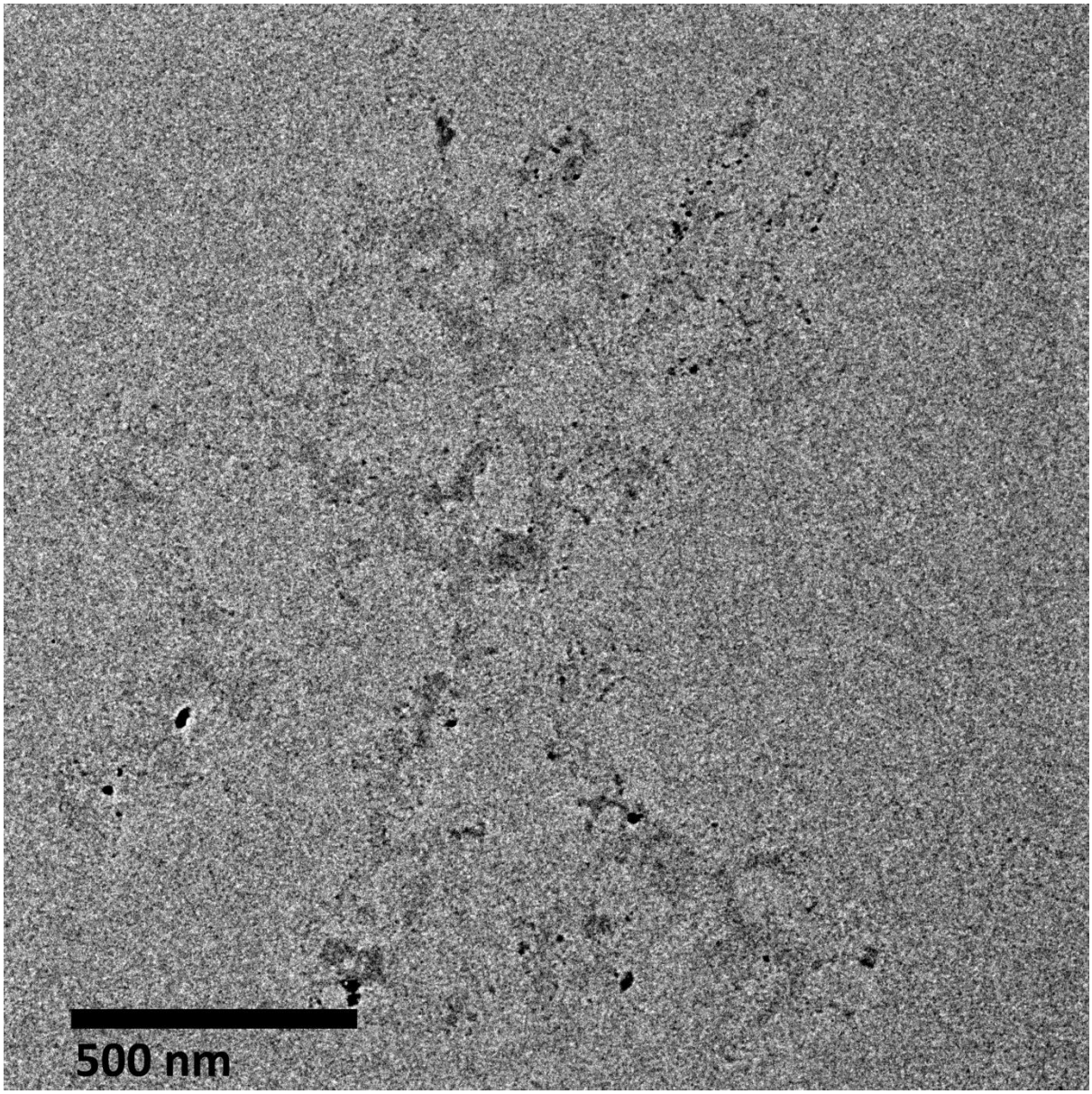

B16. TEM image of **PDI-2-TANI** in 1:50 (v/v) chloroform:ethyl acetate at room temperature, 1:1 seed:unimer ratio - [**PDI-2-TANI**] = 6 x 10^{-5} M.

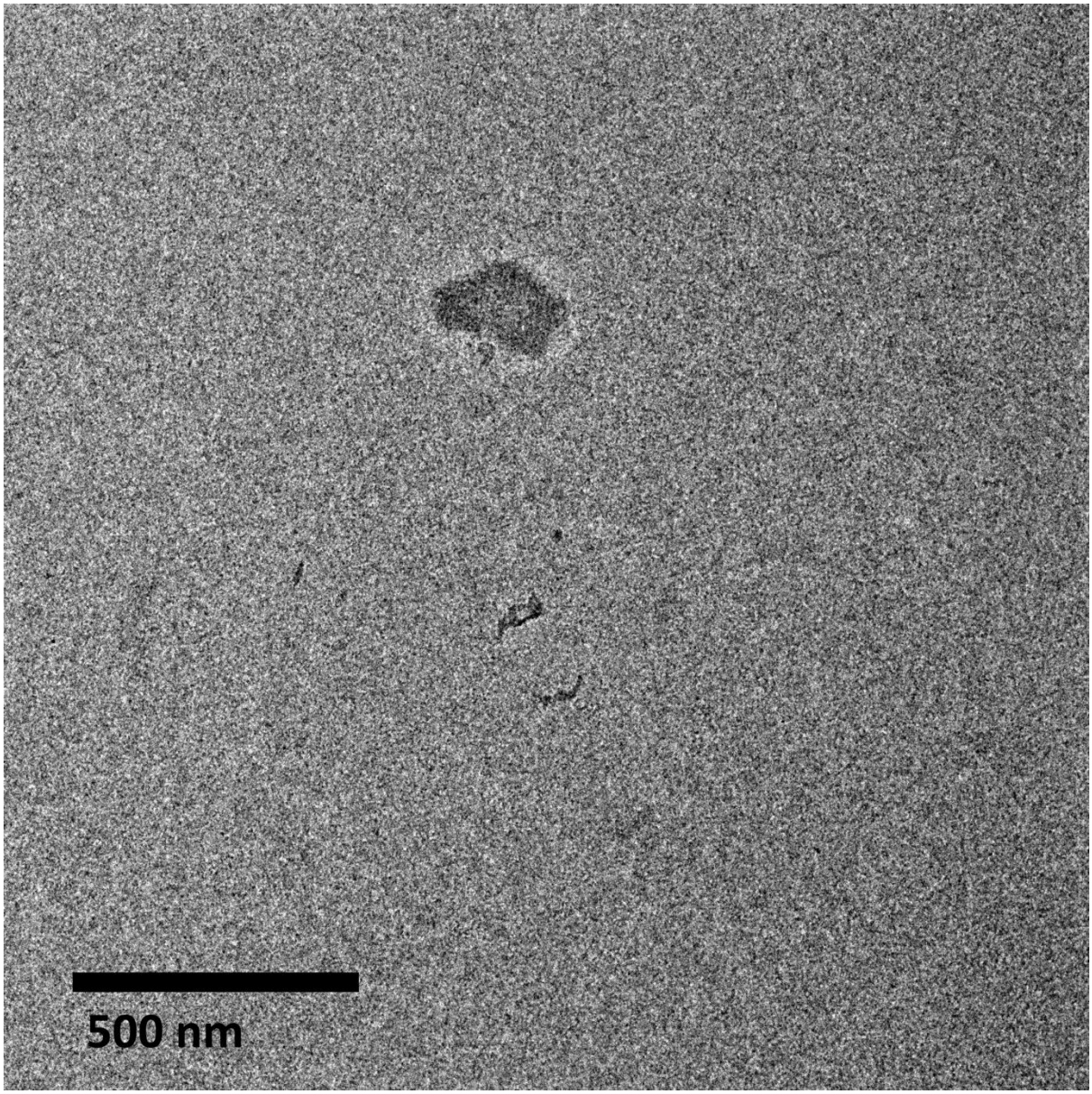

B17. TEM image of thermally self-seeded **PDI-2-TANI** in ethyl acetate, after 2 days of ageing at room temperature, prior to sonication - [**PDI-2-TANI**] = 6 x 10^{-5} M.

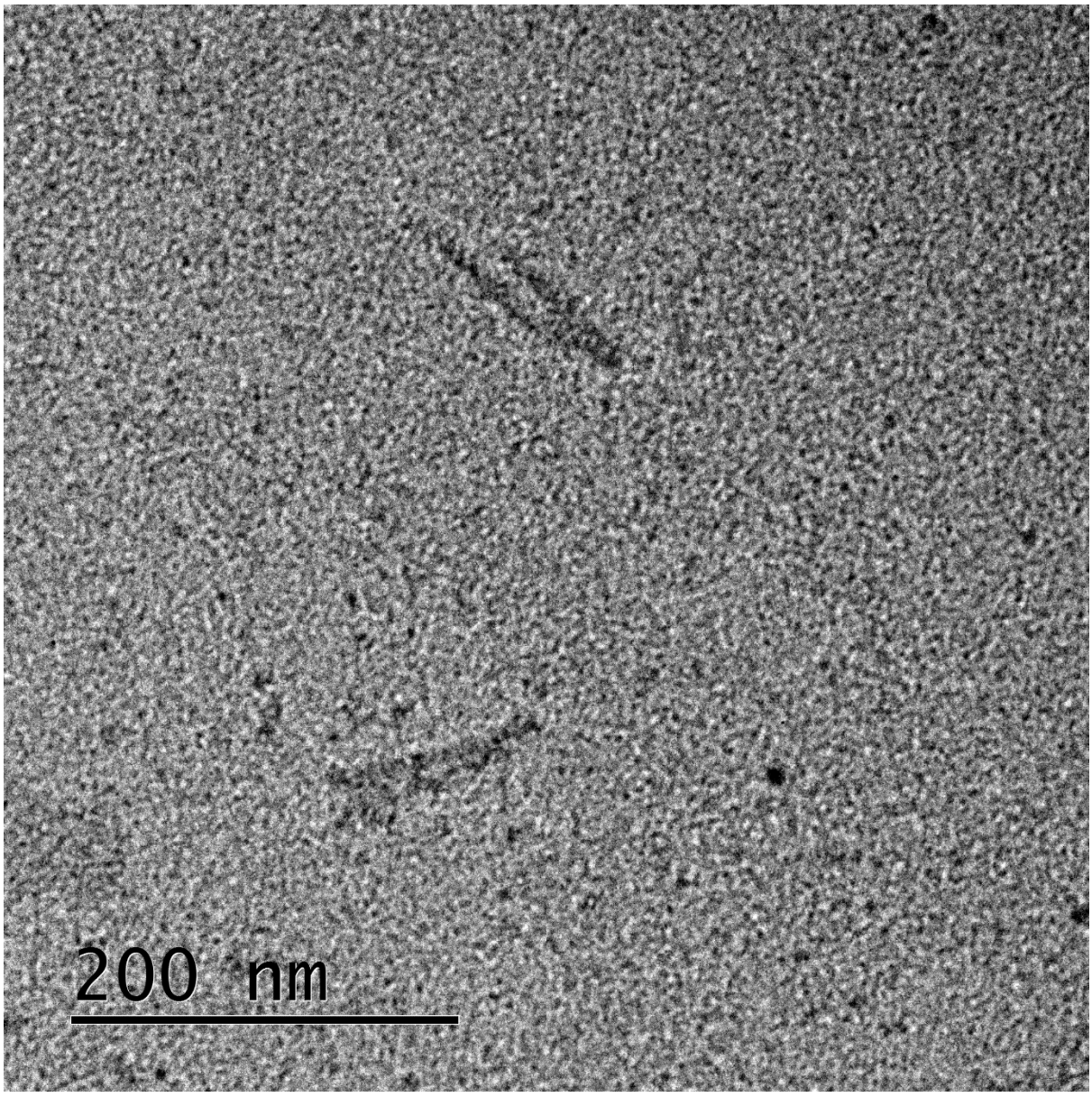

B18. TEM image of thermally self-seeded **PDI-2-TANI** in ethyl acetate, after 2 days of ageing at room temperature, prior to sonication - [**PDI-2-TANI**] = 6 x 10^{-5} M.

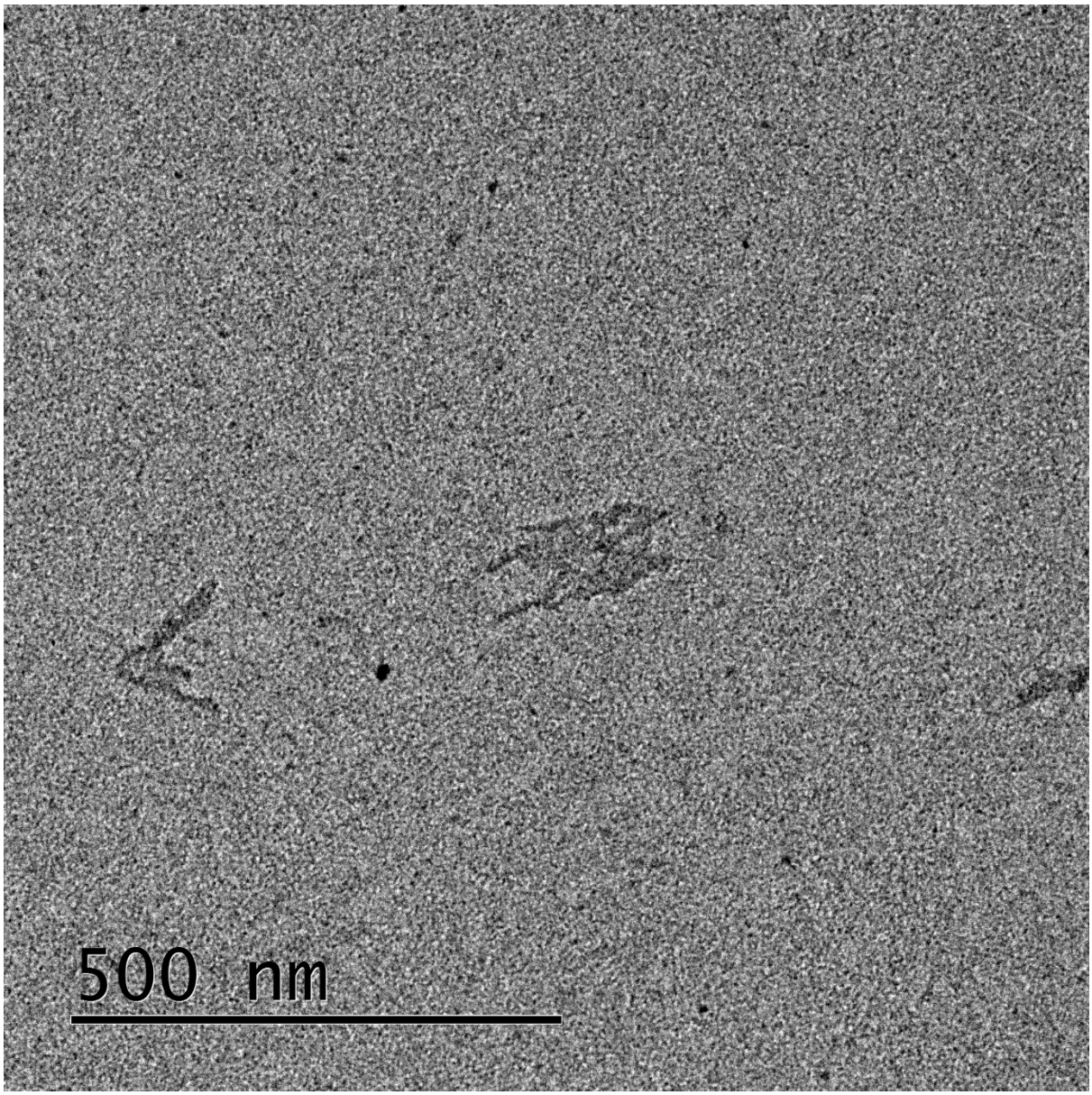

B19. TEM image of thermally self-seeded **PDI-2-TANI** in ethyl acetate, after 2 days of ageing at room temperature, prior to sonication - [**PDI-2-TANI**] = 6 x 10^{-5} M.

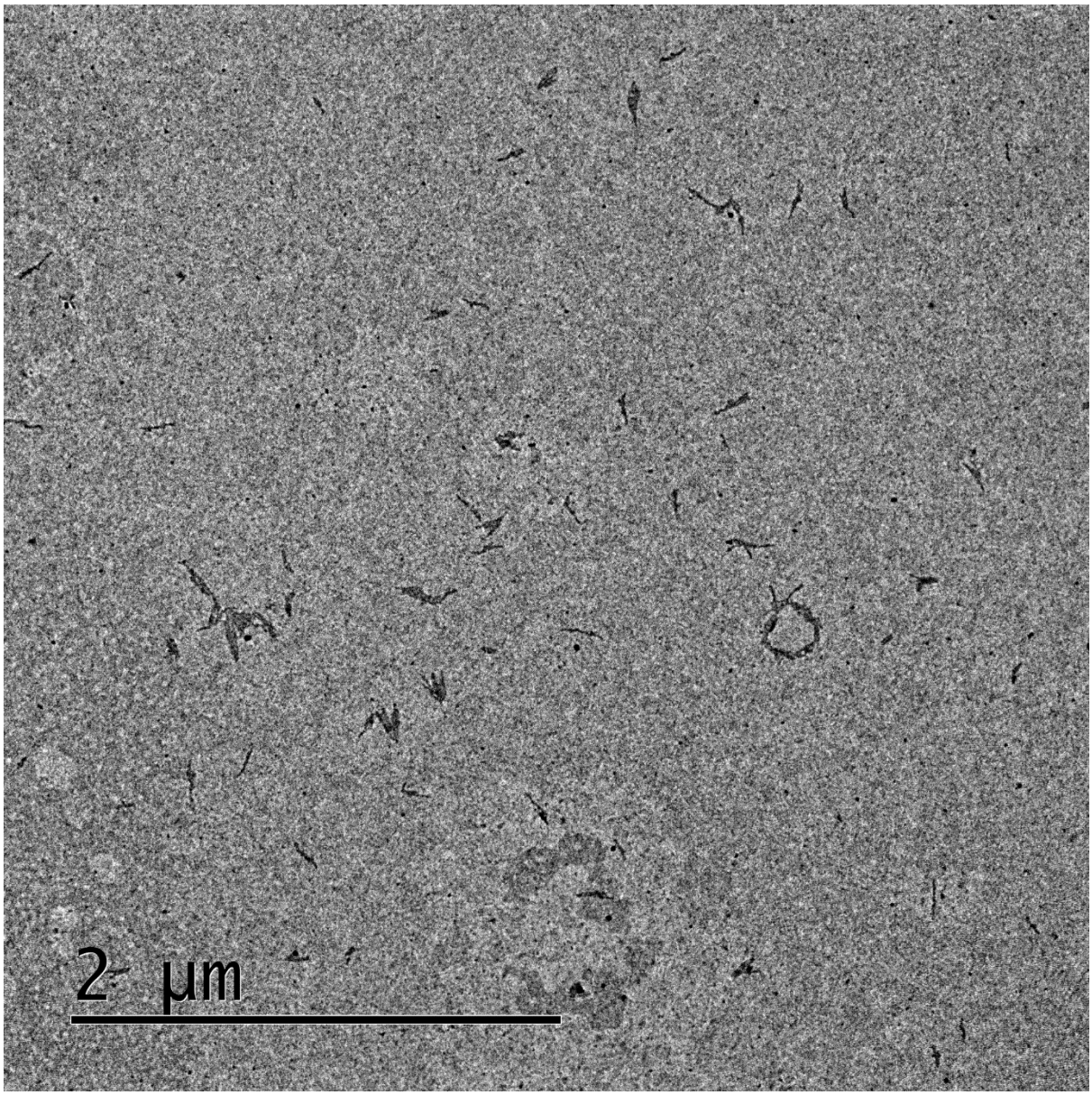

B20. TEM image of thermally self-seeded **PDI-2-TANI** in ethyl acetate, after 2 days of ageing at room temperature, prior to sonication - [**PDI-2-TANI**] = 6 x 10^{-5} M.

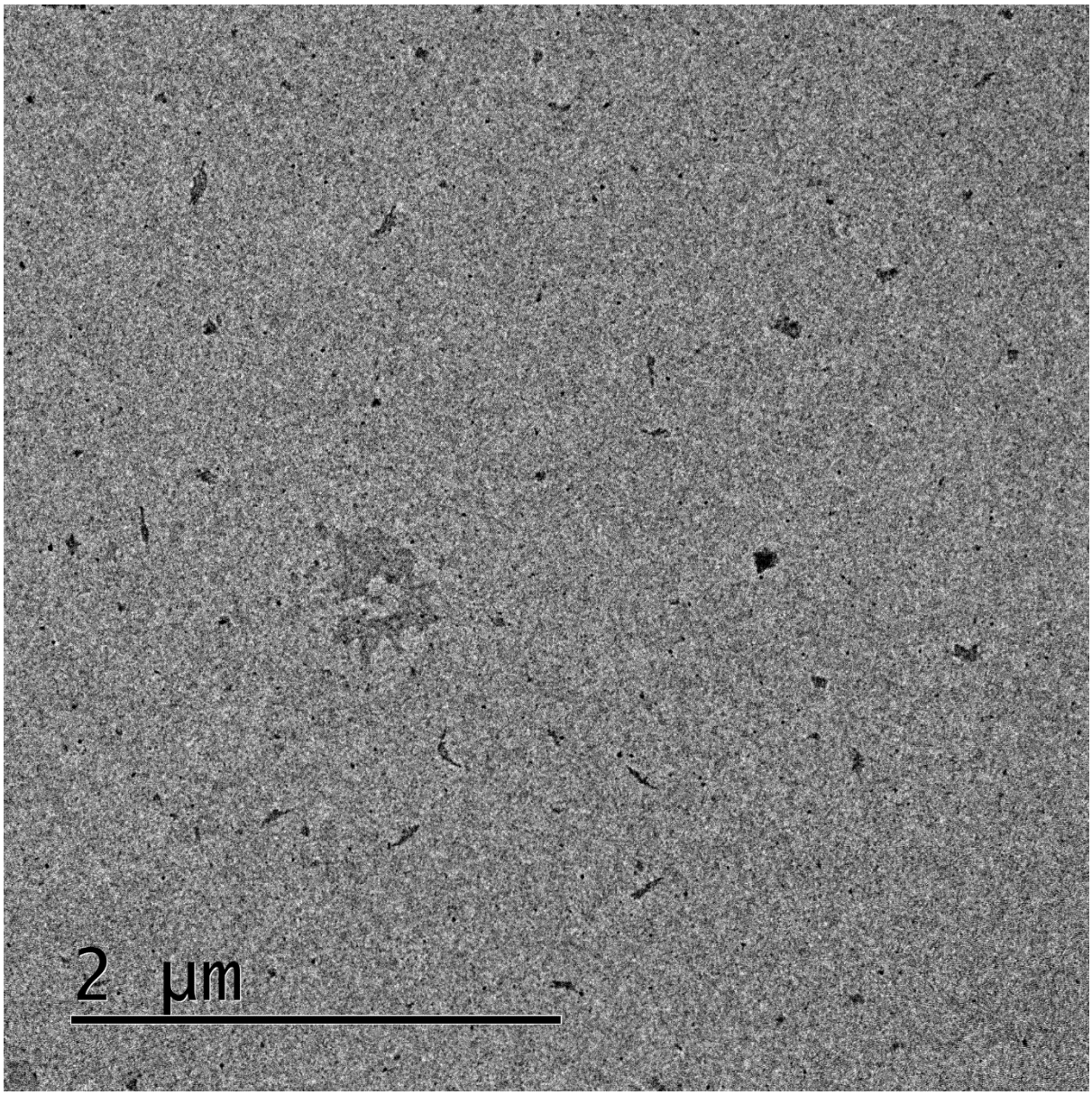

B21. Tabulated fibre lengths of thermally self-seeded **PDI-2-TANI** in ethyl acetate after 2 days of ageing at room temperature, prior to sonication - [**PDI-2-TANI**] = 6 x 10^{-5} M.

Count	Fibre length *L* (nm)	L^2 (nm^2)	Count	Fibre length *L* (nm)	L^2 (nm^2)	Count	Fibre length *L* (nm)	L^2 (nm^2)
1	76	5718	**50**	91	8264	**99**	34	1133
2	82	6651	**51**	113	12776	**100**	108	11576
3	39	1526	**52**	67	4525	**101**	69	4787
4	78	6116	**53**	165	27130	**102**	55	3062
5	76	5766	**54**	70	4922	**103**	103	10629
6	73	5286	**55**	78	6029	**104**	99	9782
7	88	7718	**56**	133	17686	**105**	70	4845
8	43	1839	**57**	72	5210	**106**	133	17712
9	81	6546	**58**	62	3864	**107**	103	10588
10	46	2156	**59**	72	5169	**108**	57	3193
11	49	2391	**60**	195	38094	**109**	53	2829
12	180	32580	**61**	54	2868	**110**	61	3702
13	92	8541	**62**	77	5970	**111**	139	19245
14	60	3636	**63**	187	34805	**112**	71	4970
15	128	16449	**64**	103	10551	**113**	127	16046
16	84	7080	**65**	41	1687	**114**	55	3012
17	43	1828	**66**	86	7393	**115**	56	3133
18	111	12393	**67**	44	1943	**116**	39	1483
19	108	11683	**68**	116	13555	**117**	31	933
20	101	10286	**69**	153	23444	**118**	97	9425
21	171	29242	**70**	96	9285	**119**	48	2333
22	90	8097	**71**	98	9624	**120**	104	10878
23	60	3624	**72**	91	8370	**121**	99	9894
24	66	4395	**73**	132	17307	**122**	117	13722
25	87	7519	**74**	51	2633	**123**	155	23977
26	106	11341	**75**	133	17686	**124**	70	4863
27	103	10617	**76**	157	24730	**125**	92	8473
28	36	1329	**77**	117	13745	**126**	188	35331
29	61	3758	**78**	95	9100	**127**	63	3924
30	132	17441	**79**	76	5843	**128**	61	3697
31	89	8001	**80**	80	6347	**129**	110	12011
32	72	5198	**81**	126	15965	**130**	89	8000
33	29	842	**82**	64	4103	**131**	122	14770
34	126	15957	**83**	32	994	**132**	56	3114
35	58	3395	**84**	143	20445	**133**	109	11883

36	81	6578	**85**	103	10596	**134**	60	3637
37	52	2704	**86**	85	7156	**135**	94	8782
38	75	5579	**87**	143	20377	**136**	177	31398
39	134	18074	**88**	57	3237	**137**	154	23679
40	98	9519	**89**	60	3596	**138**	76	5781
41	84	7035	**90**	68	4651	**139**	135	18279
42	57	3234	**91**	112	12522	**140**	117	13753
43	100	9922	**92**	101	10268	**141**	116	13530
44	74	5415	**93**	55	3044	**142**	101	10130
45	88	7792	**94**	86	7322	**143**	84	7071
46	60	3628	**95**	60	3543	**144**	58	3331
47	70	4919	**96**	40	1602	**145**	147	21699
48	70	4933	**97**	88	7724	**146**	68	4689
49	109	11867	**98**	47	2180			

B22. TEM image of thermally self-seeded **PDI-2-TANI** in ethyl acetate, after 2 days of ageing at room temperature and sonication (**PDI-2-TANI** seeds) - [**PDI-2-TANI**] = 6 x 10^{-5} M.

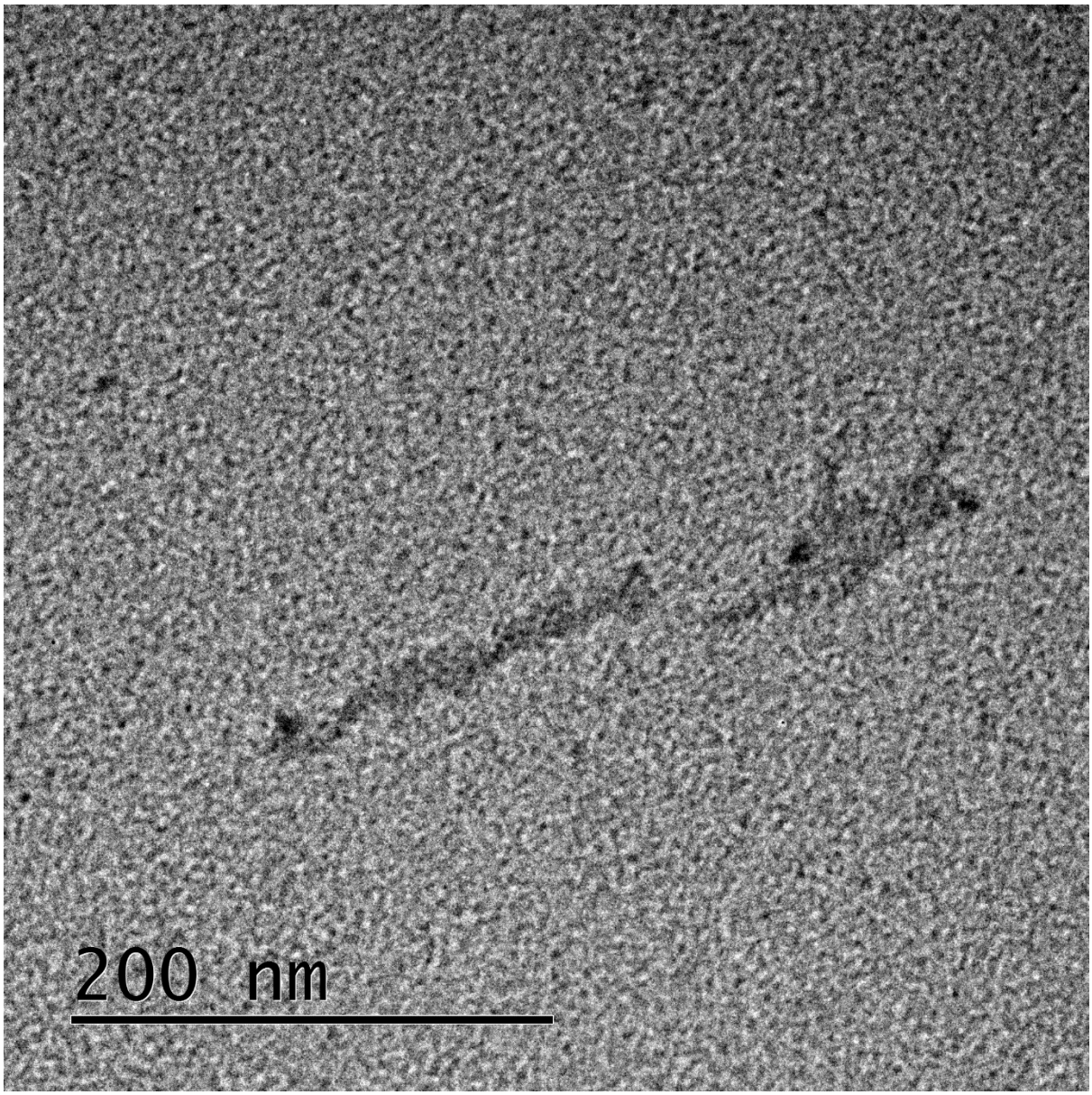

B23. TEM image of thermally self-seeded **PDI-2-TANI** in ethyl acetate, after 2 days of ageing at room temperature and sonication (**PDI-2-TANI** seeds) - [**PDI-2-TANI**] = 6 x 10^{-5} M.

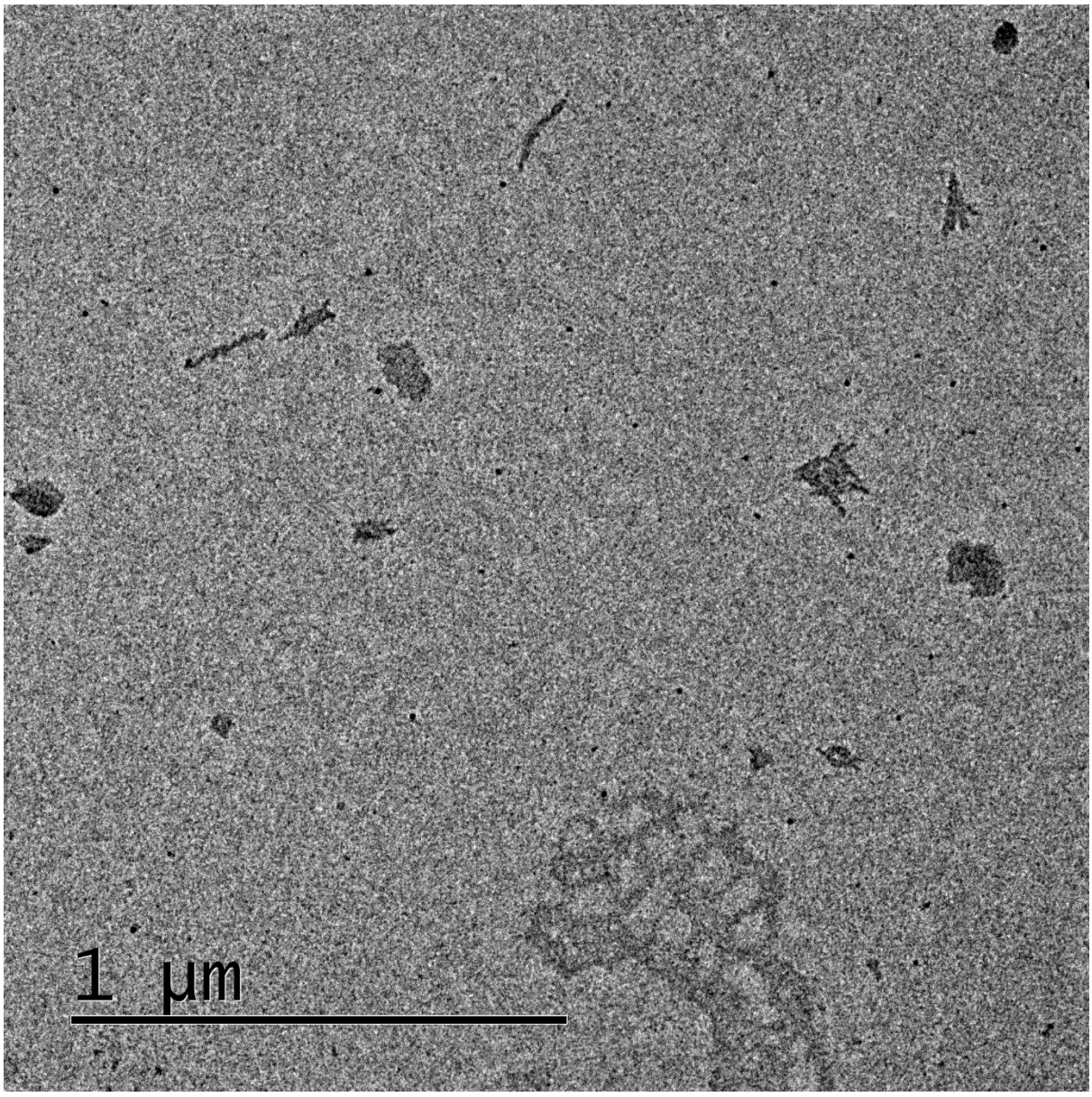

B24. TEM image of thermally self-seeded **PDI-2-TANI** in ethyl acetate, after 2 days of ageing at room temperature and sonication (**PDI-2-TANI** seeds) - [**PDI-2-TANI**] = 6 x 10^{-5} M.

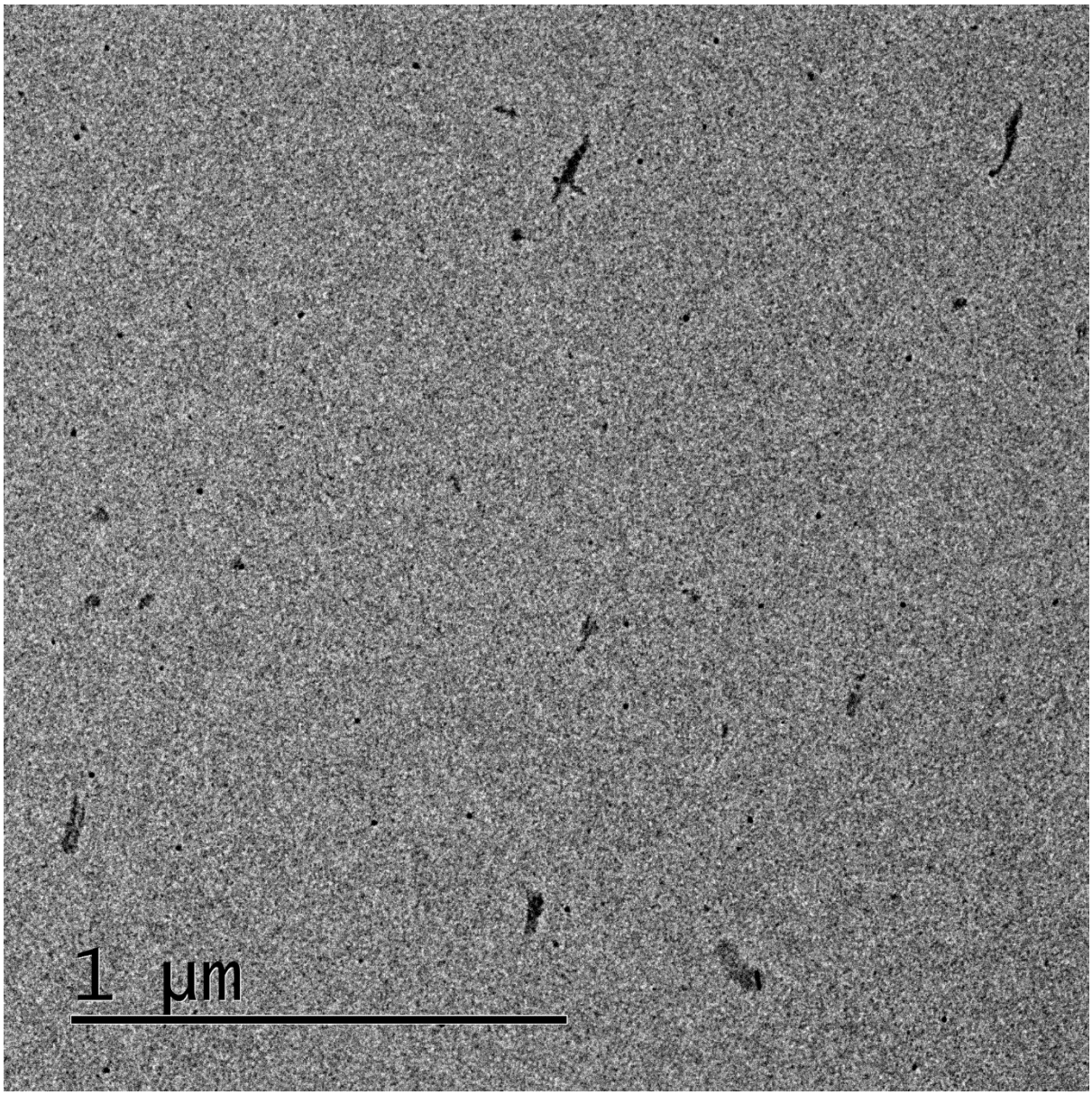

B25. TEM image of thermally self-seeded **PDI-2-TANI** in ethyl acetate, after 2 days of ageing at room temperature and sonication (**PDI-2-TANI** seeds) - [**PDI-2-TANI**] = 6 x 10^{-5} M.

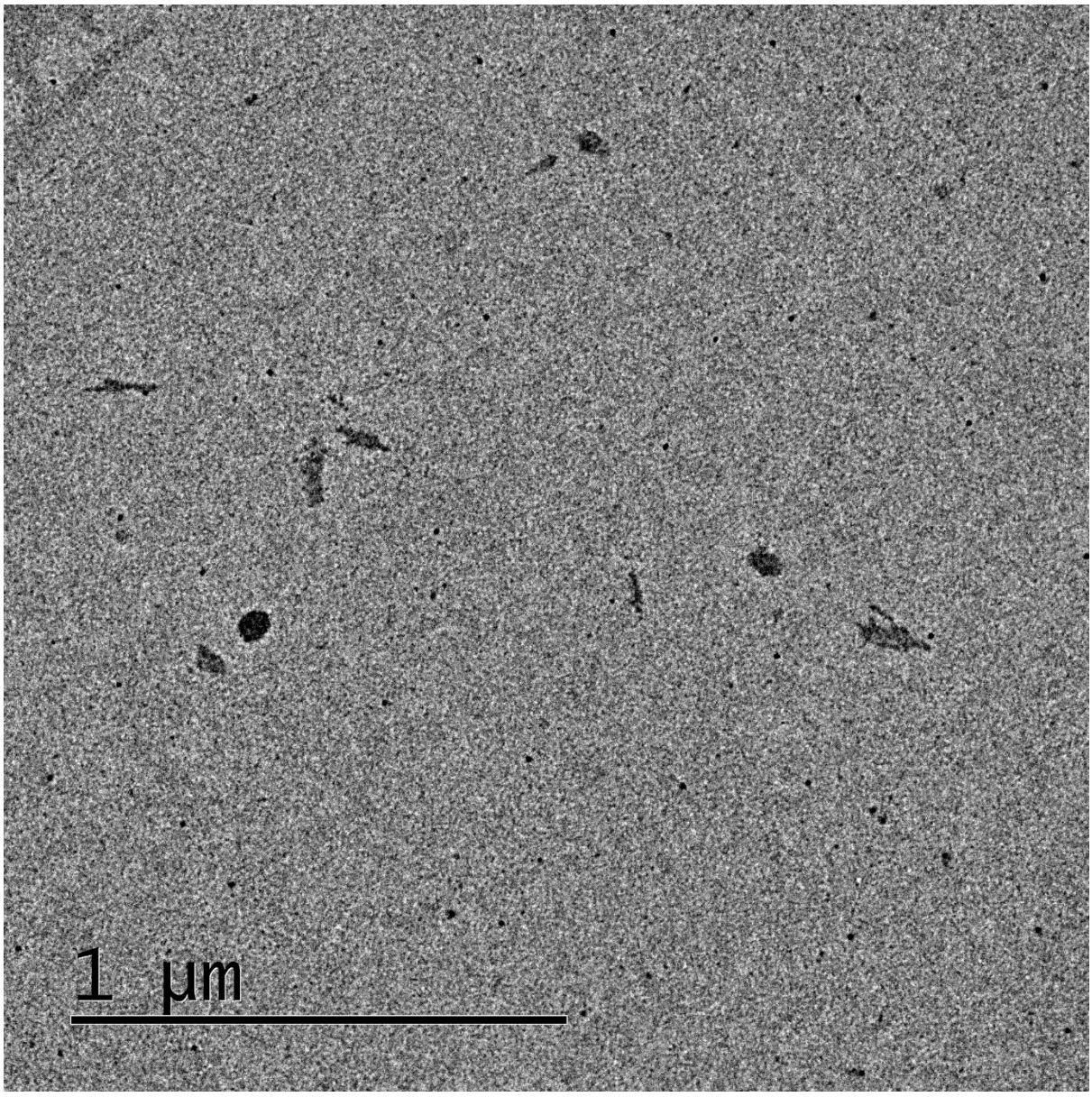

B26. Tabulated fibre lengths of thermally self-seeded **PDI-2-TANI** in ethyl acetate after 2 days of ageing at room temperature and sonication (i.e. **PDI-2-TANI** seeds) - [**PDI-2-TANI**] = 6 x 10^{-5} M.

Count	Fibre length *L* (nm)	L^2 (nm^2)	Count	Fibre length *L* (nm)	L^2 (nm^2)	Count	Fibre length *L* (nm)	L^2 (nm^2)
1	113	12705	**35**	63	4031	**69**	77	5856
2	91	8354	**36**	120	14290	**70**	117	13641
3	132	17488	**37**	69	4811	**71**	73	5304
4	83	6886	**38**	75	5666	**72**	59	3464
5	36	1325	**39**	66	4364	**73**	52	2725
6	83	6962	**40**	61	3715	**74**	92	8541
7	54	2929	**41**	75	5578	**75**	60	3572
8	44	1948	**42**	76	5773	**76**	28	773
9	36	1311	**43**	49	2365	**77**	118	13913
10	19	370	**44**	24	571	**78**	38	1417
11	42	1736	**45**	110	12038	**79**	87	7631
12	45	1986	**46**	61	3690	**80**	102	10473
13	93	8587	**47**	47	2186	**81**	39	1485
14	50	2539	**48**	96	9171	**82**	29	819
15	52	2700	**49**	80	6361	**83**	73	5303
16	35	1221	**50**	114	12947	**84**	72	5188
17	69	4724	**51**	46	2089	**85**	79	6215
18	81	6569	**52**	49	2358	**86**	47	2194
19	161	25975	**53**	123	15232	**87**	47	2183
20	87	7510	**54**	29	842	**88**	44	1929
21	92	8386	**55**	78	6045	**89**	41	1661
22	79	6219	**56**	68	4588	**90**	47	2177
23	124	15445	**57**	87	7590	**91**	123	15234
24	67	4430	**58**	114	13051	**92**	50	2533
25	40	1631	**59**	79	6266	**93**	31	962
26	53	2828	**60**	95	8963	**94**	82	6766
27	51	2651	**61**	60	3563	**95**	32	1026
28	111	12275	**62**	110	12206	**96**	64	4047
29	53	2778	**63**	64	4123	**97**	54	2866
30	62	3877	**64**	42	1784	**98**	48	2257
31	93	8565	**65**	48	2350	**99**	70	4917
32	88	7777	**66**	20	403	**100**	50	2460
33	96	9230	**67**	65	4227	**101**	54	2864
34	56	3101	**68**	81	6560			

B27. TEM image of **PDI-2-TANI** fibres in ethyl acetate prepared using a 1:1 seed:unimer ratio (seeds prepared via thermal self-seeding and sonication) - [**PDI-2-TANI**] = 6 x 10^{-5} M.

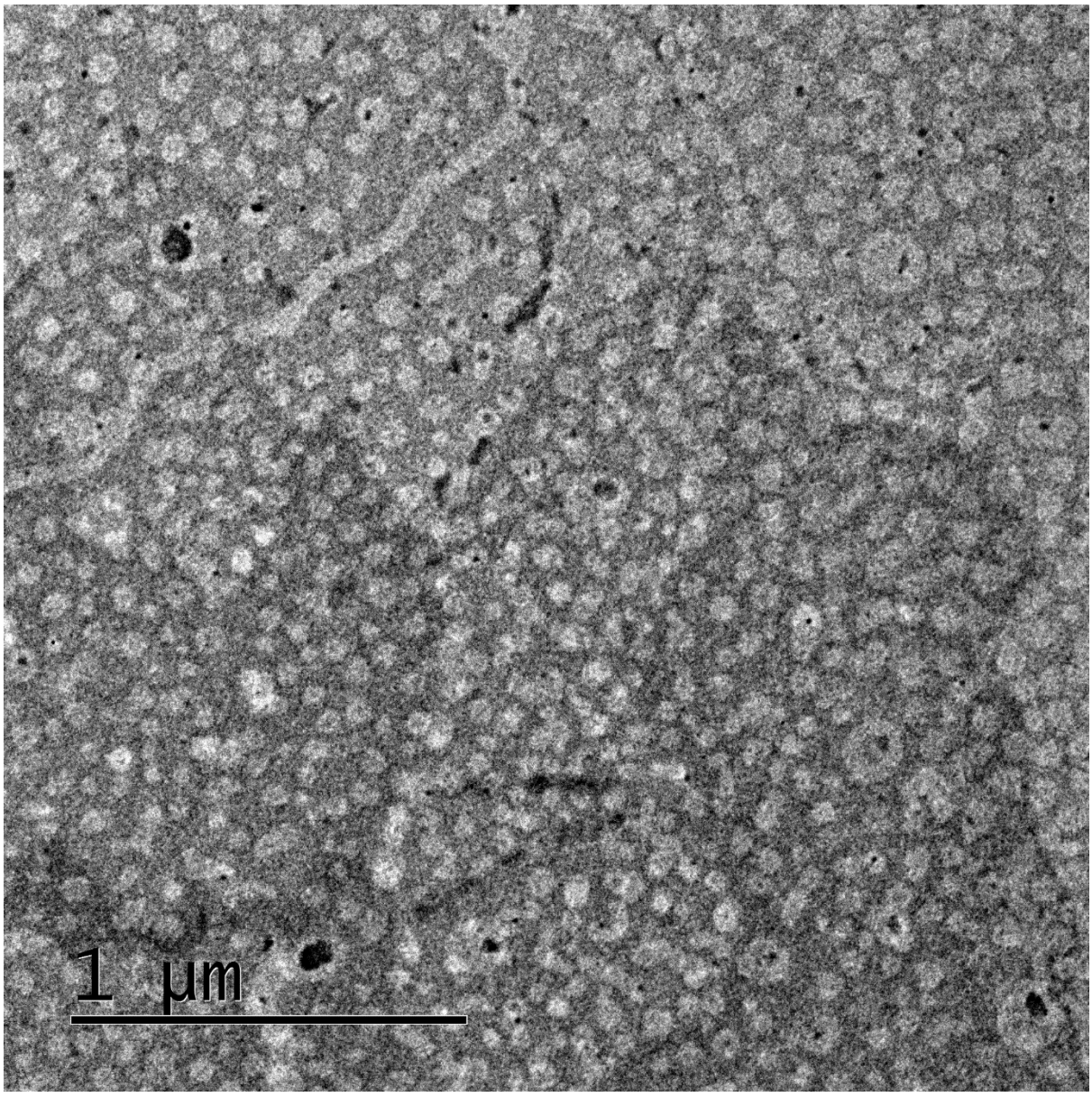

B28. TEM image of **PDI-2-TANI** fibres in ethyl acetate prepared using a 1:1 seed:unimer ratio (seeds prepared via thermal self-seeding and sonication) - [**PDI-2-TANI**] = 6 x 10^{-5} M.

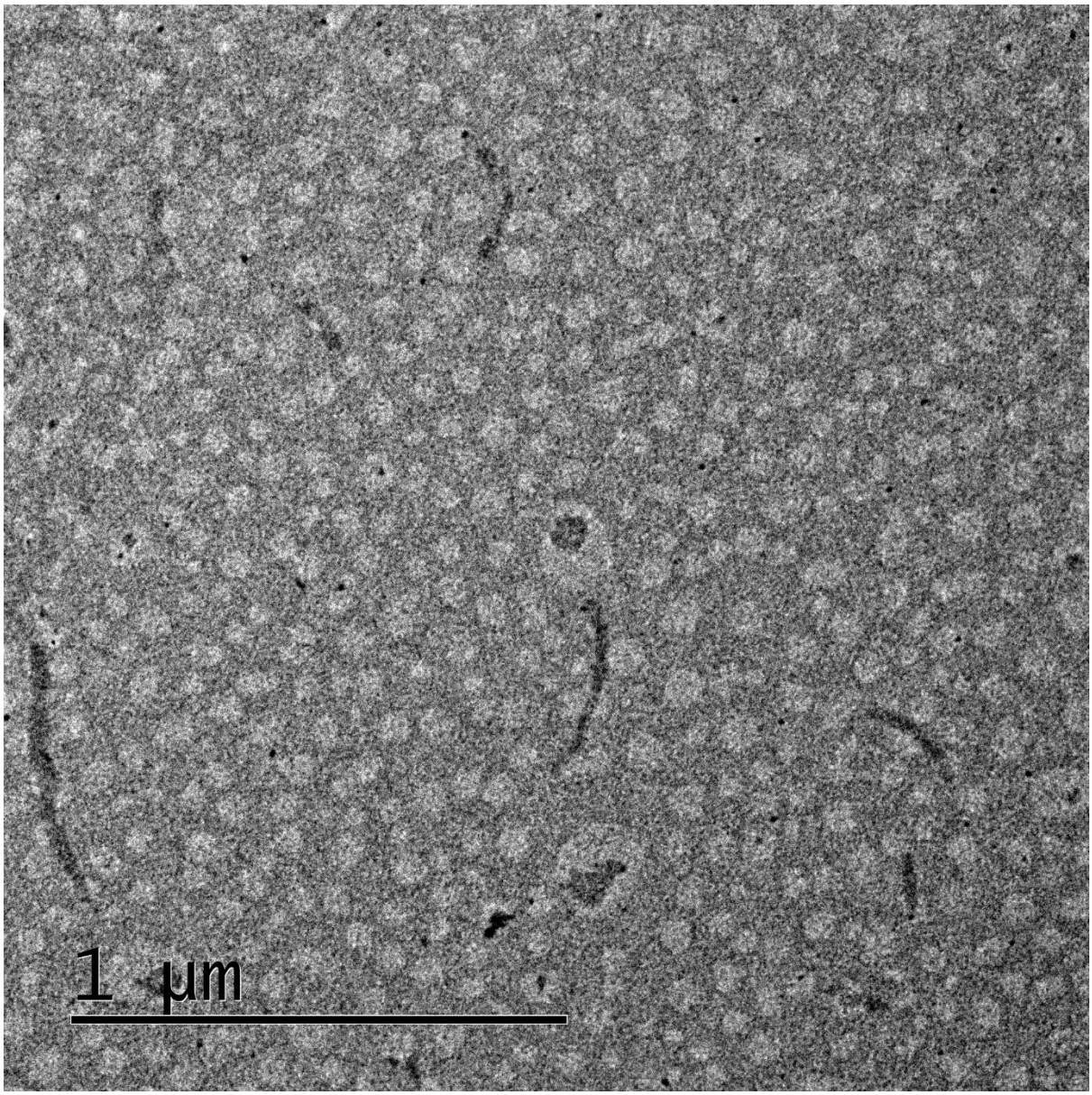

B29. TEM image of **PDI-2-TANI** fibres in ethyl acetate prepared using a 1:1 seed:unimer ratio (seeds prepared via thermal self-seeding and sonication) - [**PDI-2-TANI**] = 6 x 10^{-5} M.

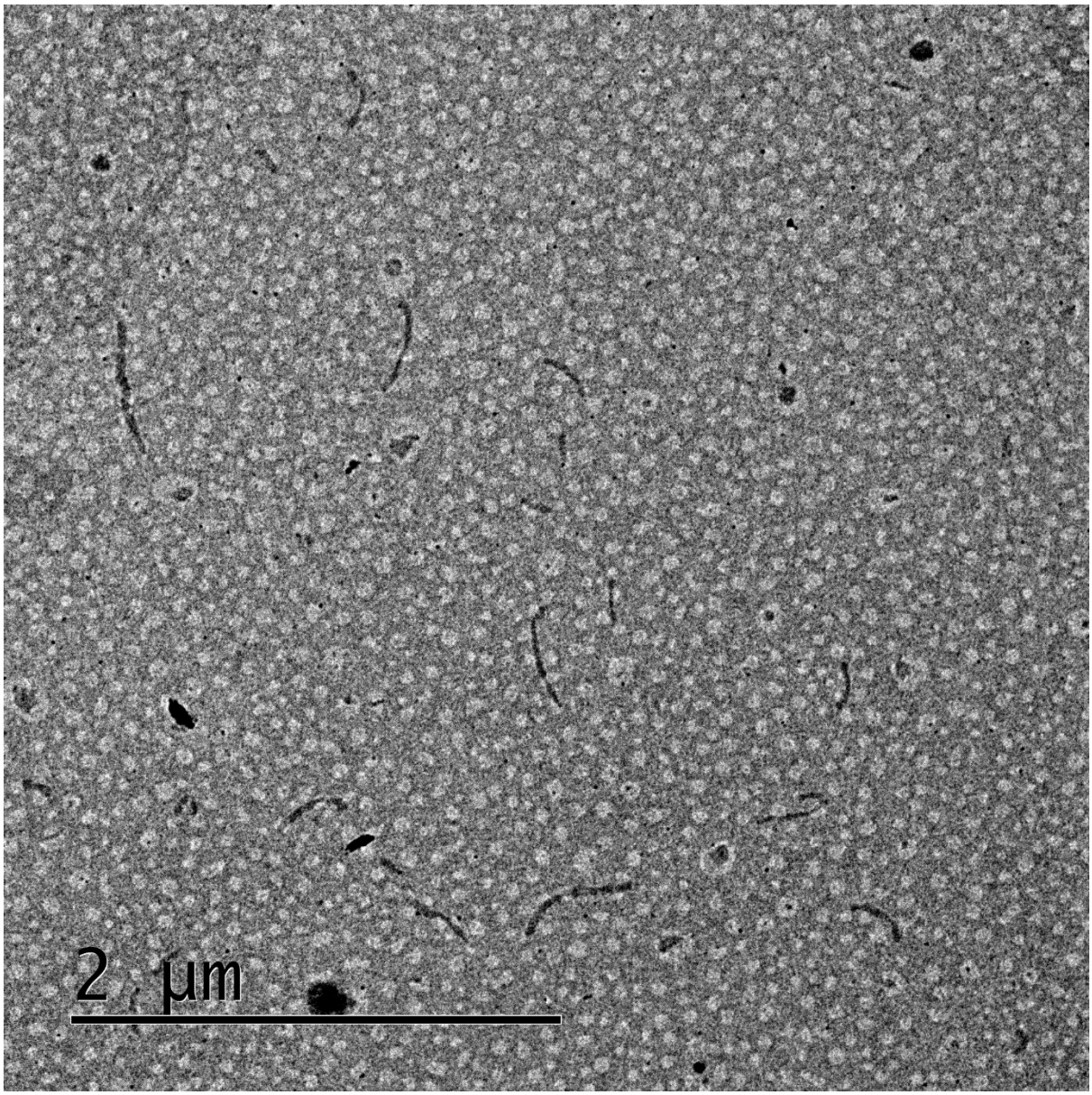

B30. TEM image of **PDI-2-TANI** fibres in ethyl acetate prepared using a 1:1 seed:unimer ratio (seeds prepared via thermal self-seeding and sonication) - [**PDI-2-TANI**] = 6 x 10^{-5} M.

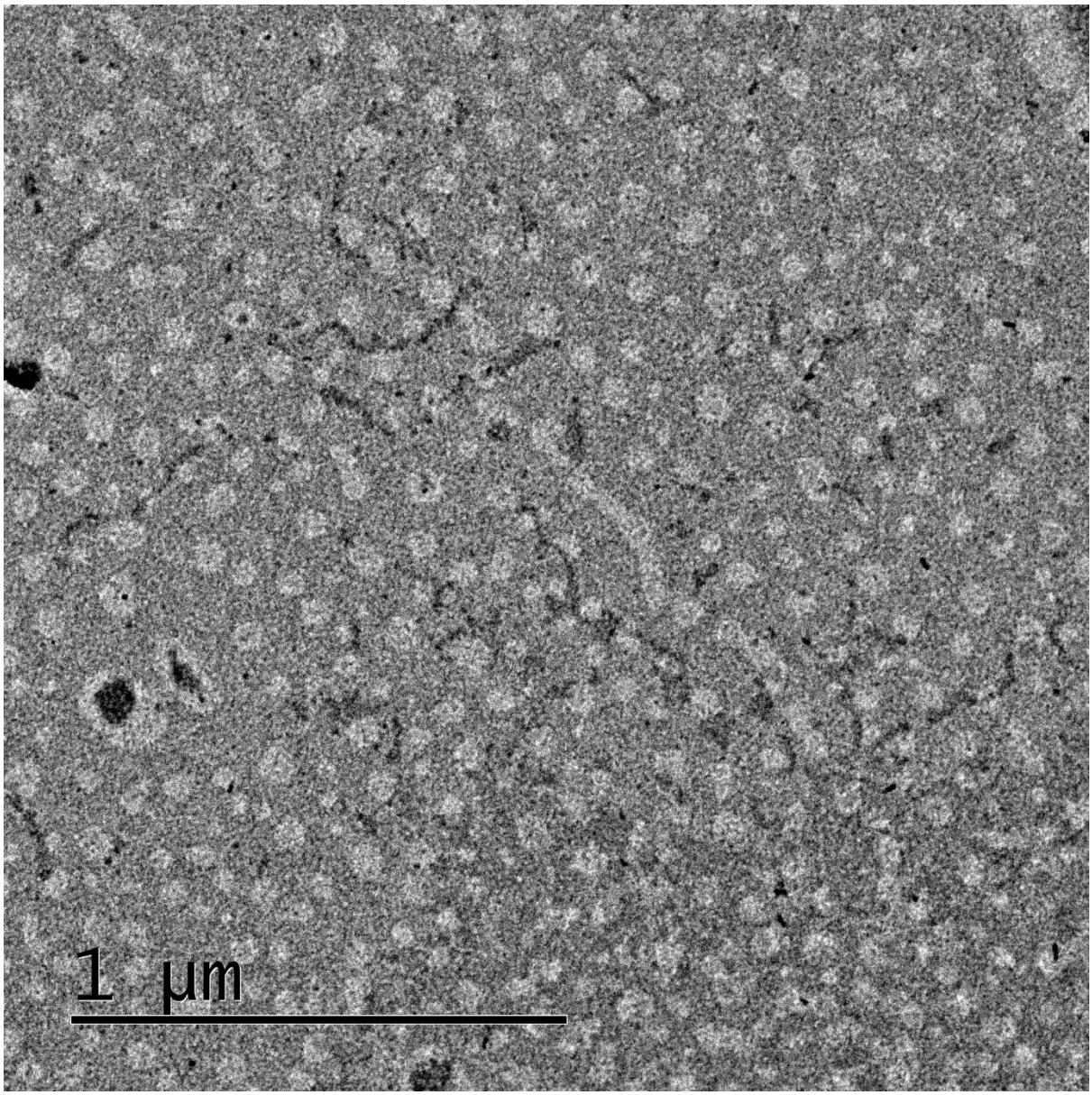

B31. Tabulated fibre lengths of thermally self-seeded **PDI-2-TANI** in ethyl acetate, 1:1 seed:unimer ratio - [**PDI-2-TANI**] = 6 x 10^{-5} M.

Count	Fibre length *L* (nm)	L^2 (nm^2)	Count	Fibre length *L* (nm)	L^2 (nm^2)	Count	Fibre length *L* (nm)	L^2 (nm^2)
1	102	10325	**34**	499	248549	**67**	247	61101
2	62	3868	**35**	499	249039	**68**	76	5702
3	505	255256	**36**	104	10799	**69**	89	7951
4	263	69141	**37**	148	21857	**70**	158	24843
5	124	15385	**38**	236	55524	**71**	128	16292
6	319	101454	**39**	569	323626	**72**	345	118815
7	106	11340	**40**	185	34145	**73**	351	123019
8	118	14032	**41**	300	90267	**74**	361	130547
9	269	72125	**42**	98	9688	**75**	189	35656
10	291	84877	**43**	265	70190	**76**	126	15903
11	199	39738	**44**	194	37707	**77**	136	18566
12	192	36721	**45**	354	125044	**78**	115	13149
13	197	38934	**46**	188	35505	**79**	85	7224
14	101	10198	**47**	279	77638	**80**	125	15526
15	181	32733	**48**	196	38423	**81**	207	42691
16	258	66758	**49**	108	11738	**82**	198	39021
17	131	17068	**50**	57	3296	**83**	135	18303
18	471	221725	**51**	129	16569	**84**	108	11729
19	222	49375	**52**	188	35274	**85**	241	57867
20	277	76475	**53**	70	4834	**86**	498	248237
21	355	126163	**54**	142	20114	**87**	182	33284
22	287	82485	**55**	128	16336	**88**	378	143093
23	225	50663	**56**	354	125631	**89**	49	2367
24	109	11971	**57**	157	24554	**90**	180	32421
25	254	64768	**58**	115	13262	**91**	270	73166
26	316	99642	**59**	147	21526	**92**	129	16612
27	388	150797	**60**	267	71249	**93**	148	21838
28	116	13431	**61**	230	52847	**94**	208	43347
29	90	8031	**62**	114	13022	**95**	250	62422
30	70	4839	**63**	159	25257	**96**	137	18709
31	302	91030	**64**	103	10670	**97**	226	51209
32	134	18077	**65**	223	49784			
33	243	59162	**66**	318	101020			

B32. TEM image of **PDI-2-TANI** fibres in ethyl acetate prepared using a 1:3 seed:unimer ratio (seeds prepared via thermal self-seeding and sonication) - [**PDI-2-TANI**] = 6 x 10^{-5} M.

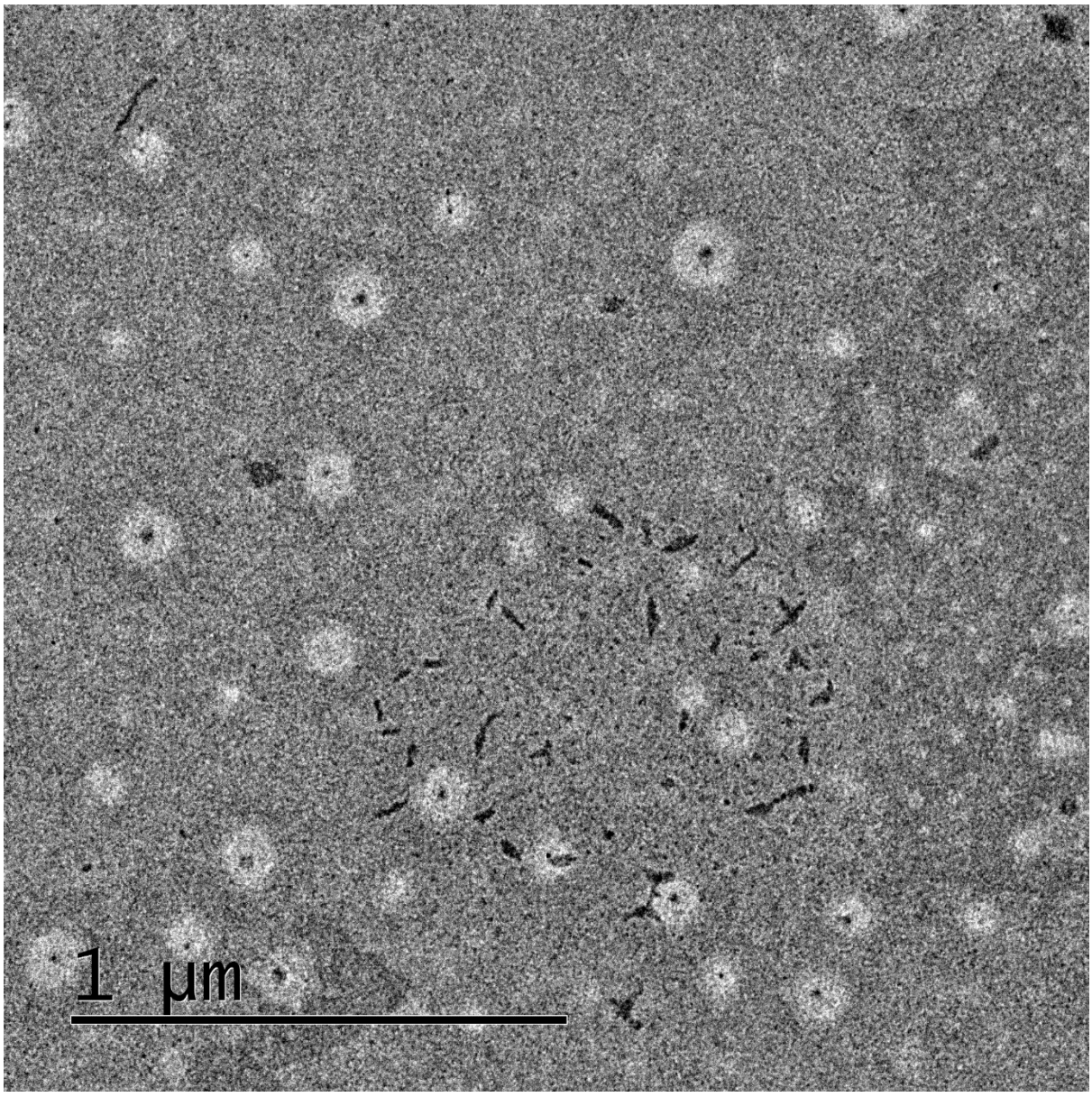

B33. TEM image of **PDI-2-TANI** fibres in ethyl acetate prepared using a 1:3 seed:unimer ratio (seeds prepared via thermal self-seeding and sonication) - [**PDI-2-TANI**] = 6 x 10^{-5} M.

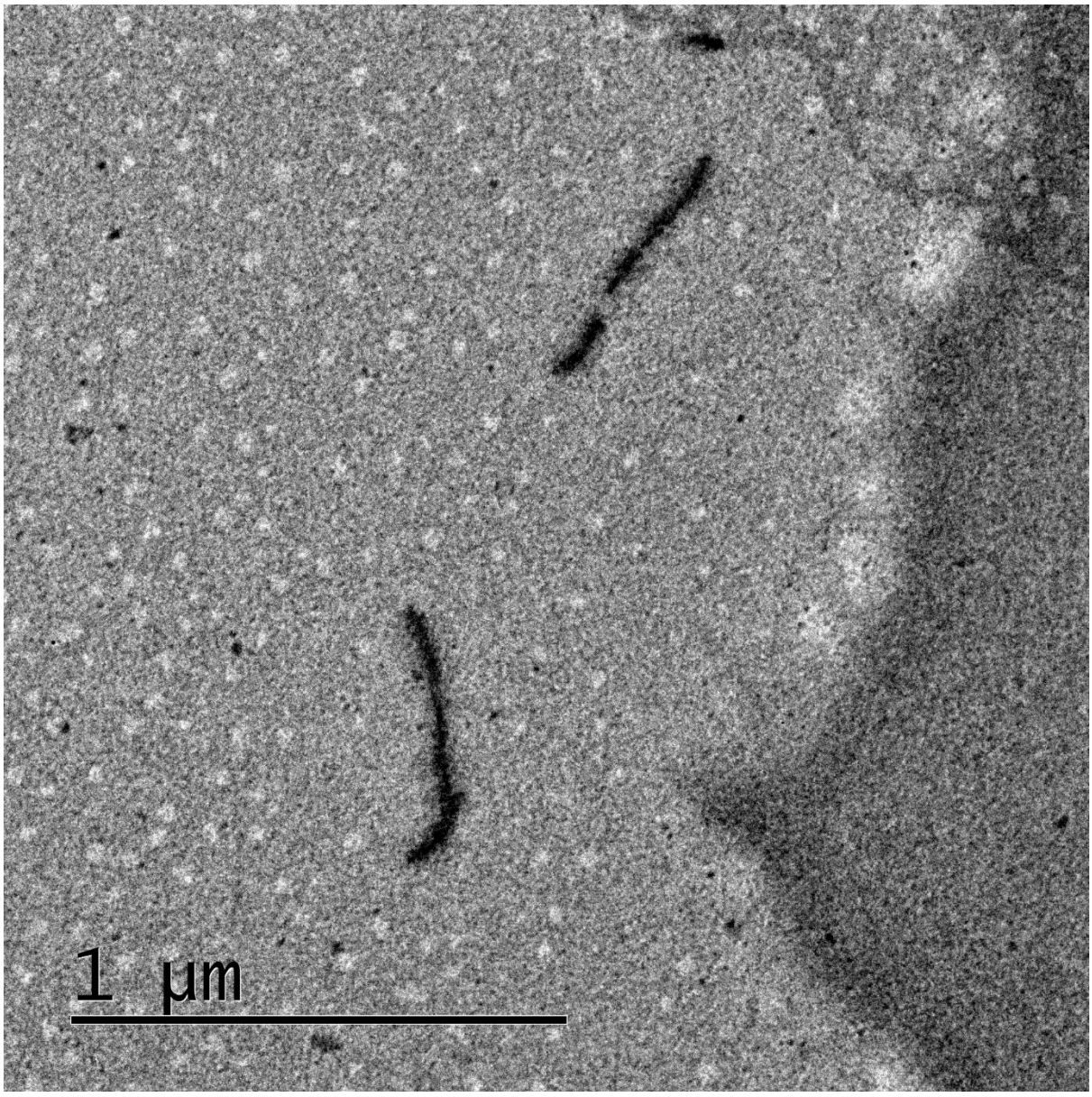

B34. Tabulated fibre lengths of thermally self-seeded **PDI-2-TANI** in ethyl acetate, 1:3 seed:unimer ratio - [**PDI-2-TANI**] = 6 x 10^{-5} M. Large, high-contrast fibres are indicated in orange.

Count	Length	Square Length	Count	Length	Square Length	Count	Length	Square Length
1	122	14787	**29**	29	864	**57**	43	1850
2	269	72362	**30**	43	1818	**58**	76	5731
3	34	1170	**31**	33	1106	**59**	94	8808
4	98	9569	**32**	39	1524	**60**	46	2123
5	92	8486	**33**	34	1161	**61**	28	775
6	98	9630	**34**	65	4278	**62**	68	4614
7	191	36420	**35**	30	889	**63**	42	1737
8	97	9432	**36**	65	4260	**64**	36	1285
9	58	3414	**37**	54	2945	**65**	46	2138
10	79	6186	**38**	44	1924	**66**	27	744
11	95	9012	**39**	54	2956	**67**	42	1780
12	94	8764	**40**	65	4186	**68**	35	1200
13	47	2174	**41**	68	4642	**69**	50	2543
14	64	4090	**42**	82	6662	**70**	39	1490
15	64	4068	**43**	37	1362	**71**	62	3852
16	125	15606	**44**	88	7696	**72**	34	1139
17	138	19051	**45**	35	1260	**73**	42	1803
18	38	1482	**46**	48	2278	**74**	43	1817
19	35	1255	**47**	44	1899	**75**	37	1347
20	98	9642	**48**	32	1052	**76**	81	6586
21	33	1057	**49**	112	12492	**1**	417	173958
22	35	1194	**50**	129	16761	**2**	173	29837
23	84	7040	**51**	62	3830	**3**	132	17320
24	52	2710	**52**	37	1384	**4**	341	116267
25	66	4310	**53**	75	5642	**5**	572	327304
26	59	3455	**54**	24	600	**6**	343	117343
27	46	2156	**55**	42	1780	**7**	289	83542
28	23	528	**56**	25	645	**8**	183	33663

B35. TEM image of **PDI-2-TANI** aggregates in ethyl acetate prepared using a 1:5 seed:unimer ratio (seeds prepared via thermal self-seeding and sonication) - [**PDI-2-TANI**] = 6 x 10^{-5} M.

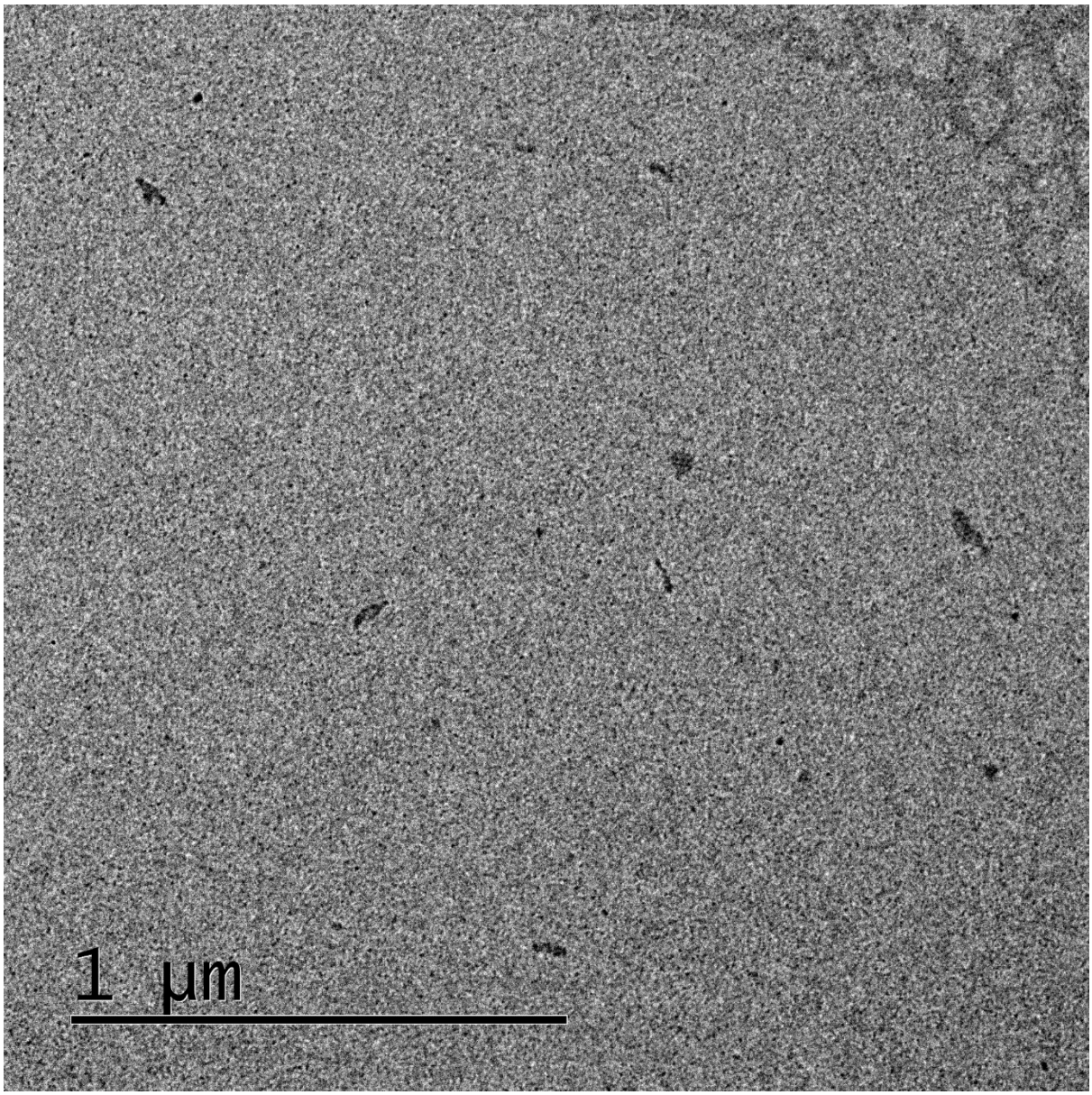

B35. TEM image of **PDI-2-TANI** aggregates in ethyl acetate prepared using a 1:5 seed:unimer ratio (seeds prepared via thermal self-seeding and sonication) - [**PDI-2-TANI**] = 6 x 10^{-5} M.

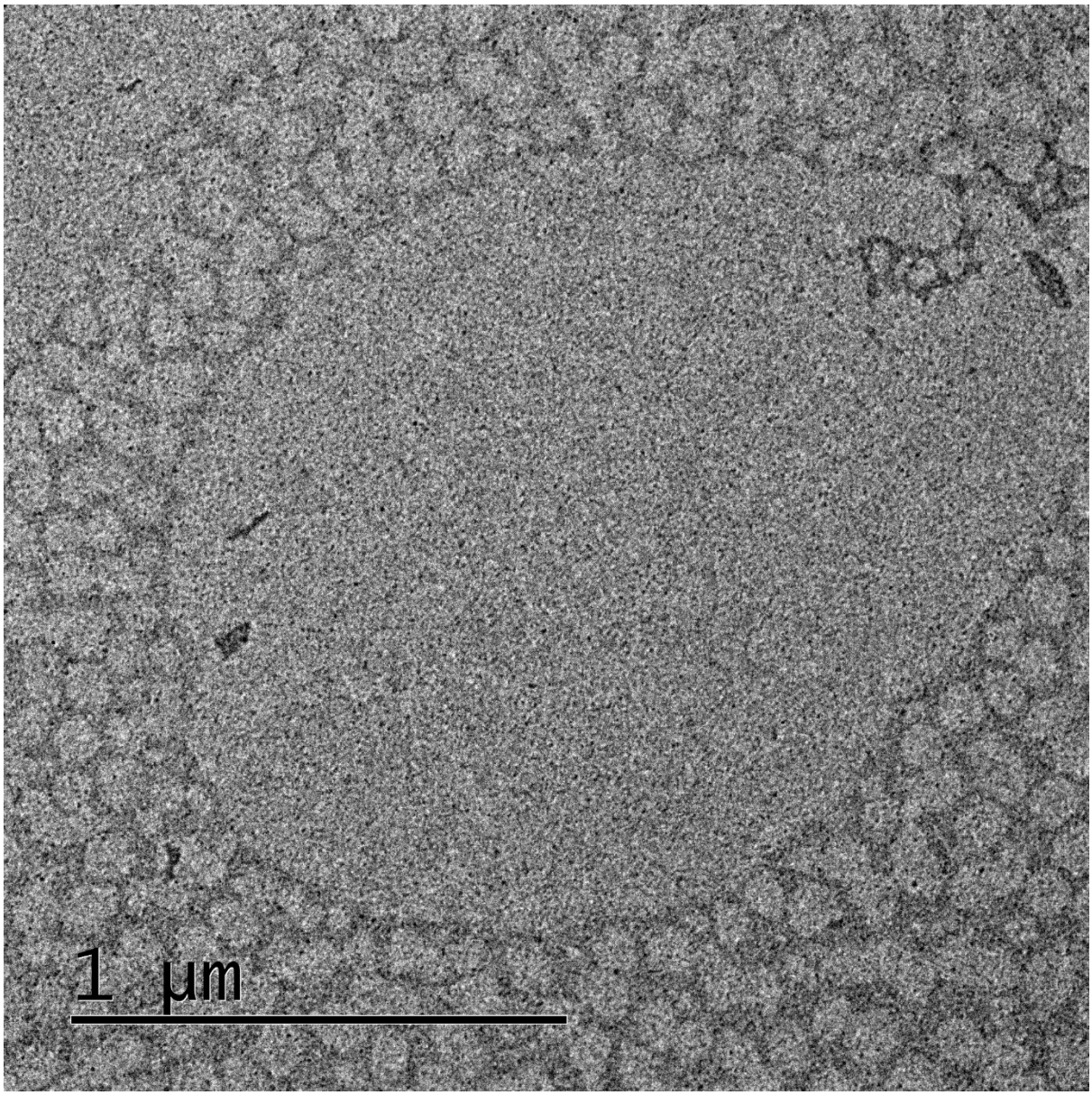

B36. TEM image of **PDI-2-TANI** aggregates in ethyl acetate prepared using a 1:5 seed:unimer ratio (seeds prepared via thermal self-seeding and sonication) - [**PDI-2-TANI**] = 6 x 10^{-5} M.

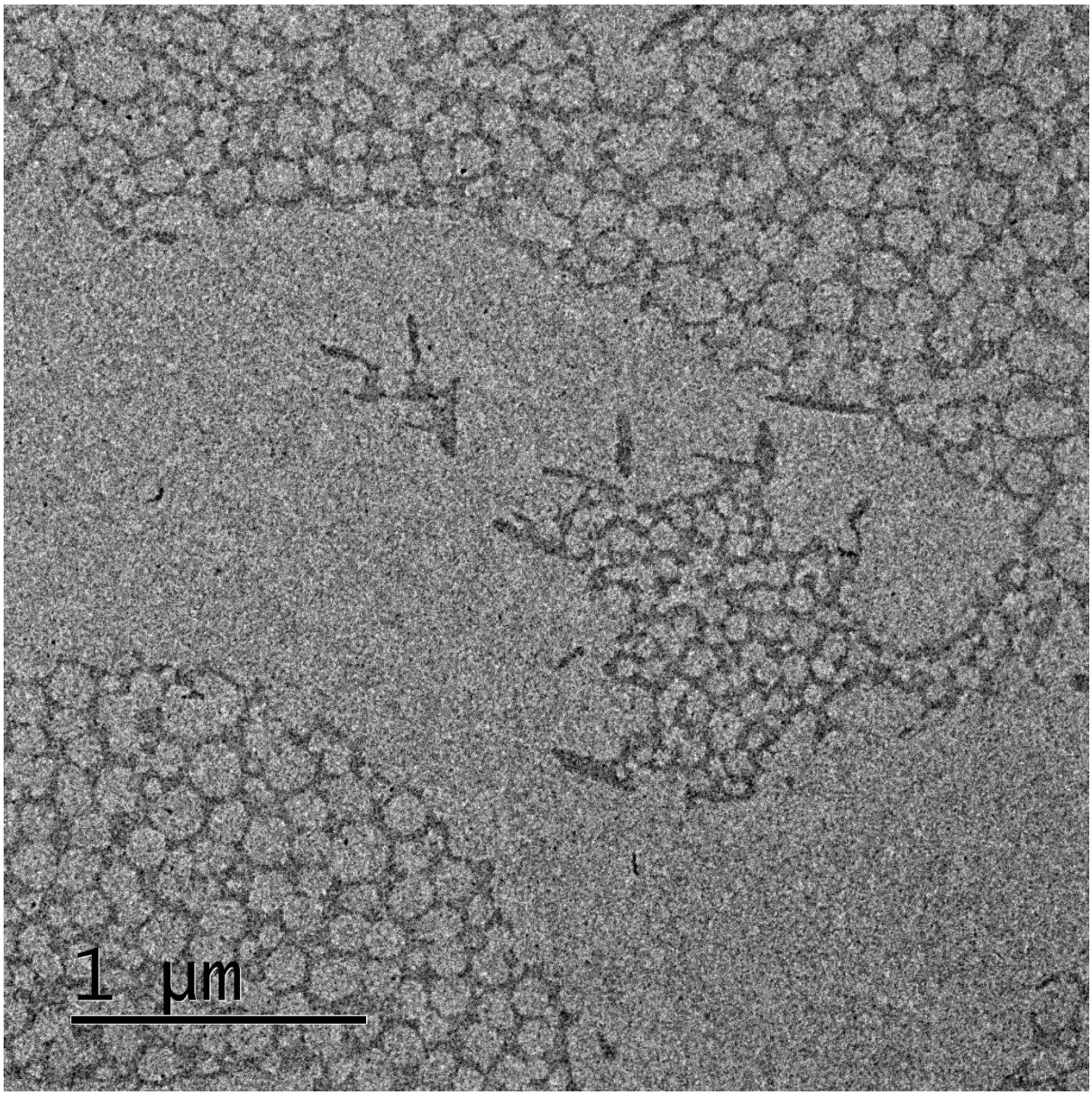

B37. TEM image of **PDI-2-TANI** aggregates in ethyl acetate prepared using a 1:5 seed:unimer ratio (seeds prepared via thermal self-seeding and sonication) - [**PDI-2-TANI**] = 6 x 10^{-5} M.